New algorithms for solving high-dimensional time-dependent optimal control problems and their applications in infectious disease models

by

Yuyang Chen

B.S., Northeastern University, 2015

AN ABSTRACT OF A DISSERTATION

Submitted in partial fulfillment of the requirements for the degree

DOCTOR OF PHILOSOPHY

Department of Industrial Manufacturing Systems Engineering
Carl R. Ice College of Engineering

KANSAS STATE UNIVERSITY
Manhattan, Kansas

2022

Abstract

Infectious diseases have been the primary cause of human death worldwide nowadays. The optimal control strategy for infectious disease has attracted increasing attention, becoming a significant issue in the healthcare domain. Optimal control of diseases can affect the progression of diseases and achieve high-quality healthcare. In previous studies, massive efforts on the optimal control of diseases have been made. However, some infectious diseases' mortality is still high and even developed into the second highest cause of mortality in the US. According to the limitations in existing research, this research aims to study the optimal control strategy via some industrial engineering techniques such as mathematical modeling, optimization algorithm, analysis, and numerical simulation.

To better understand the optimal control strategy, two infectious disease models (epidemic disease, sepsis) are studied. Complex nonlinear time-series and high-dimensional infectious disease control models are developed to study the transmission and optimal control of deterministic SEIR or stochastic SIS epidemic diseases. In addition, a stochastic sepsis control model is introduced to study the progression and optimal control for sepsis system considering possible medical measurement errors or system uncertainty. Moreover, an improved complex nonlinear sepsis model is presented to more accurately study the sepsis progression and optimal control for sepsis system. In this dissertation, some analysis methods such as stability analysis, bifurcation analysis, and sensitivity analysis are utilized to help reader better understand the model behavior and the effectiveness of the optimal control.

The significant contributions of this dissertation are developing or improving nonlinear complex disease optimal control models and proposing several effective and efficient optimization algorithms to solve the optimal control in those researched disease models, such as an optimization

algorithm combining machine learning (EBOC), an improved Bayesian Optimization algorithm (IBO algorithm), a novel high-dimensional Bayesian Optimization algorithm combining dimension reduction and dimension fill-in (DR-DF BO algorithm), and a high-dimensional Bayesian Optimization algorithm combining Recurrent Neural Network (RNN-BO algorithm). Those algorithms can solve the optimal control solution for complex nonlinear time-series and high-dimensional systems. On top of that, numerical simulation is used to demonstrate the effectiveness and efficiency of the proposed algorithms.

New algorithms for solving high-dimensional time-dependent optimal control problems and their applications in infectious disease models

by

Yuyang Chen

B.S., Northeastern University, 2015

A DISSERTATION

Submitted in partial fulfillment of the requirements for the degree

DOCTOR OF PHILOSOPHY

Department of Industrial Manufacturing Systems Engineering
Carl R. Ice College of Engineering

KANSAS STATE UNIVERSITY
Manhattan, Kansas

2022

Approved by:

Major Professor
Chih-Hang Wu

Copyright

Abstract

Infectious diseases have been the primary cause of human death worldwide nowadays. The optimal control strategy for infectious disease has attracted increasing attention, becoming a significant issue in the healthcare domain. Optimal control of diseases can affect the progression of diseases and achieve high-quality healthcare. In previous studies, massive efforts on the optimal control of diseases have been made. However, some infectious diseases' mortality is still high and even developed into the second highest cause of mortality in the US. According to the limitations in existing research, this research aims to study the optimal control strategy via some industrial engineering techniques such as mathematical modeling, optimization algorithm, analysis, and numerical simulation.

To better understand the optimal control strategy, two infectious disease models (epidemic disease, sepsis) are studied. Complex nonlinear time-series and high-dimensional infectious disease control models are developed to study the transmission and optimal control of deterministic SEIR or stochastic SIS epidemic diseases. In addition, a stochastic sepsis control model is introduced to study the progression and optimal control for sepsis system considering possible medical measurement errors or system uncertainty. Moreover, an improved complex nonlinear sepsis model is presented to more accurately study the sepsis progression and optimal control for sepsis system. In this dissertation, some analysis methods such as stability analysis, bifurcation analysis, and sensitivity analysis are utilized to help reader better understand the model behavior and the effectiveness of the optimal control.

The significant contributions of this dissertation are developing or improving nonlinear complex disease optimal control models and proposing several effective and efficient optimization algorithms to solve the optimal control in those researched disease models, such as an optimization

algorithm combining machine learning (EBOC), an improved Bayesian Optimization algorithm (IBO algorithm), a novel high-dimensional Bayesian Optimization algorithm combining dimension reduction and dimension fill-in (DR-DF BO algorithm), and a high-dimensional Bayesian Optimization algorithm combining Recurrent Neural Network (RNN-BO algorithm). Those algorithms can solve the optimal control solution for complex nonlinear time-series and high-dimensional systems. On top of that, numerical simulation is used to demonstrate the effectiveness and efficiency of the proposed algorithms.

Table of Contents

List of Figures

List of Tables

Acknowledgements

First, I would like to express my sincerest thanks to my advisor Dr. Chih-Hang Wu for his valuable guidance, understanding, and support throughout my career as a graduate student. He has not only taught me the knowledge to be a good researcher, but also taught how to be professional and better in my life. Dr. Wu, thank you for this incredible mentorship. I will never forget your advice. Your advice will inspire me to be more professional in my future career.

I would like to thank my Ph.D. supervisory committee members Dr. David Ben-Arieh, Dr. Ashesh Kumar Sinha, Dr. Mingjun Wei, and Dr. Eugene Vasserman for their time and guidance during my graduate studies. Their insightful comments and suggestions strengthened this dissertation's research substantially.

I thank Dr. Bradley Kramer for his constant financial support to develop my research and professional skills. I appreciate Dr. Bradley Kramer provide me the opportunity to participate the design, management, and maintenance of NSF CAREER Proposal Writing Workshop website. I also offer my sincere appreciation to all faculty and staff from the department of Industrial and Manufacturing Systems Engineering at Kansas State University for their support, knowledge, and assistance.

Last but not least, I would like to thank my family, friends, and colleagues who helped me during my academic and professional journey. Their encouragement, support, and willingness also made this work possible.

Chapter 1 - Research Summary

1.1 Introduction and Research Background

With the increasing importance and complexity of the problems facing in the healthcare domain, various industrial engineering techniques and concepts have been widely used to provide more efficient and effective solutions or theoretical analysis for healthcare issues or challenges [1], such as disease prevention and intervention, the method to reduce medical error, the impact of human behavior on disease progression, healthcare cost reduction, mathematical modeling and numerical simulation of complex disease system, etc. [2]. In healthcare, disease prevention and intervention are significant and widespread issue to realize health promotion and achieve high-quality health [3]. Effective disease control and intervention can also reduce medical errors, improving the quality of healthcare [4]. In the meantime, human behavior impacts the progression, prevention, and control of the disease [5]. Disease prevention and intervention are also closely associated with healthcare costs and health outcomes. Besides that, mathematical modeling and numerical simulation of disease systems provide researchers a powerful way to study the dynamics of diseases and research how disease prevention and intervention affect the progression or transmission of diseases [6].

Over the past decades, studies about the mathematical model of complex disease systems have made significant progress. There are some popular epidemic mathematical models such as the SIR model [7], SIS model [8], SEIR model [9], etc. Researchers usually utilize those models to study the epidemiological dynamic of epidemic diseases such as Ebola, Zika virus disease, influenza, COVID-19, etc., [10 - 18]. In addition to the epidemic disease, the mathematical modeling of severe infectious diseases such as sepsis has attracted increasing attention in healthcare. Sepsis is a life-threatening medical emergency disease, which is the body's extreme

immune response to infection. Its deaths increase each year [19]. Sepsis is the second highest cause of death in the United States [20]. Many studies also proposed mathematical models to research the sepsis development and immune response mechanism [21 - 24]. Whether the epidemic disease or infectious disease, however, only studying disease progression using mathematical modeling is not enough to help us reduce the mortality rate and prolong patient's life.

As the healthcare field develops, considering the optimal control strategy into the mathematical disease model became an essential and hot research issue. Optimal control strategy on disease means the medical therapy treatments or intervention measures to control the progression or spread of disease, minimize side effects of drugs, reduce medical errors, reduce disease mortality, or improve patients' quality of care in the clinic [25, 26]. For example, the optimal control strategy in the epidemic disease model can be vaccination, quarantine, hospitalization, travel restriction, mask-wearing, drug treatment, etc. [25]. The optimal control strategy in the sepsis disease model can be medical treatment, hospitalization, antimicrobial therapy, immunological therapy, etc. [27]. Researching the disease optimal control strategy is a meaningful and necessary process to prevent disease progression, reduce human mortality, and save lives.

In the disease optimal control model, the optimal control strategies usually are significantly associated with financial costs or the changes of essential system components. Suppose policymakers don't take any control strategy to control the progression of diseases. In that case, it may cause inevitable economic costs or harmful outcomes, such as workforce losses due to outbreaks, increased community healthcare costs, local business downturns, and high mortality rates. Thus, the financial cost and the critical system components associated with control strategy can be defined as an objective function of solving the optimal control strategy. To simplify the

problem and process of solving the optimal control strategy, most existing studies described the objective function of the disease control model as convex [28 - 31]. However, the objective function related to the control strategy is possible non-convex in the real-world [32]. Therefore, considering the possible non-convex objective function may make the theoretical optimal control strategy of the disease optimal control model have practical significance.

On top of that, solving the optimal control strategy in the disease optimal control model can be viewed as optimization of time-series nonlinear problem [33, 34]. Time-series means that the values of the model's variables (e.g., system state variables and control variables) at the current time will affect subsequent variable values. The control variables and the system states are time-series and stage-dependent. In addition to the time-series character, the disease control model is high-dimensional. For example, the epidemic disease usually lasts for a few hundred days or even a couple of years. The control strategy in day unit carried out in the epidemic may contain up to hundreds of thousands of time epochs. The control strategy for severe infectious diseases such as sepsis is in hour unit, which is usually carried out for dozens even up to hundreds of hours (time epochs) [35 - 37]. If each time epoch (each day or each hour) is considered as a time dimension, as the number of time epochs increases, solving the time-series disease optimal control strategy will be a complex nonlinear time-series and high-dimensional optimization problem.

If the objective function is convex, Pontryagins maximum principle is a popular approach to solve the optimal control strategy for the disease optimal control model [38 - 40]. Most general optimization algorithms such as gradient descent [41] or heuristic algorithms can also solve this type of optimization problem [42]. If the objective function is possible non-convex, the optimization will become more complicated. Pontryagins maximum principle is no longer suitable to solve it. Moreover, suppose the system contains many state variables. In that case, it is necessary

to calculate the values of each state variable at each time epoch and sum up each epoch's cost to evaluate the overall cost for one control strategy. It is too time-consuming to assess the overall cost of a high-dimensional system for a single control strategy. The conventional optimization algorithms and heuristic algorithms (such as Particle Swarm Optimization (PSO) algorithm [43], genetic algorithm [44], simulated annealing [45]) usually can reach an outstanding optimization performance in the low-dimensional systems. However, they may not be computationally efficient and highly accurate algorithms to solve the optimal control strategy for such a complex time-series high-dimensional disease optimal control model with the non-convex objective function.

Unlike conventional global optimization algorithms, standard Bayesian Optimization (BO) is a promising and powerful global optimization algorithm capable of solving the non-convex optimization problem. Still, the standard BO algorithm is challenging for dealing with high-dimensional optimization problems [46]. Some new high-dimensional BO algorithms are proposed to address this challenge. Those new BO algorithms utilize the dimension reduction knowledge to realize the high-dimensional optimization purpose. But they take a significant amount of time to reconstruct all system variables from low-dimensional space back to the original high-dimensional space at each optimization iteration. They then calculate the corresponding objective function value in high-dimensional space [47 - 50]. Therefore, they don’t improve the implementation efforts and running time. Also, those new high-dimensional BO algorithms mainly focus on simple time-independent systems, which may not be accurate and efficient enough to solve the complex time-series systems.

Therefore, all the evidence and challenges above addressed the necessity of developing more effective and efficient optimization algorithms to solve the optimal control strategy for

complex nonlinear time-series and high-dimensional disease optimal control systems in future healthcare research.

1.2 Research Motivation, Objective and Tasks

Several studies have contributed to disease mathematical modeling and disease control in healthcare. For example, Hossain *et al.* leveraged the SIR model to mathematical model the outbreak of Ebola virus disease [11]. Eikenberry and Gumel reviewed the mathematical modeling for malaria transmission dynamics and studied climate's possible impact on malaria progression [12]. Ivorra *et al.* developed a mathematical model of COVID-19 to learn the importance of the percentage of the detected cases on the impact of COVID-19 [16]. Yamanaka *et al.* constructed a nonlinear mathematical sepsis model to research how inflammation resulting from immune activity caused septic shock [21]. Wu *et al.* improved an existing mathematical model of sepsis to study immune response to infection and sepsis progression in detail [24]. However, those mathematical modeling of disease systems only focus on disease progression and transmission, which cannot help controlling further deterioration.

In addition to disease mathematical modeling, many researchers used mathematical models to study the disease control strategy. Albuquerque *et al.* established a control model for combating bancroftian filariasis to theoretically and conceptually study the necessary control strategies at each level [51]. Mandal *et al.* mathematically modeled the transmission of COVID-19 by considering optimal intervention control strategies, which aimed to figure out the impact of travel restrictions on the local outbreak of COVID-19 and research if its transmission can be mitigated by quarantine intervention control of symptomatic patients [52]. Neilan and Lenhart studied the optimal control in a disease system with simple ordinary differential equations [53]. Oke *et al.* studied the optimal control therapy on a mathematical breast cancer model to minimize the

number of cancerous cells [54]. Fish *et al.* researched the optimal antimicrobial therapy for achieving the best possible outcomes of sepsis [55]. However, those works studied the disease control strategy on oversimplified disease models.

Although the previous studies provided some contributions in disease mathematical modeling and disease control, the oversimplified disease model may not be an excellent way to study disease's exact progression and dynamics. In addition, these disease models usually considered the objective function associated with disease control strategy as convex, which is too simple to research the practical and meaningful disease control strategy in the real world. For example, the cost of control strategy in the epidemic disease system is affected by various factors like inpatient days, cost of treatment equipment, wages, logistics, and infrastructure. The cost may be different at different times, so the cost function may be possible non-convex in the real-world [56].

On the other hand, the current contributions on the methodology to solve disease optimal control are still limited. Many studies used the Pontryagins maximum principle to solve the optimal control strategy due to the system's simplicity [38], which is only suitable to solve the disease control system with the convex objective function. Some studies applied the optimization algorithms such as gradient descent, genetic algorithm, and simulated annealing to solve the optimal control strategy [41]. However, these methods are not computationally efficient and highly accurate for complex disease systems. Significantly few works provided effective and efficient optimization algorithms to find the optimal control strategy for complex enough, nonlinear, time-series, and high-dimensional disease optimal control systems.

Hence, this research aims to construct disease optimal control models (deterministic and stochastic) by considering different types of the objective function (convex and possible non-

convex). And develop the disease model that can accurately describe the disease progression. On top of that, this research attempts to propose more effective and efficient optimization algorithms that can solve the optimal control strategy for complex nonlinear disease systems, including three main research tasks as follows:

Task 1, construct disease optimal control models by considering different types of objective functions for epidemic disease: mathematically modeling different disease optimal control models based on the standard disease models (standard disease model means the original basic disease model without control variable). To better reflect the cost associated with control strategy in the real world, different types of objective function were considered. During task 1, the specific tasks are as follows:

1. Construct deterministic or stochastic epidemic disease optimal control models.
2. Define the objective function with different types: convex and possible non-convex, to better and comprehensively reflect the cost function associated with control strategy in the real world.
3. Provide the stability and sensitivity analysis for the model.

Task 2, construct a complex nonlinear disease optimal control model for a severe infectious disease named sepsis: improving an existing mathematical sepsis model to precisely describe the sepsis progression and develop the improved sepsis model into an optimal control model. During task 2, the specific tasks are as follows:

1. Improve an existing nonlinear mathematical sepsis model by reconstructing more detailed and accurate subsystems and developing it into a sepsis optimal control model.
2. Define the objective function using some important and effective biomarkers recommended and authorized by previous clinic practices.

3. Discuss the behavior of the complex nonlinear sepsis model through bifurcation analysis.

Task 3, propose more effective and efficient optimization algorithms: proposing new optimization algorithms to solve the optimal control strategy for the complex disease optimal control models. During task 3, the specific tasks are as follows:

1. Propose a more effective and efficient optimization algorithm by combining machine learning algorithm to solve the optimal control strategy for stochastic disease optimal control model.
2. Propose three more effective and efficient high-dimensional Bayesian Optimization algorithms to solve the optimal control strategy for complex nonlinear time-series and high-dimensional disease optimal control models with different types of objective function.
3. Implement numerical simulations to demonstrate the effectiveness and efficiency of proposed algorithms.

1.3 Proposed Methodologies

Several industrial engineering techniques and concepts are applied to the complex disease models to sufficiently study the impact of the optimal control strategy on the transmission or progression of diseases. This research used mathematical modeling to study how human fear affects behavior to choose the control strategy to defend epidemic disease and define the convex objective function associated with the optimal control strategy. This research also used mathematical modeling to construct time-series and high-dimensional epidemic disease optimal control models, and define the possible non-convex objective function associated with the optimal control strategy. Besides the epidemic disease, this research used mathematical modeling to

construct the stochastic sepsis optimal control model, considering both system and measurement errors. This research also utilized mathematical modeling to reconstruct a more complex nonlinear sepsis optimal control model.

After constructing disease optimal control models using mathematical modeling, according to different control models (nonlinear, time-series, high-dimensional, convex\possible non-convex, deterministic\stochastic), this research proposed several effective and efficient optimization algorithms to solve the optimal control strategy for the studied control models.

Several analysis methods, including stability analysis, sensitivity analysis, bifurcation analysis, and global convergence analysis, were used to study the model behavior or the effectiveness of the proposed optimization algorithms.

Finally, numerical simulations were carried out to demonstrate the effectiveness and efficiency of the proposed optimization algorithms by comparing them with other popular optimization algorithms. Numerical simulations also were used to study the impact of the optimal control strategy generated by the proposed optimization algorithms on disease transmission or progression.

1.4 Research Map

This research plans to provide scientific and practical mathematical disease optimal control models. At the same time, more effective and efficient optimization algorithms are proposed to solve the optimal control strategy for all studied disease optimal control models. Furthermore, different analysis and numerical simulation experiments are carried out to better understand the model, proposed algorithms, and the impact of the optimal control strategy on disease outcomes.

Figure 1.1 shows a research map describing the research objectives, methodologies, and potential research contributions.

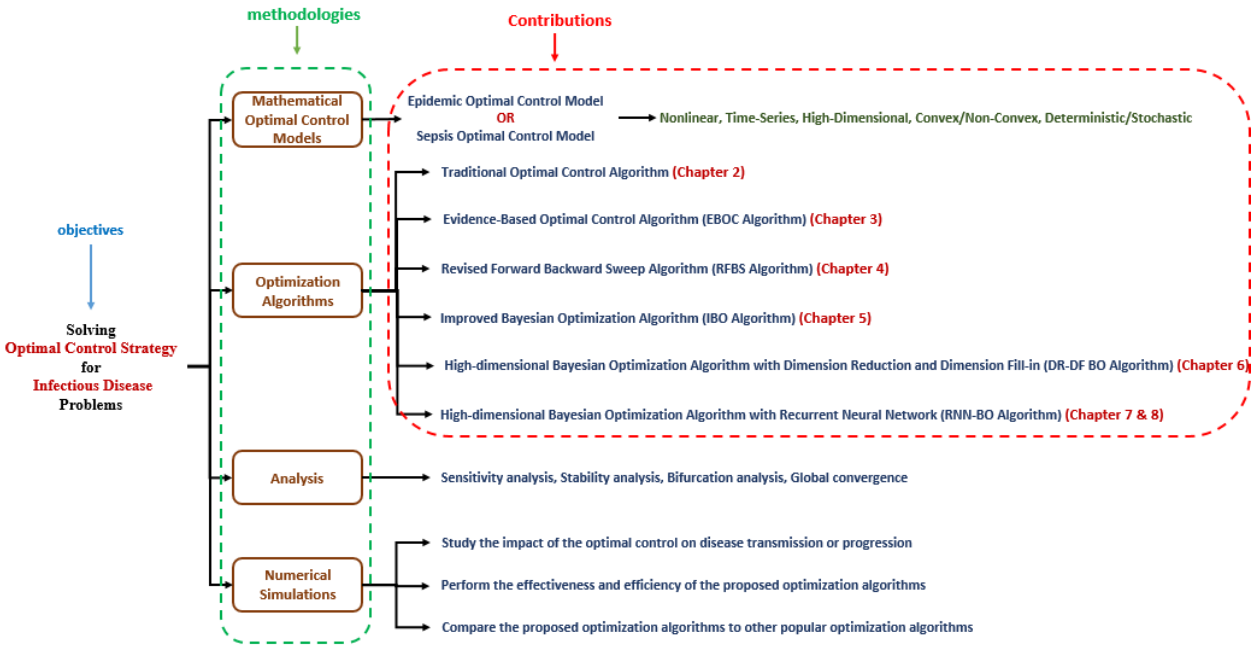

Figure 1.1 Research Map of the dissertation

1.5 Dissertation Outlines

The rest of the dissertation is organized into eight chapters: Chapter 2 is a published journal paper in Chaos, Soliton & Fractals [57], which mathematically modeled how human fear affects the behavior to choose the control strategy and solved the optimal control strategy for the epidemic disease optimal control model. Chapter 3 is a published journal paper in Computers & Industrial Engineering [58], which proposed an effective algorithm to solve the optimal control strategy for a stochastic sepsis optimal control model with considering system and measurement errors. Chapter 4 is an ongoing working paper that is ready to submit, which proposed an optimization algorithm to solve the optimal control strategy for the stochastic epidemic optimal control model with the convex objective function. Chapter 5 is an ongoing working paper that is ready to submit, which proposed an improved Bayesian Optimization algorithm (IBO algorithm) to solve the optimal control strategy for complex time-series and high-dimensional epidemic optimal control model with the non-convex objective function. Chapter 6 is an ongoing working paper that is ready

to submit, which proposed a novel high-dimensional Bayesian Optimization algorithm by considering dimension reduction and different dimension fill-in strategies (DR-DF BO algorithm). This algorithm can solve the optimal control strategy for complex deterministic or stochastic time-series and high-dimensional epidemic optimal control models with the non-convex objective function. Chapter 7 is an ongoing working paper ready to submit, which proposed a new high-dimensional Bayesian Optimization algorithm combining Recurrent neural network (RNN-BO algorithm). This algorithm can learn the historical optimal control strategy data. Accurately and quickly predict the optimal control strategy for the epidemic disease in different regions or due to different virus types. The RNN-BO algorithm is effective and efficient in solving complex deterministic or stochastic epidemic time-series and high-dimensional epidemic optimal control models with the non-convex objective function. Chapter 8 is an ongoing working paper ready to submit, which reconstructed a complex nonlinear sepsis model by improving the monocyte subsystem and adaptive immune system, then developed the improved model into a sepsis optimal control model. Also, the NN-BO algorithm was applied to predict the optimal control strategy for this complex nonlinear sepsis optimal control model. Chapter 9 summarizes this dissertation's main conclusion and contributions and discusses the potential future works.

Chapter 2 - A Individual Fear Factor Model for Information Transmission and Human Behavior with Stability Analysis

Chapter 2 is based on the manuscript “A Individual Fear Factor Model for Information Transmission and Human Behavior with Stability Analysis” Published in Chaos, Soliton & Fractals [57].

Abstract

This paper proposes a new, information-transmission-based behavior-switch that applies the individual fear factor (IFF) to describe how information regarding current disease epidemics can cause human behavior change in a disease-dynamic system. This research is a first attempt to mathematically model how an individual's emotions influence behavior. The approach can be used to study the relationship of information dissemination (e.g., broadcasting, public health education, news media, etc.) and human behaviors during disease outbreaks. The expression of IFF and a mathematical IFF model that combines human behaviors with a classic SIR model is presented, and an optimal strategy that reduces the number of infected individuals and financial loss due to switch behaviors is proposed. In particular, model stability is analyzed and corresponding necessary conditions are determined. This novel modeling approach shows that information transmission influence individual fear, resulting in a variety of human behaviors and leading to numerous disease consequences.

Keywords: individual fear factor, disease dynamic, behavior change, stability analysis, optimal control.

2.1 Introduction

Human behavior changes throughout an infectious disease epidemic have recently been identified as a dominating factor in epidemics and have attracted considerable attention in the literature [59-62]. Increased understanding of the interconnectedness of human behavior changes and the underlying epidemic could help governments and public health agencies develop more effective protective measures and mitigation strategies. Because individuals receive disease information from various sources, e.g., news broadcast, social media contacts, updated prevalence on a disease, etc., each person may exhibit unique behaviors, such as utilization of protective masks, vaccination, social distancing, self-quarantine, or other self-protections to reduce the chances of infection. On the other hand, individuals may refuse to implement protective measures because they think the measures could be inconvenient or expensive. These unique, spontaneous behavior patterns based on diverse knowledge or opinions derived from similar information may lead to a variety of disease epidemic results; therefore, the primary objective of this article is to model and study human behavior changes and subsequent impacts on the underlying disease epidemic.

During an epidemic outbreak, individuals may possess distinctive viewpoints on and responses to long-term disease risks. Lemerise *et al.* [63] found that social information can influences emotional and cognitive processes. Similar research discovered that human emotion can be formed based on the information acquired [64], and Shiota *et al.* [65] determined that emotions are unique. Zhao *et al.* [66] used a spatial evolutionary game to investigate how prevalence information in a disease can influence human behaviors. In 2010 Funk *et al.* [59] reviewed current human behavior models and researched the impact of human behavior on infectious disease dynamics. Johnston *et al.* [67] identified that fear, a common emotional

expression of individuals during disease outbreaks, can initiate human protection motivation. In 1965 Geer [68] first proposed the concept and measure of the fear factor which is the result in external stimuli.

To the best of our knowledge, no research has investigated how disease information result in human opinion and emotion then how to act on human behaviors throughout a disease epidemic. Public health agencies are often unable to fully control spontaneous changes of human behavior during an epidemic because, although individuals may receive similar information regarding a disease, each individual uniquely interprets the knowledge and forms distinctive opinions that affect his or her decisions and behavior. Actually, in 2009 Funk *et al.* [69] proposed the spread of awareness could affect the spread of disease, although it could not stop the disease, it can lower the infection rate significantly. Their paper considered the awareness just can spread through the media which is the information disseminated in global, and they provided some analysis to support the impact of spread of awareness on epidemic. The difference of ideas between their paper and this paper is that their paper proposed the spread of awareness could influence the spread of disease because it is related to the infection rate. However, the idea of this paper is that propose the mathematical definition of individual fear factor and consider individual fear factor can change human behavior, which is not considered in their paper. In this paper we mathematically model the individual fear factor (IFF) and analyze its connection to epidemic information and spontaneous human behavior. Our study of IFF is based on the perceptual and rational aspects of information, considering local and global information. We also propose an expression of individual fear factor in three different parts: inertia part, perceptual part, and rational part. The inertia aspect of information indicates the impact of one's IFF on the next IFF for all individuals. For the perceptual aspect of information, our model considers how emotions from in the population

spread and affect the IFF of an individual, including unprecedented consideration of self-mood. The rational aspect of information reflects how official or objective data pertaining to the number of infected individuals and switched susceptible individuals effect IFF.

The primary objective of this paper is to demonstrate how IFF is connected to susceptible individuals' changes in human behavior during a disease epidemic. Our aim is to increase model suitability for population over a contact network in which a disease can transmit over physical contacts and information can travel over social contacts. The proposed mathematical model incorporates IFF into the classic SIR model. First, we focus on the expression of individual fear based on various aspects of information sources, and then we adopt the particle swarm optimization (PSO) method to calculate IFF when an individual receives information regarding a disease epidemic. Second, we investigate how IFF affects changes in human behavior by analyzing how many individuals alter their current behaviors due to IFF and then inputting the number of switching susceptible individuals into the well-known SIR model. In order to precisely define the relationship between IFF and the SIR model, however, we use a multiple regression model to analyze numerical results of the regression model (IFF-SIR model). Third, stability analysis of the IFF model and IFF-SIR model is conducted using stability study and its related theories, including investigation of stability conditions. Assuming that corporate social performance of individuals can be controlled or manipulated, the optimal control strategy is used in our model to research how to effectively and economically decrease the number of infected individuals during the outbreak of disease. Our control policy is based on decreasing benefits (payoffs) due to switching behaviors and the number of infected individuals. Finally, we determine and present continuous control of optimal social reduction function with numerical simulations.

The paper is organized as follows. Section 2.2 describes construction of the IFF model and IFF-SIR dynamic systems model. Section 2.3 introduces the simulation strategy for the IFF model and regression analysis. Section 2.4 presents stability analysis for the IFF and IFF-SIR dynamic systems models and corresponding verification using simulation, and Section 2.5 includes discussion of the optimal control model and strategy of the IFF-SIR model as well as calculations for numerical solutions. Section 2.6 provides summary and discussion.

2.2 Mathematical Model

2.2.1 Disease Transmission

In this paper we use the SIR model first formulated by Lowell Reed and Wade Hampton Frost in the 1920s [70] to describe disease transmission. The classic SIR model is a host-host transmission pathway [71]. In our SIR model we consider the disease-spreading process among N population in which each individual is in one of three states: susceptible, infected, or recovered. In addition, because some individuals in the real world are born or die over one time epoch, we add newborn individuals and remove dead individuals at a rate μ. In the real-world individuals randomly contact individuals in other states, potentially becoming infected or infecting others at an average rate β. Infected individuals can choose measures to recover and acquire immunity, thereby guaranteeing they do not suffer from this disease at a recovery rate γ.

Considering the SIR model of transmission, individuals can be divided into three states: susceptible individuals, infected individuals, and recovered individuals. The following is the classic SIR model with demography that assumes that birth rate is equal to death rate [72], then

$$\frac{dS}{dt} = -\frac{\beta SI}{N} + \alpha(N - S) \tag{2.1}$$

$$\frac{dI}{dt} = \frac{\beta SI}{N} - \gamma I - \mu I \tag{2.2}$$

$$\frac{dR}{dt} = \gamma I - \mu R \tag{2.3}$$

Where S is the number of susceptible individuals, I is the number of infected individuals, R is the number of recovered individuals, β is the infection rate of individuals, γ is the recovery rate, μ is the death rate, and α is the birth rate. In here $\alpha = \mu$.

2.2.2 Individual Fear

As stated, Geer [68] first introduced the concept of a fear factor that could quantify the human emotion of fear. Parkinson *et al.* [73] reviewed emotional contagion and social appraisal and proposed that people can obtain similar emotions from their contact network via communication, meaning that fear can spread among individuals. Epstein *et al.* [74] incorporated fear into classic mathematical epidemiology by distinguishing behaviors of infected and recovered individuals as motivated by fear and unfear. Chen [75] investigated the relationship between information and disease transmission, such as whether an individual's fear of a disease is aggravated by information from face-to-face communication, social media, or TV broadcast, and how fear of a disease relates to the individual (e.g., individual's robustness or happiness).

In this paper we categorize IFF into perceptual, rational, and inertia parts, as shown in Figure 2.1.

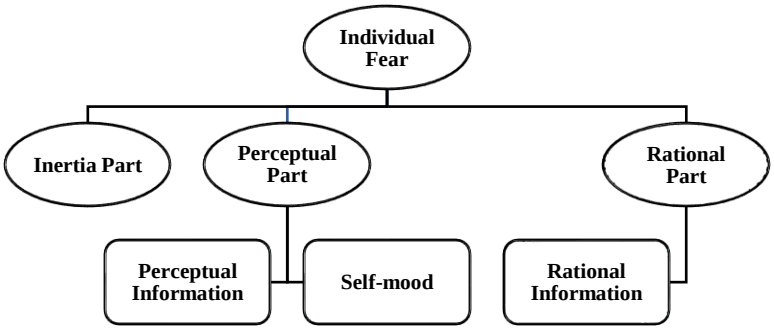

Figure 2.1 Flowchart of individual fear composition

The perceptual part contains perceptual information and self-mood [76]. Perceptual information is affected by a local social network (i.e., face-to-face contacts such as friends, colleagues, and family members), a global social network (i.e., face-to-screen contacts such as friends in social media and people in the news), and an individual's previously fostered self-fear. Consequently, people in one's social network (local and global) can transfer fear into an individual. Although self-mood is a random factor, it can also affect an individual's fear factor. For example, a person may experience decreased fear toward a disease if he or she wins a large sum of money.

The rational part, however, contains rational information such as the numbers of infected and switch individuals in a local social network and a global social network. Consequently, the more people who are infected in one's social network, the more fear an individual will feel. Moreover, if an individual perceives that others are increasing use of protective measures such as masks, then that individual could also experience increased fear.

Emotions have commonly been recognized as continuous in the time series [77, 78]. Suls *et al.* [79] first introduced the concept of emotional inertia to describe emotional fluctuation, meaning that a person's previous emotions or feelings of fear can be influenced by current emotions. Researchers have observed that emotions can be high or low in fluctuation and high or low in inertia, high in fluctuation, or low in inertia [80 - 82]. However, because researchers cannot agree on the proportion between fluctuation and inertia, we use inertia weight w in the inertia part to describe this uncertain relation, meaning that the inertia part of IFF may have different number in different situation.

2.2.3 Changes in Human Behavior

Zhao *et al.* [83] recently proposed a methodology that combines information dissemination, contact networks, and human behavior changes in order to model the dynamics of infectious

diseases. Their study divided susceptible individuals into switch and normal individuals. Switch individuals indicated fear of the disease and potentially protected themselves by wearing masks, becoming vaccinated, or limiting their travel. Normal individuals demonstrated no change in their behavior and did not take any preventive measures to reduce their chances of infection. Although their research defined a switch behavior game for susceptible individuals, the game was based only on information and did not include mental activity.

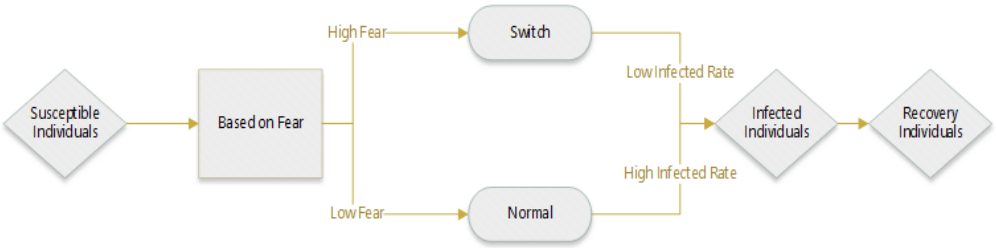

Figure 2.2 Flowchart of SIR population transition and switch behavior

Steimer [84] defined fear as a motivational state aroused by specific stimuli that results in defensive behavior or escape, meaning that switch behavior depends on an individual's degree of fear. Individuals with fear (or concerns) will likely take actions to protect themselves from a disease. Although research has shown that stress and fear reactions in response to infectious disease are normal and potential adaptation or protection [85], the research has not related fear to switch behavior. Therefore, in this paper, we assume that the fear factor is highly relevant to the level of switch behavior (Figure 2.2), meaning that if the fear factor is high, individuals will likely choose switch behavior to protect themselves. If the fear factor is low, however, individuals will likely demonstrate normal behavior, and if the fear factor is moderate, then the potential for an individual to switch his or her behavior is more indifferent. We assume that the relationship between the fear factor and switch behavior is not constant i.e., each individual would choose to switch randomly with a probability based on the logistic probability distribution [86]. However,

switch behavior is not always ideal for susceptible individuals since switching their current behaviors almost always incur certain associate costs directly or indirectly. For example, an individual may need to purchase protective measures such as face masks and vaccines, or individuals may experience loss of income or business opportunities due to reduced travel level. This paper discusses the trade-offs between protection and reduction of unnecessary cost in Section 2.5, and considers the reduction of possible financial loss and decreased numbers of infected individuals in the objective function.

2.2.4 Contact Network

A contact network originates from a computer network, which frequently applied in the fields of electrical engineering, telecommunications, and computer science [87]. Other people in an individual's contact network can be divided into local and global contacts. Local contacts have a close relationship with the individual (e.g., family members and colleagues). Individuals 2, 3, 5, and 8 in Figure 2.3 are local contacts of individual 6, and all individuals in the group are global contacts of individual 6. Meyers *et al.* [88] studied contact networks by inserting the concept of a contact network into a compartmental SIR model. Scoglio *et al.* [87] introduced a generalized epidemic modeling framework (GEMF) in order to show an individual-based network. Sahneh *et al.* [89] researched competitive epidemic spreading on multilayer networks, these networks include both disease transmissions and information contact networks.

Local and global contacts are considered in our model. Local contacts can transfer diseases and fear to an individual, while global contacts can only transfer fear by information and emotion. Hence, the effects on disease information from local contacts frequently are more influential than that from global contacts. Since each individual cannot know exactly how many infectious and

switch individuals are present in their contact network, we utilize a (random) discount between the real information and the individual received information.

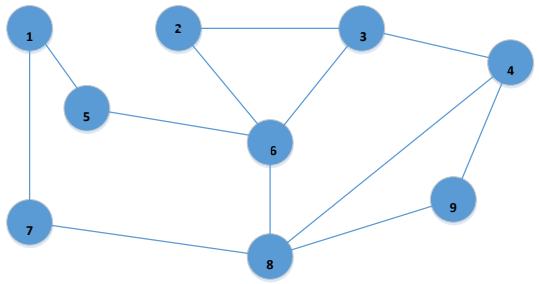

Figure 2.3 Local contact networks of individuals

2.2.5 Particle Swarm Optimization (PSO)

Kennedy *et al.* [90] developed traditional PSO in an effort to produce computational intelligence by exploiting social interaction that originated from the feeding behavior of a bird flock. PSO is an evolution process from disorder to order that assumes individuals in the group as sharing information such that the entire group can determine the optimal solution. Initially, all the birds did not know where the food was, but they knew the distance between themselves and the food. Each bird shared information with other birds in the group in order to increase understanding of the food and determine more efficient behavior in order to increase their proximity to the food. Inertia caused each bird's movement to be influenced by its local known position, and all birds were guided by information in the search-space. The entire group of birds engaged in social learning (i.e., sharing information) in order to improve direction and determine the most efficient path to food.

Based on information transmission analysis, each individual in a group shares information with others. Albert Bandura *et al.* [91] stated that individual behavior can be shaped and controlled by environmental influences and internal dispositions. In the same article, the authors stated that individuals gain understanding of diseases and experiences via information derived from personal

experiences and others in their group. That information is then used to determine subsequent actions. Such social learning occurs unintentionally in an individual's immediate environment. As shown in Figure 2.4, individuals gain information, learn from experiences influence knowledge, and change human behavior. Human behavior is regarded as self-information that influences subsequent human behavior, similar to the feeding behavior of the bird flock.

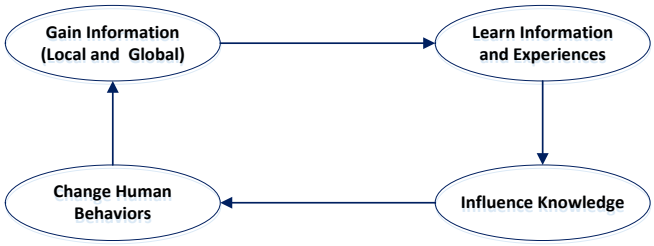

Figure 2.4 Information-behavior process

As shown in Figure 2.5, $x(t)$ represents the original position of a particle in our model (the original IFF of each individual), p_g shows the best position in the global contact networks, and p_p is the best position for the individual. Based on global and local information and in conjunction with original information, the particle would go to $x(t+1)$ along the direction of $v(t+1)$. In our model $x(t+1)$ would be the response to the next IFF and p_g, p_p would be the information an individual receives. Based on original, local, and global information, the next IFF would also tend to $x(t+1)$ along the direction of $v(t+1)$.

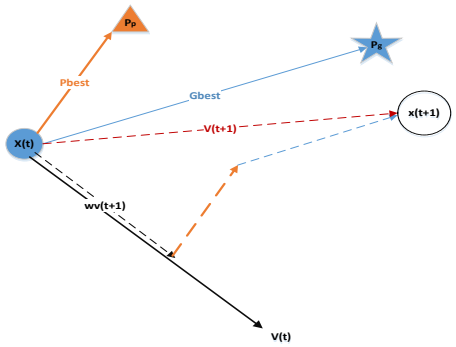

Figure 2.5 Particle swarm optimization

In PSO with inertia weight the velocity and position of particle p at iteration t are

$$v_p(t+1) = wv_p(t) + c_1 r_{1,p}(t)\big(p_p(t) - x_p(t)\big) + c_2 r_{1,p}(t)\big(p_g(t) - x_p(t)\big) \quad (2.4)$$

$$x_p(t+1) = x_p(t) + v_p(t+1) \quad (2.5)$$

Where $v_p(t)$ is velocity of the pth particle $\big(v_p(t+1) \in [-V_{max}, +V_{max}]\big)$, which represents decrement of IFF; $x_p(t)$ is position of the pth particle, which represents IFF in this paper; $p_p(t)$ is the best position found by the pth particle; $p_g(t)$ is the best position found by the swarm; $r_{1,p}(t)$ and $r_{2,p}(t)$ are two independent random numbers uniformly distributed on $[0,1]$; c_1 is the cognitive learning factor, which represents the attraction of a particle to its own success $p_p(t)$; c_2 is the social learning factor, which represents the attraction of a particle to the swarm's best position $p_g(t)$; and w is inertia weight.

We unprecedentedly use the PSO method to describe the decrement of IFF. Since IFF could change over time, a decrement factor $dIFF/dt$ appraises the difference between previous and present fear factor. The PSO method accurately generalizes information from global and local contact networks. The PSO can be also used to describe that the IFF will change as the change of individual's emotion or opinions. We also known individual's emotion is sensitive [92], which means that his/her emotion would lead IFF tending to move to the best IFF (the best IFF will be discussed in Section 2.2.6).

2.2.6 Individual Fear Factor Definition

This paper summarizes concepts of the PSO method, contact network, and individual fear in order to formally model and quantify the IFF. A negative IFF indicates increased confidence for an individual and a low probability that he or she would choose to switch. A positive IFF indicates less confidence for an individual and potentially higher probability of switching behavior. We

suppose the maximum IFF to be 1 and the minimum IFF to be –1 and then calculate the possibility of switch base on the IFF We order the highest IFF in global contact network as 1 and the lowest IFF as -1 and assign other IFFs by linear scaling.

As stated in Section 2.2.2, IFF is divided into perceptual part, rational part, and inertia part, for which we use perceptual fear factor P_f, rational fear factor R_f, and inertia factor $wr_0(t)$ (w is inertia weight, t is epoch t). Perceptual fear factor P_f contains two parts, P_{fi} and P_{fm}, which represent perceptual fear from information and perceptual fear from mood, respectively. Rational fear factor R_f contains R_{fi}, which represents rational fear from information.

We use the PSO model to analyze individual behavior as

$$\frac{dIFF(t+1)}{dt} = w\frac{dIFF(t)}{dt} + P_f + R_f \tag{2.6}$$

where:

$$P_f = P_{fi} + P_{fm} \tag{2.7}$$

$$R_f = R_{fi} \tag{2.8}$$

2.2.6.1 Perceptual Fear Factor from Information P_{fi}

Increasing development of transportation and communication technologies has increased the dissemination of disease information and subsequent fear of disease. People can obtain P_{fi} from local social networks as well as global social networks such as social media. Therefore, P_{fi} contains $P_{fi-local}$ and $P_{fi-global}$, which represent P_{fi} from local contact network, global contact network, and the individual oneself. All individual moves their IFF to a position of optimal personal advantage. Undoubtedly, this position is the smallest IFF at each level when no individual is infected since an individual would switch to the smallest probability in order to

minimize the cost of switch behavior. No individual is infected, so no disease spreading occurs. The information of infected individuals is rational information.

Therefore, in the perceptual part, people tend to move forward to the smallest IFF position in their local and global contact networks. Let $p_l(t)$ and $p_g(t)$ denote the smallest IFF in local and global contact networks, respectively, when no individual is infected until time t. In addition, perceptual information may contain errors between the transmitter and the receptor, so IFF may be amplified or shrunk in information transition. We assume $r_{1,p}(t)$, $r_{2,p}(t)$ to be two identical independent random numbers following Uniform distribution between [0, 1] to represent this perceptual information transition error, and we control the proportion of different information sources, where c_1 and c_2 are social learning factors of local and global social learning.

$$P_{fi} = P_{fi-local} + P_{fi-global} \tag{2.9}$$

where

$$P_{fi-local} = c_1 r_{1,p}(t)(p_l(t) - IFF(t)) \tag{2.10}$$

$$P_{fi-global} = c_2 r_{2,p}(t)\big(p_g(t) - IFF(t)\big) \tag{2.11}$$

2.2.6.2 Perceptual Fear Factor from Mood P_{fm}

Self-mood has been shown to influence fear factor [93]. For example, even though no one around an individual chooses to switch, other events such as weather, work issues could influence the mood of an individual to choose to switch. We use $m_p(t)$ which denotes a random number representing an individual's self-mood; c_3 is a self-learning factor from self-mood; and $r_{3,p}(t)$ is assumed to be an independent random variable following Uniform distribution between [0, 1].

$$P_{fm} = c_3 r_{3,p}(t) m_p(t) \tag{2.12}$$

2.2.6.3 Rational Fear Factor from Information R_{fi}

Since high percentages of infected individuals and switch individuals intensifies fear within one's contact networks, the rational fear factor is based on how many infected individuals are present in a social contact network and how many individuals choose to switch in local and global contact networks. In Eqns. (2.13)-(2.15), R_{fi} contains $R_{fi-local}$ and $R_{fi-global}$, which represent R_{fi} from the local contact network, and the global contact network, respectively. $S_{l-switch}(t)$ and $S_{g-switch}(t)$ represent the numbers of switch individuals in local and global contact networks, respectively, at time t; $r_{4,p}(t)$, $r_{5,p}(t)$ are independent random numbers following Uniform distribution between [0, 1] that represent errors between real facts and rational information obtained by an individual, respectively; c_4 and c_5 are rational factors related to the number of infected individuals in a local contact network; and $n_{11}, n_{12}, n_{21}, n_{22}$ are weights to balance the proportion of various factors.

$$R_{fi} = c_4 r_{4,p}(t)\ R_{fi-local} + c_5 r_{5,p}(t)\ R_{fi-global} \tag{2.13}$$

where:

$$R_{fi-local} = n_{11} I_{local}(t) + n_{12} S_{l-switch}(t) \tag{2.14}$$

$$R_{fi-global} = n_{21} I_{global}(t) + n_{22} S_{g-switch}(t) \tag{2.15}$$

2.2.6.4 Probability of Switching

Section 2.2.2 described switch behavior based on IFF with a random relation that follows logistic distribution [86]. Therefore, we use function $f(IFF(t))$ to represent the probability that an individual chooses to switch under IFF. Responses are classified based on their IFF to two cases: switch and not switch. θ is the coefficient to amplify IFF since IFF is only a number at [-1,1], we assume $\theta = 100$ to make sure that exp $(IFF(t)\theta)$ approaches to zero in our IFF model simulation.

Probabilities for a normal individual to switch behaviors (e.g., taking protective measures) can be defined as follows:

$$P(do\ switch) = f(IFF(t)) = \frac{exp\ (IFF(t)\theta)}{1+exp\ (IFF(t)\theta)} \tag{2.16}$$

$$P(do\ not\ switch) = 1 - f(IFF(t)) = \frac{1}{1+exp\ (IFF(t)\theta)} \tag{2.17}$$

In Eqns. (2.16)-(2.17), if $IFF(t) \to 1$, then $P(do\ switch) \to 1$; otherwise if $IFF(t) \to -1$, then $P(do\ not\ switch) \to 1$. Each individual is evaluated a decision variable $S^p(t)$ used to record switch behaviors of individual p. $S^p(t)$ is calculated based on binomial distribution of $P(do\ switch) = f(IFF(t))$. If $S^p(t) = 1$, then an individual is expected to choose switch behavior to protect himself; if $S^p(t) = 0$, then the individual is expected to choose the behavior like normal. The total switch individuals of susceptible individuals at time t is

$$S_{switch}(t) = \sum_{p=1}^{S} S^p(t) \tag{2.18}$$

Each susceptible individual occupies $\frac{1}{S(t)}$ of susceptible individuals, their switch probability is $f(IFF(t)^p)$, and the switch probability for the average IFF of all individuals is $f\left(\overline{IFF(t)}\right)$. Since the variable $\overline{IFF(t)}$ must describe IFF in an entire population as described in Section 2.2.7, we assume the total switch population to be equal to the average fear variable multiple susceptible population:

$$S_{switch}(t) = S(t)\sum_{p=1}^{S}\frac{f(IFF(t)^p)}{S(t)} \approx S(t)f\left(\overline{IFF(t)}\right) \tag{2.19}$$

Therefore,

$$\frac{dS_{switch}(t)}{dt} = \frac{d\left[S(t)f\left(\overline{IFF(t)}\right)\right]}{dt} = f\left(\overline{IFF(t)}\right)\frac{dS(t)}{dt} + S(t)\frac{df\left(\overline{IFF(t)}\right)}{dt}$$

$$= f\left(\overline{IFF(t)}\right)\frac{dS(t)}{dt} + \frac{S(t)d\left(\frac{\exp\left(\overline{IFF(t)}\theta\right)}{1+\exp\left(\overline{IFF(t)}\theta\right)}\right)}{dt}$$

$$= f\left(\overline{IFF(t)}\right)\frac{dS(t)}{dt} + \frac{S(t)\left(\theta\exp\left(\overline{IFF(t)}\theta\right)\right)}{\left(1+\exp\left(\overline{IFF(t)}\theta\right)\right)^2}\frac{d\overline{IFF(t)}}{dt} \quad (2.20)$$

2.2.7 The IFF-SIR Model

A classic SIR model is typically used to analysis long-term epidemics. Zhao *et al.* [83] and Shakeri *et al.* [94] compiled switch behaviors into an SIR model. Sections 2.2.2 and 2.2.6 described how IFF can affect switch behaviors, but this section extends IFF to the SIR model.

$$\frac{dS(t)}{dt} = \mu N(t) - [\beta_a S_{switch}(t) + \beta_b(S(t) - S_{switch}(t))] - \mu S(t) \quad (2.21)$$

$$\frac{dI(t)}{dt} = [\beta_a S_{switch}(t) + \beta_b(S(t) - S_{switch}(t))] - \mu I(t) - \gamma I(t) \quad (2.22)$$

$$\frac{dR(t)}{dt} = \gamma I(t) - \mu R(t) \quad (2.23)$$

$$\frac{dS_{switch}(t)}{dt} = f\left(\overline{IFF(t)}\right)\frac{dS(t)}{dt} + \frac{S(t)\left(\theta\exp\left(\overline{IFF(t)}\theta\right)\right)}{\left(1+\exp\left(\overline{IFF(t)}\theta\right)\right)^2}\frac{d\overline{IFF(t)}}{dt} \quad (2.24)$$

$$\frac{d\overline{IFF(t)}}{dt} = \frac{dF(S(t),I(t),R(t),S_{switch}(t))}{dt} \quad (2.25)$$

In Eqns. (2.21)-(2.25), $S(t)$ denotes the number of susceptible individuals at time *t*; $I(t)$ is the number of infected individuals at time *t*; $R(t)$ denotes the number of recovered individuals at time *t*; $S_{switch}(t)$ is the number of susceptible individuals who adopt switch behaviors at time *t*; $N(t)$ is the total number of individuals at time *t*, of which $N(t) = S(t) + I(t) + R(t)$; β_a and β_b are infection rates of susceptible individuals who choose switch or normal behavior, respectively; γ is the recovery rate; and μ is the death rate. (The birth rate is assumed to be equal to the death rate.)

We consider IFF to be the primary factor for an individual who decides to switch or not, but we are unable to add all IFF of each individual as variables into our dynamic system for simplify the calculation efforts when deal with the total population is large. Since we already

defined $\overline{IFF(t)}$ as the average of all IFF in switch individuals at time *t*, we can calculate $\overline{IFF(t)}$ for any time $t = 0, 1, 2, 3, \dots,$ n. However, because we do not know the mathematical relationship between $\overline{IFF(t)}$ and $S(t), I(t), R(t), S_{switch}(t)$, we will use simulation to establish these relationships in Section 2.3.1 and conduct linear regression to obtain the mathematic relationship function.

2.3 Simulation and Regression Analysis

2.3.1 Numerical Simulation

This section details a MATLAB simulation of epidemic transmission and the corresponding fear factor. The simulation runs span 50 days, each time epoch is 1 day [66]. We also assume that the total number of individuals in global contact network is $N = 200$: 185 susceptible individuals, 15 infected individuals, 0 recovered, and 0 switched susceptible individuals. To simplify the simulation, we assume the status changing probability from infected to recovered is 14% at each day. The values of other parameters are given in Table 2.1.

Table 2.1 Table of parameter values for numerical simulation

Parameters	Description	Estimated values	Source
w	inertia weight	0.729	[95]
c_1	social learning factor toward to p_p^t	1.494	[95]
c_2	social learning factor toward to p_g^t	1.494	[95]
c_3	perceptual factor due to self-mood	0.001	Assume
c_4	rational factor of local contact network	0.02	Assume
c_5	rational factor of global contact network	0.005	Assume
θ	coefficient number	1000	Assume
μ	death rate (equal to birth rate)	0.019896	[96]
β_a	infection rate of switch individuals	0.006	Assume
β_b	infection rate of normal individuals	0.02	Assume
γ	recovery rate	0.14	Assume

Figure 2.6 illustrates the change in the number of individuals in each state. The red solid line represents recovered individuals, the green dash-dot line represents infected individuals, the blue dashed line represents susceptible individuals, and the black dotted line represents switched susceptible individuals. As shown in the figure, the disease was active almost 20 days, with the highest number of infections occurring around day 7. Susceptible, infected, and recovered individuals stay the same after day 20, with only rare occurrences of individuals choosing switch behavior after 20 days.

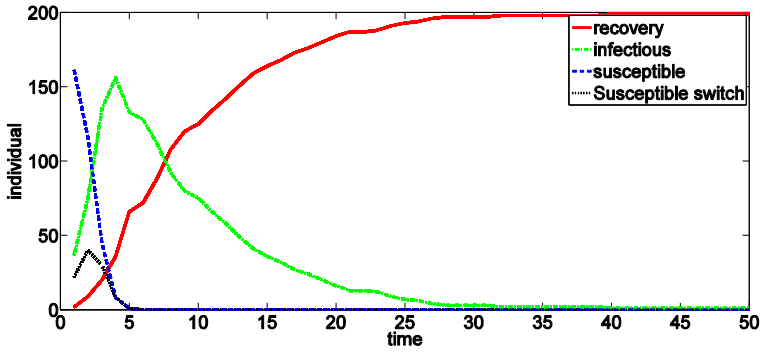

Figure 2.6 Populations in each state during the epidemic

Figure 2.7 shows the average IFF for all susceptible individuals over the first 50 days in a disease. In SIR model, all individuals just can be infected one time, after recovery they will never be infected, thus considering the IFF of recovered individuals and infected individuals is meaningless for our model. Therefore, we just consider switch individuals from susceptible individuals. In addition, since the delay of time, switch behaviors this time will have influence on IFF in next time rather than immediately influence their IFF this time, which is demonstrated by the trend of infected and switch individuals shown in Figure 2.6. This phenomenon explains how the past information persistently effects the current emotion when people face to a disease. After the increasing number of infectious and switch individuals on day 3 and day 4, the average IFF

suddenly increased on day 5. After day 15, as infected and switch individuals tend to stable, the IFF also tend to stable.

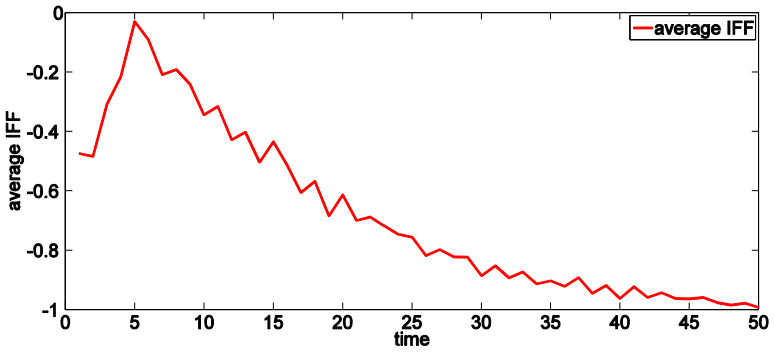

Figure 2.7 Average IFF of susceptible individuals during the epidemic

2.3.2 Regression Analysis

In order to establish a precise relationship between $\overline{IFF(t)}$ and population sizes in each state, we make multiple-variate linear regressions of $\overline{IFF(t)}$ and susceptible individuals using the statistical analysis tool Minitab. For model simplicity, we only considered nonlinear cross-term in regression but did not use the nonlinear regression.

We use $\overline{IFF(t)}$ as the dependent (response) variable y and $S(t), I(t), R(t), S_{switch}(t)$ as independent variables. The data of regression was based on the average variable numbers (by 10 replications) with initial $N = 200; S = 185;\ I = 15; R = 0;\ S_{switch} = 0$. Then we find the regression relationship using the optimized response regression toolbox in Minitab. We reject the last section $r_5 I(t)$ due to the high *P*-value and low *F*-value and *T*-value, as shown in Table 2.2. The correlation coefficients between $I(t)$ with $S(t)I(t)$ and $S_{switch}(t)I(t)$ are 0.924 and 0.925, respectively, proving that $I(t)$ is not significant in this model. Although $I(t)$ becomes significant when we try to make linear regression without cross-terms, the *R*-square of the new regression model decreases significantly.

$$\overline{IFF(t)} = r_0 + r_1 S(t) + r_2 S_{switch}(t) + r_3 S(t) I(t) - r_4 S_{switch}(t) I(t) + r_5 I(t) \quad (2.26)$$

where $r_0 = -0.5902, r_1 = -0.01172, r_2 = 0.09768, r_3 = 0.000363, r_4 = 0.002846,$ and $r_5 = -0.00008$.

Table 2.2 Variance of Average IFF Regression Analysis

Source	Degree of Freedom	Coef	*F*-value	*T*-value	*P*-value
I	1	−0.00008	0.00	−0.02	0.983
S	1	−0.01172	28.91	−5.39	0.000
S_{switch}	1	0.09768	139.11	11.79	0.000
I*S	1	0.000363	9.36	3.06	0.004
I* S_{switch}	1	−0.002846	46.75	−6.84	0.000
Lack-of-Fit	4		0.84		0.508

The *P*-value result to be less than 0.001 [97], proving that the regression model is statistically significant. Because we used the optimized response regression, all five sections (including constant term r_0) in our regression model are significant. Figure 2.8 also shows the *R*-square number of the model to be 92.59%, meaning that 92.59% of the variation in $\overline{IFF(t)}$ can be explained by the regression model. The optimized response indicates a potentially higher *R*-square with the use of more sections, but the effect is not sufficiently significant. In addition, the absolute value of a majority of residuals is less than 0.02, meaning that most $\overline{IFF(t)}$ can be accurately represented by the regression model in Eq. (2.26). The highest absolute value of residual is approximately 0.05, proving general reliability of the regression model.

2.4 Stability Analysis

2.4.1 Stability Analysis of the IFF Model

In order to conduct stability analysis of the IFF model and determine necessary conditions we first need to define the stable status. Two kinds of stability are typical: absolute stability and

asymptotic stability. Because several random numbers in our system represent self-mood and the random weight of various information, determining a clear definition of the convergence domain of asymptotically stable status is difficult. Therefore, in this section we discuss only absolute stability.

Definition 2.1 [98]: For a continuous nonlinear system, $\dot{x} = f\big(x(t)\big), x(0) = x_0$, where $x(t) \in S \subseteq \mathbb{R}^n$ are system-state variables, S is an open set on $\mathbb{R}^n$, and f is a continuous function on S. The system is Lyapunov stable in equilibrium state x_e if for every $\epsilon > 0$ there is $\delta > 0$ such that

$$\|x(0) - x_e\| < \delta \tag{2.27}$$

Then for every $t \geq 0$,

$$\|x(t) - x_e\| < \epsilon \tag{2.28}$$

Theorem 2.1: If the IFF model is stable, then $IFF(t) = -1$ and $R_{fi} = 0$.

Proof: To prove contradiction, first we assume that $IFF(t)$ is not constant, and assume there are two different IFF values presenting in the system with a total of N individuals. Then n individuals have $IFF(t) = IFF(1)$ and $N - n$ individuals $IFF(t) = IFF(2)$.

Let $IFF(1) > IFF(2)$. Then based on the meaning of P_{fi}, $IFF(1)$ will move toward $IFF(2)$, while some individuals with fear factors of $IFF(1)$ will switch because $IFF(1) > IFF(2) \geq -1$, and then $S_{switch} > 0$ and $R_{fi} > 0$. In this situation, $N - n$ individuals will increase, meaning the IFF model is unstable. If $IFF(1) < IFF(2)$, then the situation is equal to $IFF(1) > IFF(2)$, resulting in a contradiction unless $IFF(1) = IFF(2)$, which means that $IFF(t)$ does not change over time when the IFF model is stable. Therefore, $IFF(t) = C$ (C is a constant) and $R_{fi} = 0$ are requirements of system stability for all individuals in the system, and stable status should occur in a disease-free situation ($S_{switch} = 0, I = 0$).

We already proved that individuals must have identical IFF in order for the IFF model to be stable, but in order to prove contradiction of $IFF(t) = -1$, now we assume that the IFF is a constant larger than -1. Since switch behaviors of individuals are based on IFF, we assume that individual would choose to switch randomly.

If individual chooses to switch as event A, the probability of event A is $P(A) = \varepsilon > 0$ (since $\varepsilon = 0$ only happened in $IFF(t) = -1$ as mentioned in Section 2.2.6), where ε is a positive number. Therefore, the probability for individual not choosing to switch is $1 - \varepsilon$. No matter how small ε is, when the time period is long enough, the probability for individual never choosing to switch is

$$(1 - \varepsilon)^t \underset{t \to \infty}{\longrightarrow} 0 \tag{2.29}$$

So this individual would choose to switch at least one time in the timeline, then $S_{switch} \neq 0$, which leads to a contradiction unless the IFF of all individuals are -1, resulting in $IFF(t) = C = -1$.

Theorem 2.2: If the IFF model is stable, then $w > \frac{1}{2}(c_1 + c_2) - 1$.

Proof: If the IFF model is stable, then $IFF(t)$ will be convergent, assuming

$$\lim_{t \to +\infty} IFF(t) = p \tag{2.30}$$

where p is an arbitrary range of the value of $IFF(t)$.

Each individual in the SIR model can be infected only once. Since susceptible individuals were never infected, we consider the fear factor of susceptible individuals to be $R_{fr} = 0$. Therefore, according to Theorems 2.1 and 2.2, when the IFF model is stable, then

$$\frac{dIFF(t+1)}{dt} = w\frac{dIFF(t)}{dt} + c_1 r_{1,p}(t)(p_l(t) - IFF(t)) + c_1 r_{2,p}(t)\big(p_g(t) - IFF(t)\big) \tag{2.31}$$

$$IFF(t+1) = IFF(t) + \frac{dIFF(t+1)}{dt} \tag{2.32}$$

Let $\emptyset_1 = c_1 r_{1,p}(t)$ and $\emptyset_2 = c_2 r_{2,p}(t)$ [41], where $\emptyset_1$, $\emptyset_2$, and w are constant. If $\frac{dIFF(t)}{dt} = IFF(t) - IFF(t-1)$ and Eq. (2.32) is replaced by Eq. (2.31), then

$$IFF(t+1) = (1 + w - \emptyset_1 - \emptyset_2)IFF(t) - wIFF(t-1) + \emptyset_1 p_l(t) + \emptyset_2 p_g(t) \quad (2.33)$$

This non-homogeneous recurrence relation can be written as a matrix-vector equation:

$$\begin{bmatrix} IFF(t+1) \\ IFF(t) \\ 1 \end{bmatrix} = \begin{bmatrix} 1 + w - \emptyset_1 - \emptyset_2 & -w & \emptyset_1 p_l(t) + \emptyset_2 p_g(t) \\ 1 & 0 & 0 \\ 0 & 0 & 1 \end{bmatrix} \begin{bmatrix} IFF(t) \\ IFF(t-1) \\ 1 \end{bmatrix} \quad (2.34)$$

The characteristic polynomial of this matrix is

$$\left| \begin{bmatrix} IFF(t+1) \\ IFF(t) \\ 1 \end{bmatrix} - \boldsymbol{\lambda} E \right| = (1-\lambda)(w + \lambda^2 - \lambda(1 + w - \emptyset_1 - \emptyset_2)) \quad (2.35)$$

which has three roots:

$$\lambda_1 = 1 \quad (2.36)$$

$$\lambda_2 = \frac{1+w-\emptyset_1-\emptyset_2+\vartheta}{2} \quad (2.37)$$

$$\lambda_3 = \frac{1+w-\emptyset_1-\emptyset_2-\vartheta}{2} \quad (2.38)$$

where

$$\vartheta = \sqrt{(1 + w - \emptyset_1 - \emptyset_2)^2 - 4w} \quad (2.39)$$

According to the recurrence relation, the explicit form of Eq. (2.35) is

$$IFF(t) = k_1 {\lambda_1}^t + k_2 {\lambda_2}^t + k_3 {\lambda_3}^t = k_1 + k_2 {\lambda_2}^t + k_3 {\lambda_3}^t \quad (2.40)$$

where k_1, k_2, k_3 are constant.

Eq. (2.34) also produces

$$IFF(2) = (1 + w - \emptyset_1 - \emptyset_2)IFF(1) - wIFF(0) + \emptyset_1 p_l(t) + \emptyset_2 p_g(t) \quad (2.41)$$

and Eq. (2.40) yields

$$\begin{bmatrix} IFF(0) \\ IFF(1) \\ IFF(2) \end{bmatrix} = \begin{bmatrix} 1 & 1 & 1 \\ 1 & \lambda_2 & \lambda_3 \\ 1 & {\lambda_2}^2 & {\lambda_3}^2 \end{bmatrix} \begin{bmatrix} k_1 \\ k_2 \\ k_3 \end{bmatrix} \tag{2.42}$$

From Eq. (2.42) we can calculate that

$$k_1 = \frac{\lambda_2\lambda_3 IFF(0) - IFF(1)(\lambda_2+\lambda_3) + IFF(2)}{(\lambda_2-1)(\lambda_3-1)} \tag{2.43}$$

$$k_2 = \frac{\lambda_3\big(IFF(0) - IFF(1)\big) - IFF(1) + IFF(2)}{(\lambda_2-1)(\lambda_2-\lambda_3)} \tag{2.44}$$

$$k_3 = \frac{\lambda_2(IFF(1) - IFF(0)) + IFF(1) - IFF(2)}{(\lambda_3-1)(\lambda_2-\lambda_3)} \tag{2.45}$$

Using the property $\lambda_2 - \lambda_3 = \vartheta$, these values can be simplified as

$$k_1 = \frac{\emptyset_1 p_l(t) + \emptyset_2 p_g(t)}{\emptyset_1 + \emptyset_2} \tag{2.46}$$

$$k_2 = \frac{\boldsymbol{\lambda_3}\big(IFF(0) - IFF(1)\big) - IFF(1) + IFF(2)}{(\boldsymbol{\lambda_2}-1)(\boldsymbol{\lambda_2}-\boldsymbol{\lambda_3})} \tag{2.47}$$

$$k_3 = \frac{\boldsymbol{\lambda_2}(IFF(1) - IFF(0)) + IFF(1) - IFF(2)}{(\boldsymbol{\lambda_3}-1)(\boldsymbol{\lambda_2}-\boldsymbol{\lambda_3})} \tag{2.48}$$

In order to identify the condition at which the IFF model is stable, we consider the relationship of w and c_1, c_2 since $\emptyset_1$ and $\emptyset_2$ are specific expressions of $c_1 r_{1,p}(t)$, $c_2 r_{2,p}(t)$ respectively. We can then determine the upper bound associated with these values using the largest value of $\emptyset_1$ and $\emptyset_2$, and the values of $c_1$and c_2 can be considered upper bounds for $\emptyset_1$ and $\emptyset_2$. Therefore, we can consider the worst-case in terms of convergence.

Convergence of $\lim_{t\to+\infty} IFF(t)$ is determined by the values of $\emptyset_1$ and $\emptyset_2$. Eq. (2.32) shows that ϑ will be a complex number with a non-zero component when

$$(1 + w - \emptyset_1 - \emptyset_2)^2 < 4w \tag{2.49}$$

or

$$(\emptyset_1 + \emptyset_2 - w - 1 - 2\sqrt{w})(\emptyset_1 + \emptyset_2 - w - 1 + 2\sqrt{w}) < 0 \tag{2.50}$$

Since ϑ is complex, λ_2 and λ_3 will be complex numbers with non-zero components.

Using the L_2 norm to measure λ_2 and λ_3, any complex number x, x^t can be

$$x^t = (\|x\|e^{-i\theta})^t = \|x\|^t e^{-i\theta t} = \|x\|^t\big(\cos(\theta t) + isin(\theta t)\big) \quad (\theta = \arg(x)) \tag{2.51}$$

$$\lim_{t\to+\infty} x^t = \lim_{t\to+\infty} \|x\|^t(\cos(\theta t) + isin(\theta t)) = 0 \; if \; and \; only \; if \; \|x\| < 1 \tag{2.52}$$

Considering the value of $\lim_{t\to+\infty} IFF(t)$, thus

$$\lim_{t\to+\infty} IFF(t) = \lim_{t\to+\infty} k_1 + k_2{\lambda_2}^t + k_3{\lambda_3}^t \tag{2.53}$$

When $\|\lambda_2\| < 1$ and $\|\lambda_3\| < 1$, then $\lim_{t\to+\infty} {\lambda_2}^t = 0$ and $\lim_{t\to+\infty} {\lambda_3}^t = 0$.

Assuming uniform distributions, $\emptyset_1 \sim U(0,1)$ and $\emptyset_2 \sim U(0,1)$, then

$$E[\emptyset_1] = c_1 \int_0^1 \emptyset_1 \, d\emptyset_1 = \frac{c_1}{2} \tag{2.54}$$

$$E[\emptyset_2] = c_2 \int_0^1 \emptyset_2 \, d\emptyset_2 = \frac{c_2}{2} \tag{2.55}$$

Thus,

$$\lim_{t\to+\infty} IFF(t) = k_1 = \frac{\emptyset_1 p_l(t) + \emptyset_2 p_g(t)}{\emptyset_1 + \emptyset_2} = \frac{\frac{c_1}{2}p_l(t) + \frac{c_2}{2}p_g(t)}{\frac{c_1}{2} + \frac{c_2}{2}} = \frac{c_1 p_l(t) + c_2 p_g(t)}{c_1 + c_2}$$

$$= (1-a)p_l(t) + ap_g(t) \quad \left(a = \frac{c_2}{c_1 + c_2}\right) \tag{2.56}$$

proving that $IFF(t)$ converges to a value from the lines $p_l(t)$ and $p_g(t)$.

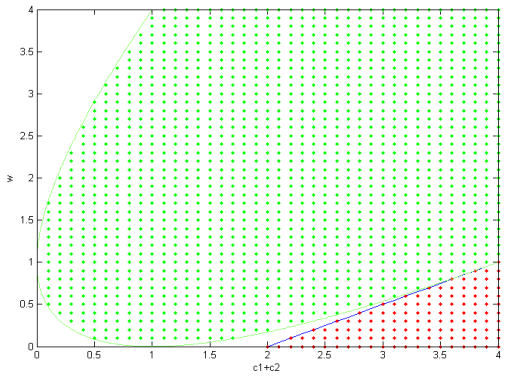

Figure 2.8 Convergence area (green area) and non-convergence area (red area) of IFF(t)

As shown in Figure 2.8, $\emptyset_1 + \emptyset_2$ represents the horizontal axis (associated with $c_1 + c_2$), w represents the vertical axis, the green area represents the region for $(1 + w - \emptyset_1 - \emptyset_2)^2 < 4w$, and the red area represents the nonconvergent region of $IFF(t)$, resulting in $\max(\|\boldsymbol{\lambda}_2\|, \|\boldsymbol{\lambda}_3\|) > 1$ [99]. In addition, $w < \frac{1}{2}(\emptyset_1 + \emptyset_2) - 1$ (blue line is $w = \frac{1}{2}(\emptyset_1 + \emptyset_2) - 1$) in the red area. As stated, we consider the upper limits of $\emptyset_1$ and $\emptyset_2$ to satisfy $\emptyset_1 \in [0, c_1]$ and $\emptyset_2 \in [0, c_2]$ in order to determine the condition. The area to the left of the blue line ensures convergence; therefore, if we want to ensure convergence, all values of w must be larger than the values of the blue line. If the IFF model is stable, $IFF(t)$ will converge and satisfy

$$w > \frac{1}{2}(\emptyset_1 + \emptyset_2) - 1 \tag{2.57}$$

Satisfaction of these four theorems ensures that the IFF model is stable.

2.4.2 Stability Analysis of the IFF-SIR Model

In order to conduct stability analysis of the IFF-SIR model, we initially combine the regression result from Section 2.2.7 into the IFF-SIR model:

$$\overline{IFF(t)} = r_0 + r_1 S(t) + r_2 S_{switch}(t) + r_3 S(t) I(t) - r_4 S_{switch}(t) I(t) \tag{2.58}$$

Then

$$\frac{d\overline{IFF(t)}}{dt} = r_1 \frac{dS(t)}{dt} + r_2 \frac{dS_{switch}(t)}{dt} + r_3 I(t) \frac{dS(t)}{dt} + r_3 S(t) \frac{dI(t)}{dt} - r_4 I(t) \frac{dS_{switch}(t)}{dt} - r_4 S_{switch}(t) \frac{dI(t)}{dt} \tag{2.59}$$

Therefore, the model can be written as the linear system (2.60)-(2.64) and stability points of this system can be determined using

$$\frac{dS(t)}{dt} = \mu N(t) - [\beta_a S_{switch}(t) + \beta_b (S(t) - S_{switch}(t))] - \mu S(t) \tag{2.60}$$

$$\frac{dI(t)}{dt} = [\beta_a S_{switch}(t) + \beta_b (S(t) - S_{switch}(t))] - \mu I(t) - \gamma I(t) \tag{2.61}$$

$$\frac{dR(t)}{dt} = \gamma I(t) - \mu R(t) \tag{2.62}$$

$$\frac{dS_{switch}(t)}{dt} = f\left(\overline{IFF(t)}\right)\frac{dS(t)}{dt} + \frac{S(t)\left(\exp\left(\overline{IFF(t)}\right)\right)}{\left(1+\exp\left(\overline{IFF(t)}\right)\right)^2}\frac{d\overline{IFF(t)}}{dt} \tag{2.63}$$

$$\frac{d\overline{IFF(t)}}{dt} = r_1\frac{dS(t)}{dt} + r_2\frac{dS_{switch}(t)}{dt} + r_3 I(t)\frac{dS(t)}{dt} + r_3 S(t)\frac{dI(t)}{dt}$$
$$-r_4 I(t)\frac{dS_{switch}(t)}{dt} - r_4 S_{switch}(t)\frac{dI(t)}{dt} \tag{2.64}$$

Theorem 2.3: The continuous-time system (2.60)-(2.64) is Lyapunov stable if the following system in Eq. (2.65) has a real solution:

$$\begin{gathered} N(t) - \left[\beta_a S_{switch}(t) + \beta_b\left(S(t) - S_{switch}(t)\right)\right] - \mu S(t) = 0 \\ \left[\beta_a S_{switch}(t) + \beta_b(S(t) - S_{switch}(t))\right] - \mu I(t) - \gamma I(t) = 0 \\ \gamma I(t) - \mu R(t) = 0 \end{gathered} \tag{2.65}$$

Proof: Based on Definition 2.1, t^* can satisfy following condition:

$$\left[\frac{dS(t^*)}{dt^*}, \frac{dI(t^*)}{dt^*}, \frac{dR(t^*)}{dt^*}, \frac{dS_{switch}(t^*)}{dt^*}, \frac{d\overline{IFF(t^*)}}{dt^*}\right] = 0 \tag{2.66}$$

Therefore, every $t \geq 0$ will produce

$$x(t) = x(t^*) = \left[S(t^*), I(t^*), R(t^*), S_{switch}(t^*), \overline{IFF(t^*)}\right] \tag{2.67}$$

and every $\epsilon > 0$ and $t \geq t^*$ will yield to the limitation $\|x(t) - x(t^*)\| < \epsilon$.

If we find a set $x(t^*)$ resulting in $\frac{d\overline{IFF(t^*)}}{dt} = 0$ and if t^* satisfies $\frac{d\overline{IFF(t^*)}}{dt^*} = 0$, then we can find a t^* that satisfies

$$\frac{dS_{switch}(t^*)}{dt^*} = f\left(\overline{IFF(t^*)}\right)\frac{dS(t^*)}{dt^*} + \frac{S(t^*)\left(\exp\left(\overline{IFF(t^*)}\right)\right)}{\left(1+\exp\left(\overline{IFF(t^*)}\right)\right)^2}\frac{d\overline{IFF(t^*)}}{dt^*}$$
$$= f\left(\overline{IFF(t^*)}\right)\frac{dS(t^*)}{dt^*} \tag{2.68}$$

Also, because $\frac{dS(t^*)}{dt^*} = 0$, the value of $f\left(\overline{IFF(t^*)}\right)$ will produce

$$\frac{dS_{switch}(t^*)}{dt^*} = f\left(\overline{IFF(t^*)}\right)\frac{dS(t^*)}{dt^*} = 0 \tag{2.69}$$

meaning that $\frac{dS_{switch}(t^*)}{dt^*}$ can be designated using $\frac{dS(t^*)}{dt^*}$ and $\frac{d\overline{IFF(t^*)}}{dt^*}$.

Therefore, the system becomes

$$\mu N(t^*) - \left[\beta_a S_{switch}(t^*) + \beta_b\left(S(t^*) - S_{switch}(t^*)\right)\right] - \mu S(t^*) = 0 \tag{2.70}$$

$$[\beta_a S_{switch}(t^*) + \beta_b(S(t^*) - S_{switch}(t^*))] - \mu I(t^*) - \gamma I(t^*) = 0 \tag{2.71}$$

$$\gamma I(t^*) - \mu R(t^*) = 0 \tag{2.72}$$

$$r_1 \frac{dS(t^*)}{dt^*} + r_2 \frac{dS_{switch}(t^*)}{dt^*} + r_3 I(t^*) \frac{dS(t^*)}{dt^*} + r_3 S(t^*) \frac{dI(t^*)}{dt^*}$$

$$-r_4 I(t^*) \frac{dS_{switch}(t^*)}{dt^*} - r_4 S_{switch}(t^*) \frac{dI(t^*)}{dt^*} = 0 \tag{2.73}$$

Moreover, $\frac{d\overline{IFF(t^*)}}{dt^*}$ can be indicated by $\frac{dS(t^*)}{dt^*}$, $\frac{dI(t^*)}{dt^*}$, $\frac{dS_{switch}(t^*)}{dt^*}$. Thus, the system (2.60)-(2.64) can rewrite as the system C below

$$C\begin{cases} \frac{dS(t)}{dt} = \mu N(t) - \left[\beta_a S_{switch}(t) + \beta_b\left(S(t) - S_{switch}(t)\right)\right] - \mu S(t) = 0 \\ \frac{dI(t)}{dt} = [\beta_a S_{switch}(t) + \beta_b(S(t) - S_{switch}(t))] - \mu I(t) - \gamma I(t) = 0 \\ \frac{dR(t)}{dt} = \gamma I(t) - \mu R(t) = 0 \end{cases} \tag{2.74}$$

From system C, the equation set can be written as

$$\begin{bmatrix} -\beta_b & \mu & \mu & -\beta_a + \beta_b \\ \beta_b & -\mu - \gamma & 0 & \beta_a - \beta_b \\ 0 & \gamma & -\mu & 0 \\ 0 & 0 & 0 & 0 \end{bmatrix} \begin{bmatrix} S(t) \\ I(t) \\ R(t) \\ S_{switch}(t) \end{bmatrix} = c \begin{bmatrix} S(t) \\ I(t) \\ R(t) \\ S_{switch}(t) \end{bmatrix} = 0 \tag{2.75}$$

Since

$$det|c| = 0 \tag{2.76}$$

system c has infinite solutions, meaning that system (2.60)-(2.64) will be stable if the SIR model is stable, also the system has infinite stability points.

In order to verify accuracy of our result, we use the regression results to check the model. We assume the total number of individuals in the global contact network is $N = 1050$, 1000

susceptible individuals, 50 infected individuals, 0 recovered, and 50 switch individuals. We observe the trend of populations in each state and the estimated $\overline{IFF(t)}$ based on the regression model in Eq. (2.26) over 100 days, as shown in Figure 2.9.

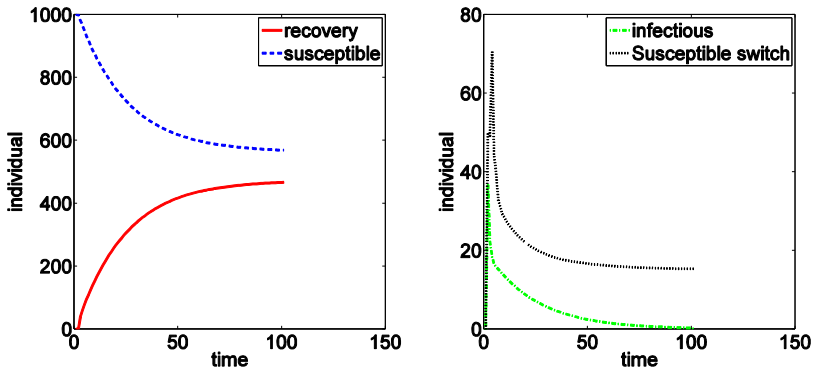

Figure 2.9 Populations in each state during the epidemic by IFF-SIR model

According to Figure 2.9, the simulation results show that the epidemic situation become stable after approximately 70 days, the number of susceptible, infectious, recovered and switch don't change significantly anymore after 70 days. According to the theorem 2.3 we prove above and the regression result in Eq. (2.58), we can know that when SIR is stable, the IFF model should be stable. Figure 2.10 shows the trend of $\overline{IFF(t)}$, it illustrates that that $\overline{IFF(t)}$ is stable when the SIR model is stable.

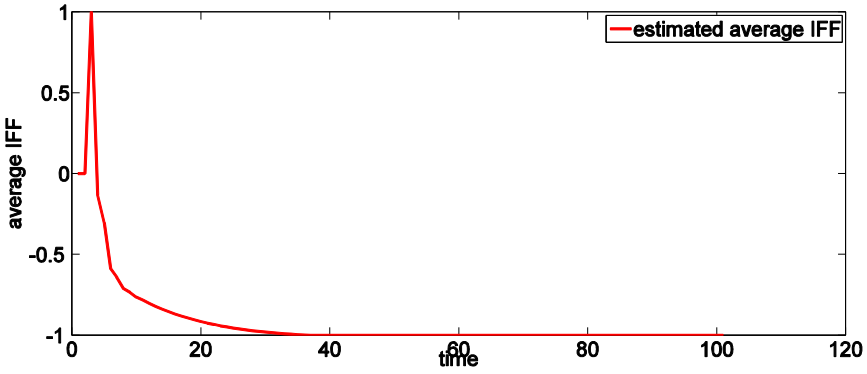

Figure 2.10 Estimated result of average IFF(t) by IFF-SIR model

In previous regression we had restricted the range of $\overline{IFF(t)}$ to [–1, 1] and used only 200 individuals for simulation. We verify our present model using 1050 individuals, so the trend of $\overline{IFF(t)}$ would exceed the range of [-1, 1] in the real world. However, our conclusion is proven accurate: an increasing $\overline{IFF(t)}$ leads to an increasing number of individuals who will switch. Sudden increase in $\overline{IFF(t)}$ around day 2 in Figure 2.9 and day 3 in Figure 2.10 show a breakout of infected and switch individuals, thereby increasing individuals' fear of the disease and resulting in a sudden increase of $\overline{IFF(t)}$.

2.5 Optimal Control

2.5.1 Definition for Control of Switch Degree

We define the switch degree as ranging from 0 to 100. Therefore, if individuals chose to switch but do not undertake any measures of switching, we assume their degrees of switching, or switch behavior, to be zero.

In order to simulate the relationship between infection rates and switching behavior, we make the following three assumptions:

- The corporate social performance of each individual can be controlled.
- Infection rate is proportional to the number of contacts, and the number of contact is proportional to the corporate social performance.
- Switching behavior is determined by the corporate social performance degrees.

We add a control variable u, to represent the decreasing degrees of corporate social performance of an individual; therefore, $(1-u)$ represents the corporate social performance. According to above assumptions, u represents the degrees of switching. If an individual decreases degrees of corporate social performance, thereby decreasing the number of contacts, that individual decreases his or her chances of being infected with the disease. More reductions of

corporate social performance degrees result in decreased degrees of corporate social performance and increased degrees of switching.

If $u = 0$, then individuals do not have any degree of switching, but they choose to switch. Since their corporate social performance has not decreased, the number of contacts is the same as the individuals who did not switch. Consequently, the infection rate does not change and stays equal to normal behavior, or β_b.

According to the second assumption,

$$\frac{\beta_a}{\beta_b} = \frac{1-u}{1}, u \in [0,1] \tag{2.77}$$

Although all individual p should have a best control u_p, the IFF set in our model may be too large and impractical to control the corporate social performance for all individual, requiring control of the average of all corporate social performances as u instead. For example, if the best controls of three individuals are assumed to be 0.3, 0.5, and 0.7, respectively, those values can be controlled by average $u = \frac{0.3+0.5+0.7}{3} = 0.5$.

Finally,

$$\beta_a = \beta_b(1-u), u \in [0,1] \tag{2.78}$$

2.5.2 Optimal Control Problem

The first part of the cost function $F(I)$ is the number of infected individuals, and the second part of the cost function $F(S_{switch})$ is associated with financial loss of switch behaviors. Switch behaviors in our model indicate that an individual chooses to decrease his or her corporate social performance. Therefore, the cost function is

$$J(u) = \int [F(I(t)) + F(S_{switch}(t))]\, dt \tag{2.79}$$

Loss function $F(I)$ relates to all infected individual, resulting in cost payoffs during the process of disease infection, such as income and revenue loss for the infected individual and associated medical costs. If all infected individual is assigned a fixed cost z, then the cost of all infected individuals can be expressed as

$$F(I(t)) = zI(t) \tag{2.80}$$

Evidence suggests that a higher degree of corporate social performance could improve financial benefits for that performance. Research [100] suggests that expected improvements in social performance could lead to improvements in financial performance, thereby decreasing financial loss. However, excessively large degrees of corporate social performance could have a negative financial impact. For example, an individual's large degree of corporate social performance could reduce payoffs from social networks [101].

Stephen *et. al.* [101] studied the relationship between corporate social performance and corporate financial performance and determined that corporate financial performance, which is a quadratic function of the corporate social performance, provides no financial payoffs to normal corporate social performance. In our model, $(1-u)$ represents corporate social performance, u represents corporate social performance reduction, and $F(S_{switch}(t))$ represents financial loss and payoffs due to the corporate social performance. According to [101] and our description, a relationship between corporate social performance and financial loss can be assumed to be a positive quadratic relation. When $u > 0$, an increasing corporate social performance degree $(1-u)$ means a decreasing number of individuals would choose to switch, leading to decreased financial loss. When no one switches and all individuals maintain normal corporate social performance, no financial loss results (i.e., when $u = 0$, then $1 - u = 1$ and financial loss is zero). However, when the corporate social performance degree reaches a specific point (e.g., $u < 0$), it generates a

negative financial impact. Therefore, the larger the corporate social performance degree $(1-u)$, the greater the financial loss.

The relationship between financial loss and corporate social performance can be expressed by

$$F(S_{switch}(t)) = b_1(1-u-b_2)^2 S_{switch}(t) \tag{2.81}$$

where *z* represents the average financial loss associated with each infected individual and b_1 and b_2 represent the scaling and shift parameters, respectively. Constraint conditions of the optimal control problems are

$$g_1 = \frac{dS(t)}{dt} = \mu N(t) - \left[\beta_b(1-u)S_{switch}(t) + \beta_b\left(S(t) - S_{switch}(t)\right)\right] - \mu S(t) \tag{2.82}$$

$$g_2 = \frac{dI(t)}{dt} = \left[\beta_b(1-u)S_{switch}(t) + \beta_b(S(t) - S_{switch}(t))\right] - \mu I(t) - \gamma I(t) \tag{2.83}$$

$$g_3 = \frac{dR(t)}{dt} = \gamma I(t) - \mu R(t) \tag{2.84}$$

$$g_4 = \frac{dS_{switch}(t)}{dt} = f\left(\overline{IFF(t)}\right)\frac{dS(t)}{dt} + \frac{S(t)\exp\left(\overline{IFF(t)}\right)}{\left(1+\exp\left(\overline{IFF(t)}\right)\right)^2}\frac{d\overline{IFF(t)}}{dt} \tag{2.85}$$

$$g_5 = \frac{d\overline{IFF(t)}}{dt} = r_1\frac{dS(t)}{dt} + r_2\frac{dS_{switch}(t)}{dt} + r_3 I(t)\frac{dS(t)}{dt}$$

$$+r_3 S(t)\frac{dI(t)}{dt} - r_4 I(t)\frac{dS_{switch}(t)}{dt} - r_4 S_{switch}(t)\frac{dI(t)}{dt} \tag{2.86}$$

2.5.3 Necessary Optimality Condition

Using Pontryagins maximum principle [102], the optimal control problem can be reduced to minimize Hamiltonian function H:

$$H(u,S,I,R) = F(I(t)) + F(S_{switch}(t)) + \sum_{i=1}^{5}\lambda_i g_i \tag{2.87}$$

where $\boldsymbol{\lambda_i}$ is the Lagrange multiplier corresponding to constraint g_i, i = 1, …, 5 as defined in Eqns. (2.82)-(2.86).

Because r_3 and r_4 are less significant than r_1 and r_2 (Section 2.3.2), the transversality conditions are complete (more than 30 sections each) if we consider r_1 to r_4.To simplify the analysis, we ignore r_3 and r_4. In addition, because Eqns. (2.85)-(2.86) and the equations of $\frac{d\overline{IFF(t)}}{dt}$ and $\frac{dS_{switch}(t)}{dt}$ have correlations with each other, $\frac{d\overline{IFF(t)}}{dt}$ can be substituted into $\frac{dS_{switch}(t)}{dt}$:

$$\frac{dS_{switch}(t)}{dt} = \frac{f\left(\overline{IFF(t)}\right)\left(1+\exp\left(\overline{IFF(t)}\right)\right)^2 + r_1 S(t)\exp\left(\overline{IFF(t)}\right)}{\left(1+\exp\left(\overline{IFF(t)}\right)\right)^2 - r_2 S(t)\exp\left(\overline{IFF(t)}\right)} \frac{dS(t)}{dt} \tag{2.88}$$

and then

$$\frac{d\overline{IFF(t)}}{dt} = \frac{\left(1+\exp\left(\overline{IFF(t)}\right)\right)^2 \left(r_1 + r_2 f\left(\overline{IFF(t)}\right)\right)}{\left(1+\exp\left(\overline{IFF(t)}\right)\right)^2 - r_2 S(t)\exp\left(\overline{IFF(t)}\right)} \frac{dS(t)}{dt} \tag{2.89}$$

Also, we substitute $N(t) = S(t) + I(t) + R(t)$ into Eq. (2.82). In the Hamiltonian function (2.87), the constraint functions g_i, i =1, …, 5, are defined as

$$g_1 = \frac{dS(t)}{dt} = \mu I(t) + \mu R(t) + \beta_b u S_{switch}(t) - \beta_b S(t) \tag{2.90}$$

$$g_2 = \frac{dI(t)}{dt} = \beta_b S(t) - \beta_b u S_{switch}(t) - \mu I(t) - \gamma I(t) \tag{2.91}$$

$$g_3 = \frac{dR(t)}{dt} = \gamma I(t) - \mu R(t) \tag{2.92}$$

$$g_4 = \frac{dS_{switch}(t)}{dt} = \frac{f\left(\overline{IFF(t)}\right)\left(1+\exp\left(\overline{IFF(t)}\right)\right)^2 + r_1 S(t)\exp\left(\overline{IFF(t)}\right)}{\left(1+\exp\left(\overline{IFF(t)}\right)\right)^2 - r_2 S(t)\exp\left(\overline{IFF(t)}\right)} \frac{dS(t)}{dt} \tag{2.93}$$

$$g_5 = \frac{d\overline{IFF(t)}}{dt} = \frac{\left(1+\exp\left(\overline{IFF(t)}\right)\right)^2 \left(r_1 + r_2 f\left(\overline{IFF(t)}\right)\right)}{\left(1+\exp\left(\overline{IFF(t)}\right)\right)^2 - r_2 S(t)\exp\left(\overline{IFF(t)}\right)} \frac{dS(t)}{dt} \tag{2.94}$$

Application of the Pontryagins maximum principle and the optimal control theory from [102] achieved the following theorem.

Theorem 2.4: Let $S(t), I(t), R(t), S_{switch}(t)$, and $\overline{IFF(t)}$ be optimal state solutions with associated optimal control variable $u(t)$ for the optimal control problem. Then adjoint (auxiliary) variables $\lambda_1(t), \lambda_2(t), \lambda_3(t), \lambda_4(t), \lambda_5(t)$ satisfy

$$\frac{\partial \lambda_1}{\partial t} = -\frac{\partial H}{\partial S} \tag{2.95}$$

$$\frac{\partial \lambda_2}{\partial t} = -\frac{\partial H}{\partial I} \tag{2.96}$$

$$\frac{\partial \lambda_3}{\partial t} = -\frac{\partial H}{\partial R} \tag{2.97}$$

$$\frac{\partial \lambda_4}{\partial t} = -\frac{\partial H}{\partial S_{switch}} \tag{2.98}$$

$$\frac{\partial \lambda_5}{\partial t} = -\frac{\partial H}{\partial \overline{IFF}} \tag{2.99}$$

with transversality conditions as

$$\lambda_i(t_f) = 0 \ \ (i = 1, 2, 3, 4, 5) \tag{2.100}$$

where t_f is the final time of the control.

Proof: Based on the Pontryagins maximum principle [102], given the fundamental system of equations

$$\frac{dx^i}{dt} = g_i(x, u) \ \ \ (i = 1, 2, 3, 4, 5) \tag{2.101}$$

and another system of equations in auxiliary variables $\lambda_1, \lambda_2, \lambda_3, \lambda_4, \lambda_5$

$$\frac{d\lambda_i}{dt} = -\sum_{i=1}^{5} \frac{\partial g_i(x(t), u(t))}{\partial x^i} \lambda_i \quad (i = 1, 2, 3, 4, 5) \tag{2.102}$$

then, in the IFF-SIR model, auxiliary variables λ_i are independent from state variables such as $S(t), I(t), R(t), S_{switch}(t)$ and $\overline{IFF(t)}$:

$$\frac{d\lambda_i}{dt} = -\sum_{i=1}^{5} \frac{\partial g_i}{\partial x^i} \lambda_i - \sum_{i=1}^{5} \frac{\partial \lambda_i g_i}{\partial x^i} = -\frac{\partial \sum \lambda_i g_i}{\partial x^i} \tag{2.103}$$

In addition, $F(I)$ and $F(S_{switch})$ are independent from state variables:

$$\frac{d\lambda_i}{dt} = -\frac{\partial \sum \lambda_i g_i}{\partial x^i} = -\frac{\partial\,(F(I)+F(S_{switch})+\sum \lambda_i g_i)}{\partial x^i} \tag{2.104}$$

Then

$$\frac{d\lambda_i}{dt} = -\frac{\partial H}{\partial x^i} \tag{2.105}$$

where x^i includes $S(t), I(t), R(t), S_{switch}(t)$ and $\overline{IFF(t)}$.

2.5.4 Existence of An Optimal Control

Theorem 2.5: Let $S(t), I(t), R(t), S_{switch}(t)$ and $\overline{IFF(t)}$ be control states with associated control variable $u(t)$ for the optimal control problem. Then unique optimal control $u^*(t)$ minimizes the Hamiltonian function H:

$$\frac{\partial H}{\partial u} = 2b_1(u^* - 1 + b_2)S_{switch} + \lambda_1\beta_b S_{switch} - \lambda_2\beta_b S_{switch} = 0 \tag{2.106}$$

Proof: The Hamiltonian function H can be normalized as

$$H = \alpha u^2 + \beta u + \gamma \tag{2.107}$$

where $\alpha \geq 0$ and β and γ are independent from u because the only quadratic term of u of H comes from

$$F(S_{switch}(t)) = b_1(1 - u - b_2)^2 S_{switch}(t) \tag{2.108}$$

Since $S_{switch} \geq 0$, then $\alpha = b_1 * S_{switch} \geq 0$, and the Hamiltonian function H has a global minimization at $u = -\frac{\beta}{2\alpha}$, meaning that the interval $u \in [0,1]$ contains only one optimal control u^* that can minimize H, whether or not the interval $u \in [0,1]$ contains $u = -\frac{\beta}{2\alpha}$.

In addition, the integrand of the objective function given by the Hamiltonian function H is convex in the control strategy set u, which is also convex and closed by definition. Conditions for the existence of optimal controls are satisfied because the model is linear in the control variables and bounded by a linear system in the state variables [101].

Then the final solution of the optimal control problem is

$$u^*(t) = \min\{\max\left(0; \frac{\beta_b(\lambda_2(t)-\lambda_1(t))-b_2+1}{2b_1}\right); 1\} \quad (2.109)$$

2.5.5 Numerical Simulations

This section provides numerical simulation to illustrate our research. Based on the final solution in Eq. (2.109), $u^*(t)$ depends on $\lambda_1(t), \lambda_2(t), \lambda_3(t), \lambda_4(t), \lambda_5(t)$. For the sake of simplicity, we use f to represent $f\left(\overline{IFF(t)}\right)$ in the following process. We calculate the necessary conditions for $\lambda_1(t), \lambda_2(t), \lambda_3(t), \lambda_4(t), \lambda_5(t)$ as

$$\frac{\partial\lambda_1}{\partial t} = -\frac{\partial H}{\partial S} = (\lambda_1 - \lambda_2)\beta_b - \frac{\exp\left(\overline{IFF(t)}\right)\left(1+\exp\left(\overline{IFF(t)}\right)\right)^2}{\gamma^2} * (\mu I + \mu R + \beta_b u S_{switch} - \beta_b S) *$$

$$(\lambda_4 r_1 - \lambda_4 r_2 f - \lambda_5 r_1 r_2 - \lambda_5 {r_2}^2 f) + \frac{\beta_b\lambda_4(f\left(1+\exp\left(\overline{IFF(t)}\right)\right)^2 + r_1 S\exp\left(\overline{IFF(t)}\right))}{\gamma} \quad (2.110)$$

$$\frac{\partial\lambda_2}{\partial t} = -\frac{\partial H}{\partial I} = -z + (\lambda_2 - \lambda_1)\mu + (\lambda_2 - \lambda_3)\gamma - \frac{\mu}{\gamma} * \phi \quad (2.111)$$

$$\frac{\partial\lambda_3}{\partial t} = -\frac{\partial H}{\partial R} = (\lambda_3 - \lambda_1)\mu - \frac{\mu}{\gamma} * \phi \quad (2.112)$$

$$\frac{\partial\lambda_4}{\partial t} = -\frac{\partial H}{\partial S_{switch}} = (\lambda_2 - \lambda_1)\beta_b u - \frac{\beta_b u}{\gamma}\phi \quad (2.113)$$

$$\frac{\partial\lambda_5}{\partial t} = -\frac{\partial H}{\partial \overline{IFF}} = -\frac{(\mu I + \mu R + \beta_b u S_{switch} - \beta_b S)\exp\left(\overline{IFF(t)}\right)}{\gamma^2}$$

$$* \{\lambda_5 r_2 S\left(1 + \exp\left(\overline{IFF(t)}\right)\right)(r_1 + r_2 f)\left(1 + 3\exp\left(\overline{IFF(t)}\right)\right)$$

$$+\lambda_5 r_2\left(1 + 2\exp\left(\overline{IFF(t)}\right)\right)\left[\left(1 + \exp\left(\overline{IFF(t)}\right)\right)^2 + S\exp\left(\overline{IFF(t)}\right)\right]$$

$$+\lambda_4\left(1 + \exp\left(\overline{IFF(t)}\right)\right)^2 [1 + 2\exp\left(\overline{IFF(t)}\right) + r_1 S$$

$$+r_2 Sf] - \lambda_4\left(1 + \exp\left(\overline{IFF(t)}\right)\right)\exp\left(\overline{IFF(t)}\right)(2r_2 Sf - 2r_1 S)$$

$$+\lambda_4(1 + 2\exp\left(\overline{IFF(t)}\right))\exp\left(\overline{IFF(t)}\right) r_2 S\} \quad (2.114)$$

where

$$\nu = \left(1 + \exp\left(\overline{IFF(\mathrm{t})}\right)\right)^2 - r_2 S \exp\left(\overline{IFF(\mathrm{t})}\right) \quad (2.115)$$

$$\phi = \left((\lambda_4 f + \lambda_5 r_1 + \lambda_5 r_2 f)\left(1 + \exp\left(\overline{IFF(\mathrm{t})}\right)\right)^2 + \lambda_4 r_1 S \exp\left(\overline{IFF(\mathrm{t})}\right)\right) \quad (2.116)$$

Using the IFF-SIR dynamic system with control in Eq. (2.79), the boundary constraints in Eqns. (2.95)-(2.99), and final solution (2.108), we calculate $u^*(t)$ by iteration algorithm [97] according to the following steps:

Step 1: Order a constant control in the first iteration (j = 1). We choose the maximum number of control $u(t)$ as this constant in order to simplify the problem.

$$u_1(t) = 1$$

Step 2: Using the IFF-SIR dynamic system expression, calculate ($S_j(t), I_j(t), R_j(t)$, $S_{switch_j}(t), \overline{IFF_j(t)}$) in the jth iteration.

Step 3: Based on the boundary constraints expression, calculate $\lambda_{i,j}(t)$ using transversality conditions as initial conditions.

Step 4: Calculate ${u_j}^*(t)$ by the final solution of the optimal control problem. We use a convex combination to calculate $u_{j+1}(t)$.

Step 5: Repeat steps 2, 3, and 4 to obtain the numerical optimal control solution $u^*(t) = u_j(t)$ until terminal condition

$$u_j(t) = u_{j+1}(t)$$

In order to verify validity of the optimal control, a simulation run compares results of the model with and without control using the iteration algorithm. Assuming that the total number of individuals in the global contact network is $N = 1000$: 980 susceptible, 20 infected, 0 recover and 300 switch individuals, let $z = 2000$ [103] and $b_1 = 60$ [104]. When $u = 0$, the financial loss is

zero and $b_2 = 1$. We observe the trend of individuals in each state and the estimated $\overline{IFF(t)}$ based on the regression relationship over the 100-day period. Observations throughout five replications revealed that the terminating condition was almost satisfied ($\left|u_j(t) - u_{j+1}(t)\right| \leq 0.001$) after the 15^{th} iteration, which means the iteration result satisfied the terminal condition at Step 5 of the iteration algorithm. Overall, the optimal corporate social performance reduction decreased through the time line, as shown in Figure 2.11. The optimal solution at the onset of a disease epidemic is to reduce almost all corporate social performance. The optimal solution at the last phase of a disease suggests that people choose normal behavior.

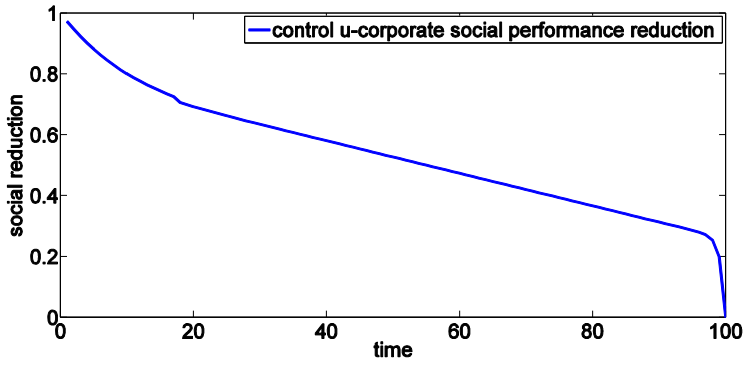

Figure 2.11 Optimal corporates with reduced social performance

In order to verify validity of the optimal control, we compare simulation results (total infections and total susceptive switch populations) of the IFF-SIR model with control and without control to various initial settings. We compare the simulations with initial population $N = 1000$ $(\mathrm{S} = 980; \mathrm{I} = 20; \mathrm{R} = 0; S_{switch} = 50)$, $N = 1000$ $(\mathrm{S} = 960; \mathrm{I} = 40; \mathrm{R} = 0; S_{switch} = 50)$, $N = 1000$ $(\mathrm{S} = 940; \mathrm{I} = 60; \mathrm{R} = 0; S_{switch} = 50)$, and $N = 1000$ $(\mathrm{S} = 920; \mathrm{I} = 80; \mathrm{R} = 0; S_{switch} = 50)$. Although the tendencies are similar, as shown in Figure 2.12, the IFF-SIR model with control has less total infectious and less total susceptive switch population. Therefore, the optimal control policy successfully reduces the financial loss of infections. Results also showed

that the switch level in the IFF-SIR model with control is not a constant, suggesting that reduction of social performance is sensitive to epidemic change, leading to the conclusion that the optimal control solution reduces unnecessary financial loss in the epidemic.

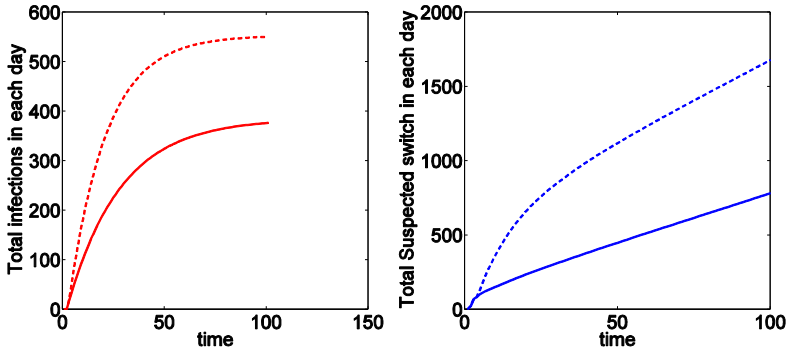

(a) With initial population $N = 1000$ ($\mathbf{S} = 980; \mathbf{I} = 20; \mathbf{R} = 0; S_{switch} = 50$)

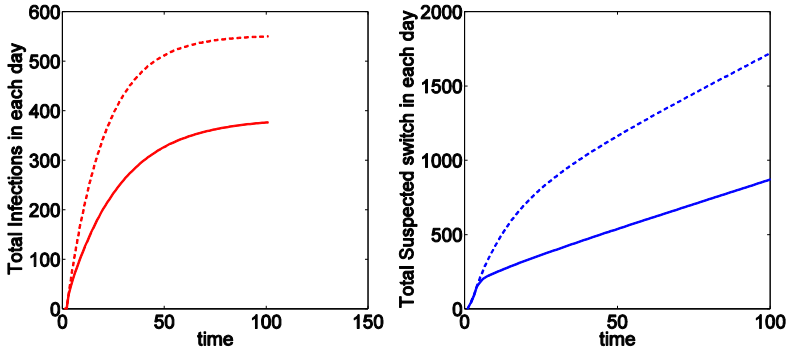

(b) With initial population $N = 1000$ ($\mathbf{S} = 960; \mathbf{I} = 40; \mathbf{R} = 0; S_{switch} = 50$)

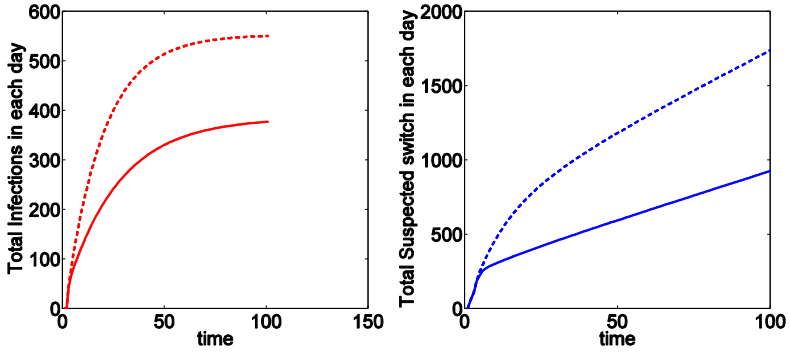

(c) With initial population $N = 1000$ ($\mathbf{S} = 940; \mathbf{I} = 60; \mathbf{R} = 0; S_{switch} = 50$)

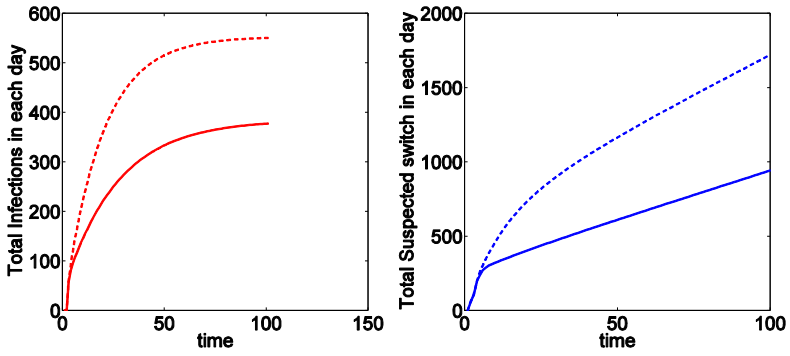

(a) With initial population $N = 1000$ ($\mathbf{S} = 920; \mathbf{I} = 80; \mathbf{R} = 0; S_{switch} = 50$)

Without control **With control**

Without control **With control**

Figure 2.12 Comparison of the IFF-SIR model with and without control in four simulations

2.6 Summary and Discussion

This paper synthesized local and global contact networks and perceptual and rational information to develop an IFF model to define the fear factor for susceptible individuals in order to determine how information affects emotion or opinion, thereby altering individuals' behavior during an epidemic. Moreover, this paper first attempted to explain how an individual's emotions and perceptions on the current information influence their switching behavior using a mathematical model. So this research can be utilized to study the complex emotion and behavior changes during disease outbreaks. Following stability analysis, we identified and proved four necessary conditions of IFF stability in order to better understand the role of IFF in epidemic transmission within the individual model. Regression analysis was used to average IFF among all susceptible individuals, revealing a statistically significant regression relationship between $\overline{IFF(t)}$ and $S(t), I(t), R(t), S_{switch}(t)$. Then we introduced an IFF-SIR dynamic system that includes differential equations of $S(t), I(t), R(t), S_{switch}(t)$, and $\overline{IFF(t)}$. Using the Lyapunov stability

theory, we found that IFF-SIR has infinite stability points. Finally, we defined financial loss as the objective function in the optimal control problem, and we proposed the optimal suggestion for reduction of social performance throughout an epidemic. Although regression analysis allows us to research IFF in disease transmission, the feasible range of population is limited by data. Therefore, future studies should include real data collection and use a multilayer method to divide a population.

Chapter 3 - A New Evidence-Based Optimal Control in Healthcare Delivery: A Better Clinical Treatment Management for Septic Patients

Chapter 3 is based on the manuscript "A New Evidence-Based Optimal Control in Healthcare Delivery: A Better Clinical Treatment Management for Septic Patients" Published in Computers & Industrial Engineering [58].

Abstract

Treatment strategy of a realistic health care system must consider both system and measurement errors. The traditional optimal control method is commonly applied to deterministic systems instead of dynamic systems with uncertain errors. Therefore, this paper considers uncertain errors and stochastic characteristics in a dynamic health care system and proposes a new evidence-based optimal control (EBOC) approach that combines the traditional optimal control and machine learning methods. Four machine learning algorithms were tested, and the most suitable algorithm was combined with the traditional optimal control method for the sepsis model. Extensive computational studies proved that, compared to the traditional optimal control method, the EBOC method more efficiently controls disease progression and decreases total cost when uncertainty or measurement errors exist in the model, no matter the machine learning algorithm utilized. Moreover, the total c^nsettings are possible when numerous parameter combinations could affect control results, meaning determination of the optimal parameter set(s) becomes an NP-hardness problem. This paper also uses the genetic algorithm to find superior parameter settings to improve the performance and effectiveness of the control strategy created by the EBOC method.

Keywords: dynamic system; sepsis, healthcare; optimal control; EBOC method; machine learning.

3.1 Introduction

Nowadays, the US healthcare industry is under increasing pressure from the quality of medical treatments and associated high cost. Healthcare planners find themselves facing the challenges of improving the efficiency and safety of their healthcare services under gradually tightened budget constraints [105]. Many research efforts to improve patients' needs and safety, along with reductions in related costs were proposed using various optimal control strategies based on certain underlining disease models [25, 106 - 109]. To reduce the number of fatalities, Ren *et al*. proposed a new approximate disease propagation model to optimize the limited resource allocation issues and control measures [110]. In 2018, Ng *et al*. studied an optimal vaccination strategy based on the influenza mathematical model to embrace the confliction among the immunization program cost, vaccination efficacy, and societal benefits [111]. Blayneh *et al*. also presented a control model based on the dynamics of vector-borne disease to regulate the disease spread while minimizing the associated costs [112]. Thus, applications of optimal controls in healthcare systems can be used to study optimal therapies or mitigation strategies for various diseases [113 - 114]. However, most current research efforts on optimal control of healthcare systems have not considered the potential system uncertainties or measurement errors, such as error due to instrument measurement approximation and medical errors due to incorrect prescriptions [115]. Regardless of the controls used, errors between real results and expected results after control exist in a dynamic system [116]. These errors may be fatal, costly, and suffer from serious medical consequences [115]. Thus, it is necessary to take these potential errors into account in various healthcare delivery systems. Also, if the system involves possible uncertainties,

the original deterministic system will become a stochastic dynamic system. The traditional algorithms to solve the deterministic optimal control problems cannot be used to obtain a meaningful solution or effective control strategies. Therefore, in this paper, we will study and explore the effective control in a healthcare system with potential existences of measurement errors or system uncertainties.

A significant amount of recent studies have shown that machine learning can be used to better describe model behaviors and the related control performances for systems with errors. Kong *et al*. presented an error-correcting technique to improve system accuracy by controlling errors by bias estimates [117]. Togai *et al*. developed a discrete control system and proposed a new supervised learning algorithm, which utilized the state variable errors of the system to obtain the optimal learning control strategy [118]. Gaudiano and Grossberg proposed an unsupervised learning model based on errors to provide the adaptive control for arm movement trajectory [119]. Also, neural network, a data structure used in supervised or unsupervised learning algorithms, has recently become a popular method for improving the system control performances [120]. Lin *et al*. proposed a general neural network model to minimize the error of a traditional fuzzy logic system and make the controls more flexible [121]. However, most existing literature related to the applications of machine learning was not directed toward the healthcare systems with measurement or system errors. Therefore, all the above research works motivated us to combine optimal controls and machine learning methods for healthcare systems with errors to improve the corresponding efficient and cost-effective. The main objective of this paper is to determine accurate and effective optimal control strategies that can improve the quality of care and increase the chances of survival for patients.

In the United States, an average of 750,000 sepsis cases reported in US healthcare systems every year, but the documented occurrences continue to rise and caused increasing concerns [24, 122]. Sepsis, a systemic inflammatory response associated with several clinical conditions, has increasingly become a leading cause of mortality in hospitals in the United States [122]. Globally, sepsis causes millions of deaths each year [123], while an average of 250,000 fatalities of sepsis in the United States annually [124]. Recent literature has shown that the hospital mortality rate of sepsis is 25%–30% and is continuously rising [125, 126]. Healthcare expenses related to sepsis treatment and management are estimated to be $60,000 per instance per patient [127]. A report from 2017 stated that sepsis is a significant healthcare burden for the United States, costing the country approximately $20 billion over the past decade [128]. Sepsis has increasingly gained attention from research and practitioner communities. To find possible reliefs for this nationwide healthcare burden, our research in this paper used an optimal control approach for control and mitigate sepsis progression, and therefore, improve related patient safety and treatment outcomes.

In this paper, we studied the results from two different situations in a sepsis model: one considered the existence of system errors, and the other one did not. Computational results from model simulations confirmed the traditional optimal control strategy is only effective for the deterministic system without measurement errors; whereas it is ill-suited for systems with stochastic or contains random errors, thereby requiring revision or improvement of the traditional optimal control strategy for stochastic systems. Four different machine learning algorithms were implemented into the traditional optimal control strategy to improve the effectiveness of optimal control for the sepsis model. This improved approach is generally referred to as the evidence-based optimal control **(**EBOC) method. Computational results showed that the sepsis model becomes a stochastic system when errors are considered in the original deterministic sepsis model. The EBOC

method resulted in a control strategy that performed more efficiently and generated more reliable control strategies than the traditional optimal control strategy to regulate the pathogen levels and pro-inflammatory mediators, subsequently, properly control the sepsis deterioration, and reduce the overall cost of a predefined objective function. Because various parameter settings could influence the results of the disease system, this paper proposes an NP-hard problem as described in Section 3.4.1, which its computational complexity increases when problem size increases [129, 130]. The model in this study contained n unknown parameters with each parameter potentially having at least c possible values, resulting in a total of c^n possibilities. Therefore, this paper suggested the use of a heuristic algorithm, genetic algorithm (GA), to obtain an enhanced control strategy for a real disease clinic problem and application of parameter settings into the EBOC method to improve method performance.

The main contribution of this paper is that the proposed EBOC method combines traditional optimal control, created using Pontryagin's maximum principle, and machine learning, thereby allowing method utilization in stochastic systems and providing an effective optimal control strategy for the systems. The EBOC method updates control solutions learned from the prior evidence and asymptotically converges to a final optimal control significantly reduces sepsis progression and overall costs. The rest of this paper is organized as follows. In Section 3.2, a sepsis disease model is presented and related limitations of applying a traditional optimal control were discussed to motivate the needs of the new EBOC approach to deal with possible system uncertainties and measurement errors. Section 3.3 presents the methodology of the Evidence-Based Optimal Control that combines several recommended machine learning algorithms with optimal control. Also, the effectiveness of the EBOC control strategy was illustrated, no matter the chosen machine learning. Section 3.4 presents a heuristic Genetic Algorithm to find the optimal

control parameters for the EBOC method. Finally, in Section 3.5, the main contributions of this research are summarized, and possible future extensions of this research are discussed.

3.2 Model of Sepsis and Model Improvement

3.2.1 Model of Sepsis

Sepsis is a life-threatening systemic inflammatory response that can lead to organ dysfunction and death if not properly treated and controlled. Acute inflammatory response (AIR), the initial stage of sepsis, is a complex process in which pathogens invade body tissue, stimulating immune cells to detect and respond to the pathogen invasion. Immune cells then transmit the signal to resting phagocytes such as neutrophil and monocytes. Some phagocytes are then activated and transferred to the infection site or damaged tissues where they begin to engulf and eliminate the pathogens. The activated phagocytes also excrete pro-inflammatory cytokines such as Interleukin-1 (IL-1), IL-6, IL-8, IL-12, tumor necrosis factor α (TNF- α), and high-mobility group box-1 (HMGB-1), which contribute to the up-regulation of the immune system response. The excreted pro-inflammatory cytokines then activate more resting phagocytes, and those activated phagocytes migrate to the infection site. Although the phagocytic cells kill the pathogens, the substances they excrete also harm healthy cells near the infected site, thereby increasing inflammation and causing activated phagocytic cells to release anti-inflammatory cytokines such as IL-4, IL-10, IL-13, and transforming growth factor β (TGF-β) to inhibit pro-inflammatory cytokines. Therefore, anti-inflammatory mediators become essential for regulating the immune system response.

This paper specifically studies sepsis based on the model proposed by Kumar *et al.* [131], which introduced a three-dimensional ordinary differential equation model to simulate the inflammatory response by focusing on the dynamic interaction between pathogen, early pro-

inflammatory mediator (such as TNF-α, IL-10), and a late pro-inflammatory mediator (such as IL-6, HMGB-1). The sepsis model is described as follows:

$$\frac{dS(t)}{dt} = k_S S(t)\big(1 - S(t)\big) - k_{Sm} m(t) S(t) \tag{3.1}$$

$$\frac{dm(t)}{dt} = (k_{mS} S(t) + l(t)) m(t)(1 - m(t)) - m(t) \tag{3.2}$$

$$\frac{dl(t)}{dt} = k_{lm} f\big(m(t)\big) - k_l l(t) \tag{3.3}$$

where

$$f\big(m(t)\big) = 1 + tanh\,(\frac{m(t)-\theta}{w}) \tag{3.4}$$

$S(t)$ represents the pathogen population at time *t*, $m(t)$ represents the early pro-inflammatory mediators at time *t*, and l(t) represents the late pro-inflammatory mediators at time *t*. k_S denotes the growing rate of the pathogens, k_{Sm} is pathogen susceptibility to the host's defense (or the pathogen death rate), k_{mS} is the activation rate of the early pro-inflammatory mediators, k_{lm} represents the recruitment rate of the late pro-inflammatory mediators, and k_l is the death rate of the late pro-inflammatory mediators. θ is the activation threshold, and w is the activation width.

Recent research on mathematical modeling of sepsis has seldom used the optimal control strategy to determine if the systemic inflammatory response to sepsis processes can be intervened to impact the outcomes of a sepsis episode. Researchers have frequently ignored potential system or measurement errors that may significantly decrease optimal control effectiveness in existing disease models. Therefore, this paper applies traditional optimal control in the sepsis model with consideration of measurement errors and proposes ways to increase control strategy effectiveness and accuracy for controlling sepsis deterioration when clinical treatment is not ideal for traditional optimal control. The above model was considered a continuous-time system.

3.2.2 Problem Statement

This paper generalized system (3.1)-(3.3) in the following general dynamic system form:

$$\dot{x}(t) = f(x(t)) \tag{3.5}$$

where $x(t) \in R^n$ is the *n*-dimensional state variable vector, $f(x(t))$ is the system function, and $\dot{x}(t) = (\frac{dS(t)}{dt}, \frac{dm(t)}{dt}, \frac{dl(t)}{dt})^T$, $f(x(t))$ is the right-hand side of the system (3.1)-(3.3). Let $x(0)$ be the initial state.

The following rational assumptions were made to explain the main problems in Eq. (3.5):

Assumption 3.1: System (3.5) is controllable, and control vector $u(t)$ can be adjunct to the system (3.5) linearly. $u(t) \in R^m$ means that m of n state variables are controllable ($m \leq n$).

Assumption 3.2: Considering system errors and measurement errors throughout the control process, the optimal control of the system is defined as $p(t)u(t)$, where $p(t) \in R^m$ represents the random error vectors.

Assumption 3.3: System state $x(t) = 0$ is an equilibrium state of the system (3.5) when the control $u(t) = 0$.

Based on the first two assumptions, system (3.5) can be rewritten in first-order dynamic constraints as

$$\dot{x}(t) = f\big(x(t)\big) + p(t)u(t) \tag{3.6}$$

where $x(t)$ is the state variable denoted by $x(t) = (x_1(t), x_2(t), \dots, x_n(t))^T$, $f \in R^n$. For a general control system (3.6), objective function *J* can usually be defined as the following system (3.7), which maximizes or minimizes the overall cost function:

$$J\big(x(t_0), u(t_0)\big) = \int_{t_0}^{t_f} U(x(t), u(t))\, dt \tag{3.7}$$

where t_0 and t_f represent the initial time and ending time, respectively. $U(x(t), u(t))$ denotes the cost function for any time $t \in [\, t_0, t_f]$, $U \in R$.

We focused on finding the optimal control method to optimize the function in Eq. (3.7), including uncertainty components presented by the system and measurement errors [132]. Consideration of system errors or measurement errors means that the system under study is stochastic; therefore, the optimal control strategy for the dynamic system cannot be calculated directly due to randomness behaviors over time. This paper applies a new EBOC approach to determine a practical optimal control strategy while considering these stochastic components.

3.2.3 Traditional Optimal Control

To establish a baseline for the proposed optimal control method, a traditional optimal control method is described in this section to solve the system (3.6) for $u^*(t)$. However, the system (3.6) contains a random error vector, $p(t)$, which are uncertain components with unknown distributions. Since the traditional optimal control strategy does not consider stochastic aspects in a dynamic system, in this case, all components in $p(t)$ are equal to 1, meaning the model ignores all errors in optimal control strategy processes.

Using Pontryagin's maximum principle [102], the optimal control problem can be reduced to minimize (or maximize) the Hamiltonian function H as follows:

$$\begin{aligned} H(x,u) &= U\big(x(t),u(t)\big) + \lambda(t)[f\big(x(t)\big) + p(t)u(t)] \\ &= U\big(x(t),u(t)\big) + \lambda(t)g(x(t),u(t)) \end{aligned} \tag{3.8}$$

where $\lambda(t)$ represents the adjoint variables vector $\lambda(t) = (\lambda_1(t), \lambda_2(t), \dots, \lambda_n(t))^T$, which corresponds to n-vector $g\big(x(t),u(t)\big) = (g_1, g_2, \dots, g_n)^T$, and g_i is the right-hand side of the dynamic constraint in Eq. (3.6), $U \in R$.

Theorem 3.1: For the optimal control problem defined in Section 3.2.2, adjoint variables vector $\lambda(t)$ satisfies

$$\frac{\partial \lambda_i}{\partial t} = -\frac{\partial H}{\partial x_i} \tag{3.9}$$

with transversality conditions as

$$\lambda_i(t_f) = 0 \tag{3.10}$$

where λ_i is the i^{th} number in vector λ, x_i is the i^{th} number in the state variable vector x, and t_f is the terminal time of the control.

Proof: Based on the assumption that all numbers in $p(t)$ are equal to 1 when the system does not consider stochastic aspects, the system equations can be defined as

$$\frac{\partial x_i}{\partial t} = g(x(t), u(t)) \tag{3.11}$$

and the constraint function can be defined as

$$\mathcal{H}(x, u, \lambda) = \lambda(t) g(x(t), u(t)) \tag{3.12}$$

Also, based on the maximum principle [102], the following system equation holds:

$$\frac{\partial \lambda_i}{\partial t} = -\frac{\partial U}{\partial x_i} - \sum_{\alpha=1}^{n} \frac{\partial g_\alpha(x,u)}{\partial x_\alpha} \lambda_\alpha \tag{3.13}$$

Using the results of (3.12) and (3.13), the necessary conditions for the existence of an optimal solution are

$$\frac{\partial \lambda_i}{\partial t} = -\frac{\partial H}{\partial x_i} = -\frac{\partial U}{\partial x_i} - \sum_{\alpha=1}^{n} \frac{\partial \lambda_\alpha g_\alpha(x,u)}{\partial x_\alpha} = -\frac{\partial U}{\partial x_i} - \frac{\partial \mathcal{H}}{\partial x_i} \tag{3.14}$$

Theorem 3.2: If the unknown random errors vector $p(t)$ in Eq. (3.6) is ignored, then the result of the traditional optimal control $u^*(t)$ is optimized for a minimization problem (or maximization problem):

$$u^*(t) = \min\left\{\max\left(u_l; \arg\left(\frac{\partial H}{\partial u} = 0, \frac{\partial^2 H}{\partial u^2} > 0 \left(or \frac{\partial^2 H}{\partial u^2} < 0\right)\right)\right); u_u\right\} \tag{3.15}$$

where u_l and u_u represent the lower and upper bounds of the control set, respectively. We also assume $u(t)$ is monotonic in both $[u_l, \arg_{u\in\mathbb{R}}(\frac{\partial H}{\partial u}=0, \frac{\partial^2 H}{\partial u^2}>0)]$ and $[\arg_{u\in\mathbb{R}}(\frac{\partial H}{\partial u}=0, \frac{\partial^2 H}{\partial u^2}>0), u_u]$, otherwise, several extremum values should be present in the control range, requiring manual comparison of the optimal control from the extremum value set.

Proof: To prove the contradiction, we first assume that control $u^{**}(t)$, $u^{**}(t) \in [u_l, u_u]$ for any $t\in [t_0, t_f]$, is better than the optimal control result $u^*(t)$ and that $H\big(x, u^{**}(t)\big) < H(x, u^*(t))$ are satisfied for an object minimization problem. Therefore,

First, if $\arg_{u\in\mathbb{R}}\left(\frac{\partial H}{\partial u}=0, \frac{\partial^2 H}{\partial u^2}>0\right) \in [u_l, u_u]$, then $u^*(t) = \arg_{u\in\mathbb{R}}\left(\frac{\partial H}{\partial u}=0, \frac{\partial^2 H}{\partial u^2}>0\right)$.

Let $u^{**}(t) = u^*(t) + \Delta u(t)$ for any $t \in [t_0, t_f]$, where $\Delta u(t)$ is the deviation and $|\Delta u(t)| < u_u - u_l$. Since we assume this problem is the minimization problem, then for any $(t) \in [u_l, u_u]$

$$\frac{\partial^2 H}{\partial u^2}\big(u^*(t)\big) = \frac{H'(u(t)) - H'\big(u^*(t)\big)}{\Delta u} > 0 \tag{3.16}$$

Then $u(t) = u^{**}(t)$, so

$$\frac{\partial^2 H}{\partial u^2}\big(u^*(t)\big) = \frac{H'(u^{**}(t)) - H'\big(u^*(t)\big)}{\Delta u} > 0, \tag{3.17}$$

meaning that $(H'(u^{**}(t)) - H'\big(u^*(t)\big)) \cdot \Delta u > 0$ holds for any $u^{**}(t) \neq u^*(t)$. When $\Delta u > 0$, then

$$H'(u^{**}(t)) > H'\big(u^*(t)\big) = \frac{\partial H}{\partial u}\big(u^*(t)\big) = 0 \tag{3.18}$$

Therefore, for any $u(t) \in [u_l, u_u]$,

$$H'(u^{**}(t)) = \frac{H(u(t)) - H\big(u^{**}(t)\big)}{-\Delta u} > 0 \tag{3.19}$$

Then $u(t) = u^*(t)$, so

$$H'(u^{**}(t)) = \frac{H(u^*(t)) - H(u^{**}(t))}{-\Delta u} > 0 \tag{3.20}$$

Therefore, $H(u^{**}(t)) > H(u^*(t))$ is a contradiction.

Also, when $\Delta u < 0$, then

$$H'(u^{**}(t)) < H'(u^*(t)) = \frac{\partial H}{\partial u}(u^*(t)) = 0 \tag{3.21}$$

$$H'(u^{**}(t)) = \frac{H(u^*(t)) - H(u^{**}(t))}{-\Delta u} < 0 \tag{3.22}$$

which also proves to be a contradiction. Therefore, for any $t \in [t_0, t_f]$ if $\arg_{u\in\mathbb{R}}\left(\frac{\partial H}{\partial u} = 0, \frac{\partial^2 H}{\partial u^2} > 0\right) \in [u_l, u_u]$, $u^*(t)$ is the minimum solution.

Second, if $\arg_{u\in\mathbb{R}}(\frac{\partial H}{\partial u} = 0, \frac{\partial^2 H}{\partial u^2} > 0) \in (-\infty, u_l] \cup [u_u, +\infty)$, then we can assume $u^*(t) = \arg_{u\in\mathbb{R}}(\frac{\partial H}{\partial u} = 0, \frac{\partial^2 H}{\partial u^2} > 0) \in (-\infty, u_l]$, where $u^*(t) = u_l$.

Let $u^{**}(t) = u^*(t) + \Delta u(t)$. Since $u^*(t)$ is the minimum solution in $(-\infty, +\infty)$but u_l is the lower bound of the control set because $u^*(t) \le u_l < u_u$ and in interval $[u', u_u]$ function H monotonically increases in $[\arg_{u\in\mathbb{R}}(\frac{\partial H}{\partial u} = 0, \frac{\partial^2 H}{\partial u^2} > 0), u_u]$, then

$$H(x, u^*(t)) \le H(x, u_l) < H(x, u_u) \tag{3.23}$$

Therefore, when $u^*(t) = \arg_{u\in\mathbb{R}}(\frac{\partial H}{\partial u} = 0, \frac{\partial^2 H}{\partial u^2} > 0) \in (-\infty, u_l]$ in control interval $[u_l, u_u]$, the minimum solution is $u^*(t) = u_l$. We can use the same proof for $u^*(t) = \arg_{u\in\mathbb{R}}(\frac{\partial H}{\partial u} = 0, \frac{\partial^2 H}{\partial u^2} > 0) \in [u_u, +\infty)$, where the minimum solution is $u^*(t) = u_u$ in the control interval $[u_l, u_u]$.

3.2.4 Evidence-Based Optimal Control Method

Section 3.2.3 discussed the effectiveness of the traditional optimal control method without considering the unknown random error matrix $p(t)$. However, because these errors exist in many

real-world applications, especially clinical disease control, the accuracy of the control strategy must be ensured under uncertain errors in the disease models. To eliminate influence due to errors, we utilized a learning reinforcement to revise results from the optimal control method. This learning reinforcement comes from historical evidence or the predicted model based on historical evidence (e.g., results obtained from regression or clustering models). Then we combined the optimal control strategy and the learning reinforcement strategy with a learning factor α, which determines the weight of the learning reinforcement strategy. The evaluation of α will be discussed in Section 3.4.

The definition of EBOC is as follows:

$$u_f(t) = (1-\alpha)u^*(t) + \alpha * u_{learning}(t) \tag{3.24}$$

where $u_f(t)$ is the final control strategy created by the EBOC method at time t ($t \in [t_0, t_f]$) for a clinical trial, $u^*(t)$ is the traditional optimal control strategy created using Pontryagin's maximum principle at time t (defined in Section 3.2.3), and $u_{learning}(t)$ is the learning control strategy at time t.

For the learning control strategy $u_{learned}(t)$, several machine learning methods can be used based on the training data, which can be initialized by evidence data obtained from traditional optimal control methods. In general, there are two kinds of learning methods. The first method is the case-based learning method, which utilizes either a supervised learning algorithm or an unsupervised learning clustering algorithm to group historical data, allowing selection of the best history data that has the most positive consequence from the corresponding group. In this method, the data can be grouped by simple classification based on only feedback after the control or by supervised classification (decision tree) labeled by several specific system variables or by unsupervised clustering that considers all system variables. The second method, the predictive

learning model, utilizes historical data to train the predictive model and then acquire predictive relationship among data. The predictive model is generated using a supervised neural network or a supervised linear/logistic regression. Each method has unique effectiveness and application scopes, as described in detail in Section 3.3.

3.3 Evidence-Based Optimal Control Methodology

This section details how to build the evidence database, and combine the machine learning algorithm with traditional optimal control method as the EBOC method, and verify the effectiveness of the EBOC method using simulated datasets for the sepsis dynamic model.

3.3.1 Evidence Database

The EBOC method first requires initialization of the evidence database. The database with s patients, including state variable values and corresponding control within 24 hours, was obtained from real data or simulation experiments since the first 24 hours is the optimal time for immunological rejection of sepsis [133]. Then each $\tau \in [0,24]$ hour was used as the time interval to calculate the numerical solution of traditional optimal control using the algorithm in [96], resulting in a total of $\frac{24s}{\tau}$ training data points. Each data point included control data and system state variables data, but these data did not include feedbacks after control. Since we wanted to use these feedbacks to judge the control, we transferred our evidence database and determined that for each patient s_i, i = 1, 2, … s, at time $t \in \{\tau, 2\tau, \dots, n\tau\}$, where $n = \frac{24}{\tau}, and\ 0 < \tau \leq 24$:

$$\Delta x(s_i, t) = x(s_i, t + \tau) - x(s_i, t), \tag{3.25}$$

where $\Delta x(s_i, t)$ denotes the feedback of control for patient s_i at time t.

This evidence database can be extended over time since new state variable values and controls can be gradually calculated using the EBOC control strategy and then added to the

database as training data. Subsequently, the EBOC control strategy becomes increasingly precise since additional evidence data are added to the evidence database over time with more training cases. A flowchart of EBOC methodology is shown in Figure 3.1.

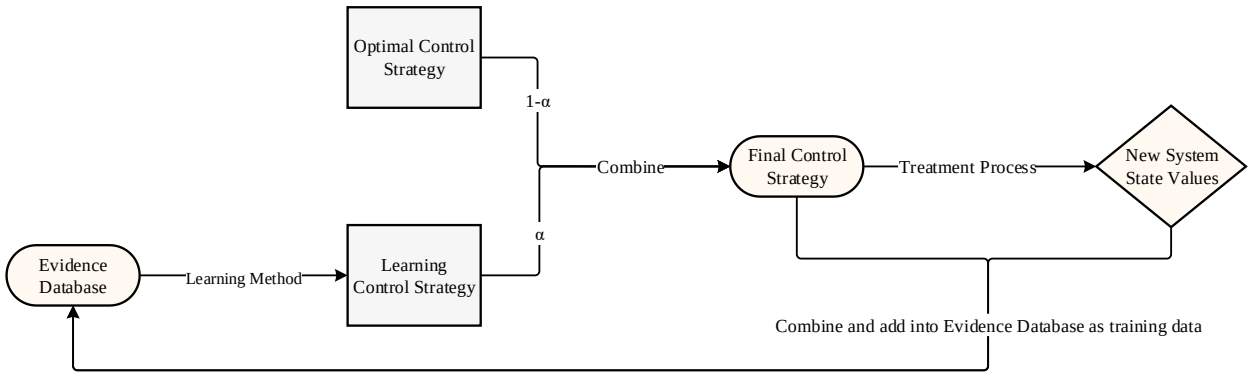

Figure 3.1 Flowchart of EBOC methodology

3.3.2 Case-Based Learning Method Based on Evidence Database

In the case-based learning method, evidence data is divided into groups with similar sepsis symptoms. When the EBOC strategy is used on a new patient s_i, the group that the new patient belongs to at each time epoch will be picked up, and then a control strategy with the most positive and effective feedbacks in this group is chosen from all possible control strategies as the learning control.

3.3.2.1 Clustering Method

Clustering is a popular approach for grouping similar data based on the Euclidean distance between a data point and a cluster center [134]. After clustering, data points in the same group (or cluster) are assumed to have similar characteristics. For each group, the EBOC method identified the best control that produces the most positive and effective feedback among all possible controls. When a new patient s_i entered the system, the EBOC method used the clustering method to

determine the most similar group S_j for this patient. Then the learned control $u_{learning}(t)$ for new patient s_i at time t was assigned using the best control that produced the most effective feedback in group S_j. After combining the learning control $u_{learning}(t)$ with the traditional optimal control $u^*(t)$ in Eq. (3.24), the EBOC method provided a final control $u_f(t)$.

3.3.2.2 Decision Tree Method

The decision tree learning method is a supervised learning method that uses a decision tree to enumerate and classify all possible combinations from the input data; this decision tree then predicts the output results for these combinations [135]. Because the decision tree learning method can only predict discrete results, however, the learning control $u_{learning}(t)$ is continuous in the control domain. First, we divided the control domain $[u_l, u_u]$ into *n* different ranges, namely, Y_1: $[u_l, u_1]$, Y_2: $[u_1, u_2]$, …, Y_u: $[u_n, u_u]$. The evidence database includes states variable values and corresponding control so that we could determine the corresponding control range $Y_j (1 \leq j \leq u)$ for the historical controls in the evidence database and use these historical state variable values and control ranges as training data to build the decision tree. When a new patient enters the system, we used the decision tree model based on the evidence database to find a control range with the highest information gain for patient application. Information gain measures how much information a feature provides about the class [136]. Therefore, the control range with the highest information gain was selected when the state variables value of the new patient was tested. Then the best historical control strategy was selected from the control range with the most positive and effective feedback to be the learning control for this new patient. Finally, the system used Eq. (3.24) to combine the learning control with the optimal control strategy.

3.3.3 Predicted Learning Method Based on Evidence Database

The predicted learning method utilizes only state variable data (i.e., evidence) and corresponding control strategy with more positive and effective feedback to train a machine learning model. Data with more positive and effective feedback can be defined as the top percent of good data that improve objective function value. The predicted learning method is primarily used to train a model to predict an exact control for each new state variable value; we did not classify the evidence database into groups as in the case-based learning method.

3.3.3.1 Supervised Regression Method

Classification is a supervised learning approach in which the output is provided with the input; it learns from the input and output, and find a relation among the input and output [137]. This determined relationship can help predict the correct output for the new input. Initially, the evidence database is divided into two sets: the good data set and bad data set, based on predefined feedback results. Then the bad data set is deleted and only trained our model using controls from good data set results in the positive and effective feedback. We labeled state variable x_i (i = 1, 2, …, n) as input and then used the corresponding control u_i (from the evidence database derived from the traditional optimal control method) as output. We then established relationships between the input x_i and the output u_i via the linear regression or logistic regression method. Finally, we utilized this relationship to predict the final learning control strategy for the new data.

3.3.3.2 Neural Network Method

Neural network, a popular tool in machine learning for predictive models [138], is comprised of hidden layers for analyzing and learning the data; each hidden layer tries to detect patterns among the input and output. When a pattern is detected, the next hidden layer is activated. First, since the predicted learning control $u_{learning}(t)$ is continuous, we divided the control $[u_l, u_u]$

into j different ranges, and we labeled each range k as the certain output variable y_k, , $k = 1, \ldots, j$. Then we applied the neural network to establish relationships between the input data and the control (output). For example, when information for a new patient was added to the database, the neural network was used to predict the corresponding output (e.g., a most-possible outcome of a sepsis episode for the patient). Finally, we suggested the control range that generated the most positive and effective predictive output as the optimal control strategy for the new patient.

3.3.4 Simulation Assumption

This section lists several assumptions related to our specific application for determining optimal control strategies for septic patients.

Day *et al.* stated that an early pro-inflammatory mediator has controllability [139]. Therefore, we added a control (considering the error), $p(t)u(t)$, into the early pro-inflammatory portion of our sepsis model. Then the model (3.1)-(3.3) becomes as the following model:

$$\frac{dS}{dt} = k_S S(t)\big(1 - S(t)\big) - k_{Sm} m(t) S(t) \tag{3.26}$$

$$\frac{dm}{dt} = (k_{mS} S(t) + l(t)) m(t)(1 - m(t)) - m(t) + p(t)u(t) \tag{3.27}$$

$$\frac{dl}{dt} = k_{lm} f\big(m(t)\big) - k_l l(t) \tag{3.28}$$

The following objective function was used to eliminate the pathogen population and pro-inflammatory mediators to ensure patients do not experience acute inflammation:

$$J = \min_{u(t)} \int_{t_0}^{t_f} a_1 S(t) + a_2 m(t) + a_3 l(t) + a_4 u(t)^2 dt \tag{3.29}$$

where a_i ($i \in \{1,2,3,4\}$) represents the weight of the pathogen population, early pro-inflammatory mediators, late pro-inflammatory mediators, and control. The parameter reference table is shown in Table 3.1.

Table 3.1 Simulation parameter reference table [139]

Parameters	Estimated values	Parameters	Estimated values
k_S	0.021–2.44/hr	k_{lm}	0.35 units of D/hr
k_{Sm}	0.6/M units hr	k_l	0.02/hr
k_{mS}	0.01/P units hr	θ	1
w	0.5	a_1	4.154
a_2	0.112	a_3	0.1
a_4	20		

3.3.5 Simulation

This section presents several simulation experiments to examine the effectiveness of the optimal control created by the EBOC method. Section 3.3.5.1 presents the simulation results of a deterministic sepsis system with no control. Section 3.3.5.2 obtains simulation results to demonstrate that the traditional optimal control works well for a deterministic system, but it is ill-suited for stochastic systems. The first simulation, which was for the deterministic sepsis system with traditional optimal control, proved that traditional optimal control is effective for the deterministic system. The second simulation applied traditional optimal control to the stochastic sepsis system with random errors. Simulation results indicated that traditional optimal control is ineffective for the stochastic system. Section 3.3.5.3 describes another designed simulation to demonstrate that the EBOC is effective for the stochastic system.

3.3.5.1 Model Simulation without Control

In a comparison among the EBOC control method, traditional optimal control method, and the empty-control method, the Runge-Kutta method was used in Eqns. (3.26)-(3.28) to obtain results of a model without control. For example, the iteration function for Eq. (3.26) should be

$$S_{t+1} = S_t + \frac{h}{6}(ks_1 + 2ks_2 + 2ks_3 + ks_4) \tag{3.30}$$

$$ks_1 = 3S_t(1 - S_t) - 30m_tS_t = S(S_t, m_t, l_t) \tag{3.31}$$

$$ks_2 = S(S_t + \frac{h}{2} * ks_1, m_t + \frac{h}{2} * km_1, l_t + \frac{h}{2} * kl_1) \tag{3.32}$$

$$ks_3 = S(S_t + \frac{h}{2} * ks_2, m_t + \frac{h}{2} km_2, l_t + \frac{h}{2} * kl_2) \tag{3.33}$$

$$ks_4 = S(S_t + h * ks_3, m_t + h * km_3, l_t + h * kl_3), \tag{3.34}$$

where S_t is the result of the pathogen population at time t; ks_i, km_i, and kl_i $(i \in 1, 2, 3, 4)$ represent the ith increment for pathogens, early pro-inflammatory mediators, and late pro-inflammatory mediator population, respectively, at time t; and h is the step length.

Using $S_0 = 0.01, m_0 = 0.05$, and $l_0 = 0.179$ as the initial setting and $h = 0.05$ as the step length, the simulation was run for the first 24 hours. The integral of objective function when we did not add control and did not consider error was 4.374. The results of the system variables and the corresponding objective function are shown in Figure 3.2.

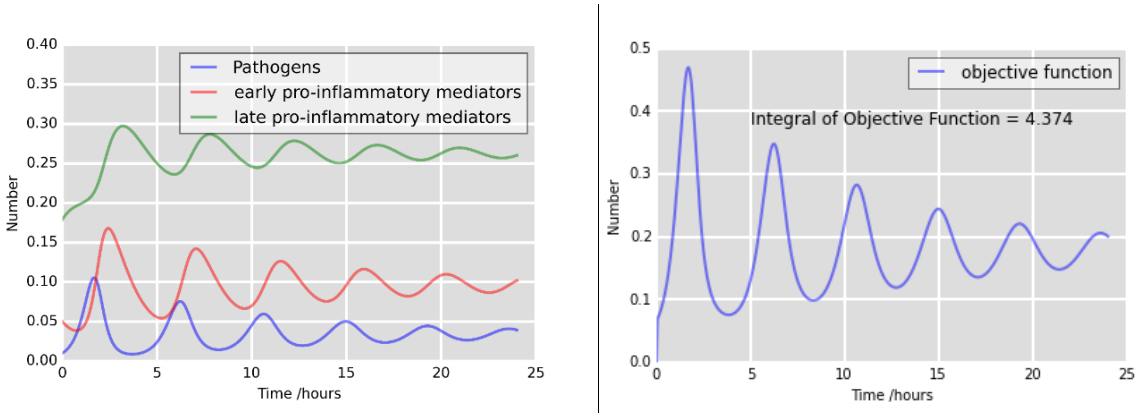

Figure 3.2 Simulation results of model without control and without error

3.3.5.2 Model Simulation with Traditional Optimal Control

Using the objective function defined in Eq. (3.29) and Section 3.2.3, the Hamilton function can be defined as

$$H(u, S, m, l) = a_1 S(t) + a_2 m(t) + a_3 l(t) + a_4 u^2 + \sum_{i=1}^{3} \lambda_i g_i, \tag{3.35}$$

where $\lambda_1, \lambda_2, and\ \lambda_3$ represent the Lagrange multipliers corresponding to pathogens, early pro-inflammatory mediators, and late pro-inflammatory mediators, respectively.

In addition, based on Theorem 3.1, the Lagrange multipliers differential equations can be obtained using the decided objective function:

$$\frac{\partial \lambda_1}{\partial t} = -\frac{\partial H}{\partial S} = -a_1 + \lambda_1 k_S(2S(t) - 1) + \lambda_1 k_{Sm} m(t) + \lambda_2 k_{mS} m(t)(m(t) - 1) \quad (3.36)$$

$$\frac{\partial \lambda_2}{\partial t} = -\frac{\partial H}{\partial m} = -a_2 + \lambda_1 k_{Sm} S(t) + \lambda_2 \big(k_{mS} S(t) + l(t)\big)(2m(t) - 1)$$

$$+\lambda_2 + \frac{\lambda_3 k_{lm}[(f(m(t))-1)^2-1]}{w} \quad (3.37)$$

$$\frac{\partial \lambda_3}{\partial t} = -\frac{\partial H}{\partial l} = -a_3 + \lambda_2 m(t)(m(t) - 1) + \lambda_3 k_l, \quad (3.38)$$

with transversality conditions $\frac{\partial \lambda_i}{\partial t} = 0$ ($i \in 1,2\ and\ 3$).

Since all conditions needed in Theorem 3.2 are contained, the optimal control strategy can be calculated using

$$\frac{\partial H}{\partial u} = 2a_4 u(t) + \lambda_2 p(t) = 0 \quad (3.39)$$

$$u^*(t) = min\{max\left(u_l; -\frac{\lambda_2(t)p(t)}{2a_4}\right); u_u\}. \quad (3.40)$$

However, the initial value problem to calculate $S(t)$, $m(t)$, and $l(t)$ in system Eqns. (3.26)-(3.28) is from t_0 (i.e., $S(t_0)$, $m(t_0)$ and $l(t_0)$ were given), whereas, the initial value problem for solving the Lagrange multipliers (i.e., $\lambda_i(t)$, for i = 1, 2, 3) in Eqns. (3.36)-(3.38) is from t_f. Therefore, an iteration algorithm is required to solve the differential equations with different initial values. Emvudu *et al.* introduced an algorithm to calculate the optimal control strategy for the tuberculosis model [96]. Our research transferred the algorithm and applied it to the acute inflammatory control strategy.

Algorithm 3.1:

Step 1. Initialize the control $u(t)$ as a constant control in the whole simulation time zone.

$$u(t) = c, t \in [0, t_f], c \in [u_l, u_u]$$

Step 2. Calculate the result of system differential Eqns. (3.26)-(3.28) based on the Runge-Kutta method with their initial status and control $u(t)$.

Step 3. Use the Runge-Kutta method to backward calculate the Lagrange multipliers by differential Eqns. (3.36)-(3.38).

Step 4. Calculate the new control $u(t)$ using Eq. (3.40).

Step 5. Use the new control to replace the previous control strategy. Repeat steps 2, 3, and 4 until the control strategy is stable.

The only uncertain component remaining was the random errors $p(t)$. If we assume no errors exist in the clinical processes, then this system is ideal and without error, which means the traditional control strategy is identical to the final control strategy. Therefore, $p(t) = 1$ is suitable for $t \in [0, t_f]$, and according to the description in Section 3.2.3, the traditional optimal control strategy is the optimal strategy.

Using $S_0 = 0.01, m_0 = 0.05, and\ l_0 = 0.179$ as the initial setting, $h = 0.05$ as the step length, and Algorithm 3.1 to calculate the optimal control strategy, the simulation was run in the first 24 hours. The integral of objective function when we added traditional control into the system without considering error was 3.586. Simulation results are shown in Figure 3.3.

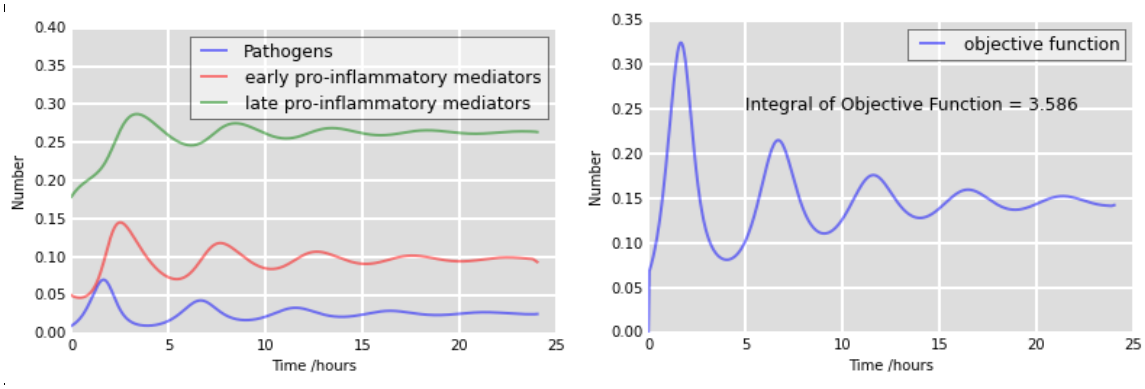

Figure 3.3 Simulation results of the model with traditional optimal control and without error

A review of Figures 3.2 and 3.3 shows that pathogens, early pro-inflammatory mediators, and late pro-inflammatory mediator populations are less in Figure 3.3 and the objective function values at each time in Figure 3.3 are significantly lower than the values in Figure 3.2. Also, the integral of the objective function was 3.586 when we applied traditional optimal control to the system and 4.374 in the no-control model. Therefore, when no random errors were considered in

the system, the traditional optimal control effectively controlled sepsis deterioration and minimized the objective function.

As mentioned in Section 3.1, because random errors cannot be eliminated in real-world clinical processes, system or measurement errors, such as error due to approximation, medical error [115], or control errors due to the uncertain stochastic system process. However, researchers often cannot find details about the error vector, $p(t)$, even these errors do exist in many real-world systems. Thus, we assume that the errors, $p(t)$, follows an unknown distribution. We have tried different distributions for the errors $p(t)$, we found from our computational results the proposed EBOC method works for all of them, and the control quality mostly impacted by the size of the variance in the error vector $p(t)$.. Therefore, in simulation analysis throughout the rest of this paper, we only present a set results with a specific uniform distribution in range (0, 1) for the errors $p(t)$.

Below we conducted a simulation to determine if the traditional optimal control method is still effective and optimal for a clinical process with random errors $p(t)$. Using $S_0 = 0.01, m_0 = 0.05, and\ l_0 = 0.179$ as the initial setting, $h = 0.05$ as the step length, and Algorithm 3.1 to calculate the traditional optimal control strategy of a model with random errors; the simulation was run in the first 24 hours. Random errors followed uniform distribution from 1 to 1.4, and the integral of the objective function was 4.964. Simulation results when we applied traditional optimal control to the system with errors are shown in Figure 3.4.

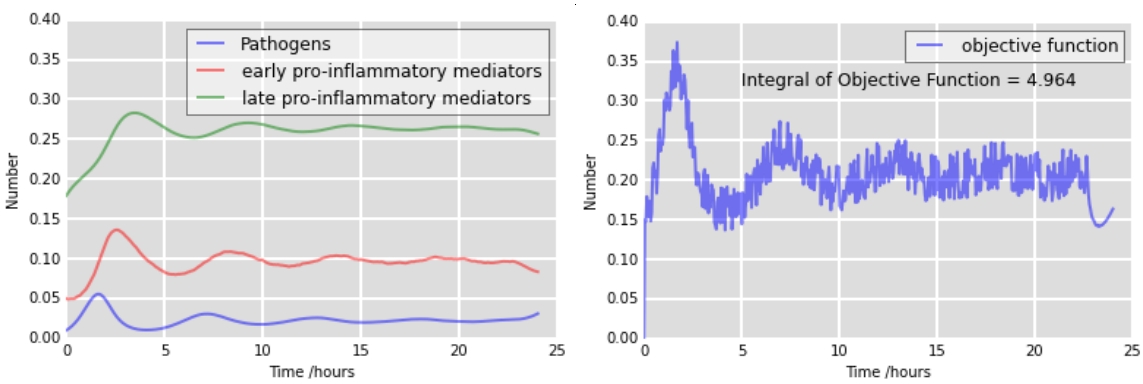

Figure 3.4 Simulation results of the model with traditional optimal control and with errors

Because the system contained errors, the tendencies of pathogens, early pro-inflammatory mediators, and late pro-inflammatory mediators showed stochastic characteristics, although the stochastic property was not obvious since we only considered the sepsis trend of the first 24 hours. The original deterministic sepsis model became stochastic when we accounted for random error in the system; thus, the model controls were also stochastic.

Figure 3.4 shows the results of implementing traditional optimal control into the stochastic sepsis model. A comparison of Figure 3.3 and Figure 3.4 shows that the objective function at each time in Figure 3.3 is lower than in Figure 3.4. Also, when we implemented the traditional optimal control to the original deterministic sepsis model without considering error, the integral of the objective function was 3.586, whereas the integral of objective function when we implemented traditional optimal control to the stochastic sepsis model with errors was 4.964. Therefore, traditional optimal control is only suitable when the system is deterministic or no existing errors are considered in the system. The simulation results in Figure 3.4 show that traditional optimal control does not perform well for stochastic systems or systems containing random errors.

In the existing literature about the model of immune systems, there is no control algorithm to solve the optimal control problem when the system considers uncertain errors. When the system

considers the system and measurement errors, it is an optimal control problem of an uncertain system. Although there is no study about the optimal control problem for immune systems with uncertain errors, a paper [140], proposed an optimal control algorithm for the uncertain system. To verify that EBOC method is more effective than other existing algorithms for the uncertain stochastic system with the same initial setting, we design another simulation for applying the algorithm in paper [140] into our sepsis system with errors. Simulation results when we applied this optimal control algorithm to the system with errors are shown in Figure 3.5.

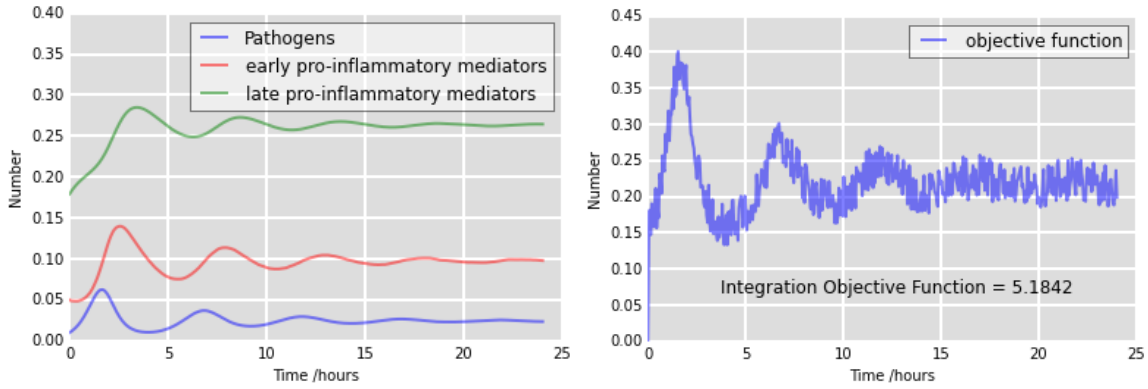

Figure 3.5 Simulation results of the model with optimal control in paper [140] and with error

When the system considers possible errors, the errors part $p(t)$ can be either positive or negative, so the lower bound of control strategy in our system is 0. Thus, the optimal control at each time period obtained by the algorithm in paper [140] is set to be either 0 or u_l. While the control value of traditional optimal control presented in Section 3.3.5.2 can be any value between $[0, u_l]$ at each time period. Therefore, it's reasonable that the results of this algorithm is slightly worse than the traditional optimal control method in our system. Therefore, we will apply the EBOC method to the stochastic sepsis model with random errors to verify suitability and effectiveness for the model in the next section.

3.3.5.3 EBOC Methods Compared to Traditional Optimal Control by Simulation

Because the traditional optimal control method is not effective when random errors are considered in the dynamic system, we attempt to verify if EBOC methods could more efficiently control sepsis deterioration and minimize the objective function. Therefore, this section simulates the application of four EBOC methods (described in Sections 3.3.2–3.3.3) to the stochastic sepsis model with random errors in the system.

An evidence database based on historical simulation data was built prior to the simulation runs. We set random initial status ($S_0 = U(0.005, 0.015), m_0 = U(0.025, 0.075), and\ l_0 = U(0.09, 0.27)$, where $U(a, b)$ is a random number following uniform distribution from a to b) for eight simulation training patients. Using the traditional optimal control method with simulation step $h = 0.05$ and assuming random error followed uniform distribution from 1 to 1.4, the simulation was run for 24 hours, resulting in 3832 data (8*(480-1) based on the database collection method (Section 3.3.1) in the evidence database.

The evidence database was set up after data collection, and then the case-based EBOC method and the predictive model EBOC method were ready for use. Using $S_0 = 0.01, m_0 = 0.05, and\ l_0 = 0.179$ as the initial setting, $h = 0.05$ as the step length, and $\alpha = 0.2$ as the assumed learning factor (parameter optimization will be discussed in Section 3.4), the learning control was calculated based on the clustering method in the first 24 clinical hours. Results of the integral of the objective function for the system using different methods are shown in Figure 3.6.

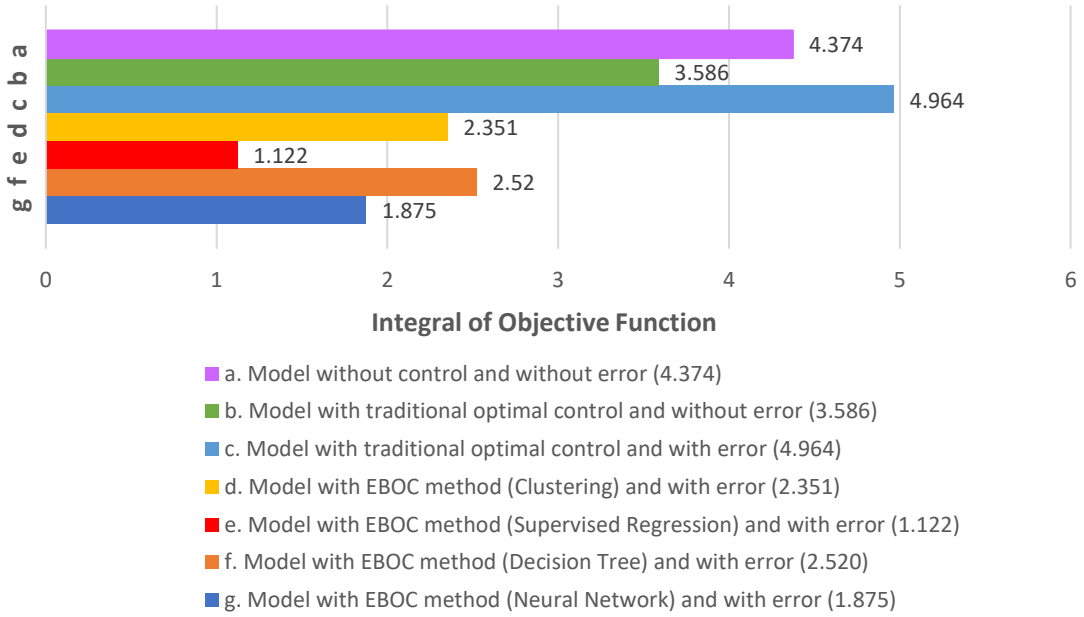

Figure 3.6 Comparison of integral of the objective function using different control strategies

Results shown in Figure 3.6 show that four EBOC methods (i.e., unsupervised clustering, supervised regression, decision tree, neural network) all performed better than traditional optimal control when the system contains random errors. Either unsupervised or supervised machine learning approach we added to the traditional optimal control strategy all controlled the progression of sepsis and decreased the total cost for the stochastic sepsis system.

3.4 Heuristic Algorithm and Simulation Results

3.4.1 Heuristic Algorithm to Determine Unknown Parameters

A comparison of EBOC algorithms with four learning methods in Figure 3.5 revealed that EBOC with the supervised regression learning method is the optimal approach for the sepsis model with the specific initial setting ($S_0 = 0.01, m_0 = 0.05, and\ l_0 = 0.179$). However, parameter settings still needed to be defined since the goal was to maximize the survival rate.

Assume n undetermined parameters and that the value of each parameter can be at least c possible numbers totaling c^n possibilities, thereby requiring determination of the ideal setting of

parameters from c^n possible solutions. Cook *et al.* identified this as an NP problem [129], and theorem 3.3 proved it is an NP-hard problem.

Theorem 3.3: Determination of the best setting of unknown parameters for the EBOC method is an NP-hard problem.

Proof: The reduction is from the quadratic program [141], which is an NP-complete problem proved by Sahni.

Quadratic Programming:

INSTANCE: Finite set X of pairs $(\bar{x}, b)$, where $\bar{x}$ is an m-tuple of rational numbers and b is a rational number, two m-tuples $\bar{c}$ and $\bar{d}$ of rational numbers and a rational number B.

QUESTION: Is there an m-tuple $\bar{y}$ of rational numbers such that $\bar{x}\bar{y} \leq 0$ for all $(\bar{x}, b) \in X$ and such that $\sum_{i=1}^{m}(c_i {y_i}^2 + d_i y_i) \geq B$, where c_i, y_i, and $d_i$denote the i^{th} components of $\bar{c}, \bar{y}$, and $\bar{d}$, respectively?

The objective function for the EBOC method is shown in Eq. (3.29). We can transform y_1, y_2, y_3, and y_4 to $S(t)$, $m(t)$, $l(t)$, and $u(t)$, respectively, and then transform c_1, c_2, c_3, and d_4 to a_1, a_2, a_3, and a_4, respectively. Also, let d_1, d_2, d_3 and c_4 equal zero.

For each time epoch t, minimizing the objective function is equivalent to or harder than finding a rational number B. Besides, because the constraints from Eqns. (3.26)-(3.28) are stricter than constraints in quadratic programming, the optimal control portion of the EBOC method is at least as hard as the quadratic programming problem.

The problem also must determine unknown parameters in the learning control portion of the EBOC method, such as the learning factor α mentioned in Eq. (3.26). In summary, the hardness of the problem to determine the ideal setting of unknown parameters for the EBOC method is at least equivalent to the computational complexity of solving the quadratic programming problem.

In 1989, De Jong *et al.* first asserted that the GA could be utilized to solve an NP problem [142]. Therefore, our research utilized the basic logic of GA to find the optimal setting of unknown parameters. The detailed algorithm is shown below.

GA algorithm to determine unknown parameters of EBOC:

Step 1: Randomly initialize 4 children solutions, where each parent solution represents one setting of parameters. Calculate the objective functions and record the best result. Also initialize the $\text{current iteration} = \text{record iteartion} = 0$.

Step 2: Then consider 4 children solutions as parent solutions. Calculate the heritability for each parent based on their objective function result.

Step 3: Birth 6 new children by the combinations of different parents ($C_4^2 = 6$). Each child will be randomly changed one number to represent the mutation process.

Step 4: Calculate the objective functions for 6 new children and record the new best result. Eliminate 2 children with the worst results and keep other 4 children based on their objective functions.

Step 5: Check if the new best result is better than the old best result. If yes, then update $\text{current iteration} = \text{current iteration} + 1; \text{record iteartion} = 0$ and return to Step 2. Otherwise, move to Step 6.

Step 6: Check if the current iteration is less than max iteration and record iteration is less than max record iteration. If yes, then update $\text{current iteration} = \text{current iteration} + 1; \text{record iteartion} = \text{record iteartion} + 1$ and return to Step 2. Otherwise, move to Step 7.

Step 7: Break the loop and export the best solution.

3.4.2 Heuristic Optimization Result

This paper has focused on two important unknown parameters: learning factor α and the size of the evidence database. Learning factor, as defined in Section 3.2.3, is used to balance the optimal control and learning control. The range of learning factor α is from 0 to 1. The size of the evidence database determines how many data is used in the learning process. The size range for the evidence database is from 0 to infinity. To make the GA algorithm available for use, the maximal size of the database was set to 4550.

We utilized the six-order binary system to represent the unknown parameters and then scaled the binary numbers into their corresponding range. For example, learning factor α in a

binary number is [0 1 0 1 1 1], so the real number of this factor is $\text{binary number} * \text{ratio} = 23 * \frac{1}{63} \approx 0.365$.

The objective function is the core of the GA iteration loop since the update process is based on the objective function result. We defined the objective function in Eq. (3.29); we integrated the objective function values over time. Using the initial setting of system variables mentioned in Section 3.3.4 (i.e., $S_0 = 0.01, m_0 = 0.05, and\ l_0 = 0.179$) and other pre-determined parameters from Table 3.1, we utilized the GA algorithm described in Section 3.4.1 by starting from four random parent parameters settings (shown in Table 3.2). The first six-digit binary number represented the size of the evidence database; the last six-digit binary number corresponded to the learning factor α.

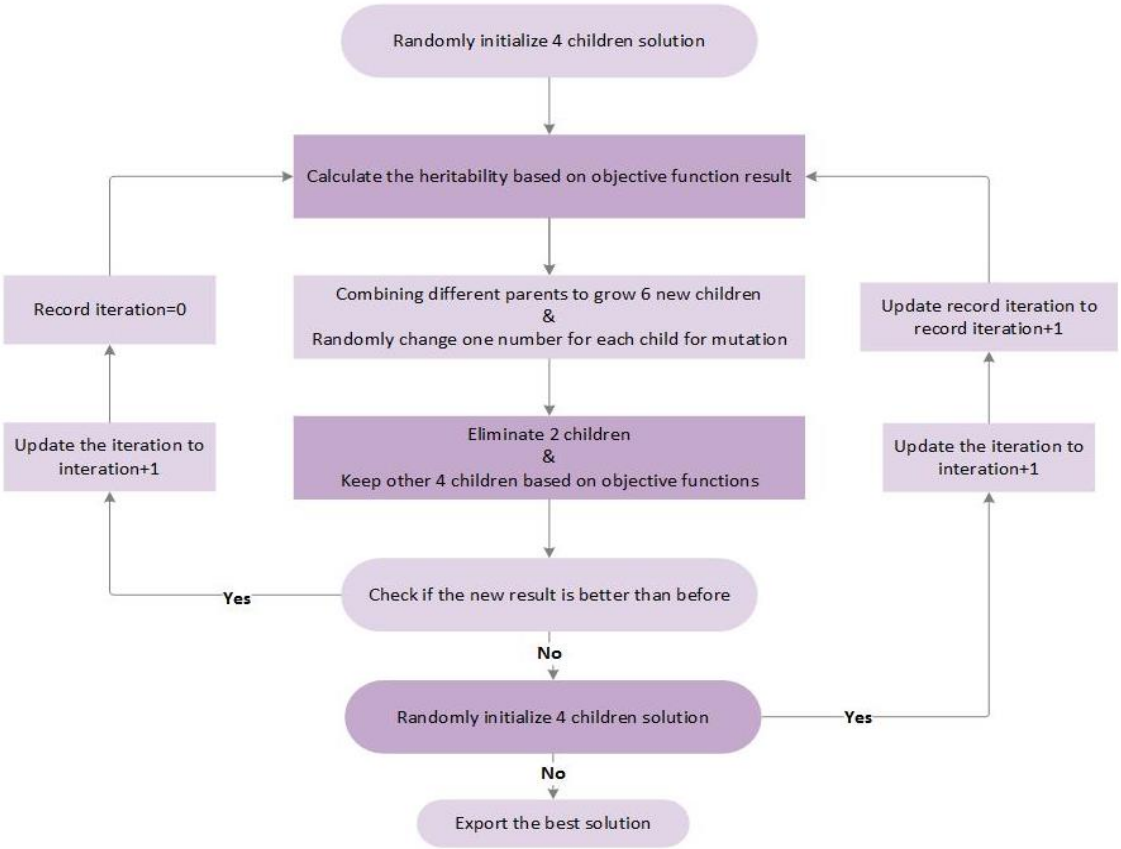

Figure 3.7 Flowchart of GA algorithm

Table 3.2 initial parent setting of unknown parameters

Parent settings	1	2	3	4
Binary number	0 0 0 1 1 0 1 1 1 0 0 1	1 0 0 1 0 0 0 0 1 0 0 1	1 1 1 0 0 1 0 0 1 1 0 1	0 1 0 0 1 1 0 1 1 1 1 1
Database size	432	2592	4104	1368
Learning factor α	0.90476	0.14286	0.20635	0.48206
Integral of objective function	1.62716	1.03110	1.05453	1.28652

To exclude contingency given by maximum iteration and maximum record iteration setting, multiple experiments with various settings were implemented. The results of the experiments are shown in Table 3.3.

Table 3.3 GA heuristic algorithm results

Experiment settings	1	2	3
Maximum iteration	100	300	500
Maximum record iteration	30	90	200
Stop iteration	48	151	342
Stop record iteration	30	90	200
Final binary number	1 1 0 1 0 0 0 0 0 1 1 0	1 1 0 0 0 1 0 0 0 1 1 0	1 1 1 0 0 0 0 0 0 1 0 0
Database size	3744	3528	4032
Learning factor α	0.09524	0.09524	0.09524
Integral of objective function	1.02784	1.02476	1.02024

Experiment settings	4	5	6
Maximum iteration	1000	2000	10000
Maximum record iteration	500	1000	5000
Stop iteration	716	1309	5317
Stop record iteration	500	1000	5000
Final binary number	1 1 0 0 0 1 0 0 0 1 1 1	1 1 0 0 0 1 0 0 0 1 0 0	1 1 0 0 0 1 0 0 0 1 1 0
Database size	3528	3528	3528
Learning factor α	0.11111	0.06349	0.09524
Integral of objective function	1.02022	1.01886	1.02063

Based on results in Table 3.3, all six integral results of objective function were similar (around 1.02), suggested sizes of databases were approximately 3,500 and suggested learning factors were around 0.1. In general, the GA heuristic algorithm is stable with different maximum iterations and maximum record iteration settings. Since the goal of this research was to minimize the objective function, the result with the lowest integral of the objective function was the optimal result, meaning the GA heuristic algorithm determines the learning factor α to be 0.06349 and the size of the evidence database to be 3528.

Implementing the simulation with parameters created by the GA heuristic algorithm and the initial setting of system variables mentioned in Section 3.3.4 ($S_0 = 0.01, m_0 = 0.05, and\ l_0 = 0.179$), this system chose only the supervised regression method to find learning control. The running time was 24 hours (h = 0.05 as step length). Simulation results for tendencies of the system variables, final EBOC control, and the objective function are shown in Figures 3.8-3.10.

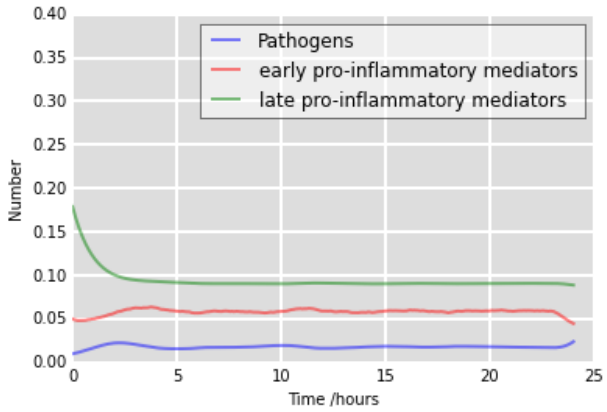

Figure 3.8 The tendency of final system variables with GA-suggested parameter values

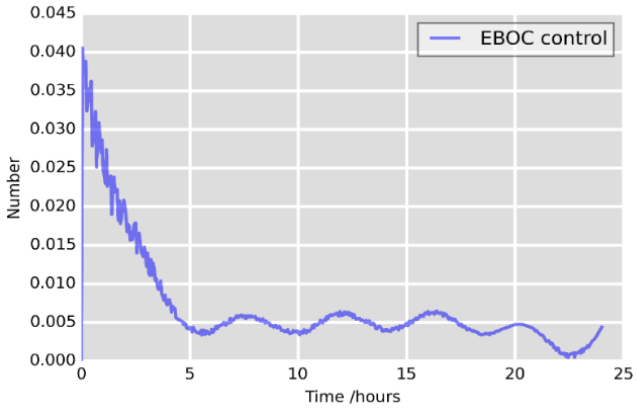

Figure 3.9 Final EBOC control with GA-suggested parameter values

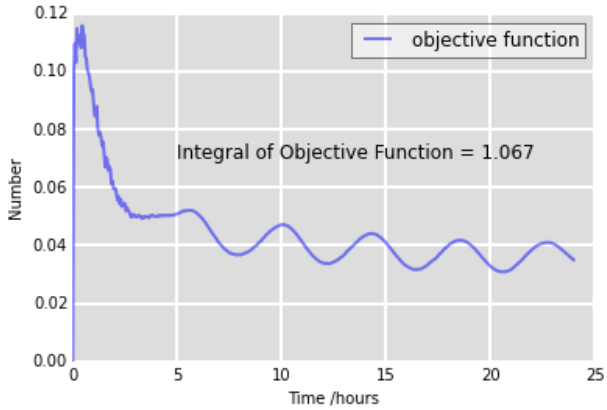

Figure 3.10 Final objective function with GA-suggested parameter values

Figures 3.8-3.10 show that the trend of pathogens, early pro-inflammatory mediators, and late pro-inflammatory mediators declined noticeably. Also, the objective function at each time decreased after we used the GA heuristic algorithm to find a parameter setting to improve the final control strategy. The integral of the objective function was 1.067, whereas Figure 3.6 shows that the integral of objective function without using parameters created by the GA algorithm was 1.122. Therefore, the parameters setting created by the GA algorithm improves the performance of the final control for preventing sepsis progression and decreasing the total cost of the objective function.

3.5 Summary and Discussion

This paper presented a new EBOC method that can be applied to stochastic optimal control systems or systems containing random errors. The EBOC method combines the traditional optimal control strategy and machine learning algorithm to provide a suitable and effective optimal control for stochastic systems. Several simulation experiments were conducted to verify the effectiveness of the EBOC method. Simulation results showed that traditional optimal control is only suitable and effective for deterministic systems, not stochastic systems or systems containing random errors. Regardless of the machine learning algorithm applied, when we applied the EBOC method to the system containing random errors, the results showed significantly better control effectiveness for suppressing disease epidemic and regulating overall cost. The EBOC method proposed in this paper is a novel and effective tool to find the optimal control strategy for stochastic systems. Based on the sepsis model (Eqns. (3.2)-(3.4)) our research results can help the healthcare providers have a better understand the sepsis progressions while determining and adjusting the corresponding treatment plans. Firstly, the optimal control problem presented utilizes the underlining sepsis model (i.e., Eqns. (3.2)-(3.4)), and incorporate possible measuring errors and uncertainties due to the physiology differences from various patients and patients' responses toward the current treatment plan. The proposed EBOC method uses the prior patient/treatment database to study the relationships between the controls (treatments) and the effects (patients' responses) after each control adjustment. Through studying the historical progressions of septic patients after applying the optimal control, the EBOC method can also help analyze the errors/uncertainties between the real effects and the theoretical effects in real clinical settings. Due to the existences of errors/uncertainties in the sepsis/treatment model, the EBOC method can be used to calibrate the

traditional optimal control, so that the treatment effects can be better predicted via the EBOC control methodology using various Machine Learning algorithms.

Because the main purpose of combining the traditional optimal control method with machine learning method is to revise and improve traditional optimal control for stochastic systems, this paper focused on only four machine learning algorithms to use with traditional optimal control. However, the EBOC method always provided more practical and effective optimal control when stochastic random errors were present, proving that other machine learning methods can be utilized, no matter the chosen machine learning. Moreover, the performance of the optimal control strategy was further improved using the EBOC method when the GA heuristic algorithm was utilized to determine the appropriate setting of unknown parameters. This paper only implemented simulation among a sepsis system with random errors, but the EBOC approach could easily be generalized to systems other than sepsis-diseased models, including other stochastic optimal systems or control systems with random or measurement errors. Since the proposed method is developed based on the traditional optimal control method, it will remain some limitations of the traditional optimal control method. So it can only be used to solve the optimal control problems with the twice differentiable convex objective functions. The control strategy generated by the proposed method is valid for a single initial state, and if the initial states changed, we would have to solve the problem again. Also, since the control obtained by the proposed method includes two parts: the traditional control and the learned control. The learned control is generated by learning from the evidence database. Therefore, the accuracy of the optimal control calculated by the proposed method relies on the size of the evidence database. When the size of the evidence database is larger, the proposed method can learn more accurately from the database, which will allow the proposed method to produce more effective and accurate control strategies.

Chapter 4 - A Computational Scheme for Stochastic Disease Optimal Control System with Variance Constraint

Abstract

Uncertainty or random behaviors in a system cause complication when solving the stochastic optimal control problem to obtain an analytical solution. Previous research of stochastic optimal control problems have primarily attempted to minimize the expected value of the objective function, but system variances may be significant, meaning the current solution may not guarantee system stability. This paper proposes a revised algorithm for a class of stochastic optimal control problems with the quadratic objective function. The revised algorithm provides an effective control strategy that minimizes expected costs and controls system variance in a specific range, thereby guaranteeing system stability.

Keywords: Computational scheme, optimal control, stochastic optimization, variance constraint.

4.1 Introduction

Optimal control is a mathematical optimization approach to finding a control policy for a given dynamic system over time. Recently stochastic optimal control systems have attracted much attention [143]. A variety of stochastic optimal control and applications have been proposed, such as neuro-optimal control for unknown nonlinear systems, power management for stochastic dynamic system with Markov process, stochastic control in delayed networked control systems, inventory control strategies for the inventory-location problem with stochastic capacity constraints and stochastic optimal control in healthcare area for solving better clinical treatment [144 - 148]. The goal of many studies about stochastic optimal control is to find an effective algorithm that can

estimate system states and find the optimal control solution to minimize the expectation of the objective function.

The stochastic maximum principle, proposed by Kushner [149] and developed by Haussmann in the 1970s [150], is a useful tool for solving the stochastic optimal control problem. Although this principle has previously been applied in various systems [151 - 155], it does not readily identify the analytical solution of stochastic optimal control problem. Some of researchers typically have used two classic numerical approaches to solve these problems: utilization of finite differences to solve the Hamilton-Jacobi-Bellman (HJB) equation [156, 157] and implementation of the finite-state Markov chain approximation method [149]. In addition, some approximating method, iteration approaches or feedback control algorithms are developed for different dynamic stochastic systems. Chavanasporn *et al.* proposed a numerical approach with quadratic splines by approximating the two-point boundary value problem solution to solve stochastic optimal control problems [158]. Simpkins *et al.* used function approximation to yield the global optimal solution [159], while Huschto *et al.* introduced a Wiener chaos method using Malliavin calculus and Markov control to solve continuous finite-horizon stochastic optimal control problems [160]. Tönissen *et al.* used the decomposition approach to study the stochastic multiple knapspack problem [161]. In [162], an iterative linear-quadratic Gaussian method is developed for solving nonlinear stochastic control problems. Hatami-Marbini *et al.* developed a new network model and combined the simulated annealing, simulation, and Taguchi experimental design to obtain the optimal control strategy [163]. With the stochastic network-induced delays and packet losses, an optimal decentralized state-feedback controllers for systems with quadratic cost function is presented in [164]. It is easy to find that most of approaches are developed for solving the optimal

control strategy that only minimizes the expected value of the objective function in stochastic systems.

However, the minimum expected value does not guarantee system invariance or remain in a specific range. The case that optimal control solution with minimum expectation for stochastic system is difficult to guarantee the system stability. Therefore, in this work, our aim is to develop an optimal control algorithm named revised forward-backward sweep (RFBS) algorithm for solving the stochastic optimal control problem that can minimize the expected value of system, at the meantime, the variance of system can be reduced or controlled. The obtained simulation results demonstrate the performance and effective of the proposed algorithm.

This paper is organized as follows: The problem statement and analyzes forms of the control strategy are given in Section 4.2. The Revised Forward-Backward Sweep (RFBS) algorithm only for minimizing the expected value of objective function is presented in Section 4.3.1. The RFBS algorithm for both minimizing the expected value and variance of system is proposed in Section 4.3.2. In Section 4.4, the related simulations are given to demonstrate the effective of the propose RFBS algorithm. Finally, a brief conclusion is drawn in Section 4.5.

4.2 Stochastic Optimal Control Problem Statement

The stochastic system can be considered as the following equation:

$$dx(t) = f\big(t, x(t), u(t)\big)dt + \sigma\big(t, x(t), u(t)\big)dW \tag{4.1}$$

where $x(t)$ is the state variable of the system at time t, and $u(t)$ is the system control at time t, where $u \in [u_l, u_u]$, in which u_l is the nonnegative lower bound and u_u is the upper bound of control vector u. The time period under control is denoted by $t \in [t_0, t_f]$, where t_0 is the start time, and t_f is the end time under study. W is the standard Wiener process, $f(t, x(t), u(t))$ is assumed to be continuous and differentiable, and $\sigma(t, x(t), u(t))$ denotes the stochastic part of the system.

Because the dynamics in stochastic optimal control problems are stochastic and uncertain, the expected values of the objective function must be minimized:

$$V(t, x(t), u(t)) = \min_{u} E[\phi(t, x(t), u(t))] \tag{4.2}$$

where $\phi(t, x(t), u(t))$ represents the cost function, which is presumably twice differentiable, and the optimal solution (t^*, x^*, u^*) that minimizes $E[\phi(t, x(t), u(t))]$ is assumed.

Based on the maximum principle, the HJB equation [165] of the stochastic problem in Eqns. (4.1) and (4.2) can be written as

$$\min_{\{u\}} \{\psi\} = 0 \tag{4.3}$$

where

$$\psi = \frac{\partial V}{\partial t} + f\big(t, x(t), u(t)\big)\frac{\partial V}{\partial x} + \frac{1}{2}\Big(\sigma\big(t, x(t), u(t)\big)\Big)^2 \frac{\partial^2 V}{\partial x^2} \tag{4.4}$$

At the minima of Eq. (4.4), the following three conditions must be satisfied:

$$\psi(u^*) = 0 \tag{4.5}$$

$$\frac{\partial \psi(u^*)}{\partial u} = 0 \tag{4.6}$$

$$\frac{\partial^2 \psi(u^*)}{\partial u^2} > 0 \tag{4.7}$$

According to Eq. (4.6), the following can be obtained:

$$\frac{\partial V}{\partial x}\frac{\partial f}{\partial u} + \sigma \frac{\partial \sigma}{\partial u}\frac{\partial^2 V}{\partial x^2} = 0 \tag{4.8}$$

The explicit form for the optimal control u^* can be obtained by solving Eq. (4.8), and then, by substituting u^* into Eq. (4.5), the partial differential equation for the value function (Eq. (4.6)) can be written as

$$\frac{\partial V}{\partial t} + f(t, x, u^*)\frac{\partial V}{\partial x} + \frac{1}{2}\big(\sigma(t, x, u^*)\big)^2 \frac{\partial^2 V}{\partial x^2} = 0 \tag{4.9}$$

with the limit condition $V\big(t_f, x, u\big) = \phi(t_f, x, u)$ when $t = t_f$.

Because $V(t,x,u)$ is assumed to be twice differentiable, explicit solutions can be calculated for special forms of $V(t,x,u)$:

- $V(t,x,u)$ is power form:

$$V(t,x,u) = \frac{x^{\gamma}}{\gamma} + a(t,x,u) \tag{4.10}$$

where $\gamma > 1$, and $a(t,x,u)$ can be any function of x and u. Then,

$$\frac{\partial V}{\partial x} = x^{\gamma-1} + \frac{\partial a}{\partial x},\ \frac{\partial^2 V}{\partial x^2} = (\gamma-1)x^{\gamma-2} + \frac{\partial^2 a}{\partial x^2} \tag{4.11}$$

Then the second-order condition is also fulfilled:

$$\frac{\partial^2 \psi}{\partial u^2}(u^*) = \frac{\partial^2 \sigma}{\partial u^2}\frac{\partial^2 V}{\partial x^2} = [(\gamma-1)x^{\gamma-2} + \frac{\partial^2 a}{\partial x^2}]\ \frac{\partial^2 \sigma}{\partial u^2} > 0\ (with\ \gamma > 1\ ) \tag{4.12}$$

Therefore, the explicit optimal control solution can be derived using Eq. (4.8).

- $V(t,x,u)$ is the exponential form:

$$V(t,x,u) = \frac{1}{c}e^{cx} + b(t,x,u) \tag{4.13}$$

where $c > 0$, and $b(\mathrm{t},x,u)$ can be any function of x and u. Then,

$$\frac{\partial V}{\partial x} = e^{cx} + \frac{\partial b}{\partial x},\ \frac{\partial^2 V}{\partial x^2} = ce^{cx} + \frac{\partial^2 b}{\partial x^2} \tag{4.14}$$

Then the second-order condition is also fulfilled:

$$\frac{\partial^2 \psi}{\partial u^2}(u^*) = \frac{\partial^2 \sigma}{\partial u^2}\frac{\partial^2 V}{\partial x^2} = (ce^{cx} + \frac{\partial^2 b}{\partial x^2})\ \frac{\partial^2 \sigma}{\partial u^2} > 0\ (with\ c > 0\ ) \tag{4.15}$$

Therefore, the explicit optimal control solution can be derived using Eq. (4.8).

4.3 Revised Forward-Backward Sweep (RFBS) Algorithm

4.3.1 RFBS Algorithm for Only Minimizing Expected Value

The uncertainty of states for each time in the stochastic system makes it difficult to obtain current system states at each time using the original FBS algorithm. The FBS algorithm sequentially calculates state values in the forward process. Because state values range from lower

bound to upper bound with various probabilities, however, the forward process of the RFBS algorithm calculates the probability of each state's values over time.

To reduce error caused by sequential calculation and obtain more accurate results during the forward process, this study replaced the sequential updates in a stochastic system with an irregular update procedure. The new irregular update procedure uses the antithetic variates in the RBFS algorithm, a common variance reduction technique [166]. Antithetic variates can be calculated as follows. For a given set of samples, $x_1, x_2, \dots, x_n$, the antithetic sample, $x_1', x_2', \dots, x_n'$ are calculated as $x_i' = 1 - x_i$ $(i = 1, 2, \dots, n)$. Therefore, the resulting variance for antithetic variates $\bar{x}_i$ is

$$var(\bar{x}_i) = var\left(\frac{x_i + x_i'}{2}\right) = \frac{1}{4}\left(var(x_i) + var(x_i')\right) + \frac{1}{2}cov(x_i, x_i') \tag{4.16}$$

Since the variables x_i and x_i' are negatively correlated, the covariance of x_i and x_i', $cov(x_i, x_i')$, is negative. Therefore, the variance term $var(\bar{x}_i)$ is smaller than $var(x_i)$. The RFBS algorithm for minimizing the expected value is given as Algorithm 4.1.

Algorithm 4.1

***Step 1*:** Let the state variable $x \in [\underline{x}, \overline{x}]$. Then divide the range into *n* segments and let the initial state variable $x_0 = (x_1, x_2, \dots, x_n)$ follow a normal distribution with mean μ and standard deviation σ.

***Step 2*:** Randomly select a set of control $(u_1, u_2, \dots, u_{tf})$, with t_f as the ending time.

***Step 3*:** Calculate the probability for each segment x at start time t_0 using the probability density function in the following equation:

$$p(x) = \frac{1}{\sqrt{2\pi\sigma^2}} e^{-\frac{(x-\mu)^2}{2\sigma^2}}$$

***Step 4*:** Apply the antithetic variables technique to implement the forward loop for the stochastic system. According to the system and the values of control, forward calculate the state values for each segment x at the next time in the following order: $x_1, x_n, x_2, x_{n-1}, \dots, x_i, x_{n-i+1}$ using the following equation, where $x_i = 1 - x_{n-i+1}$:

$$x(t+1) = x(t) + \frac{dx(t)}{dt}$$

***Step 5*:** Calculate the probability of each segment x at each time. For any segment x (i.e., x_i, x_j, x_k) at time t, t = 1, 2, …, t_f. If they all transfer to the same segment x_{new} at time t+1, the probability of segment x_{new} at time t + 1 is equal to the sum of probability of all segments (x_i, x_j, x_k) at time t.

***Step 6*:** After obtaining the probability for each segment x at time t, determine the expected value of the state at time t by

$$E(x) = \sum_{i=1}^{n} x_i p(x_i)$$

***Step 7*:** Calculate the expected value of the objective function for time t = 1, 2, …, t_f.

Step 8*:** Calculate the total expected value $E(obj)$ of the objective function, which is the sum of all expected values of the objective function at time t = 1, 2, …, t_f obtained in ***Step 7.

***Step 9*:** After obtaining the total expected values of the objective function, combine the transversality conditions to calculate the expected values of λ_t over time t = 1, 2, …, t_f in a backward manner.

Step 10*:** Determine the expected value $E(u^*)$ of control u^* through λ_t obtained in ***Step 9 using $E(u^*)$ as the value of u^* to update the control.

Step 11*:** Repeat ***Steps 4–***10*** until it satisfies the following convergence condition, where k is the iteration step, and ε is an enough small value:

$$\frac{\left\| E(obj)^{(k)} - E(obj)^{(k+1)} \right\|_1}{\| E(obj)^{(k)} \|_1} \leq \varepsilon$$

4.3.2 RFBS Algorithm for Minimizing Expected Value and Variance

The goal of previous research on optimal stochastic control systems have mostly tended to optimize the expected value of the objective function. However, minimizing the expected value of the system does not guarantee the system stability due to the stochastic nature of the underlining processes. Therefore, this study added one more variance constraint into the RBFS algorithm to make the control strategy obtained by the RBFS algorithm more efficient for the stochastic system. The objective was to minimize the expected objective function value and reduce the system variance.

Using the RFBS algorithm, this study also utilized the Adam algorithm to update the control values. The Adam approach, proposed by Diederik Kingma and Jimmy Ba [167], provides the individual adaptive learning rate through the first moment (mean) and the second moment

(uncentered variance) of the gradients, which combines the benefits of two stochastic gradient descent methods: adaptive gradient algorithm (AdaGrad) and root mean square propagation (RMSProp) [167]. Thus, Adam was added to the RFBS algorithm process to update the control set. Details of the RFBS algorithm for minimizing expected objective and controlling variance is shown in Algorithm 4.2. The flowchart of Algorithm 4.2 is shown in Figure 4.1.

Algorithm 4.2

***Step 1*:** Let the state variable $x \in [\underline{x}, \overline{x}]$. Divide the range of *x* into *n* segments and let the initial state variable $x_0 = (x_1, x_2, \dots, x_n)$ follow a normal distribution with mean μ and standard deviation σ.

***Step 2*:** Randomly select a set of control $(u_1, u_2, \dots, u_{tf})$, with tf as the ending time.

***Step 3*:** According to the probability density function in the following equation, calculate the probability for each segment x at start time t_0:

$$p(x) = \frac{1}{\sqrt{2\pi\sigma^2}} e^{-\frac{(x-\mu)^2}{2\sigma^2}}$$

Step 4: Repeat ***Steps 4–8*** in **Algorithm 4.1**.

Step 5: Calculate the variance of the objective function at each time as $Var(t, x, u)$.

Step 6: Repeat ***Steps 9–11*** in **Algorithm 4.1**.

Step 7: When the expected value of the objective function satisfies the convergence condition and the set of control $u(t)$ is obtained, determine if all variances satisfy range constraint a $\leq Var(t, x, u) \leq b$ at each time. For any variance $Var(t, x, u)$ that satisfies the range constraint, the current control *u*(*t*) remains unchanged. For any variance $Var(t, x, u)$ that does not satisfy range constraint, update the corresponding control $u(t)$ using the Adam method as following:

$$gt = \nabla f\big(u(t)\big)$$

$$mt = \beta_1 * mt + (1 - \beta_1) * gt$$

$$vt = \beta_2 * mt + (1 - \beta_2) * gt^2$$

$$mcap = \frac{mt}{\left(1 - {\beta_1}^2\right)}$$

$$vcap = \frac{vt}{\left(1 - {\beta_2}^2\right)}$$

$$u(t) = u(t) - \frac{\alpha * mcap}{\sqrt{vcap} + \epsilon}$$

Step 8: Repeat ***Steps 4–7*** of **Algorithm 4.2** until all variances $Var(t, x, u)$ satisfy range constraints.

Figure 4.1 Flowchart of Algorithm 4.2

4.4 Simulation

Healthcare agencies and individuals can effectively prevent or mitigate disease epidemics if stochastic transmission processes of infectious diseases can be precisely modeled and controlled. To verify the effectiveness of the RBFS algorithm, the following stochastic susceptible-infected (SI) disease control model was applied for all simulation experiences in this paper [168]:

$$dI(t) = \big(\beta S(t)I(t) - (\mu + \gamma + u)I(t)\big)dt + \sigma S(t)I(t)dW \tag{4.17}$$

where β is the transmission rate, μ is the death rate (assuming the birth rate is equal to the death rate), and γ is the recovery rate. σ and W are defined in Eq. (4.1).

Effective measures to control the spread of disease may reduce infection rate but increase associated costs for executing control. Therefore, the following objective function can be used to potentially reduce the infection rate and minimize implementation costs:

$$minimize \;\; E[a_1 I(t) + a_2 u(t)^2] \tag{4.18}$$

Where the parameter a_1 indicates the treatment cost for the infected population during the period of infection (e.g., medicine, hospitalization expenses, etc.), a_2 is the cost of implementing control before the infection period (e.g., vaccines, cost for environment improvement, etc.).

For example, the World Health Organization (WHO) declared the tuberculosis epidemic in North America in 1993 to be a global emergency [169]. Therefore, this research used the percentages of tuberculosis infections and susceptible populations in San Francisco as a case study for simulation experiments. The total population was defined as $S + I = 1$, with the initial value of infected population I following a normal distribution with a mean of 0.35 and a standard deviation of 0.1. The total time of the simulation experiments was 50 days, and the numerical discrete step length was 0.05 days. In this research, a_1 was the cost of hospitalization and drug treatments for 100% infected people per day. Previous research summarized the approximate

treatment cost for each tuberculosis patient were approximately $47,266 for 19-years of illness [170], while hospitalization expenses for each tuberculosis patient were approximately $16,775 for 6-years of illness [171]. Because the population of San Francisco is approximately 870,887, then $a_1 = 870887 * (\frac{16775}{6*365} + \frac{47266}{19*365})$ per day. A previous study showed prevention costs for each tuberculosis patient to be approximately $3,724 for 6 years [172], thus the cost of implementing control a_2 was assumed to be 870,887*$\frac{3724}{6*365}$ per day. The values of other parameters were $\beta = 0.326655$, $\gamma = 0.04123$, and $\mu = 0.000035$ [171].

Although use of the RFBS algorithm can reveal a set of theoretical optimal control for a system, the control set must be verified as useful and practical for disease prevention. Thus, this research applied theoretical optimal control to the simulation result without control to compare simulation results. To avoid influences due to stochastic components, the results of 20 replications of simulation runs for both settings (i.e., with or without controls) were compared, and the following performance metric was used to compare the control settings:

$$ratio(t) = \frac{I_{wo}(t) - I_w(t)}{I_{wo}(t)} \tag{4.19}$$

where $I_{wo}(t)$ is the infection population without control at time t, and $I_w(t)$ is the infection population with control at time t. Based on the equation, $ratio(t) \leq 1$. If $ratio(t) \leq 0$, then the infection population without control is less than or equal to the infection population with control at time t, indicating that the effect of adding the theoretical optimal control is unnecessary. If $ratio(t) > 0$, then the infection population without control is more than the infection population with control at time t, meaning the addition of the theoretical optimal control was effective. The larger the value of $ratio(t)$, the higher the effectiveness of the control.

4.4.1 Simulation Results of Algorithm 4.1: RFBS Algorithm for Only Minimizing Expected Value

In this section, we provide the simulation and result analysis for Algorithm 4.1 that only minimizes the expected value of system. Figure 4.2 and Figure 4.3 show the simulation results for systems with initial value of $I(0) = 0.369$. Figure 4.2 shows the ratio values to be equal to or greater than 0. After about 10 days, however, the ratio increased, nearing 1 after 40 days, demonstrating that the theoretical optimal control generated by the RFBS algorithm helped mitigate the spread of disease. Figure 4.3 shows the accumulated expected value of the objective function over time; the lines are plotted with error bands showing a confidence interval. As depicted in Figure 4.3, the expected cost function value for the system without control was constantly higher than or equal to the system with control, meaning the theoretical optimal control generated by the RFBS algorithm can lower expected costs.

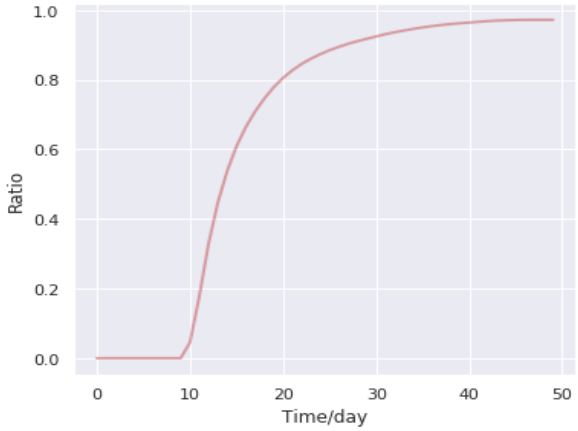

Figure 4.2 Ratio of infected population without variance constraint (initial value: I(0)=0.369)

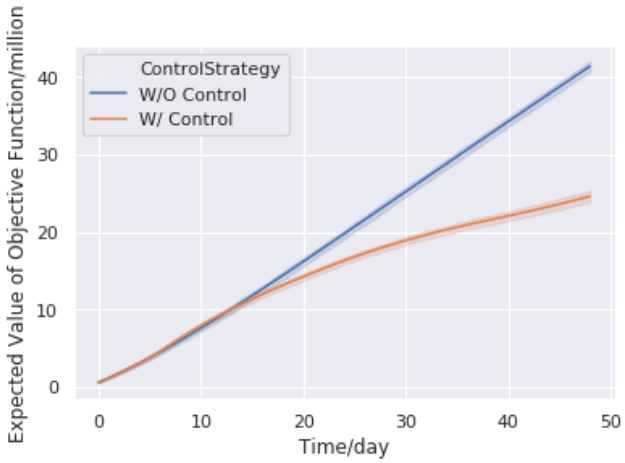

Figure 4.3 Expected value of objective function for 20 tests without variance constraint (initial value: I(0)=0.369)

Since the initial value was fixed, the simulation could not prove that the theoretical optimal control obtained by the RFBS algorithm is always effective for the stochastic system. Therefore, another simulation used the paired *t*-test to verify that the theoretical optimal control is significantly more effective with different initial values. A total of 20 initial system state values were randomly generated, and for each initial system state value, two corresponding expected values were calculated: one for the system with control, and one for the system without control. These two expected values were regarded as the paired sample for the *t*-test analysis, totaling 20 pairs of samples.

Before the *t*-test, the *F*-test was applied to determine if the variances for two samples differed significantly. For expected costs without control, the average variance of the group was 1.574, with a sample size of 20. For expected costs with controlled interventions, the average variance of the group was 1.794, with a sample size of 20. The null hypothesis and alternative hypothesis were

$$H_0: \text{ No difference in } variances \text{ for these two groups}$$

H_1: Difference in variances *for* these two groups

The following equation was used to calculate the *F* critical value, or the highest variance divided by the lowest variance:

$$F\ statistic = \frac{1.794}{1.574} = 1.14 \tag{4.20}$$

The degrees of freedom for both groups was 19, the significance level was $\alpha = 0.025$ (total 5% type I errors for a two-tailed test), and the critical *F* value was $F_{19,19;0.025} = 2.526$. Since *F* statistics calculated from the data were smaller than the critical value from the *F* table, the null hypothesis of no difference in variance for the two groups could not be rejected.

The *t*-test was then used to determine if the means (i.e., expected costs) differed significantly. The null hypothesis and alternative hypothesis were

$$H_0: \ E(with\ control) - E(without\ control) = 0$$

$$H_1: \ E(with\ control) - E(without\ control) \neq 0$$

where $E(with\ control)$ is the expected value of the objective function for the system with control, and $E(without\ control)$ is the expected value of the objective function for the system without control. The null hypothesis indicated no difference between the two systems. The mean and standard deviation of differences were $\overline{d} = -16.803$, $s_d = 1.022$, so the standard error of the mean difference was

$$SE\left(\overline{d}\right) = \frac{s_d}{\sqrt{n}} = \frac{1.022}{\sqrt{20}} = 0.229 \tag{4.21}$$

where *n* = 20. The *t*-statistic (*t*-score) is

$$\frac{\bar{d}}{SE(\bar{d})} = -\frac{16.803}{0.229} = -73.375 \tag{4.22}$$

According to the t-score value in Eq. (4.22), we calculated that the *P*-value is $p < 0.00001$, meaning the control generally leads to improvements. However, calculation of a confidence

interval for the mean difference would beneficially reveal what limits the true difference is likely to lie [173]. The formula of 95% confidence interval for the true mean difference was

$$\overline{d} \pm t_{n-1,1-\frac{\alpha}{2}} \frac{s_d}{\sqrt{n}} \tag{4.23}$$

where $t_{n-1,1-\frac{\alpha}{2}}$ is the 2.5% point of the *t*-distribution on *n* −1 degrees of freedom. Simulation results (Table 4.1 and Table 4.2) showed that the mean difference was −16.803, while the 2.5% point of the *t*-distribution on 19 degrees of freedom was 2.093. Therefore, the 95% confidence interval for the true mean difference was

$$\overline{d} \pm t_{n-1,1-\frac{\alpha}{2}} \frac{s_d}{\sqrt{n}} = -16.803 \pm (2.093 * 0.229)$$

$$= -16.803 \pm 0.479 = (-17.282, -16.324) \tag{4.24}$$

The result can be shown as following tables:

Table 4.1 One-Sample Statistics

	N	Mean	Std. Deviation	Std. Error Mean
Difference	20	–16.803	1.022	0.229

Table 4.2 One-Sample Test

	Test Value = 0					
	t	df	Sig. (2-tailed)	Mean Difference	95% Confidence Interval	
					Lower	Upper
Difference	–73.375	19	.000	–16.803	–17.282	–16.324

Table 4.2 shows that the 95% confidence interval increased from -17.282 to -16.324; since the interval did not contain 0, sufficient evidence was available to reject the null hypothesis, leading to the conclusions that a statistically significant difference in the effectiveness of control was present at the given level of confidence and that the theoretical optimal control could significantly control the spread of disease and lower the total cost. The simulation indicated that if

the RFBS algorithm focuses only on minimizing the expected value of the objective function, it can optimize the objective function without system variance.

4.4.2 Simulation Results of Algorithm 4.2: RFBS algorithm for Minimizing Expected Value and Variance

In this section, we provide the simulation and result analysis for Algorithm 4.2 that minimizes the expected value and the variance of system. Like Section 4.4.1, the same stochastic system with parameter values and initial conditions were used in simulation experiments to verify efficiency of theoretical control to minimize the expected value of the objective function and control the range of system variance.

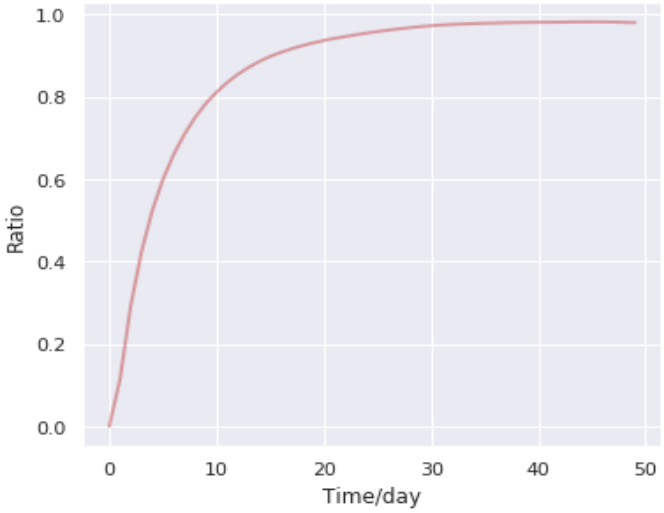

Figure 4.4 Ratio of infected population with variance constraint (initial value: I(0)=0.369)

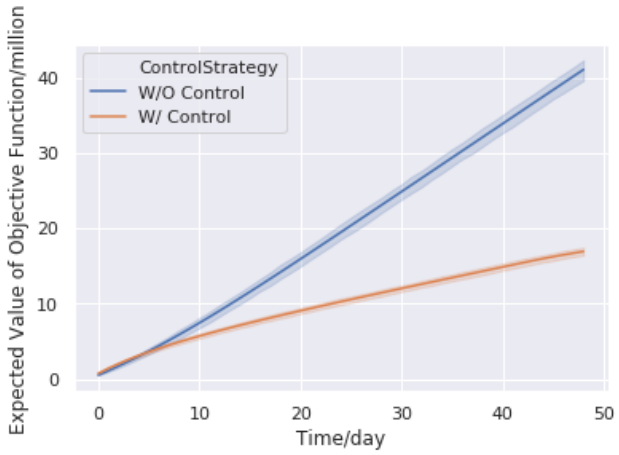

Figure 4.5 Expected value of objective function for 20 tests with variance constraint (initial value: I(0)=0.369)

Figure 4.4 and Figure 4.5 show the simulation results for the RFBS algorithm with variance constraint. According to Figure 4.4, the ratio sharply increased from 0, reaching 1 after approximately 20 days, meaning the control effectively and efficiently reduced the infection population when the variance constraint was added to the RFBS algorithm. Figure 4.5 shows the accumulated expected values of objective function for a system with and without control. The expected value of the cost function for the system without control was significantly larger than or equal to the expected value of the cost function for the system with control over time. The results demonstrate that the controls were more effective when the variance constraints were added into the RFBS algorithm, and the number of infected populations decreased significantly with the same system parameters and initial conditions as the RFBS algorithm without the variance constraint (Algorithm 4.1).

To verify that the theoretical optimal control obtained by the RFBS algorithm when the constraint about variance is added into Algorithm 4.2 not only can reduce the infection population and minimizes the expected value of the objective function, also can control the variance of system,

we did the following *F*-test and *t*-test. For the *F*-test and *t*-test, each sample size of the two groups was 20. Based on simulation results, the variance was 1.843 for the group of expected value without control, and the variance was 0.597 for the group of expected value with control. The null hypothesis and alternative hypothesis were

$$H_0: \text{ No difference in varian}ces\ for\ these\ two\ group$$

$$H_1: \ Difference\ in\ variances\ f\text{or these two group}$$

The following equation can calculate the *F* critical value by dividing the highest variance by the lowest variance:

$$F\ statistic = \frac{1.843}{0.597} = 3.087 \tag{4.25}$$

The degrees of freedom for the two groups were each 19, and the significance level was $\alpha = 0.025$. Therefore, the critical F was

$$F_{19,19;0.025} = 2.526 \tag{4.26}$$

Since the *F* statistics in Eq. (4.26) were greater than the critical value from the *F* table, then the null hypothesis was rejected, meaning a significant difference in variances was observed between the two groups. In addition, the highest sample variance was observed for the system without control, and the lowest sample variance was observed for the system with control. Thus, proving that the addition of a variance constraint into the RFBS algorithm significantly and effectively controls and reduces system variance.

Because the variances for the two groups differed, the Welch *t*-test, an adaptation of Student's *t*-test, was used to compare the means of the two groups with unequal variances. The null hypothesis and alternative hypothesis were

$$H_0: \ E(without\ control) - E(with\ control) = 0$$

$$H_1: \ E(without\ control) - E(with\ control) \neq 0$$

The Welch *t*-statistic formula can be expressed as

$$t' = \frac{m_1 - m_2}{\sqrt{\frac{s_1^2}{n_1} + \frac{s_2^2}{n_2}}} \tag{4.27}$$

where the subscript *1* represents the group without control, and subscript *2* represents the groups with control. In Eq. (4.27), m_1 and m_2 represent the means of two groups, and s_1^2 and s_2^2 represent the standard deviation of two groups. The terms n_1 and n_2 are sample sizes for the two groups, respectively. Simulation results were

$$m_1 = 40.82, m_2 = 16.197, s_1^2 = 1.843, s_2^2 = 0.597, n_1 = n_2 = 20$$

Therefore, the Welch *t*-statistic was $t' = 70.351$. The degree of freedom of the Welch *t*-test was calculated as

$$df = \left(\frac{s_1^2}{n_1} + \frac{s_2^2}{n_2}\right)^2 / \left(\frac{(s_1^2/n_1)^2}{n_1 - 1} + \frac{(s_2^2/n_2)^2}{n_2 - 1}\right) \tag{4.28}$$

Thus, the degree of the data was $df = 314$. The *P*-value was less than 1.0*e*-6, which means the control led to improvements when a variance constraint was added to Algorithm 4.2. Using the *t*-table, $t_{313,0.025} = 1.968$ was obtained. Using Welch's *t*-interval formula,

$$m_1 - m_2 \pm t_{24,0.025}\sqrt{\frac{s_1^2}{n_1} + \frac{s_2^2}{n_2}}. \tag{4.29}$$

A 95% confidence interval for the difference (*E(without control)-E(with control)*) was obtained via

$$40.82 - 16.197 \pm 1.968 * \sqrt{\frac{1.843}{20} + \frac{0.597}{20}} = 24.623 \pm 0.349 = (24.274, 24.972) \tag{4.30}$$

Because the interval did not contain 0, the null hypothesis that suggested the average objective function values differed significantly was rejected. In addition, a statistically significant difference between expected costs for the system with controls and the theoretical optimal control

significantly decreased the spread of disease when a variance constraint was added to the RFBS algorithm.

In the first simulation, although the RFBS algorithm without variance constraint minimized expected costs, the system was unstable because system variance was uncontrolled. Simulation and analysis of the RFBS algorithm with variance constraint showed that the algorithm effectively minimized the expected costs and controls and reduced system variance, making the system stable.

4.5 Summary and Discussion

This paper presented an RFBS algorithm with variance constraint to identify a control strategy for stochastic optimal control problems. Previous research of stochastic optimal control have primarily focused on minimizing the expected value of the objective function. However, reaching the minimum expected value of the total cost does not ensure system stability. Therefore, the RFBS algorithm was proposed to minimize the expected value of the objective function and reduce the system variance. Application of the optimal control strategy obtained by the RFBS algorithm minimized the expected value of the cost and guaranteed system stability.

Chapter 5 - Exploring Disease Optimal Control Strategies Using An Improved Bayesian Optimization Algorithm and Related Computational Studies

Abstract

This paper presents an Improved Bayesian Optimization (IBO) algorithm to solve complex high-dimensional and time-dependent epidemic models' optimal control solutions. Evaluating total objective function value for disease control models with hundreds of thousands of control time-periods is high computational cost. In this paper, we improve the conventional Bayesian Optimization (BO) approach. The existing BO methods optimize the minimizer step for once time during each acquisition function update process. To find a better solution for each acquisition function update, we do more local minimization steps to tune the algorithm. When the model is high dimensions, and the objective function is complicated non-convex, only some update iterations of the acquisition function may not find the global optimum. The theoretical analysis for the feasible solution of researched model and convergence analysis of the final optimal solution solved by the IBO algorithm are provided. Comparative simulation experiments using different kernel functions and acquisition functions have shown that the IBO algorithm is effective and suitable for handing complex high-dimensional and time-dependent epidemic optimal control models under study. The proposed IBO algorithm is compared with four other global optimization algorithms on three well-known synthetic test functions. The effectiveness and robustness of the IBO algorithm are also demonstrated through some simulation experiments to compare with the Particle Swarm Optimization algorithm and Random Search algorithm. With its reliable

convergence behaviors and straightforward implementation, the IBO algorithm has a great potential to solve other complex optimal control problems with high dimensionality.

Keywords: Bayesian improvement, complex system, high-dimension, time-dependent model, optimal control.

5.1 Introduction

Today, optimal control for disease or epidemic has received increasing attention, which became a meaningful and popular issue in healthcare. Optimal control can affect the progression and transmission of diseases and achieve high-quality healthcare [3]. There are many works about the optimal control in the healthcare domain, such as optimal control of epidemic problem [174], optimal control of COVID-19 [175], optimal management of sepsis treatment [58], optimal control of HIV [176], etc. In general, disease control measures would be associated with certain financial costs, directly or indirectly. If the health agencies take a series of prevention or intervention measures to control the ongoing epidemic, e.g., vaccination, quarantine, disinfection, or regional closures, these measures would have associated costs of mass vaccination and economic costs related to the medical resources and disinfection products [177]. Suppose health agencies do not take any control measure towards the ongoing epidemic. In that case, it may also cause inevitable economic consequences, such as workforce losses due to outbreaks, increased community healthcare costs, local business downturns, and declined related travels. Thus, the goal of an optimal control problem is to balance the cost of control and the cost of null control. During the optimization process, it is necessary to calculate the value of state variables at each time-period and sum up each period's cost to evaluate the overall cost for only a control strategy. It could be too time-consuming to assess the overall cost, even for a single control strategy. In addition, most of the existing epidemic models assume the cost function associated with interventions as convex.

However, the costs of control measures are not simply constant nor linear. The costs could vary attributed to different control strategies implemented at different phases of the ongoing epidemic. For example, for the COVID-19, the control measure at the beginning of the epidemic is self-isolation. And, during the middle phase of the epidemic, the control measure is medical treatments and increasing hospital capacity. The medical and hospitalization costs are very different from the individual opportunity cost due to self-isolation in these two different phases [178]. The costs also could be greatly affected by diverse human behaviors or other factors such as seasonal weather patterns, short-term executive mandates, and time varied public health policies. Thus, the costs of control measures may not be convex [179, 180]. That means there will be multiple local optima when the objective function of the epidemic control model is non-convex.

In addition, the time-period epidemic control model is high-dimensional. Since the epidemic frequently lasts for hundreds of days or even a couple of years, one control decision needs to be carryout at each time-period in the model. Therefore, the overall control strategies containing up to hundreds of thousands of time-periods will result in a high-dimensional model. Besides the challenge of high-dimension, time-dependent is another challenging issue for solving the epidemic optimal control problems. In dynamic epidemic systems, the control decision at the current time would affect the epidemic progression in the near future. For example, vaccination may reduce the probability of infection and subsequently curb the infected population in the next few months. Then, the intervention decisions would be adjusted and refocused in the next few months according to trends and prevalence of the ongoing epidemic. Therefore, the control decisions and the epidemic status are both time-dependent and stage-dependent in nature. The resultant epidemic optimal control problems are multi-stage and multi-period decision-making models. These are different from conventional optimization problems with stage-independent

decisions. Thus, solving the optimal control of the high-dimensional and time-dependent epidemic control model with non-convex objective function is a complicated and challenging global optimization problem.

In the past few decades, many state-of-the-art global optimization methods have been proposed, such as the Cutting plane method [181], Branch and bound methods [182], Monte-Carlo methods [183], Genetic algorithms [184], Simulated annealing [185], Particle swarm optimization [186]. Several improved global optimization algorithms also have been developed to handle different types of global optimization problems raised in real-world applications. An extended cutting plane method is introduced and applied to solve convex mixed-integer nonlinear programming problems [187]. A bi-objective branch-and-bound method was proposed to solve a subclass of multi-objective mixed integer programming problems with two allowed objectives and binary variables [188]. A variety of improvements have been proposed to improve the Particle Swarm Optimization (PSO) algorithm or address its shortcomings by combining genetic algorithms. For example, a genetic learning Particle Swarm Optimization is proposed to use the genetic evolution to breed exemplars to PSO algorithm, then guidance the examples by the historical search experience of particles [189]. These algorithms help them to reach good performance. However, their applications are well-suited for lower-dimensional systems with independent variables, and their optimization processes require frequent evaluation of the objective functions if they are non-convex. The challenges mentioned above motivate our research using a new Bayesian optimization algorithm.

Standard Bayesian optimization (BO) utilizes an acquisition function to approximate the original objective function so that the reevaluations of the objective values can be done more effectively and efficiently at each iteration [190, 191]. It has been shown that BO algorithm is a

prevalent and efficient method for solving global optimization problems with low-dimensional systems. The BO algorithm is a novel framework dealing with exploration and exploitation within the solution domain spaces and sampling during the search process. In [50], BO algorithm leveraging gradients in hyperparameter tuning is applied to reduce the number of objective function evaluations in low dimensional problems. For multi-response surface optimization problems, a new BO approach incorporating both expected loss and its variances into a Bayesian modeling uniform framework was also proposed [192]. This proposed approach considers the uncertainty of model parameters and measures the reliability of an acceptable optimization result. A BO algorithm with an elastic Gaussian process is also introduced and tested in the optimization problem with less than a hundred dimensions [193]; this algorithm enables local gradient-dependent algorithms to move through the flat terrain. For COVID-19, researchers combined deep learning and Bayesian optimization to predict the COVID-19 time-dependent data [194].

Although the standard BO algorithm performs well on the global optimization of low-dimensional systems with non-convex objective function, it is not enough good for solving the global optimal solution when the system is high-dimensional and time-dependent. These previously mentioned challenges inspired the necessity to improve the BO algorithm and streamline its implementation process to make it become suitable, more effective, and efficient to the high-dimensional and time-dependent epidemic control model with non-convex objective function. Ensure that the improved BO algorithm has capacity to capture a better solution at each optimization process to seek out the global optimum soon. In this paper, we improved the BO algorithm from framework and implementation and named it Improved Bayesian Optimization (IBO) algorithm, then utilized the improved algorithm to solve the optimal control solution for

high-dimensional and time-dependent SEIR epidemic control system with non-convex objective function. Therefore, the contributions of this paper are as follows:

(1) Improved the BO algorithm and demonstrated that it can solve the global optimal solution for both low-dimensional optimization problems and complex high-dimensional and time-dependent epidemic optimal control model with non-convex objective function within limited number of iterations.

(2) Theoretically analyzed the feasible solution of the high-dimensional and time-dependent optimal control model with non-convex objective function. Provided convergence analysis of the final optimal solution generated by the IBO algorithm.

(3) Validation and comparison on both well-known synthetic functions and researched high-dimensional and time-dependent SEIR control model to demonstrate the effectiveness and robustness of the IBO algorithm.

The remainder of this paper is organized as follows. Section 5.2 formulates the high-dimensional and time-dependent epidemic optimal control problem. In Section 5.3, presents the IBO algorithm framework in detail. Section 5.4 presents the theoretical analysis about the feasible solution of the researched model and the convergence analysis of the IBO algorithm. Then, the computation studies and their results are presented to demonstrate the effectiveness and efficiency of the IBO algorithm in Section 5.5. Conclusions and potential future studies are summarized in this final section.

5.2 Problem Formulation

In this paper, we attempt to solve the optimal control problem with SEIR control model that is revised according to the SEIR epidemic model in [195]. The status variables in epidemic model are time dependent, it means that the status values in current moment have impact on the

status in the next moment. If the government or the health organizations tend to minimize the overall cost due to control measures and infectious population under null control condition, they not only need to calculate the cost at each moment, but also figure out how current status affect the status at the next moment and then affect the cost. Therefore, solving the time-dependent optimal control in epidemic model is complex. In addition, the epidemic usually last for some months even more than one year, such as the ongoing COVID-19 epidemic. This means the optimization problem of the epidemic models will be high-dimensional. It is necessary to calculate the cost at each time dimension and sum of them at each optimization iteration. Thus, the optimal control problem with time-dependent epidemic model what we research is dynamic, complex, and high-dimensional with expensive computational efforts.

Our main goal is to solve the optimal control strategy in time series that not only controls the infected population but also minimizes the overall related financial cost. The control strategy in our researched epidemic model can represent the practical meanings of public health of real world, which means the possible disease intervention or treatment measures, such as vaccination, quarantines, safeguard procedures, hospitalization, or medical treatment. The control strategy variables in different parts of the researched epidemic model have different meanings.

Consider the control period in the researched model is $[0, t_f]$, t_f is the final time. The high-dimensional and time-dependent SEIR optimal control problem with practical meanings can be formulated as shown in Eqns. (5.1)-(5.6). The dynamic transfer chart of the model is shown in Figure 5.1.

$$\text{Min } V(u_1, u_2) = \int_0^{t_f} C_1 I(t) + C_2 f(u_1, u_2, t) \tag{5.1}$$

$$\textit{s. t.} \quad \frac{dS(t)}{dt} = \tau - (1 - u_1(t))\beta S(t) I(t) - \tau S(t) \tag{5.2}$$

$$\frac{dE(t)}{dt} = \big(1 - u_1(t)\big)\beta S(t)I(t) - \alpha E(t) - \tau E(\mathrm{t}) \tag{5.3}$$

$$\frac{dI(t)}{dt} = \alpha E(t) - (\gamma + u_2(t))I(t) - \tau I(t) \tag{5.4}$$

$$\frac{dR(t)}{dt} = (\gamma + u_2(t))I(t) - \tau R(t) \tag{5.5}$$

$$S(t) + E(t) + I(t) + R(t) = 1 \tag{5.6}$$

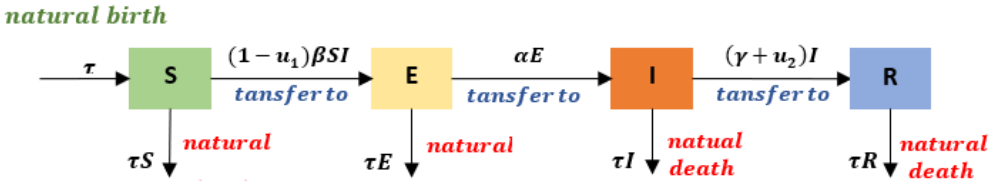

Figure 5.1 Dynamic transfer chart of SEIR epidemic control model

In the SEIR optimal control system, the population is divided into four states: susceptible S, exposed E, infected I and recovery R, which represent four different infection statuses of individuals. In the system defined in Eqns. (5.1)-(5.6), $S(t)$, $E(t)$, $I(t)$, $R(t)$ denote the state variables of the system. They represent the fraction of susceptible, exposed, infected and recovery population at time t, respectively. Susceptible population means the individuals who can contract the disease, exposed population means the individuals who have been infected but are not yet infectious, infected population means the individuals who are capable to transmit the disease, recovery population means the individuals who have become immune. Each person in real world will belong to one of those four disease statuses.

System parameter τ denotes the natural birth rate. In current model, we assume that the natural death rate and natural birth rate are identical. Thus, in Eqns. (5.2)-(5.6), $\tau S(t), \tau E(t), \tau I(t), \tau R(t)$ represent the number of natural deaths for each system state at time t, respectively. In Eq. (5.2), system parameter β denotes the contact rate of S against I, then $\beta S(t)I(t)$ represents the number of S transferring to exposed state when contacting with I at time

t. In Eq. (5.3), system parameter α denotes transfer rate from E to I, then $\alpha E(t)$ represents the number of E transferring to infected state at time t. In Eq. (5.4), system parameter γ denotes the natural recovery rate of I, then $\gamma I(t)$ represents the number of I naturally transferring to recovery state without medical treatment at time t.

u_1, u_2 are the system decision variables, which are also called control variables. $u_1(t)$ in Eq. (5.2) and Eq. (5.3) and shown in Figure1 represents the prevention control strategies that can slow down the population's transformation from state S to state E. $u_2(t)$ in Eq. (5.4) and Eq. (5.5) and shown in Figure 5.1 represents the intervention control strategies that can speed up the population's recovery from state I to state R. $u_1(t)$ and $u_2(t)$ mean the level/degree of different types of control strategies that are applied to different population at time t. Each type of control is t_f -dimensions variable defined as $u_1(or\ u_2) = \{u(0), \dots, u(t), \dots, u(t_f)\},\ t \in [0, t_f],\ u(t) \in [0,1]$.

Control variables can represent practical meanings in real world. Different variables located in different terms in the model can represent different practical meanings. In Eq. (5.2) and Eq. (5.3), type 1 control variable $u_1(t)$ can represent the practical intervention control strategies, such as restrictions on activities, vaccination, wearing mask, and restriction on social distance that are applied to susceptible population, which can reduce the contact between susceptible person and the infected person [196]. $u_1(t)$ also can represent the control strategy such as quarantines or isolation applied to the infected population, which can reduce the contract possibility that susceptible person will be infected by the infected person [197]. The above control strategies have impacts on the value of contact rate β. Then term $(1 - u_1(t))\beta$ means how much the contact rate will be affected by control u_1 at time t. There will be lower contact possibility between S and I if the level/degree of control strategy $u_1(t)$ is high and close to 1. In Eq. (5.4) and Eq. (5.5), type 2

control variable $u_2(t)$ can represent the practical control strategies like intense medical care or improvement of hospitalization facilities applied to the infected population, such as hospital facility of respirator in the COVID-19 epidemic, which can speed up the infected person's recovery [197, 198].

In the objective function defined in Eq. (5.1), V represents the overall cost of the system due to control measures and the cost of infected population if there is no null control in time interval [0, t_f]. The parameters C_1 and C_2 represent the loss of each infected person under null control condition and the control cost per individual if individuals take control measures at each time moment, respectively. For simplification, we only consider the minimization problem in this paper. A maximization problem can be easily converted to a minimization problem by setting the negative of the objective function V.

$f(u_1, u_2, t)$ is the cost function associated with the current levels of control strategy. In the existing epidemic control models, the cost function f associated with the control strategy usually is considered as a convex function [199 - 201]. However, in real world, the cost function doesn't always perform convex. For example, when the epidemic outbreaks suddenly, there are less masks available for supplying, the price of mask at this time may sharply increase. Then this phenomenon will spur suppliers to produce a mass of masks so that there are more masks available suddenly on the market, even occur the situation that supply exceed demand. At this moment the price of mask will decrease. Also, the individuals' social behaviors have influence on the medical cost [202]. For instance, individuals may perform less activities or reduce the frequency of going out during the winter, the phenomenon would be inverse during the spring. In those situations, the sellers may lower the medicine or mask price to stimulate consumption when individuals are active during the spring, and increase the price to earn more profits for every deal when individuals are less active

during the winter. Therefore, the cost of control strategy may perform the nature of seasonal. Thus, in this paper, we will consider the cost function due to the control strategy as a non-convex function. Then, the objective function V in this paper also is a high-dimensional non-convex function.

Current serious COVID-19 epidemic can be considered as one case of the SEIR epidemic model [196, 198, 203]. The challenges and reasons discussed above indicate that studying the time-dependent optimal control in a high-dimensional and complex SEIR control model is meaningful and useful. In the introduction of the IBO algorithm and simulation parts, we will only consider the type 2 control variable u_2. It means we will assume that type 1 control variable $u_1(t)$ is assumed to be zero in the simulation part. For simplification, we directly use symbol u to represent the control strategy u_2 in the rest of the paper, which is $u_2 = u = \{u(0), \dots, u(t), \dots, u(t_f)\}$.

To provide an intuitive display of the complication of our researched system, we show a 3D plotting of an example of non-convex objective function with control strategy in Figure 5.2, the control variable in the shown example only has two dimensions (time-periods). We can see that there is complex and with multiple local optima only for 2D control model with non-convex objective function. However, our researched model is with t_f dimensions where practically t_f could equal to several hundred time-periods.

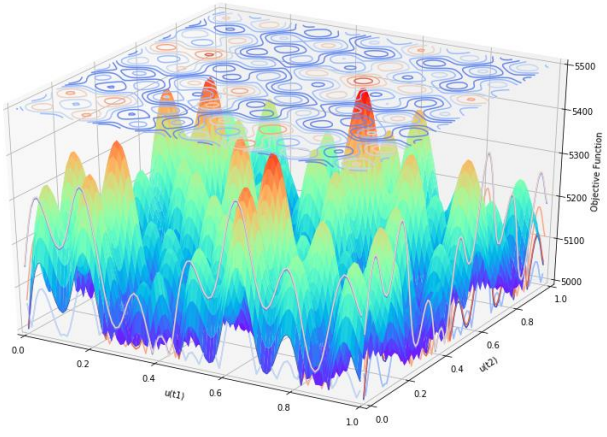

Figure 5.2 3D plotting of objective function of SEIR control model

5.3 The Improved Bayesian Optimization Algorithm

This section explains the reason for choosing and improving the BO algorithm to solve the complex high-dimensional and time-dependent SEIR epidemic control model. Then introduces the essential related works of the IBO algorithm. We presented various studies with different structures of the probabilistic models, the kernel functions, the acquisition function, and the sampling strategies.

The standard BO algorithm framework is thoroughly reviewed in the article [204]; there are two essential parts for BO: the probabilistic model of objective function and acquisition function. The probabilistic model evaluates the model uncertainty based on the observed sampling data, and the acquisition function mainly balances the exploration and exploitation during the optimization process [205]. We briefly summarize the general procedures as follows: (1) Initial a start sampling point; (2) Construct the probabilistic model. Generally, the posterior model is considered as the probabilistic model of objective function $V(x,u)$ for Bayesian optimization; (3) Optimize the acquisition function to select a next sampling point; (4) Calculate the corresponding objective function value $V(x,u)$ for this sampling point; (5) Update the probabilistic model by adding the new sampling point and corresponding objective function value; (6) Repeat (3) – (5) for some iterations and return the best objective function value and corresponding sampling point. To make the BO algorithm more effective, we will add some improvements and name the improved version of BO algorithm as IBO algorithm. In the IBO algorithm, we will remain some those important procedures.

5.3.1 Gaussian Processes

Due to the complication of the high-dimensional non-convex objective function, the computational effort will be expensive if we solve the optimal control based on the original

objective function. Therefore, we will leverage a probabilistic model to approximate the original objective function, which is more tractable to calculate and can be constantly refined itself with the historical data to become more accurate on the estimation of original objective function.

There are many methods to construct the probabilistic model, such as neural networks, support vector machines, random forests, and the Gaussian Process (GP). When a function follows a GP, then the likelihood is Gaussian, and its posterior also is a GP. Since the property and flexibility of the GP, it becomes a common and popular choice of probabilistic model for the IBO algorithm to estimate the original objective function.

The GP is a probability distribution over function. Assume the original objective function $V(u)$ follows a GP, consider the objective function value as $V(u)$ when the control strategy is $u = \{u(0), \dots, u(t_f)\}$. Then

$$V(u) \sim \mathcal{GP}(m(u), k(u, u')) \tag{5.7}$$

where $m(u)$ is mean function and $k(u, u')$ is covariance function [205], the covariance function is also named kernel function, where u and u' represent two different control strategies. The mean function is usually defined as a linear function or directly defined as zero [206]. Without loss of generality, the mean function in this paper is given as $m(u) = 0$.

Any finite number of the objective function values, $V(u)$, follow multivariate Gaussian distribution [207]. Let a set of historical control strategies $\{u^1, \dots, u^i\}$, superscript value i denotes the ith control strategies. Each control strategy is t_f-dimensions as $u^i = \{u^i(0), \dots, u^i(t_f)\}$. Then $V = [V(u^1), \dots, V(u^i)]^T$ is a vector of corresponding objective function values of control strategies set $\{u^1, \dots, u^i\}$, then V is Gaussian distributed with mean vector M and covariance matrix K as below:

$$M = [m(u^1), \dots, m(u^i)]^T = [0, \dots, 0]^T \tag{5.8}$$

$$K = \begin{bmatrix} k(u^1, u^1) & \cdots & k(u^1, u^i) \\ \vdots & \ddots & \vdots \\ k(u^i, u^1) & \cdots & k(u^i, u^i) \end{bmatrix} \tag{5.9}$$

where $k(u^j, u^{\mathrm{i}})$ $(1 \leq j \leq i)$ references to the kernel function and K references to kernel (covariance) matrix. k and K are used to theoretically estimate the covariance information of the original objective function at two points.

For any new sampling point u^{i+1} that is not in the historical control strategies set and corresponding objective function value $V(u^{i+1})$, let

$$V' = \begin{bmatrix} V \\ V(u^{i+1}) \end{bmatrix}, M' = \begin{bmatrix} M \\ m(u^{i+1}) \end{bmatrix}, \Sigma = \begin{bmatrix} K & K'^T \\ K' & K'' \end{bmatrix} \tag{5.10}$$

where

$$K' = [k(u^{i+1}, u^1), k(u^{i+1}, u^2), \ldots, k(u^{i+1}, u^i)] \tag{5.11}$$

$$K'' = k(u^{i+1}, u^{i+1}) \tag{5.12}$$

Then the posterior distribution of $V(u^{i+1})$ for any new sampling point u^{i+1} based on all known historical data V will Gaussian distributed with mean $\mu(V(u^{i+1})|V, u^{i+1})$ and variance $\sigma(V(u^{i+1})|V, u^{i+1})$, which can be written as:

$$V(u^{i+1})|V, u^{i+1} \sim \mathcal{GP}(\mu(V(u^{i+1})|V, u^{i+1}), \sigma(V(u^{i+1})|V, u^{i+1})) \tag{5.13}$$

where the posterior mean and the variance at point u^{i+1} can be derived as:

$$\mu(V(u^{i+1})|V, u^{i+1}) = m(u^{i+1}) + K'K^{-1}(V - M) = K'K^{-1}V \tag{5.14}$$

$$\sigma(V(u^{i+1})|V, u^{i+1}) = K'' - K'K^{-1}K'^T \tag{5.15}$$

For simplification, we will use $\mu(u)$ and $\sigma(u)$ represent the posterior mean $\mu(V(u)|V, u)$ and posterior variance $\sigma(V(u)|V, u)$ at a new point u in the rest of paper, respectively.

5.3.2 Choices of Kernel Function

The kernel function is used in Eq. (5.9) of Gaussian Process, which is an essential part of the Gaussian Process regression modeling. Kernel function can evaluate the pattern or shape of original objective function in high-dimensional space, also provide the dependence information between the objective function values at any two different data points u^j and u^{i} in the feasible solution space. Different kernel function used in Gaussian Process would affect the shape and smoothness of the regression acquisition function discussed in Section 5.3.3 using Eq. (5.14) and Eq. (5.15). There are several kernel function choices that can be used in the IBO algorithm, such as Matern32, Matern52, Radial Basis Function (RBF), Exponential, Linear, Brownian, Periodic, Polynomial, Warping, Coregionalize, RationalQuadrati (RQ). In most existing literatures about the BO algorithm, Matern32, Matern52 and Radial Basis Function (RBF) are the three more popular choices [208]. The expression of these three popular kernel functions is defined as below, respectively.

$$k_{Matern32}\left(u^j, u^{\mathrm{i}}\right) = \left(1 + \frac{\sqrt{3}\left\|u^j - u^{\mathrm{i}}\right\|}{l}\right) exp\ (-\frac{\sqrt{3}\left\|u^j - u^{\mathrm{i}}\right\|}{l}) \tag{5.16}$$

$$k_{Matern52}\left(u^j, u^{\mathrm{i}}\right) = \left(1 + \frac{\sqrt{5}\left\|u^j - u^{\mathrm{i}}\right\|}{l} + \frac{5\left\|u^j - u^{\mathrm{i}}\right\|^2}{3l^2}\right) exp\ (-\frac{\sqrt{5}\left\|u^j - u^{\mathrm{i}}\right\|}{l}) \tag{5.17}$$

$$k_{RBF}\left(u^j, u^{\mathrm{i}}\right) = exp\ (-\frac{\left\|u^j - u^{\mathrm{i}}\right\|^2}{2l^2}) \tag{5.18}$$

where l is the kernel length-scale, its value reflects the smoothness of the objective function.

The impacts of different kernel function choices on the global performance of the IBO algorithm to apply in the researched optimal control model will be detailed discuss in the simulation part.

5.3.3 Acquisition Functions

Acquisition function is used to approximate the original objective function with cheaper computational effort. In minimization problems, it can provide a probability lower bound for the objective function. The expression of acquisition function takes the probabilistic mean and variance obtained from Gaussian process at each sampling point on the objective function. The choice of kernel in the acquisition function can control shape of the approximation function for the objective function.

Acquisition function can evaluate how desirable the next sampling position would be. An adequately designed acquisition function in BO algorithm should represent a trade-off between exploration and exploitation. The exploration suggests that objective function values could be highly uncertain. On the other hand, exploitation implies that the next sampling point could have a lower objective function value for the minimization problem [209]. Several popular approaches can be applied as the acquisition function including, Lower Confidence Bound (LCB), Probability of Improvement (PI), Expected Improvement (EI).

LCB acquisition function is defined as [210]:

$$LCB(u) = \mu(u) - \nu\sigma(u) \tag{5.19}$$

where ν is the parameter that balances exploration and exploitation. If $\nu = 2$ means the LCB acquisition function approximates the shape of the objective function with two standard deviations below the posterior mean at each point.

PI acquisition function is defined as [210]:

$$PI(u) = \Phi\left(\frac{V(u^+) - \mu(u) - \xi}{\sigma(u)}\right) \tag{5.20}$$

where u^+ represents the best point so far based on the historical control strategies set $\{u^1, \dots, u^i\}$. Φ is the CDF of standard normal distribution. Parameter ξ estimates the noise. As recommended in previous research, to guarantee the exploration, ξ is set as $\xi = 0.01$ [210].

EI acquisition function is defined as [210]:

$$EI(u) = \big(V(u^+) - \mu(u)\big)\Phi(Z) + \sigma(u)\phi(Z) \tag{5.21}$$

and

$$Z = \frac{V(u^+) - \mu(u)}{\sigma(u)} \tag{5.22}$$

where ϕ is the PDF of standard normal distribution.

The purpose is to solve the optimal control solution that minimizes the original objective function value and subjects to the high-dimensional and time-dependent SEIR control model. The acquisition approximates the original objective function, which provides the probability lower bound for the objective function. Therefore, the purpose is equivalent to minimize the acquisition function. The t_f-dimensional solution u^{i+1} is chosen as a minimizer of acquisition function:

$$u^{i+1} = \arg\min_{u \in \mathcal{U}} AC(u) \tag{5.23}$$

and

$$\mathcal{U} = [0, 1]^{t_f} \backslash \{u^1, \dots, u^i\} \tag{5.24}$$

where $AC(u)$ represents the acquisition function, it can be $LCB(u)$, $PI(u)$, or $EI(u)$.

The impact of different acquisition functions on the IBO algorithm to apply in the researched high-dimensional optimal control model is analyzed in the simulation part through some computational experiments.

5.3.4 Candidate Sampling Strategies

Using an acquisition function to estimate the high-dimensional non-convex objective function may still encounter difficult issues when dealing with high-dimensional and time-dependent optimal control model. Since the feasible region is continuous and high-dimensional, it is impossible to traverse the entire feasible solution space to solve the optimal solution in a reasonable amount of time. Therefore, an efficient and effective sampling approach is the key to optimize the acquisition function.

The IBO algorithm selects the candidates through uniform random distribution and do some gradient descent steps for candidates to obtain the best point as the next sampling point. Uniform random search can guarantee the candidates at any locations have probability to be selected. Let $\mathcal{D}$ be s set of known historical data. $(u^{last}, V(u^{last}))$ be the last data of $\mathcal{D}$, which is also the optimal sampling point selected from the last optimization iteration so far. Consider $(u^{last}, V(u^{last}))$ as one of the candidates for the next sampling point. Specify a uniform distribution for each dimension of $(u^{last}, V(u^{last}))$, and randomly sample k values for each dimension from this distribution, and then compose k control strategy candidates. Consider the acquisition function as the loss function, then we will do some gradient descent steps for each candidate. Eventually, select the point after gradient descent process that minimizes the acquisition function as the next sampling point and add into the database for the update of the GP model.

5.3.5 Framework of The IBO Algorithm

The IBO algorithm attempts to perform several optimization steps during each candidate sampling process based on the acquisition function. This improvement can efficiently pick out the better sampling point when the model is high-dimensional. Besides, during implementation process, the IBO uses the acquisition function rather than the original objective function

information to determine the next sapling point. We know that the acquisition function is an approximation way of the original objective function based on the known historical data information, which is not exactly precise original objective function. Thus, to increase the accuracy of final optimal solution, a series of Adam-based steps is added as a local search process after the acquisition function optimizations. This local search process will use the original objective function instead of the acquisition function as derivative information. Therefore, the IBO algorithm framework for the high-dimensional and time-dependent optimal control problem can be summarized in detail as follows:

Algorithm 5.1 The Improved Bayesian Optimization Algorithm

1: Randomly initial some control strategy inputs with multi-dimensions $(u^1, \dots, u^i)$

2: Compute the state variables through the control inputs and the given high-dimensional control model

3: Calculate the corresponding objective function values for each control strategy input and same them to compose

a dataset $\mathcal{D} = \{\left(u^1, V(u^1)\right), \dots, \left(u^i, V(u^i)\right)$

4: Train the Gaussian process model by using dataset $\mathcal{D}$

5: **for** iteration1 = 1, 2, …, m **do**

6: Select control u^{last} from the last data in dataset $\mathcal{D}$ to be one of the new candidates

7: Randomly generate k sampling candidates from the uniform distribution based on u^{last}

8: **for** each candidate **do**

9: **for** q = 1, 2, …, n **do**

10: Calculate the acquisition function value

11: Use *autograd.backward* to obtain the derivate information of acquisition function and then update the step size of optimizer for acquisition function

12: **end for**

13: **end for**

14: Find point that minimizes the acquisition function to be the next sampling point

15: Add the candidate and corresponding objective function value to the dataset $\mathcal{D}$

16: Update the Gaussian process model

17: **end for**

18: **Obtain** a best control u with the lowest acquisition function value from all sampling points during iterations

19: **Repeat** (initial iteration2 $l = 0$)

20: Use *autograd.backward* to obtain the derivate information of the objective function, and update the step size to do the local optimization for the objective function

$l = l + 1$

21: **Until** the objective function V converges

22: **Return** the global optimal control solution

The IBO algorithm was implemented in Python 3.7 using PyTorch and Pyro libraries. The codes were executed on a Personal Computer with Intel i5 Center Process Unit and 32 GB of Random-Access Memory for more than a hundred times to find the more suitable values of parameter m – main loops, the number of candidates, k, and parameter l – number of local minimization steps. For the given high-dimensional control system, our experiment results show that the IBO algorithm can almost find the global optimal solution when m is about 10, the number of candidates k is around 5, l is set to 15.

5.4 Theoretical Analysis

In this section, the theoretical analysis about the feasible solution of the researched optimization system will be provided. We also want to analyze the validity and rationality of the improvement of the IBO algorithm. Before that, we generalize the model in Eqns. (5.2)-(5.5) as

$$\dot{x}(t) = g(x(t), u(t), t) \tag{5.25}$$

where $x(t) = (S(t), E(t), I(t), R(t))^T$.

Theorem 5.1. $\forall t \in [0, t_f]$, there are infinite feasible values for the state variables in the researched SEIR control model if the control strategy is continuous at each time period t. The total number of feasible points is k^{t_f}.

Proof. According to Eq. (5.25), then we have

$$x(t+1) = x(t) + g(x(t), u(t), t) \tag{5.26}$$

Obviously, the state variable x is continuous function regarding to u and t. Since the objective function is non-convex, the optimal solution may not exist in the corner or bound of the feasible region. The value range of the control strategy u at each time period t is $u(t) \in [0,1]$, $u(t)$ is also continuous. Assume we select $k(k \geq 1)$ possible values as candidates for $u(t)$ at each time period t, the total number of feasible points for control strategy $u = \{u(0), \dots, u(t_f)\}$ will be:

$$\prod_0^{t_f} k = k^{t_f} \tag{5.27}$$

Since $k \geq 1$, $t_f > 0$, then k^{t_f} is monotonically increasing and $k^{t_f} > 1$. When the number of possible values of $u(t)$ that the algorithm selects is infinite, then

$$\lim_{k \to +\infty} k^{t_f} \to +\infty \tag{5.28}$$

From Eq. (5.26), we know that $\forall t \in [0, t_f]$, the values of state variables are related to $u(t)$. Therefore, the number of feasible values of state variables will be infinite if the number of possible values of $u(t)$ is infinite.

Lemma 5.1. According to **Theorem 5.1**, for high-dimensional and time-dependent optimal control system with non-convex objective function, to solve the optimal control solution in a reasonable amount of time, the value of k should be bounded.

Convergence analysis of the IBO algorithm The acquisition function is an approximate probability lower bound of the original objective function, which is constructed through the Gaussian process regression. The reason for choosing the Gaussian process regression rather than other regression methods is because general regression methods tend to find the best function to fit the known historical data, but they do not exactly pass through the data points [211]. However, Gaussian process regression can utilize the posterior information to find a function that passes through the known historical data [212]. The confidence intervals shown in Figure 5.3 to Figure 5.5 mean the probability that the original objective function value will fall between the values

around the acquisition function. In here, the percentage of probability is 95%. Then the objective function value will be outside of the confidence interval with 5% confidence level. The 95% confident interval of the area that is closer to the known historical data points will be smaller, conversely the 95% confident interval of the area that is far from the known historical data points will be larger. Therefore, according to the difference between Gaussian process regression and other regression methods, the confidence intervals of other regression methods for the known historical data points are not exactly equal to 0, because their regression functions do not exactly pass through those points that represent the original objective function values. The confidence intervals of Gaussian process regression at those known historical data points are exactly equal to 0 since the Gaussian regression function exactly cross the data points. The confidence intervals of the area between any two known data points would be large than 0 due to the uncertainty. The confidence intervals of a point would be smaller if this point is closer to one of two known data points. To provide an intuitive display, there only consider one dimension for the control strategy to show the acquisition function generated using Gaussian process regression knowledge and analyze the convergence of the IBO algorithm.

In Figure 5.3, assume it shows the situation at the first iteration, four green points are the initial points or historical points. The solid blue line represents the acquisition function fitted by Gaussian regression, which passes all the historical points. According to the Theorem 5.1 and Lemma 5.1, we know that the number of candidates used in the IBO algorithm is bounded and finite. Assume the number of candidates in this example are 3. The IBO algorithm generates the candidates through uniform random distribution, which can make sure the candidates at any locations can be selected with probability. In Figure 5.3, assume the red rhombus points represent the candidates generated by the IBO algorithm. Since the IBO algorithm only considers limited

candidates rather than traverse all feasible points to minimize the acquisition function. Therefore, one improvement of the IBO algorithm is to do some gradient descent steps for each candidate during implementation process. Thus, shown as Figure 5.3, the black dotted arrows indicate the direction of the gradient descent for three candidates. From the figure, candidate 2 and candidate 3 will go to the same local minimum (red star point) of the acquisition function, which is also lower than the acquisition function value obtained from gradient descent of candidate 1. Then the red star point will be selected as the best sampling point for the next iteration.

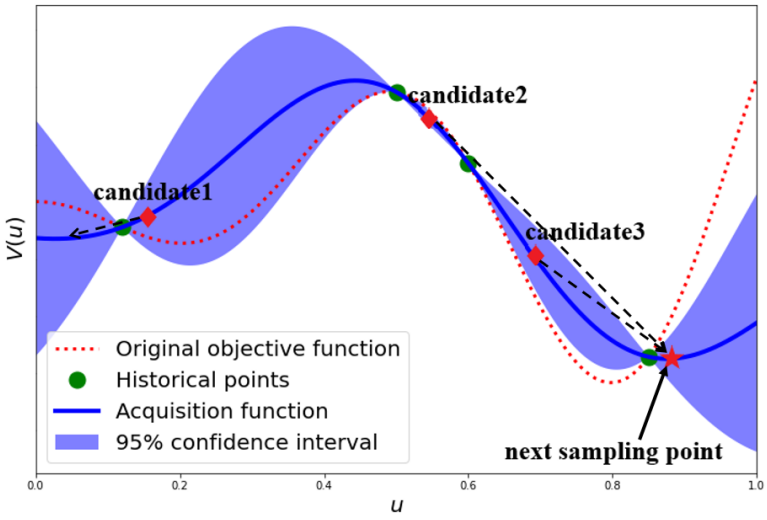

Figure 5.3 The position of the next sampling point obtained from the 1st iteration

At the second iteration shown in Figure 5.4, the sampling point obtained from the first iteration has been added into the historical data set. Then we will consider three new candidates for finding the next sampling point. From Figure 5.4, candidate 1 and candidate 2 will go to the same local minimum of the acquisition function. However, compared to candidate 1 and candidate 2, candidate 3 will obtain a better minimum acquisition function value after some gradient descent steps. Then the new red star point in Figure 5.4 will be the next sampling point for the next iteration.

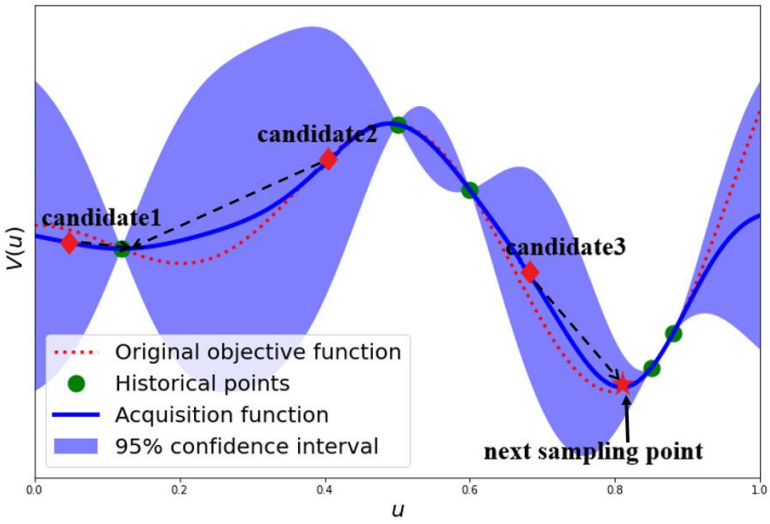

Figure 5.4 The position of the next sampling point obtained from the 2nd iteration

After the second iteration, this sampling point obtained is also added into the historical data set shown in Figure 5.5. Assume the IBO algorithm only carried out for 2 iterations on the acquisition function optimization process. The current optimal point is closer to the actual optimal solution of the original objective function.

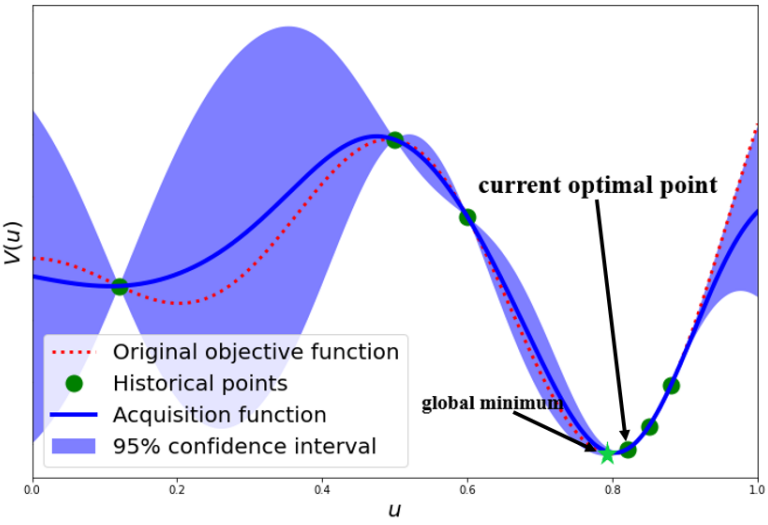

Figure 5.5 The positions of current optimal point after two iterations

According to the analysis of possible positions for the optimal solution, obviously it's necessary to add a local search after the acquisition function optimizations for further optimization,

which can increase the accuracy of the final optimal solution. Since the acquisition function is a probability lower bound of the original objective function based on the known historical information, it doesn't exactly fit to the original objective function. Thus, another improvement of the IBO algorithm is to add a series of Adam-based steps as a local search after the acquisition function optimizations to increase the accuracy of the final optimal solution. In this example, during this local search process, the current optimal point will gradually move toward the exactly global minimum. Therefore, two improvements of the IBO algorithm guarantee the convergence of the final optimal solution.

5.5 Experiment Simulations

In this section, some simulation experiments are conducted to evaluate the performance of the IBO algorithm. We will focus on the simulations on the researched SEIR control model, but before that, to better demonstrate the effectiveness and efficiency of the IBO algorithm, we firstly provide a brief simulation to test the global optimization ability of the IBO algorithm on low-dimensional global optimization problems in Section 5.5.1. After that, from Section 5.5.2 to 5.5.4, we implement detailed simulations to demonstrate the effectiveness and convergence of the IBO algorithm focusing on high-dimensional time-dependent SEIR control system. All simulation experiments are conducted on Python version 3.7 with Intel Core i5 CPUs and 32G memory. The kernel function and acquisition function selected for the IBO algorithm in the following simulation experiments are Matern52 kernel and lower confidence bound acquisition function, respectively.

5.5.1 Benchmarking Using Synthetic Test Functions

Before implementing the simulation experiments on the researched SEIR control model, we use three synthetic test functions (Eggholder function, Rosenbrock function, McCormick function) to test and prove the excellent optimization performance of the IBO algorithm on low-

dimensional global optimization problems. Since these three low-dimensional optimization problems are not key researched system, we just show the brief simulation results in this Section, the detailed process and discussion are provided in Appendix 1.

The part is to test the global optimization performance of the IBO algorithm for solving the global optimal solution on three functions: Eggholder function, Rosenbrock function, McCormick function. We also compare the IBO algorithm with other four global optimization algorithms: simplicial homology global optimization algorithm (SHGOA) [213], dual annealing optimization algorithm (DAOA) [214], differential evolution algorithm (DEA) [215], and basin-hopping algorithm (BHA) [216]. The simulation experiments are conducted 10 times for each algorithm to calculate the average result. The running time of the IBO and other four algorithms are very close when they solve the same test function, which are about 5 seconds. The final optimal solutions generated by different algorithms are summarized in Table 5.1. According to the results on three synthetic test functions, the IBO algorithm always shows the best global optimization performance with the similar running time by comparing other four algorithms.

Table 5.1 Optimal solution of different algorithms on three synthetic test functions

	Eggholder function	**Rosenbrock function**	**McCormick function**
Theoretical Solution	(512, 404.2319, −959.6407)	(1, 1, 0)	(−0.54719, −1.54719, −1.9133)
IBO algorithm	(512, 404.2661, −959.4893)	(1, 1, 0)	(−0.54719, −1.54719, −1.9132)
SHGOA	(439, 453.9774, −935.338)	(1, 1, 0.1996)	(−1.21944, −1.44547, −1.9002)
DAOA	(439,453.9775, −935.3379)	(1, 1, 0.8999)	(−0.54719, −1.54719, −1.9132)
DEA	(−466, 385.7367, −894.579)	(1, 1, 0)	(−0.54720, −1.54720, −1.9132)
BHA	(−106, 423.1532, −565.998)	(1, 1, 0.3204)	(2.59440, 1.59440, 1.2284)

5.5.2 Impact of Different Kernel Functions on the Global Performance of The IBO Algorithm

From Section 5.5.2 to 5.5.4, the computational studies will focus on applying the IBO algorithm to high-dimensional time-dependent SEIR epidemic control model with a control variable defined in Eqns. (5.1)-(5.6). Under investigation, the SEIR control model has a control variable with 100 time-periods, so the problem's dimensionality is 100. Based on the discussion about the cost function in Section 5.2, we assume that the objective function of the researched optimal control problem that will be used in Section 5.5.2 to Section 5.5.4 is:

$$\text{Min } V = \int_0^{t_f} C_1 I(t) + C_2 \left| \begin{matrix} 0.3\, sin\big(10u(t)\big) + sin\big(13u(t)\big) \\ +0.9\, sin(42u(t)) + 0.2\, sin(12u(t)) + u^2(t) \end{matrix} \right| \quad (5.13)$$

The reason why we assume the function shown as Eq. (5.13) is that the objective function in this paper is non-convex and it may perform seasonal characteristics as discussed in Section 5.2. Also, to increase the difficulty of the researched model and better to demonstrate the effectiveness and global optimization ability of the proposed IBO algorithm, we hypothetical design the objective function as this function shown in Eq. (5.13), which has no practical significance.

For a control strategy with 100 time periods, it is necessary to calculate all state variables values at each time-period using the SEIR model in Eqns. (5.2)-(5.6). Then it needs to calculate the cost using this complicated objective function 100 times for one control strategy. Therefore, computationally calculate the total cost is time-consuming. Figure 6 shows a 2D plotting of the relationship between the control variable and the objective function. In Figure 5.6, the control variable only has two time-period, and the objective function has multiple local minima. Doubtlessly, the objective function in the studied SEIR model with 100 time periods is more complicated.

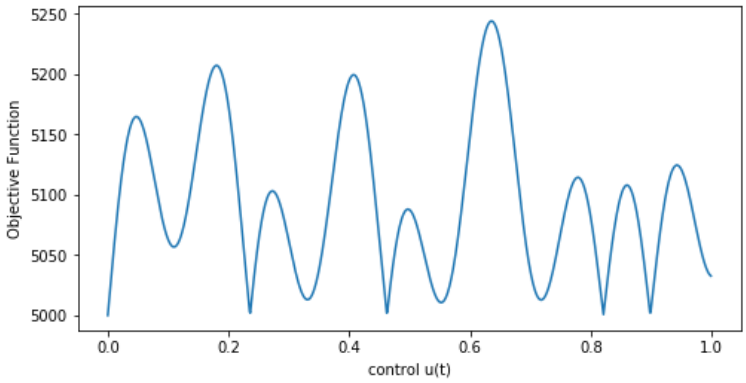

Figure 5.6 2D plotting for 1-dimensional control strategy and objective function

In Section 5.3.2, the theoretical knowledge and expression of kernel function are introduced. Since there are many choices for kernel function, the purpose of this section is to find out which kernel function is more effective to use in IBO algorithm. Several kernel function types were tested in this section. For each kernel function choice, we repeatedly implemented tests on the given high-dimensional control model 20 runs with the same initial conditions and model parameters values, and summarized the mean of all results for each kernel function. All simulation experiments were implemented and tested in Python version 3.7 programming language. Figure 5.7 shows the average objective function values for different kernels choices. Our computational experiments have shown that the RBF, Warping, and Matern52 kernels produce better objective function values than others for the given control model. Figure 5.8 shows the average running times for different GP kernels. Brownian, RBF, Linear, and Coregionalize are more efficient than the other kernels. Consider those simulation results, and we can see that RBF and Matern52 reach a better all-around performance than other kernel choices. Both RBF and Matern52 kernels are stationary kernels. RBF kernel is also known as the "squared exponential" kernel. Matern kernel is a generalization of the RBF kernel that contains an additional parameter that can control the resulting function's smoothness. Therefore, they are two popular kernel options for the GP.

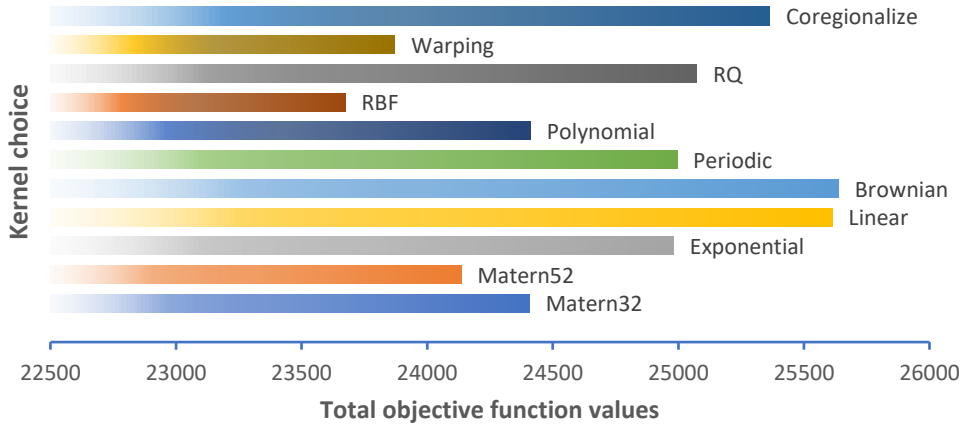

Figure 5.7 The mean of total objective function values for different kernels choices

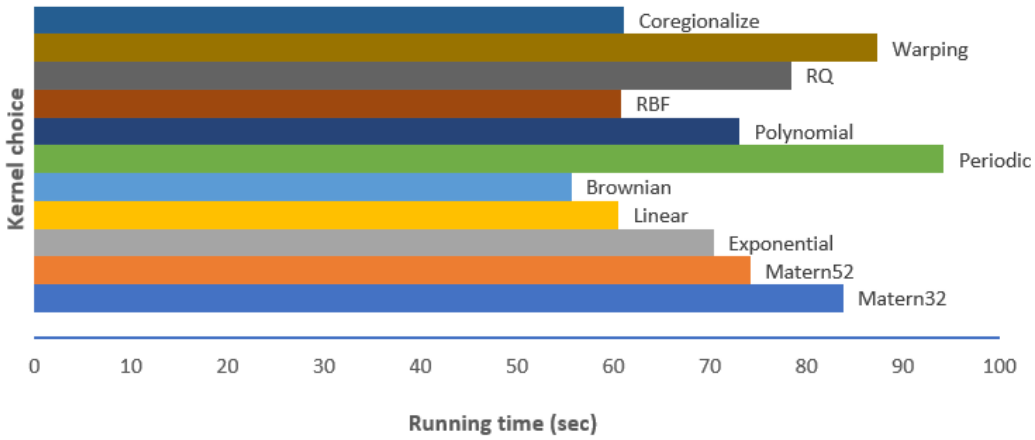

Figure 5.8 The running time for different kernels choices

5.5.3 Impact of Different Acquisition Functions on the Global Performance of The IBO Algorithm

To test the influences of the acquisition functions on the IBO algorithm, some simulation experiments were carried out using the three most popular acquisition functions: LCB, PI, and EI. For each acquisition function, 20 replications of simulation experiments are conducted by Python and summarized as the average performance more than 50 iterations. Due to the results of three different acquisition function choices after 25 iterations tend to be constant and almost coincide.

Thus, we will only show up the results of 26 iterations. Figure 5.9 shows the results for three different acquisition function choices within 26 iterations. Although these three acquisition functions perform differently before about the first iterations, they reach similar optimization results eventually after about 20 iterations. Thus, For IBO algorithm, three different acquisition function choices do not have impacts on the final results. In addition, all of three results have a sudden downward trend at about the 16^{th} iteration. Before they decrease sharply, the lines represent the results during the acquisition function optimization iterations. From about the 16^{th} iterations, the smooth descent curves represent the results when the IBO algorithm does the local search. It shows that adding the local search after the acquisition function optimization part is important and necessary for the accuracy of final solution.

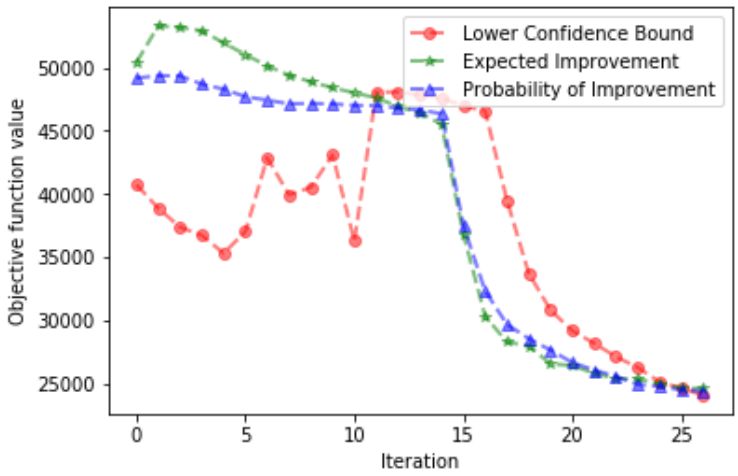

Figure 5.9 The convergence performance for different acquisition functions choices

5.5.4 Solving High-Dimensional Time-Dependent SEIR Optimal Control Problem Using the IBO Algorithm

This section we will study global optimization ability of the IBO algorithm for solving the optimal control solution on high-dimensional SEIR control model. Figure 5.10 shows the comparison results of the SEIR epidemic model with control and without any control. The black

and red dotted lines represent the trend for exposed and infected populations without control over time. The black and red solid lines represent the trend for exposed and infected populations with optimal control generated by the IBO algorithm. From Figure 5.10, we can find that the infected population raised sharply initially when the model is without control and declined very slowly to zero. However, the optimal control strategy created by the IBO algorithm effectively and quickly control the epidemic once it starts to break out.

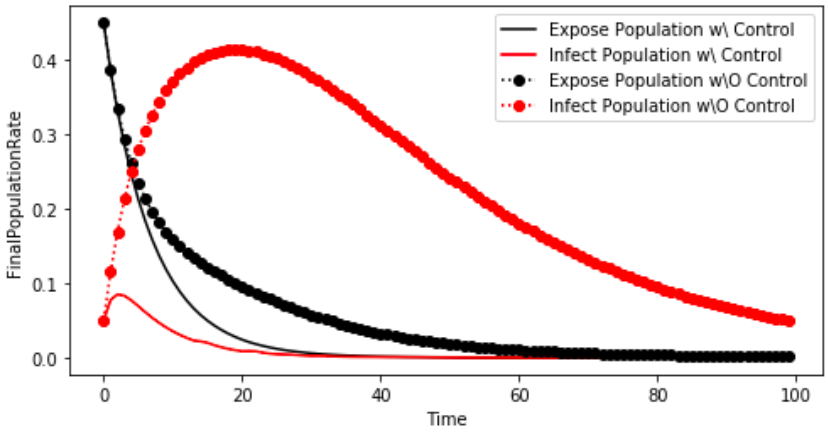

Figure 5.10 The comparison of population rate for the IBO algorithm and null control

Next, the position updates of the consecutive sampling points are tracked from iteration to iteration. In our simulation experiments, we set the value of $l = 1$ in **Algorithm 5.1**, which means the IBO algorithm only retains one best candidate from all sampling candidates to be the next sampling point. The convergence plots in Figures 5.11 and 5.12 depict how the distance changes between consecutive sampling points and how many iterations are required to find the global optima. The total iterations are the sum of the iterations m of sampling the new next point and the iterations of local search. From Figure 5.11, we can see that in the first 15 iterations, the distances between consecutive sampling points are relatively large and jumpy. It indicates that the sampling point is explored and updated by the global search, which was implemented from lines 5 to 17 in **Algorithm 5.1**. After that, the IBO algorithm starts to carry out more local searches within the

while loop. Thus, it is easy to see the gradual downward trend in the later iterations. Figure 5.12 shows the corresponding objective function values for the best sampling point at each iteration. Since we select the next sampling point according to the acquisition function value rather than the objective function value, that is why the trend line does not decrease monotonously within the first 15 iterations. After the local search process started, the IBO algorithm starts to perform searches based on the objective function value. Therefore, the trend line descends monotonously after the 15^{th} iteration. From both Figures 5.11 and 5.12, one can observe a good convergence performance of the IBO algorithm. It almost explores the global optima around 30 iterations with the solution time is around 70 seconds. These computational studies indicate that the IBO algorithm works well and effective for especially high-dimensional search spaces.

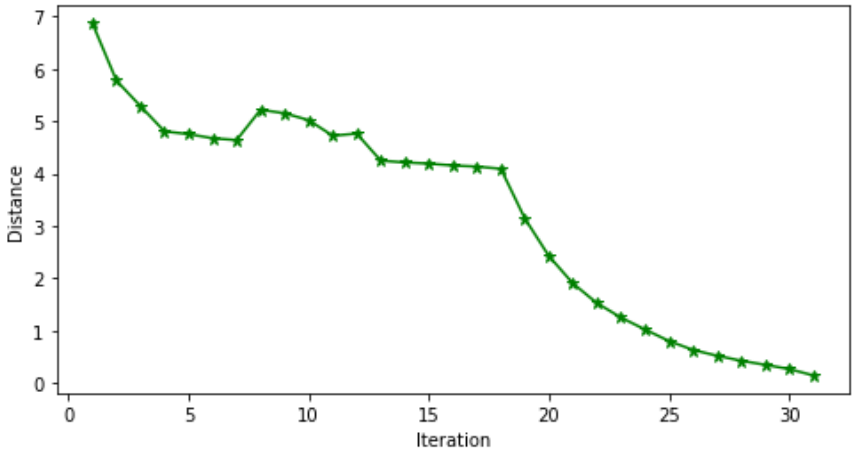

Figure 5.11 The distance change between consecutive sampling points during iterations

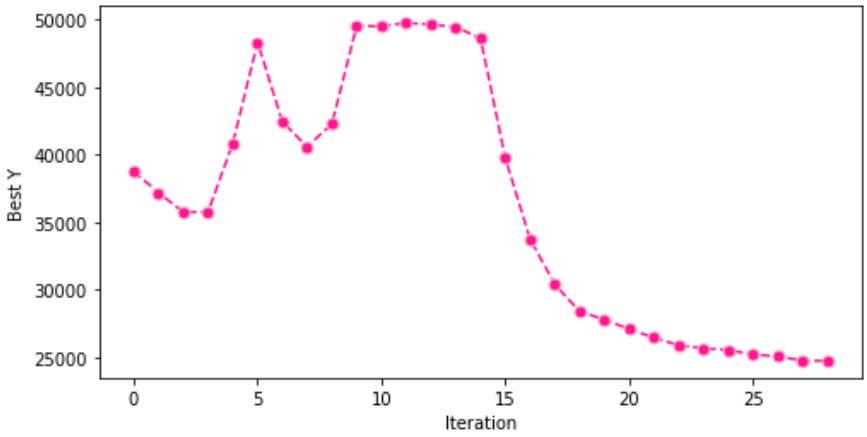

Figure 5.12 The objective function value change between consecutive sampling points during iterations

5.5.5 Comparisons of the IBO Algorithm, Random Search, PSO Algorithm, and Standard BO Algorithm

This section we will investigate how IBO algorithm performs compared to the standard BO algorithm, and two popular evolutionary optimization algorithms (Random Search algorithm and PSO algorithm). We compare the convergence performance of four algorithms on the time-dependent SEIR epidemic control model under the same parameter settings. For each compared algorithm, we conducted 15 simulation runs with random initial control strategies for each run. We display the means and standard deviations of the objective function value for all four algorithms over the same 25 optimization iterations. For PSO algorithm, there are four key parameters: the number of particles N, the inertia weight w, the cognition and social learning factors c_1 and c_2, we refer readers to [217] and [218] for more detailed and exact definitions and value settings of those parameters. The result of PSO algorithm in Figure 5.13 is under the parameter setting as $N = 50$, $w = 0.9$, $c_1 = c_2 = 2$. For IBO algorithm, the number of candidates defined in Section 5.3.4 is assumed as 5, the iteration values of main loop and local optimization

loop defined in Algorithm 5.1 in Section 5.3.5 are assumed as $m = 10$ and $l = 15$, so the total number of iterations of IBO algorithm during comparison simulation implementation is 25. For PSO algorithm, it takes about 18 seconds running time over 25 iterations for each run; Random search takes about 2 seconds running time over 25 iterations for each run; both standard BO algorithm and IBO algorithm take about 40 seconds running time over 25 iterations for each run.

Figure 5.13 plots the comparison results of the average of the objective function values along with corresponding standard deviation from 15 runs of four algorithms. The figure shows that eventually the IBO algorithm significantly reaches better objective function value than other algorithms. Note that the IBO algorithm sharply downs to different level after about 10^{th} iterations. This means that the local optimization search helps the IBO algorithm to find more accurate final solution based on its current best candidates gained from main implementation loop. In contrast, PSO algorithm, Random Search and the standard BO algorithm fail to minimize the objective function value of the researched high-dimensional and time-dependent SEIR control model within relatively less iterations. In addition, although the standard deviations of the IBO algorithm are larger before about the first 15 iterations, the standard deviations at last 5 iterations are obviously smaller than other three algorithms. This fact means that the IBO algorithm always may find the similar final optimal solutions within the same small feasible region over those 15 simulation tests. Hence, the IBO algorithm performs convergence to the same final optimal solution. Therefore, new IBO algorithm outperforms other algorithms in term of solution quality with reasonable amount of running times and number of optimization iterations. Besides the results of PSO algorithm shown in Figure 5.14, consider that the values of parameters may affect its global optimization performance on this time-dependent SEIR control model, we also test some other parameter value settings that usually assumed in related PSO algorithm implementation studies

[219, 220], i.e., $N = 50$, $w = 0.9$, $c_1 = 0.5$, $c_2 = 0.3$; $N = 100$, $w = 0.9$, $c_1 = 1.5$, $c_2 = 1.5$; $N = 50$, $w = random(0.1,0.5)$, $c_1 = random(1.5,2.0)$, $c_2 = random(1.5,2.0)$. We test the PSO algorithm over 50 iterations with similar running time as the IBO algorithm as well. The best result of PSO algorithm obtained from all tests for the researched SEIR model is that the minimum objective function value is about 30000.

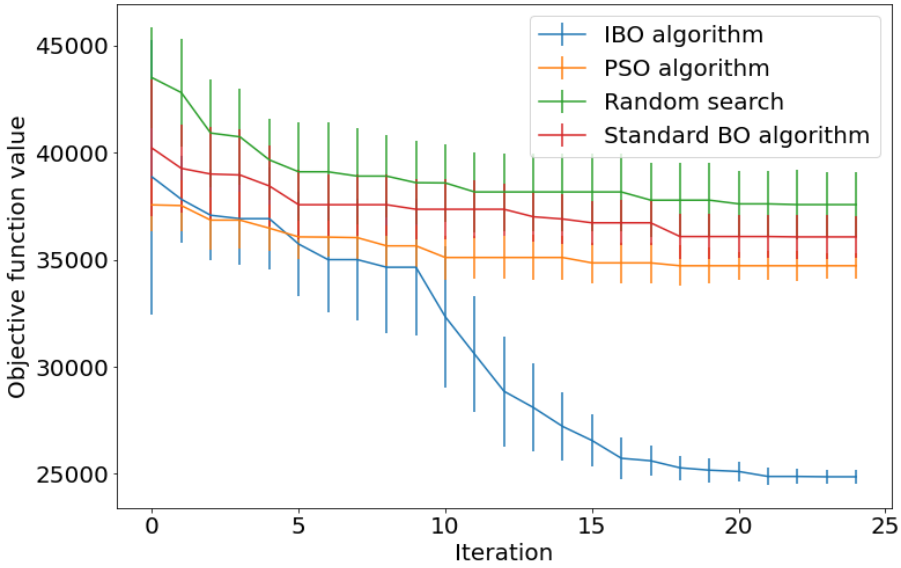

Figure 5.13 Comparison of the average of the objective function values from 15 simulation runs along with standard deviation

Besides, we conduct simulation experiments to study the robustness of the IBO algorithm comparing Random Search, PSO algorithm and the standard BO algorithm with the different initial control strategy inputs, and the results are summarized in Figure 5.14. The horizontal axis represents the initial control input of the algorithm that each dimension is set up the constant $\varphi \in [u_l, u_u]$ that is $u^0 = \left(u_0^0 = \varphi, \dots, u_{t_f}^0 = \varphi\right)$ $(\varphi = 0\ or\ 0.05\ or\ 0.1\ or\ 0.15, \dots or\ 1.0)$. For each compared algorithm, we conducted 10 simulation runs for each same initial control strategy input. We display the means and standard deviations of the objective function value for all four

algorithms over the same 10 optimization iterations for each input setting. The bar represents the average values of 10 runs, the black line upon the bar represents the corresponding standard deviation.

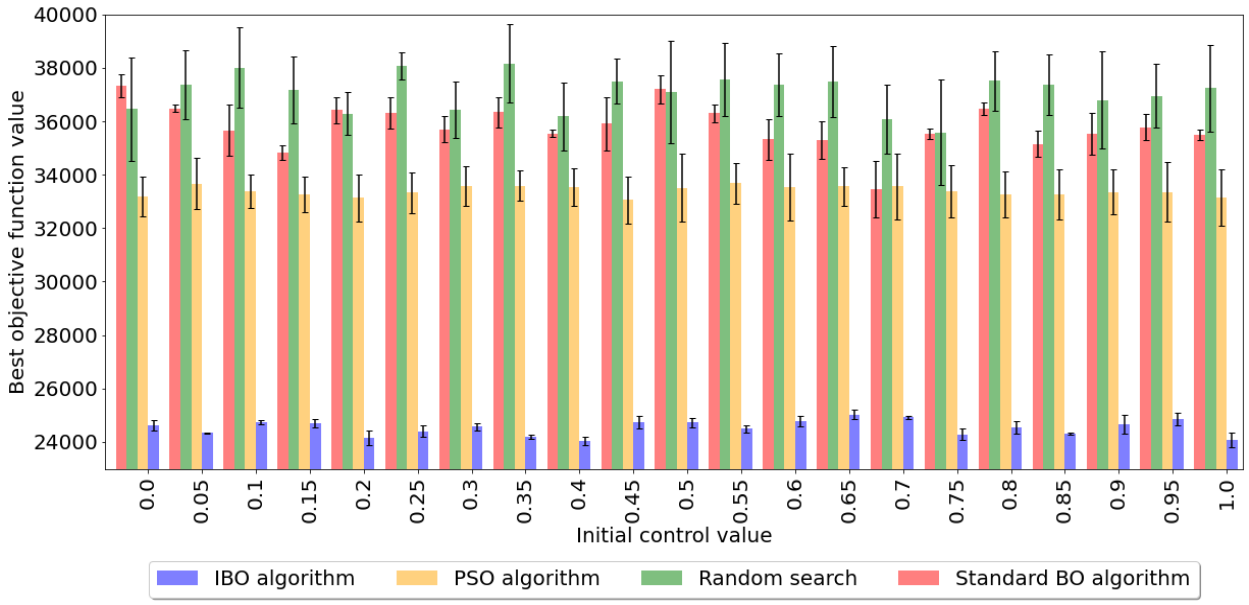

Figure 5.14 Sensitivity analysis of different initial control inputs for four algorithms

Figure 5.14 shows that over 10 simulation runs, the PSO and Random Search have larger standard deviations than the standard BO algorithm and IBO algorithm. The average values of IBO algorithm and PSO algorithm over the whole input range are more stable. For all different initial control inputs, PSO algorithm has smaller averages but large standard deviations than the standard BO algorithm, Random Search performs the worst results, which is most sensitive to the initial control inputs. Whether the standard deviations or averages, their values of the IBO algorithm are all significantly smaller than other three algorithms for all different initial control inputs. Hence, according to those results, it seems that the IBO algorithm performs nicely robustness than the PSO algorithm, Random Search, and standard BO algorithm. Besides, Random Search and PSO algorithms have a poor performance to reach the global optima. The IBO algorithm performs

relatively stable with different initial control inputs, it consistently searches out the global minimum for the given high-dimensional and time-dependent optimal control model.

5.6 Conclusion

In this paper, we improved the standard BO algorithm by considering more suboptimal steps for optimizing the acquisition function process. Also, an Adam-based local optimization process is used to improve the current solution even further when the best candidate is generated from acquisition function optimizations. The theoretical analysis for the feasible solution of the high-dimensional and time-dependent optimal control model with non-convex objective function is provide. Different kernel functions and acquisition function choices are discussed to study their impacts on the IBO algorithm's performances. We extend the IBO algorithm to solve both low-dimensional optimization problems with multiple local minima and high-dimensional and time-dependent optimal control model. Computational benchmarks of the IBO algorithm are also compared against four existing optimization algorithms, namely Simplicial homology global optimization, Dual annealing optimization, Differential evolution, and Basin-hopping algorithm, on three widely used single-objective test functions. Our benchmark tests showed that the IBO algorithm could reach the most precise solutions for all three test functions. The IBO algorithm performs an excellent optimization characteristic in low-dimensional optimization problems. Also, the trajectory of distances between consecutive sampling points indicates that implementing a local optimization process after the acquisition function optimizations is useful and necessary. Besides, compared with the Random Search, PSO algorithm and standard BO algorithm, the experimental results demonstrate that the IBO algorithm can achieve better optimization results for the high-dimensional and time-dependent optimal control model. The IBO algorithm is also more robust

with different initial control strategy inputs than Random Search, PSO algorithm and standard BO algorithm.

Despite the improvement, the IBO algorithm still performs a longer running time than some other global optimization algorithms within same number of iterations. Also, during candidates' selection process, the IBO algorithm tends to choose the candidate closer to the global optimal position among all candidates generated by uniform random distribution. That means some candidates are useless to be generated. Hence, our future works could focus on how to improve the running time of the IBO algorithm by using dimension reduction knowledge. Also, consciously and selectively sampling candidates is also one possible research direction for the extension of our IBO algorithm, once a more effective and efficient IBO algorithm combining these two thoughts becomes available, it would possible accurately catch a better candidate with high belief as the next sampling point within lower running time.

Chapter 6 - A New High-Dimensional Bayesian Optimization Algorithm for Complex Epidemic Optimal Control Models

Abstract

At present, high-dimensional global optimization problems with time-series models have received much attention from engineering fields. Bayesian optimization (BO) has quickly become a popular and promising approach for solving global optimization problems since it was proposed. However, the standard BO algorithm is insufficient to solving the global optimal solution when the model is high-dimensional and time-series. Hence, this paper presents a novel high-dimensional BO algorithm by considering dimension reduction and different dimension fill-in strategies. Five different dimension fill-in strategies were discussed and compared in this study. In addition, most existing literatures about BO algorithms did not discuss the sampling strategies to optimize the acquisition function. This study also proposes a new sampling method based on both the Multi-Armed Bandit and Random Search, which can more effectively and consciously determine the better solution for optimizing the acquisition function. Besides, though some computational experiments and comparisons with other BO algorithms, the proposed BO algorithm shows significantly excellent performances on either the final optimal solution or the running time for solving both deterministic and stochastic high-dimensional time-series epidemic optimal control systems.

Keywords: High-dimensional Bayesian Optimization; Time-series model; Optimal control; Global optimization.

6.1 Introduction

Effective and efficient disease control decision is important to mitigate the spread of epidemic, thus, driving the optimal control strategy for dynamic epidemic control model has attracted increasing attention in healthcare domain [221]. The health organizations or agencies usually take a series of prevention or intervention control strategies for local outbreaks, e.g., shelter-at-home, social distancing, person-protection-equipment, vaccination, quarantine, disinfection, or regional closures. All these control strategies have significant associated financial costs. If health organizations or agencies do not take any control strategies to prevent the epidemic, it may also cause inevitable economic consequences and costs, such as workforce losses due to outbreaks, increased community healthcare costs, local business downturns, and declined related travels. Thus, solving optimal control strategy that minimizes the financial cost associated with controls strategy and controls the epidemic progression has become an object. Most of existing studies defined the objective function of epidemic control model as convex [28 - 31]. However, the cost of control strategy could be affected by various factors like inpatient days, cost of treatment equipment, wages, logistics and infrastructure, the cost may be different at different time as well [56]. Hence, the objective function associated with controls strategy is possible non-convex [32]. That means the optimal control problem of epidemic control model is a global optimization problem that exists multiple local optimal solutions.

Besides, dynamic epidemic control model is time-series and high-dimensional. Time-series means that the values of the variables (e.g. system state variables and control variables) of the model at current time will affect subsequent variable values. Therefore, the control variables and the epidemic states are both time-series and stage-dependent in nature, which is different from conventional optimization problems with time-independent nature. In addition to the time-series

character, the epidemic control model is high-dimensional. An epidemic usually lasts for a few hundred days or even a couple of years, the control strategies carried out in the epidemic may contain up to hundreds of thousands of time epochs. If each time epoch is considered as a dimension of the system, solving the optimal control strategy of epidemic control model will be a time-series and high-dimensional optimization problem.

As the number of time epochs increases, especially when the model is complex and nonlinear, the optimization challenges for such high-dimensional time-series system are rising. When there are many state variables in the model, it is necessary to calculate the values of each state variable at each time epoch and sum up each epoch's cost to evaluate the overall cost for one control strategy. It could be too time-consuming to evaluate the overall cost of system containing hundreds of thousands of dimensions, even for a single control strategy. Thus, general conventional global optimization algorithms, such as Particle Swarm Optimization (PSO) algorithm [43], genetic algorithm [44], Simulated annealing [45], may be not enough sufficient to solve this type of optimization problem. Although these conventional algorithms can reach a good performance for the lower-dimensional systems [222, 223], they may suffer from relatively long running time or get stuck in a local optimum for high-dimensional complex dynamic systems, or even not suitable for solving time-series optimization systems. The above challenges hinted us to think about Bayesian Optimization.

Standard Bayesian Optimization (BO) is a promising and powerful global optimization approach to optimize complex dynamic systems with low dimensions [46]. However, it may be challenging for dealing with high-dimensional time-series systems. Recently some new BO algorithms were proposed especially for handling the high-dimensional challenge. For example, Moriconi *et. al.* proposed a high-dimensional BO algorithm by learning a nonlinear feature

mapping to reduce the inputs' dimension to easily optimize the acquisition function in low-dimensional space [47]. Zhang *et al.* introduced a sliced inverse regression method to BO to learn the intrinsic low-dimensional structure of the objective function in high-dimensional space [48]. Li *et al.* developed a new method for high-dimensional BO using a dropout strategy to minimize dimensions and optimize a subset of variables [49]. Rana *et al.* proposed a high dimension BO algorithm to solve the acquisition function with a flat surface by gradually reducing the length-scale of the Gaussian process [50]. This paper reduces the variable dimensions by reducing the length-scale during the Gaussian regression part, which is different from other high-dimensional BO algorithms we reviewed in this paper. It can only reduce the dimension of Gaussian processes rather than optimizing the acquisition function in a low-dimensional space, which may lead to an inaccurate solution while it does calculation efficiency.

Although the above high-dimension BO algorithms utilize the dimension reduction knowledge to realize the high-dimensional optimization purpose, they take a significant amount of time to reconstruct the system variables from low-dimensional space back to original high-dimensional space at each optimization iteration, and then calculate the corresponding objective function value in high-dimensional space. They may not enough efficiently realize the dimension reductions if the systems contain hundreds of thousands of dimensions, the implementation efforts and running time were not significantly improved. Also, those new high-dimensional BO algorithm focus on time-independent systems. Thus, we attempt to propose a new more efficient and effective high-dimensional BO algorithm that is suitable for the time-series systems, and can solve more accurate solution for high-dimensional time-series epidemic control systems with less implementation efforts and running time.

In this paper, we innovatively propose a high-dimensional BO algorithm combining dimension reduction and dimension fill-in (DR-DF BO algorithm). This algorithm effectively resolves the shortcomings from the most existing high-dimensional BO algorithms and obtains remarkable performance improvements in solving the global optimization solutions for high-dimensional time-series epidemic control models with non-convex objective function. Compared with the existing literature about high-dimensional BO algorithms and standard BO algorithms, the main contributions of this paper are listed as follows:

(1) This paper presents a new high-dimensional BO algorithm for solving the optimal control strategy of the high-dimensional time-series control model. The proposed algorithm combines both dimension reduction and dimension fill-in strategies. In this manner, the algorithm can efficiently solve the global optimal control for the high-dimensional control models with time-dependent or dimensions-dependent variables.

(2) The proposed DR-DF BO algorithm proposes a variable dimension reduction strategy that is suitable for the variables in the studied system are time-series. The proposed algorithm also doesn't require reconstructing the variable dimensions into original dimensional space at each acquisition optimization iteration, which significantly reduces the computational effort and shortens the implementation running time.

(3) This paper proposes a new sampling strategy to optimize the acquisition function by utilizing the multi-armed bandit concept and random search. This sampling strategy helps the proposed DR-DF BO algorithm learn the history known data and more quickly and effectively optimize the acquisition function at each iteration.

(4) This paper introduces five strategies for the dimension fill-in for the proposed DR-DF BO algorithm, which may provide more options to meet different system requirements for

further applications' use. Several fill-in strategies are tested and compared in this paper to increase the final solution's accuracy and study which fill-in strategy is better for the researched high-dimensional time-series control systems.

The remainder of this paper is organized as follows. Section 6.2 formulates two high-dimensional time-series optimal control epidemic systems, including one deterministic SEIR control system and one stochastic SIS control system. Section 6.3 presents each part of the proposed DR-DF BO algorithm in detail. Then the numerical simulation experiments are conducted to evaluate the proposed algorithm's performances in Section 6.4. Finally, Section 6.5 provides the conclusions and discusses our future work.

6.2 Problem Formulations

This section aims to show two time-series control models with non-convex objective function. To better demonstrate the effectiveness and efficiency of the proposed DR-DF BO algorithm, we select two different systems: deterministic and stochastic. The proposed high-dimension BO algorithm is expected to efficiently and accurately solve the global optimal control strategy that minimizes the non-convex objective function and subjects to the researched high-dimensional time-series control model.

In general, the control measures are not defined as variables in SEIR and SIS epidemic models [193, 224]. However, when the outbreak starts, health organizations or agencies tend to determine the disease intervention to control the spread of the epidemic more effectively, such as vaccination, quarantine, disinfection, or wearing masks. Those are all considered as control measures affecting the contact rate of infective individuals [197]. This paper considers the control variables in general SEIR and SIS epidemic models to balance the control measures on mitigating disease spread and relieving government financial burden.

6.2.1 Deterministic Time-Series SEIR Epidemic Optimal Control System

The deterministic SEIR epidemic optimal control system can be defined as following representation:

$$\text{Min} \quad V(u_1, u_2) = \int_{t_0}^{t_f} C_1 I(t) + C_2 f(u_1, u_2, t) \tag{6.1}$$

$$s.\,t. \quad \frac{dS(t)}{dt} = \tau - (1 - u_1(t))\beta S(t) I(t) - \tau S(t) \tag{6.2}$$

$$\frac{dE(t)}{dt} = \big(1 - u_1(t)\big)\beta S(t) I(t) - \alpha E(t) - \tau E(t) \tag{6.3}$$

$$\frac{dI(t)}{dt} = \alpha E(t) - \big(\gamma + u_2(t)\big) I(t) - \tau I(t) \tag{6.4}$$

$$\frac{dR(t)}{dt} = \big(\gamma + u_2(t)\big) I(t) - \tau R(t) \tag{6.5}$$

$$S(t) + E(t) + I(t) + R(t) = 1 \tag{6.6}$$

where t_0 is the start time, t_f is the final time, assume the start time $t_0 = 1$ in this paper; C_1 and C_2 are the financial cost of system without control and with control, respectively; $f(u_1, u_2, t)$ represents the cost function of control variable regarding time. In real world, since the cost of disease control may be possible non-convex [32], which is affected by various environment factor or control treatment condition [56] such as inpatient days, cost of treatment equipment, wages, logistics and infrastructure, etc. Hence, in this paper, we assume $f(u_1, u_2, t)$ is non-convex.

$S(t)$, $E(t)$, $I(t)$, $R(t)$ are the system state variables, represent the susceptible, exposed, infectious and recovered population rate at time t, respectively. S means the individuals who can contract the disease; E means the individuals who have been infected but are not yet infectious, in this model E is not contagious; I means the individuals who are capable to transmit the disease; R means the individuals who have become immune.

System parameter τ in Eqns. (6.2)-(6.5) represents the rate of natural birth, the rate of natural death is assumed to be equal to the natural birth rate; system parameter β in Eqns. (6.2)-

(6.3) represents natural contact rate between susceptible individual S and infectious individual I when there is no control measures such as vaccination, quarantine or activity restriction; system parameter α in Eqns. (6.3)-(6.4) represents the transfer rate from exposed individual E to infectious individual I; system parameter γ in Eqns. (6.4)-(6.5) represents natural recovery rate from infection status without using any control treatment such as medicine treatment or hospitalization.

u_1, u_2 in Eqns. (6.1)-(6.5) denote the system decision variables, sometimes it can be named as control variables. The control variable in this paper will indicate the level\degree\density of corresponding control measure. u_1 represents the level\degree\density of prevention control strategies. In real work, this type of prevention control strategies can be activities restrictions, vaccination, wearing mask, and social distance restriction, those control strategies can slow down the probability of susceptible individual S being infected by infectious individual I. u_2 represents the level\degree\density of intervention control strategies at time t. This type of intervention control strategies has practical meanings in real work, such as intense medical care or hospitalization facilities or equipment (e.g. respirator in COVID-19 epidemic), which can speed up the population's recovery from status I to status R. Control variables u_1 and u_2 are t_f-dimensions, which can be expressed as $u_1 = \{u_1(1), \dots, u_1(t_f)\}$ and $u_2 = \{u_2(1), \dots, u_2(t_f)\}$, $u_1(t), u_2(t) \in [0,1]$, $u_1(t)$ and $u_2(t)$ represent the level\degree\density of corresponding control measure at time t.

6.2.2 Stochastic Time-Series SIS Epidemic Optimal Control System

Consider the effective contact rate β of infectious individual in the deterministic epidemic model in Eqns. (6.2)-(6.3), this parameter is constant. Then each infectious individual makes βdt the effective contacts with other susceptible individuals during the time interval $[t, t + dt)$. Now

we assume that the contact rate β changes to a stochastic parameter $\bar{\beta}$ caused by certain stochastic environmental factors such as seasonal variations, climate change, air humidity, etc. In a stochastic model, the contact rate in the time interval $[t, t+dt)$ will make is assumed as:

$$\bar{\beta}dt = \beta dt + \sigma dB(t) \tag{6.7}$$

where $B(t)$ is a standard Brownian motion, Eq. (6.7) means that the stochastic contact rate is normally distributed with mean βdt and variance $\sigma^2 dt$, we refer readers to paper [224] to get more exact details and definitions of $B(t)$ and σ.

The stochastic SIS epidemic optimal control system with a stochastic contact rate is supposed as:

$$\text{Min} \quad V(u_1, u_2) = \int_{t_0}^{t_f} C_1 I(t) + C_2 f(u_1, u_2, t) \tag{6.8}$$

$$s.\,t. \quad \frac{dS(t)}{dt} = \tau - \big(1 - u_1(t)\big)\beta S(t) I(t)$$

$$+\big(\gamma + u_2(t)\big) I(t) - \tau S(t) - \sigma S(t) I(t) dB(t)/dt \tag{6.9}$$

$$\frac{dI(t)}{dt} = \big(1 - u_1(t)\big)\beta S(t) I(t) - \big(\gamma + u_2(t)\big) I(t) - \tau I(t) + \sigma S(t) I(t) dB(t)/dt \tag{6.10}$$

$$S(t) + I(t) = 1 \tag{6.11}$$

where the definition of system state variables, control variables and system parameters in system Eqns. (6.8)-(6.11) are the same defined in system Eqns. (6.1)-(6.6). In stochastic SIS epidemic control model, it will only consider two system state variables: susceptible population S and infectious population I.

In the rest section of this paper, we will only consider the type 2 control variable u_2. It means type 1 control variable u_1 is assumed to be zero. For simplification, we directly use symbol u to represent the control strategy u_2 in the rest of the paper, that is $u_2 = u =$

$\{u(1), \ldots, u(t), \ldots, u(t_f)\}$ $(1 \leq t \leq t_f)$. Then the objective function defined in Eq. (6.1) will be rewrite as:

$$V(u) = \int_{t_0}^{t_f} C_1 I(t) + C_2 f(u,t) \tag{6.12}$$

Since the cost function regarding control strategy can be possible non-convex [32], in this paper, we assume $f(u,t)$ is a non-convex function. Also, to increase the difficulty of the researched model and better to study the capability of the proposed DR-DF BO algorithm in solving the optimal control strategy for the researched high-dimensional time-series control models. Hence, we hypothetical design the same cost function $f(u,t)$ as a non-convex function shown in Eq. (6.13) for both SEIR and SIS control systems, which has no practical significance.

$$f(u,t) = 0.3|sin(10u(t))| + 2.1|sin(u(t))| + u^2(t) \tag{6.13}$$

6.3 The Proposed DR-DF BO Algorithm

The standard BO algorithm only considers the surrogate model, acquisition function, and random sampling for candidates' selection of the acquisition function optimization, which is only sufficient to optimize low-dimensional models. Standard BO algorithm doesn't perform well for high-dimensional models, especially for the time-series models. Time-series property would lead the complexity of global optimization straightly raise. Therefore, this paper proposes an effective and efficient high-dimensional BO algorithm based on dimension reduction and dimension fill-in. The proposed DR-DF BO algorithm includes six important steps: variable dimension reduction, surrogate model, acquisition function, sampling strategies for candidates' selection of the acquisition function optimization, local search with a series of Adam-based steps, variable dimension fill-in. Each step is detailed introduced in this section.

6.3.1 Variable Dimension Reduction

When the model is high-dimensional, solving the optimal solution is usually computationally intractable. For example, the control variables u in this paper is t_f-dimensions. If t_f is larger than hundreds or even thousands, solving a global optimal control strategy with time-series property in such a high-dimensional space will become almost impossible. Dimension reduction is an effective way to transfer data from high-dimensional space into low-dimensional space while retaining as much important information and meaningful properties of the original model as possible.

Most conventional dimension reduction methods can effectively deal with dimension reduction of high-dimensional variables in many fields. The variables in those application fields have a common property, that is the remaining dimensions before and after dimension reduction are both independent, and the removed dimensions usually contain less meaningful information of the original variables. However, the control variables in high-dimensional models researched in this paper follow a time-series correlation. The control strategy of the model at each time epoch (time dimension) is dependent on the strategies at previous epochs, it also would affect the control strategies at subsequent time. The control value $u(t)$ at time t will affect the model's state variables values at time t, and then the state variables values will affect the control values at next moment. Thus, conventional dimension reduction methods may not be well-suited to handle the variables with time-series nature.

The control variables of SEIR and SIS models under study have t_f dimensions. Since the control value at each time epoch are equally important and time-dependent, hence the proposed DR-DF BO algorithm will evenly select $d < t_f$ ($d \in Z^+$) dimensions to realize the dimension reduction. We call d dimension reduction value in this paper, the variable will remain d

dimensions after reduction. **Figure 6.1** provides some examples that the DR-DF BO algorithm determines the reduced dimensions in time.

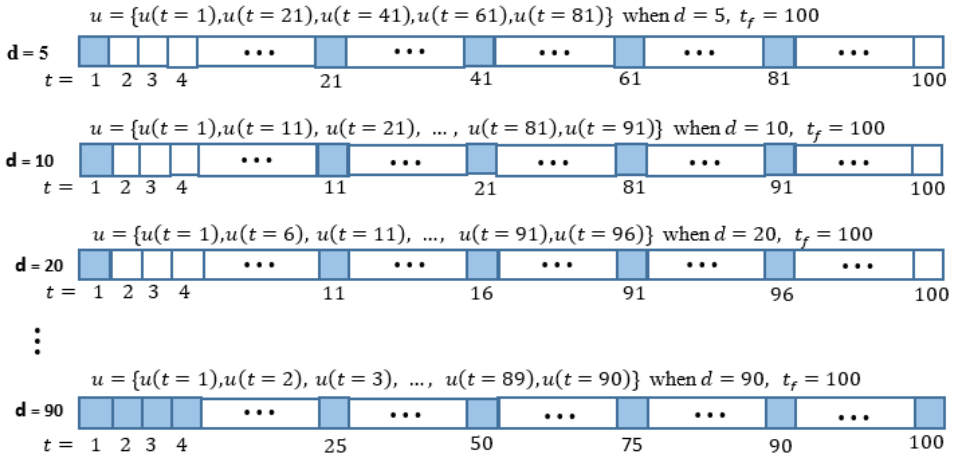

Figure 6.1 The DR-DF BO algorithm selects the time dimensions for different d (the color boxes represent the selected dimensions)

6.3.2 Surrogate Model

The surrogate model is an approximation model constructed by using a data-driven approach. There are many choices for many existing BO algorithms to construct the surrogate model, for example, neural networks, random forests, and Gaussian Process. But Gaussian Process is a more popular choice to construct the surrogate model for BO algorithm [225].

The Gaussian Process is a probability distribution over function. Herein, suppose the objective function $V(u)$ follows a Gaussian Process. Define $V(u^i)$ is the objective function value for i-th control strategy u^i, where $i \in Z^+$, i is used to number the control, the control strategy with different superscript only represents different control strategy. In here, simply denote the control strategy u^i as d-dimensional control variable after dimension reduction. Then there is:

$$V(u^i) \sim \mathcal{GP}(m(u^i), k(u^i, u^j)) \tag{6.14}$$

and

$$u^i = \{u^i(t=1), \dots, u^i(\cdot)\} = \{u_1^i, \dots, u_d^i\} \tag{6.15}$$

where $m(u^i)$ is called the mean function; $k(u^i, u^j)$ is the covariance function [49], the covariance function is also called kernel function; where u^i and u^j are two different control strategies. Oftentimes, the mean function is defined as either a linear function or directly defined as zero [204]. Without loss of generality, the mean function in this paper is defined as $m(u^i) = 0$.

Since the objective function follows the Gaussian Process, any finite number of the objective function values $V(u^i)$ will follow the multivariate Gaussian distribution [205]. Let the set of historical objective function values $V = [V(u^0), \dots, V(u^i)]^T$ and u^i is *i*-th control strategy, then V is Gaussian distributed with mean vector $M = [m(u^0), \dots, m(u^i)]^T$ and covariance matrix (kernel matrix) K as below:

$$K = \begin{bmatrix} k(u^0, u^0) & \cdots & k(u^1, u^i) \\ \vdots & \ddots & \vdots \\ k(u^i, u^0) & \cdots & k(u^i, u^i) \end{bmatrix} \tag{6.16}$$

The kernel function k and covariance matrix (kernel matrix) K are used to theoretically estimate the covariance information of the original objective function at any two control strategies (sampling points).

For any new control strategy u^j (a control strategy is also named as a sampling point in the introduction or implementation of the DR-DF BO algorithm), the corresponding objective function value is $V(u^j)$, let

$$V' = \begin{bmatrix} V \\ V(u^j) \end{bmatrix}, M' = \begin{bmatrix} M \\ m(u^j) \end{bmatrix}, \Sigma = \begin{bmatrix} K & K'^T \\ K' & K'' \end{bmatrix} \tag{6.17}$$

where $K' = [k(u^j, u^0), k(u^j, u^1), \dots, k(u^j, u^i)]$, $K'' = k(u^j, u^j)$. Then the posterior distribution of $V(u^j)$ for any new control strategy (sampling point) u^j based on the known dataset V will

Gaussian distributed with mean $\mu\left(V\left(u^j\right)|V,u^j\right)$ and variance $\sigma\left(V\left(u^j\right)|V,u^j\right)$, which can be written as:

$$V\left(u^j\right)|V,u^j \sim \mathcal{GP}(\mu(V\left(u^j\right)|V,u^j),\sigma(V\left(u^j\right)|V,u^j)) \tag{6.18}$$

where the posterior mean and the variance can be derived as:

$$\mu\left(V\left(u^j\right)\middle|V,u^j\right) = m\left(u^j\right) + K'K^{-1}(V-M) = K'K^{-1}(V-M) \tag{6.19}$$

$$\sigma\left(V\left(u^j\right)\middle|V,u^j\right) = K'' - K'K^{-1}K'^{T} \tag{6.20}$$

In the Gaussian Process, kernel function $k\left(u^i,u^j\right)$ is an important concept. The reason why it is important has been discussed in paper [226]. BO algorithm may perform different results with different kernel functions. Some popular kernel function choices include Matern32, Matern52, Radial Basis Function, Exponential, Linear, Brownian, Periodic, Polynomial, Warping, Coregionalize, RationalQuadrati [227]. For the proposed DR-DF BO algorithm in this paper, Matern52 kernel is selected as the kernel function $k\left(u^i,u^j\right)$, which is expressed as:

$$k\left(u^i,u^j\right) = (1+\sqrt{5}*\frac{|u^i-u^j|}{l}+\frac{5}{3}*\frac{|u^i-u^j|^2}{l^2})\exp\left(-\sqrt{5}*\frac{|u^i-u^j|}{l}\right) \tag{6.21}$$

where l is the length-scale hyperparameter, its value reflects the smoothness of the objective function.

6.3.3 Acquisition Function

Acquisition function is used to approximate the original objective function with less efforts, which is based on the historical data information got from Gaussian Process. The system in this paper is time-dependent, then the values of state variables at current moment will affect their values at the next moment. When calculating the overall objective function value if the model contains many state variables, it is necessary to calculate the values of state variables at each time epoch and sum up each epoch's cost to evaluate the overall cost of a control strategy. It could be too time-

consuming to evaluate the overall cost for a single control strategy. Therefore, this paper attempt to use the acquisition function to approximate the original objective function for reducing the calculation effort and computational time. The acquisition function also is an excellent way to define a trade-off between exploitation and exploration The exploitation will guide the algorithm to sample the next points leading to a lower objective function value, which can be expressed by posterior mean got from Gaussian Process. The exploration will guide the algorithm to sample the next points that the objective function values could be highly uncertain, which can be expressed by posterior variance got from Gaussian Process.

Through the Gaussian Process, the acquisition function obtains the posterior mean and variance at a new sampling point u^j. The acquisition function can leverage the posterior distribution information to calculate a value that represents how desirable it is to sample next at this new point u^j. Some well-known choices of acquisition functions can provide a trade-off between exploration and exploitation for various applications. For example, lower confidence bound (LCB) [210], expected improvement (EI) [228], probability of improvement (PI) [229], Thompson sampling [230]. The original name of LCB is named Gaussian Process Upper Confidence Bound [231], it's originally proposed for the maximization problem. Since the optimization problem in this paper is a minimization problem, we use LCB here. PI is an alternative expression of EI. But PI is biased towards the exploitation over the exploration. When the variable is a single dimension, Thompson sampling usually performs better than other choices on running time.

This paper chooses LCB as the acquisition function of the proposed DR-DF BO algorithm. The expression is defined as:

$$\mathrm{LCB}(u^j; k) = \mu\left(V\left(u^j\right)\middle|V, u^j\right) - k\sigma\left(V\left(u^j\right)\middle|V, u^j\right) \tag{6.22}$$

where k is the weight to balance the posterior mean (exploitation) and variance (exploration). The purpose of the original optimization problem is temporally changed to find a control strategy, u^j, using the proposed DR-DF BO algorithm to minimize the Eq. (6.22).

6.3.4 Sampling Strategies

Most of the current research works of BO do not discuss the sampling strategies for optimizing the acquisition function. The construction of the acquisition function is essential, but the sampling strategy to optimize the acquisition function also is the key to solve the global optimization problems efficiently. It does not efficiently handle the original optimization problem if we search the whole feasible solution space to find a solution that optimizes the acquisition function. Random search is a simple and popular strategy to select the next sampling point for optimizing the acquisition function. However, if unlucky, the random search may either catch many similar sampling points that provide redundant information or never being able to locate the points closer to the global optima. This paper introduces the Multi-Armed Bandit concept and considers the sampling point process as a Multi-Armed Bandit problem.

Multi-Armed Bandit is a classic example of the exploration-exploitation trade-off. In the Multi-Armed Bandit, at each time, the player decides to choose one or some machines from all machines, whether to continue with the current machine or try a different machine [232]. Each machine is configured with a reward probability of how you will likely earn a reward at each decision. In the proposed DR-DF BO algorithm, we refer to different sampling value zones as different machines and refer to the number of sampling points at each value zone as the reward of the corresponding zone. The referred details will be presented in Section 6.3.4.1. The aim of using Multi-Armed Bandit concept in the proposed algorithm is to choose the best selection strategy at each iteration to achieve maximum long-term rewards. At each iteration, the decision logic is set

up so that the algorithm can continuously gather more information to make better decisions later, which is referred to as the reinforcement learning process. Therefore, the DR-DF BO algorithm is proposed to combine the advantage of the Multi-Armed Bandit and Random Search for the sampling point process. It can optimize the acquisition function effectively.

6.3.4.1 Sample Points Based on Multi-Armed Bandit

After dimension reduction, each control strategy u^i should be d-dimensional, which is in Eq. (6.15). Therefore, the sampling point (a sampling point represents a control strategy) is d-dimensional as well. The d -dimensional sampling point is expressed as $u^i = \{u^i(t = 1), \dots, u^i(\cdot)\} = \{u_1^i, \dots, u_d^i\}$. The DR-DF BO algorithm is based on the Multi-Armed Bandit that evenly divides the feasible region $[0, 1]$ into n separate zones. For each zone, the DR-DF BO algorithm samples m points and there will be m control strategies in each zone. It means for each iteration, each zone samples m control strategies, each control strategy is d dimensions, then there should sample $n * m$ control strategies in all n zones. Therefore, at each zone, m sampling points $u^1, \dots, u^m \in \mathbb{R}^d$ were selected.

We refer the number of sampling points at each zone as the reward of this zone. So, assume the initial reward of each zone is equal to m, then the n-dimensional reward matrix regarding all zones is $R = (m, m, \dots, m)$. This reward matrix R also represents the matrix of the number of sampling points in all zones. Calculate all acquisition function values corresponding to $n * m$ sampling points, find the sampling points with the smallest and largest acquisition function values and locate the corresponding zones these two sampling points belong to. We decide that the zone where the sampling point with the smallest acquisition function value belongs to receives a reward (for minimization problem), the zone where the sampling point with the largest value belongs to loses a reward. It means that in the next sampling iteration, one zone will be sampled with one less

point, and one zone will be sampled with one more point. This reward and reinforcement process can be generalized with other possible schemes. For example, we can define the zone where the sampling point with the second smallest value belongs to will earn p rewards, the section where the sampling point with the largest value belong to will lose q rewards, etc. Besides, among all $n * m$ sampling points, select the sampling point with the smallest acquisition function value as u_M^* (the best control strategy selected based on Multi-Armed Bandit), and express the corresponding acquisition function value as y_M^*.

6.3.4.2 Sample Points Based on Random Search

On the other hand, the DR-DF BO algorithm also takes advantage of Random Search to help with sampling points. The DR-DF BO algorithm specifies a uniform distribution with initial lower limit L and initial upper limit P for each dimension of control strategy u^i. The initial lower limit L is equal to 0, initial upper limit P is equal to 1 in this paper. Then randomly sample value from the uniform distribution for each dimension of control strategy. In such case, the algorithm tries to use this sampling way to generate N sampling points $u_R^1, u_R^2, \dots, u_R^N$. Each sampling point is d dimensions. Calculate all acquisition function values corresponding to these N sampling points. Also, among all N sampling points, the algorithm selects a sampling point with the smallest acquisition function value as u_R^* (the best control strategy selected based on Random Search), and express the corresponding acquisition function value as y_R^*.

During each iteration of the DR-DF BO algorithm, the best d-dimensional control strategy can be selected as:

$$u^* = \begin{cases} u_M^*, & y_M^* < y_R^* \\ u_R^*, & otherwise \end{cases} \tag{6.23}$$

To more effectively sample points via Random Search in each iteration, the DR-DF BO algorithm tries to update the lower limit and upper limit for the uniform distribution as:

$$L = \begin{cases} L + \alpha, & y_M^* < y_R^* \\ unchange, & otherwise \end{cases} \tag{6.24}$$

$$P = \begin{cases} P - \beta, & y_M^* < y_R^* \\ unchange, & otherwise \end{cases} \tag{6.25}$$

where α and β are constant parameters. The values of α and β in each iteration must satisfy the following condition:

$$u_l \leq L + \alpha < P - \beta \leq u_u \tag{6.26}$$

The purpose of updating the bound limit is to gradually and effectively narrow the feasible space utilizing the information from previous sampling process. To better determine the values of α and β, we need to understand that α can be set as 0 or a smaller value if u_M^* is closer to the control strategy's lower bound 0, and β can be set as 0 or a smaller value if u_M^* is closer to the control strategy's lower bound 1.

6.3.5 Local search with Adam-Based Steps

The existing BO algorithms usually conclude that the algorithms find the final global optimal solution when they are done optimizing the acquisition function, we considered a local search with Adam-based steps in an improved BO algorithm and reached a better final optimal solution in another paper [226]. The paper [226] provides the reason and theoretical analysis to explain why we add a local search after the acquisition function optimization process. We refer readers to that paper for more details about the local search with Adam-based steps. To increase the solution's accuracy, the DR-DF BO algorithm decides to add such a local search process after the acquisition function optimization, which can significantly improve the solution quality in our computational experiments.

6.3.6 Variable Dimension Fill-In

Many existing high-dimensional BO algorithms [47, 48, 50] consider reducing the variable's dimensions before optimizing the acquisition function. These algorithms find a low-dimensional sampling point with the optimal acquisition function value. Then the algorithms tend to transfer these low-dimension sampling points back to their original high-dimensional space to reconstruct a corresponding high-dimensional point. After that, they calculate the original objective function values corresponding to this high-dimensional solution space. Finally, the algorithms add this high-dimensional point and its objective function value into the database to update the surrogate model.

The BO algorithms transform the models into a lower dimension space and then transfer the decision variables back into original dimension at each iteration, which results in not much computational time saving due to recalculating the original objective function values in its high-dimensional space at each iteration. It seems that these high-dimensional BO algorithms do not successfully and efficiently realize the purpose of dimension reduction. Besides, it is unreasonable that those algorithms update the surrogate model using the high-dimensional reconstruction point and its corresponding objective function value. The surrogate model learns the posterior information and the relationship between the high-dimensional variables and objective function values. But the algorithms use that information to optimize the acquisition function value in low-dimensional space and find the best low-dimensional point, which is inconsistent and may lower the solution's accuracy. That is why the DR-DF BO algorithm decides to do the variable dimension fill-in for low-dimensional sampling point after finishing all acquisition function optimization iterations and an Adam-based local search process.

Considering the control strategy after the Adam-based local search process, we need to fill in the low-dimensional control strategy from the left $t_f - d$ dimensions to evaluate the real objective function values in the whole space. The following section will introduce five different strategies to realize the variable dimension fill-ins.

6.3.6.1 Identical Value Fill-In

Identical value fill-in strategy means to fill in the left dimensions with the same values as the d dimensions we obtain. We know that the control strategy u^i after dimension reduction can be exactly expressed in Eq. (6.15), then the control values between time interval $[1, \left\lfloor \frac{t_f}{d} \right\rfloor + 1)$ can be filled with the same value $u^i(t=1)$. To simplify, we use $u(t=1)$ to denote $u^i(t=1)$, and assume $\varphi = \left\lfloor \frac{t_f}{d} \right\rfloor$. The control values between time interval $[\varphi + 1,\ 2\varphi + 1)$ can be filled with the same value $u(t=\varphi+1)$, and so on. **Figure 6. 2** Shows the identical value fill-in process example when $d = 20$ and $t_f = 100$.

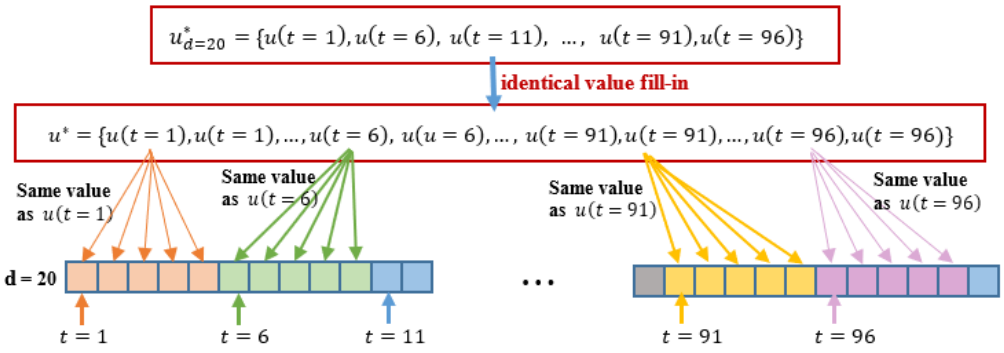

Figure 6.2 Identical value fill-in strategy

6.3.6.2 Uniform Distribution Fill-In

Uniform distribution fill-in means to fill in the left dimensions by using the uniform distribution. For the d-dimensional control strategy:

$$u_d^* = \{u(t=1), u(t=\varphi+1), \ldots, u(t=(d-1)\varphi+1)\} \tag{6.27}$$

The control values between time interval $\Delta = [q\varphi + 1, (q+1)\varphi + 1)$ can be filled by using the uniform distribution with the lower bound and upper bound as the following expression, respectively:

$$lower\ bound = \min\left(u(t = A), u(t = B)\right) \tag{6.28}$$

$$upper\ bound = \max\left(u(t = A), u(t = B)\right) \tag{6.29}$$

where $A = q\varphi + 1, B = (q+1)\varphi + 1$.

6.3.6.3 Linear Approximation Fill-In

Linear approximation fill-in means to fill in the left dimensions by using linear approximation approach. For the control values between time interval Δ (defined in Section 6.3.6.2), we can approximate the control value using following equation ($2 \leq m \leq \varphi$):

$$u(t = A) + (m-1)\frac{u(t=B) - u(t=A)}{\varphi} \tag{6.30}$$

6.3.6.4 Normal Distribution Fill-In

The normal distribution fill-in means to fill in the left dimensions by using a normal distribution. For the control values between time interval Δ (defined in Section 6.3.6.2) can be filled by using the normal distribution with the mean and standard deviation of control strategies $u(t = A)$ and $u(t = B)$ as the following, respectively:

$$mean = mean(u(t = A), u(t = B)) \tag{6.31}$$

$$std = std(u(t = A), u(t = B)) \tag{6.32}$$

6.3.6.5 Gaussian Regression Fill-In

Gaussian regression fill-in means to fill in the left dimensions by using the Gaussian regression model [233]. For the d-dimensional control strategy, the DR-DF BO algorithm learns the Gaussian regression model based on d control values of this d-dimensional control strategy.

For the control values between time interval Δ (defined in Section 6.3.6.2), the algorithm uses the learned Gaussian regression model to predict the corresponding control values.

The flowchart of the DR-DF BO algorithm is shown in **Figure 6.3.** The complete implementation steps of the DR-DF BO algorithm are summarized in **Algorithm 6.1**.

Algorithm 6.1 The DR-DF BO Algorithm

1: Initialize control strategy and state values of the model
2: Evenly select d dimensions of the control strategy
3: Construct the Gaussian process model
4: **for** loop = 1, 2, … **do**
5: **for** i = 1, 2, … n sections **do**
6: Evenly generate m d-dimensional sampling points
7: Find the best sampling point u_M^* and corresponding acquisition function value y_M^*
8: **end for**
9: **for** j = 1, 2, … N **do**
10: Randomly generate N sampling points $u_R^1, u_R^2, \ldots, u_R^N$
11: Find the best sampling point u_R^* and corresponding acquisition function value y_R^*
12: **end for**
13: Find the best d-dimensional control strategy u^* by comparing y_M^* and y_R^*
14: Check if need to update the lower limit L and upper limit P
15: Calculate $y^* = f(u^*)$, where f is the original objective function
16: Add the data (u^*, y^*) into a database to update the Gaussian process model
17: **end for**
18: **obtain** the control strategy u^* with best $f(u^*)$ recorded during iterations
19: **do** local search based on series of Adam-based steps starting from the point u^*
20: Fill in the point u^* by using one of five strategies for dimension fill-in
21: **return** the final optimal control strategy and corresponding objective function value

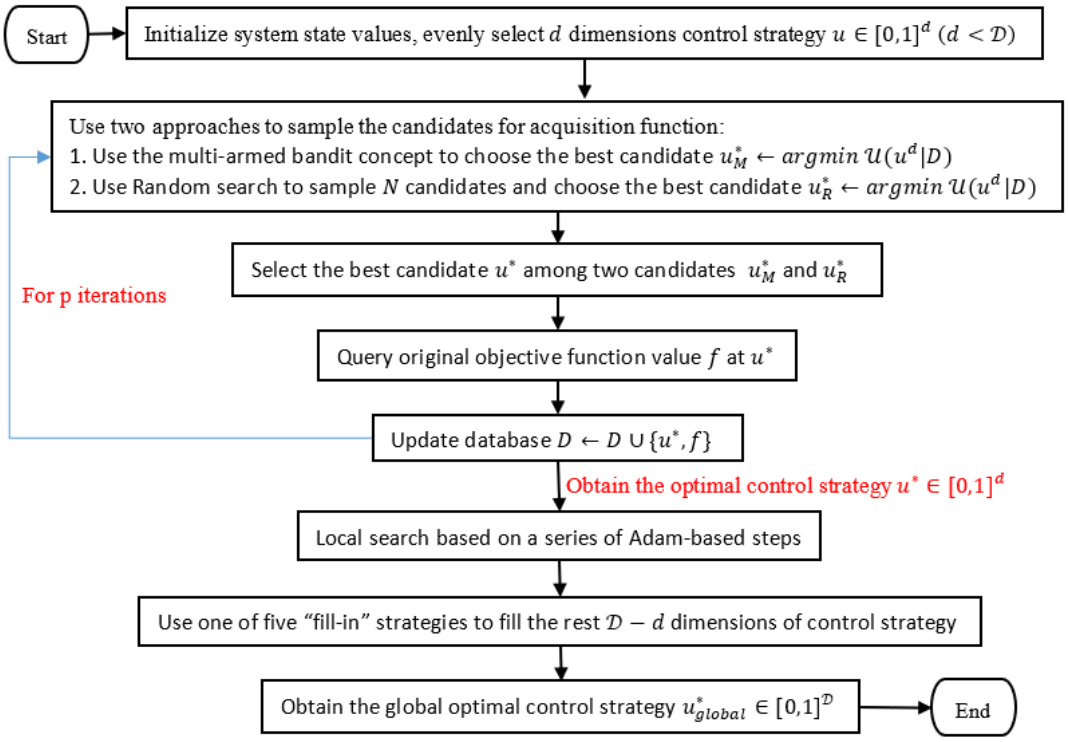

Figure 6.3 The flowchart of DR-DF BO algorithm

6.4 Numerical Simulation

This section evaluates the proposed DR-DF BO algorithm's performance on two high-dimensional time-series epidemic systems and compares it with other global optimization algorithms: standard Bayesian optimization algorithm [234], and a high-dimensional BO algorithm proposed in [49]. In this study, all simulation experiments are conducted on Python version 3.7 with Intel Core i5 CPUs and 32G memory, the Python libraries what we used includes Torch, Pyro, Scikit-learn. The kernel function selected in the following simulation experiments is Matern52, and the lower confidence bound function is defined as the acquisition function.

6.4.1 DR-DF BO Algorithm on Deterministic High-Dimensional Time-Series SEIR Epidemic Optimal Control System

This part verifies the global optimization performance of the DR-DF BO algorithm on the deterministic high-dimensional time-series SEIR control system defined in Eqns. (6.1)-(6.6), the global optimal control strategy is expected to not only control the epidemic spread but also minimize the overall financial cost. Under investigation, the deterministic SEIR model has the control variable with 100 time-epochs, so this problem's dimensionality is 100.

Figure 6.4(a) shows the SEIR epidemic model's infectious population rate with the control of different d and without any control when the fill-in strategy is a linear approximation. The solid red line represents the trend of infectious population rate without any control over time. The other color lines represent the trend of the infectious population rate with optimal control generated by the DR-DF BO algorithm when the algorithm selects different dimension reduction value d. As can be seen from Figure 6.4(a), the infectious population increases sharply initially when the model is without control and declines very slowly to zero. However, no matter the dimension reduction value, the optimal control strategies generated by the DR-DF BO algorithm effectively and quickly control the epidemic once it breaks out.

Figure 6.4(b) shows the trends of accumulated objective function value of the deterministic SEIR model with different d and without any control when the fill-in strategy is a linear approximation. The small figure in Figure 6.4(b) is a partial zoom figure between time interval $[40,100]$. We can see that the accumulated objective function when the model is without control is significantly higher than the values with control. Also, when d value is about 40, the DR-DF BO algorithm can achieve a closer effect without dimension reduction (when $d = 100$). Figure 6.4(c) shows the final best objective function values and running time comparison results for

different d when the fill-in strategy is a linear approximation. To make the results more intuitive, we use the ratio to express the results. We name the ratio of accumulated objective function value as AOFV ratio, and the ratio of running time as RT ratio, their expressions are defined as:

$$AOFV\ ratio\ (d) = \frac{AOFV(d)}{AOFV(d=100)} \tag{6.33}$$

$$RT\ ratio\ (d) = \frac{RT(d)}{RT(d=100)} \tag{6.34}$$

where $AOFV(d)$ and $RT(d)$ mean the accumulated objective function value and running time when dimension reduction value is d, respectively.

The ratio results for the SEIR control model are summarized in Table 6.1. The smaller the value of the ratio, the better the result. In our simulation experiments of the SEIR control model, $AOFV(d = 100)$ is about 15500, $RT(d = 100)$ is about 13 seconds. According to the simulation results, we can see that the DR-DF BO algorithm performs relatively well on both the final objective function value and running time when the dimension is reduced to 40. The proposed DR-DF BO algorithm can reach an excellent final solution using a reduced dimension of 40 with around 8 seconds of running time. The DR-DF BO algorithm shows an excellent global optimization performance for the deterministic SEIR model. It efficiently solves the optimal control strategy for the model to control the epidemic spread and significantly reduce the financial cost.

Table 6.1 AOFV ratio and RT ratio for different d in SEIR model

d	5	10	20	30	40	50	60	70	80	90	100
AOFV ratio	1.218	1.218	1.218	1.1336	1.061	1.098	1.076	1.028	0.994	1.0	1.0
RT ratio	0.307	0.385	0.462	0.538	0.615	0.615	0.692	0.769	0.846	0.923	1.0

Figure 6.4(d) shows the deterministic SEIR control model's best objective values of different d when the DR-DF BO algorithm chooses different fill-in strategies. We can directly see

that these five different fill-in strategies all provide good approximations on the deterministic SEIR control model. All of them perform similar trends, they also can reach almost same better objective function values at $d = 40$. These observations indicate that the DR-DF BO algorithm can solve the optimal control solution within a reasonable running time no matter which fill-in strategy it uses.

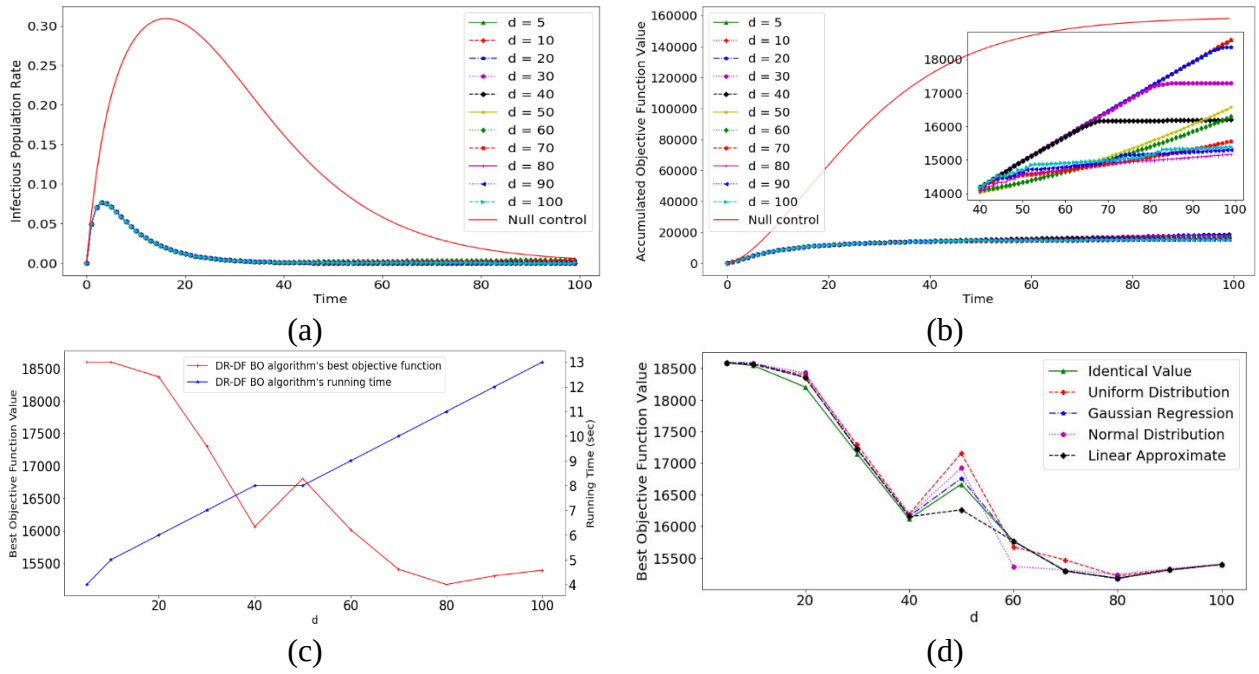

Figure 6.4 Simulation results of the DR-DF BO algorithm on deterministic SEIR control model. (a) Infectious population rate over time for different d. (b) Accumulated objective function values over time. (c) Best objective function values and running time for different d. (d) Best objective function values of different fill-in strategies.

6.4.2 DR-DF BO Algorithm on Stochastic High-Dimensional Time-Series SIS Epidemic Optimal Control System

This part verifies the global optimization performance of the DR-DF BO algorithm on the stochastic high-dimensional time-series SIS control model defined in Eqns. (6.8)-(6.11).

Stochastic SIS epidemic model has seasonal characteristics. Thus, we will study the SIS control model in a more extended period. Under this investigation, the stochastic SIS control model has the control variable with 200 time-epochs, so this problem's dimensionality is 200.

Figure 6.5(a) shows the stochastic SIS epidemic model's infectious population rate with the control of different d and without any control or interventions when the fill-in strategy is a linear approximation. The solid red line represents the trend of infectious population rate without any control over time. The other color lines represent the trend of infectious population rate with optimal control generated by the DR-DF BO algorithm when the algorithm selects different d. As can be seen from Figure 6.5(a), the infectious population of the stochastic SIS model has richer dynamic properties than the infectious population in the deterministic SEIR model studied in section 6.4.1. The trend of the epidemic performs the oscillation characteristics. The disease will come back again and again if there is not any control. However, no matter the dimension reduction value, the optimal control strategies generated by the DR-DF BO algorithm effectively and quickly control the epidemic once the epidemic breakouts; it also effectively prevented the recurrence of the epidemic.

Figure 6.5(b) shows the trends of accumulated objective function value of the stochastic SIS model with different d and without any control when the fill-in strategy is a linear approximation. The small figure in Figure 6.5(b) is a partial zoom figure between time interval $[100, 200]$. We can see that the accumulated objective function when the SIS model is without control is significantly higher than the values with control. When d value is about 40, the DR-DF BO algorithm can achieve a closer effect to that without dimension reduction (when $d = 200$). It means that for any d in range $[40, 200]$, the optimal control strategies generated by the DR-DF BO algorithm perform similar and sufficient control effects on the epidemic. Figure 6.5(c) shows

the final best objective function values and running time comparison results for different d when the fill-in strategy is a linear approximation. To well understand the results, in this part we also use the AOFV ratio and RT ratio defined in Eqns. (6.33)-(6.34) to present. The ratio results for the SIS model are summarized in Table 6.2. From the results in the table and figures, we can see that the DR-DF BO algorithm performs well both on objective function value and running time when d is 80. It can reach good global optimization results when d is 80 and the running time is around 30 seconds. The DR-DF BO algorithm shows an excellent global optimization performance for the stochastic SIS model. It solves the optimal control strategy for the model in a fraction of the time. The generated control strategy can control the epidemic spread and significantly reduce the financial cost.

Table 6.2 AOFV ratio and RT ratio for different d in SIS model

$\boldsymbol{d}$	5	20	40	60	80	100	120	140	160	180	200
$\boldsymbol{AOFV\ ratio}$	6.552	3.141	1.707	1.544	1.283	1.37	1.087	1.053	1.0	1.0	1.0
$\boldsymbol{RT\ ratio}$	0.146	0.204	0.288	0.377	0.461	0.540	0.648	0.739	0.813	0.916	1.0

Figure 6.5(d) shows the stochastic SIS control model's best objective values with different d when the DR-DF BO algorithm chooses different fill-in strategies. As shown in Figure 6.5(d), compared to the other four fill-in strategies, the Gaussian regression fill-in strategy does not perform well if d is smaller than 40. However, these five different fill-in strategies have good effect on global optimization if d is larger than 40. All of them can reach an excellent and similar objective function value, which indicates that the DR-DF BO algorithm can solve the optimal control solution within a short running time no matter which fill-in strategy it uses at which $d = 40$.

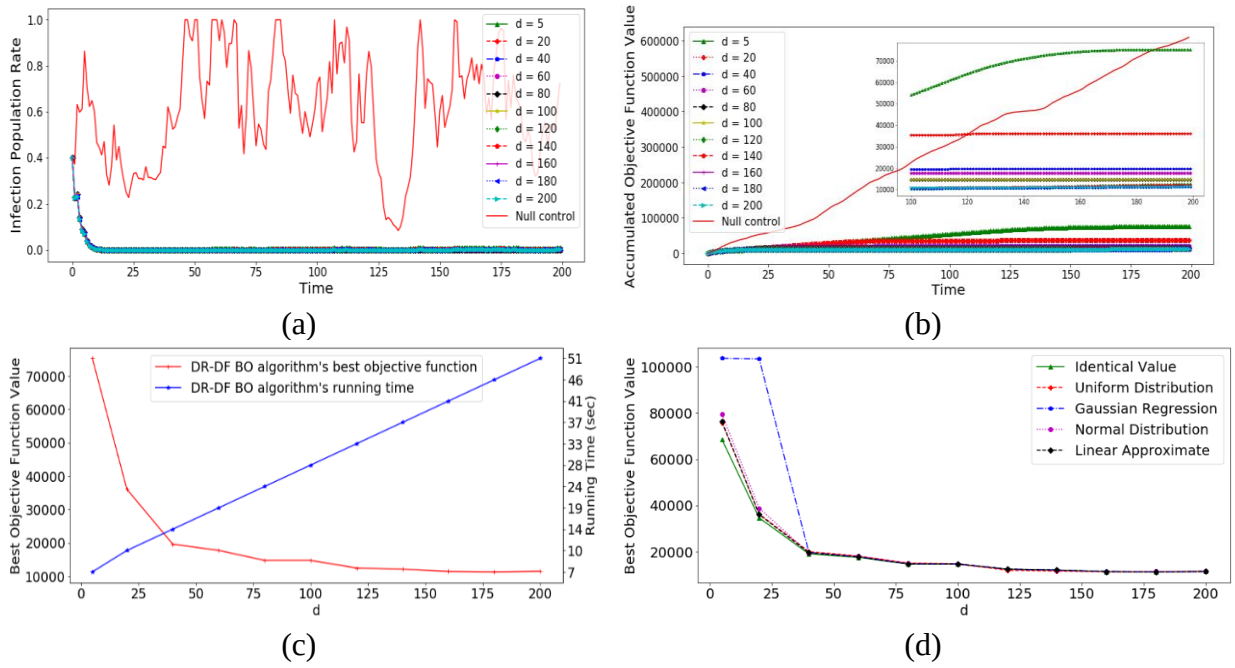

Figure 6.5 Simulation results of the DR-DF BO algorithm on stochastic SIS control model. (a) Infectious population rate over time for different d. (b) Accumulated objective function values over time. (c) Best objective function values and running time for different d. (d) Best objective function values of different fill-in strategies.

6.4.3 Comparisons of the DR-DF BO Algorithm, and Other Two BO Algorithms

This part compares the proposed DR-DF BO algorithm with the standard BO algorithm and a high-dimensional BO algorithm proposed in [49]. In this section, we will call the high-dimensional BO algorithm in [49] **Referenced BO algorithm**. We test four algorithms on the same deterministic SEIR and stochastic SIS control models with the same parameter values and state conditions. In this section, linear approximation is selected as the fill-in strategy of the DR-DF BO algorithm, the dimension reduction value of the DR-DF BO algorithm is chosen as $d = 40$ for both SEIR and SIS control model. For each compared algorithm, we conducted 15 simulation runs with random initial control strategies for each run. We display the means and standard

deviations of the objective function value for all three algorithms over the same 25 optimization iterations. Since the Referenced BO algorithm also considers dimension reduction, we test $d = 40$ for the Referenced BO algorithm as well. But after the comparisons of the DR-DF BO algorithm, the standard BO algorithm, and Referenced BO algorithm, we will provide a comparison of the DR-DF BO algorithm and Referenced BO algorithm with different dimension reduction values d. When the model is deterministic SEIR control model (total time dimensions = 100), for 25 iterations, the running time of the standard BO algorithm is about 61 seconds, the running time of Referenced BO algorithm is about 70 seconds, the running time of the DR-DF BO algorithm is about 11 seconds. When the model is stochastic SIS control model (total time dimensions = 200), the standard BO algorithm takes about 90 seconds to run, the Referenced BO algorithm takes about 100 seconds, the DR-DF BO algorithm takes about 10 seconds.

The difference between the DR-DF BO algorithm and other two BO algorithms is that other two compared BO algorithms calculate the objective function value in original high-dimensional space. The standard BO algorithm doesn't consider dimension reduction. Reference BO algorithm considers the dimension reduction, but it reconstructs the control strategy back to original high-dimensional space, and then calculates the corresponding objective function values to use them update the surrogate model at each iteration. However, the DR-DF BO algorithm doesn't consider reconstruct the control strategy during the acquisition function optimization process and the local search process. It just does the dimension fill-in after local search process. This means that the DR-DF BO algorithm reconstructs the optimal control strategy from low-dimensional space back to high-dimensional space at the last iteration. In this section, the DR-DF BO algorithm determines to optimize the acquisition function over 10 iterations, after that, it does the local search for 15 iterations. Then fill in the left dimensions based on the optimal solution got

from the last iteration of local search. There are 25 iterations in total. Thus, the objective function values of the DR-DF BO algorithm before 24 iterations are just the values calculated in low-dimensional space ($d = 40$).

Figure 6.6(a) and Figure 6.6(b) plot the comparison results of three algorithm implementing on the deterministic SEIR and stochastic SIS control model, respectively. The results show the average of the objective function values along with corresponding standard deviation from 15 runs of three algorithms. Since the objective function values of the standard BO algorithm and Referenced BO algorithm over 25 iterations are both calculated in high-dimensional space (100 time dimensions), their objective function values are significant higher than the values of the DR-DF BO algorithm. Hence, for the previous 24 iterations, we mainly focus on the analysis of trends and standard deviations. According to the results from both SEIR and SIS control models, the standard BO algorithm and Referenced BO algorithm have the similar trends, but the standard deviation of the standard BO algorithm at about the first 8 iterations are larger than the standard deviation of the Referenced BO algorithm. However, compared to other two algorithms, the DR-DF BO algorithm keeps smallest standard deviations over 25 iterations. The results also show that the local search process helps the algorithm to increase the final solution's accuracy. After dimension fill-in process, the final objective function value of the DR-DF BO algorithm in original high-dimensional space is significantly lower than the standard BO algorithm and Referenced BO algorithm.

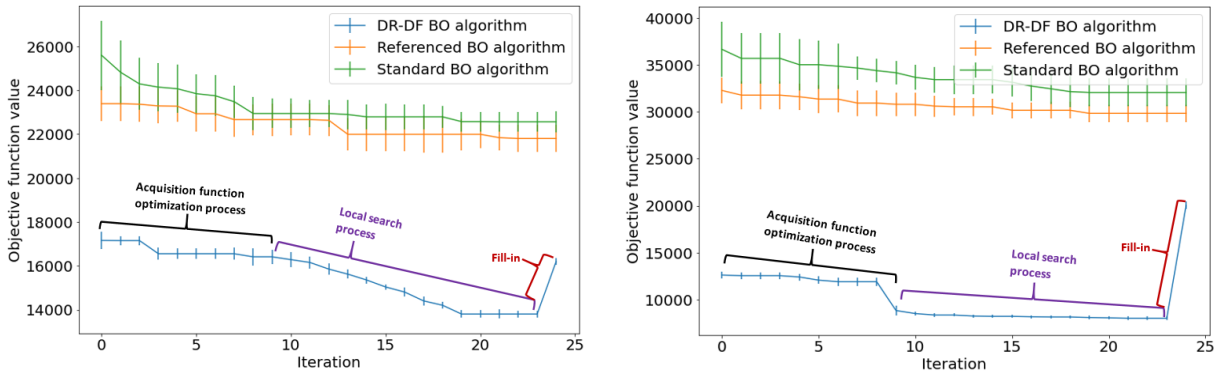

Figure 6.6 Comparison of the averages and standard deviations of the objective function values from 15 simulation runs. (a) on the deterministic SEIR control model with 100-dimensions. (b) on the stochastic SIS control model with 200-dimensions.

To further demonstrate the proposed DR-DF BO algorithm's effectiveness and efficiency, we compare it to Referenced BO algorithm for different dimension reduction value d. For each d, we conducted 10 simulation runs with the same initial control strategy for both algorithms. We display the means and standard deviations of the final objective function value over 10 simulation runs for each d. Each run is implemented for 25 optimization iterations.

Figure 6.7(a) and Figure 6.7(c) show the averages and standard deviations of the best objective function values over 10 runs for different d on the deterministic SEIR and stochastic SIS control models, respectively. Figure 6.7(b) and Figure 6.7(d) show the average running time over 10 runs for different d on the deterministic SEIR and stochastic SIS control models, respectively. From the results, we can see that for both SEIR and SIS control models, the Referenced BO algorithm solves similar best objective function values with almost same running time although the dimension reduction value d is different. It seems that the Referenced BO algorithm isn't effective and suitable for solving the time-series models. When it does the dimension reduction, it shows the same performances with that doesn't do the dimension reduction, which indicates that

the dimension reduction of the Referenced BO algorithm has no good effect on the researched time-series models. However, the DR-DF BO algorithm shows different performances when d is different, it means that the dimension reduction of the DR-DF BO algorithm is meaningful. Although the DR-DF BO algorithm reaches a larger final objective function value when d is smaller, it takes very fast running time. It's reasonable that the larger the value of d, the longer the running time. The DR-DF BO algorithm can find the similar final objective function values at smaller d values with very short running time. In addition, in the SEIR model, the best objective function values and running times of the DR-DF BO algorithm for all different d are significantly better than the Referenced BO algorithm. In SIS model, except the objective function value at $d = 20$, the DR-DF BO algorithm always perform more excellent than the Referenced BO algorithm as well. Therefore, the DR-DF BO algorithm is more effective and efficient algorithm to solve the optimal control solution for the researched high-dimensional time-series models compared to the Referenced BO algorithm.

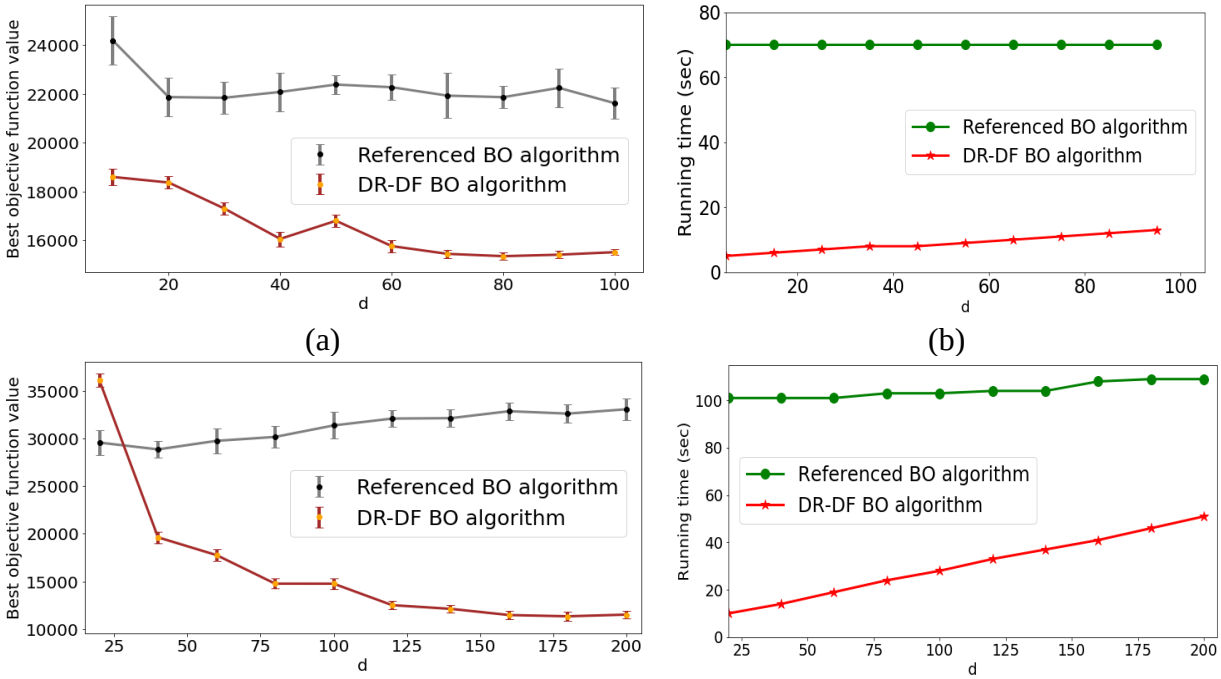

Figure 6.7 Figure 6.7 Comparison results of the DR-DF BO algorithm and Referenced BO algorithm for different *d*. (a) The averages and standard deviations of the best objective function values on the deterministic SEIR control model. (b) Running time on the deterministic SEIR control model. (c) The averages and standard deviations of the best objective function values on the stochastic SIS control model. (b) Running time on the stochastic SIS control model.

6.5 Conclusions

In this paper, we have proposed a high-dimensional DR-DF BO algorithm. This algorithm is improved based on the standard BO algorithm. However, the proposed algorithm is effective in solving the high-dimensional time-series models. The proposed algorithm successfully implements dimension reduction and dimension fill-in with different fill-in strategies. Also, the proposed algorithm discusses a new sampling strategy to optimize the acquisition function effectively, this new sampling strategy effectively utilizes the knowledge of Multi-Armed Bandit and Random search to determine better solution point for optimizing the acquisition function. Moreover, the DR-DF BO algorithm is not necessary to do the dimension fill-in at each acquisition function optimization process. It means that the DR-DF BO algorithm doesn't repeatedly reconstruct the system's variables from low-dimensional space back to the original high-dimensional space, it only needs to do it at the last iteration. This improvement guarantees the computational efficiency of the DR-DF BO algorithm. While ensuring running time efficiency, the proposed algorithm also demonstrates its effective global optimization ability through some simulation experiments. During those simulation experiments, the DR-DF BO algorithm shows more excellent performances than the standard BO algorithm and a high-dimensional BO

algorithm proposed in [49] on solving the final optimal solution for both deterministic and stochastic time-series epidemic control systems.

However, when the system condition is changed (such as the value of the key system parameter is changed), the DR-DF BO algorithm and most of existing BO algorithms need to implement the whole optimization process to solve the optimal solution. It will waste a lot of time if the model contains millions of dimensions. Thus, one possible research direction would be the extension of our proposed DR-DF BO algorithm based on machine learning. It is expected to generate a learning model combining the DR-DF BO algorithm and machine learning method, which can predict the optimal solution with less computational efforts when the system condition is changed. If it becomes available, there will be no necessary to implement the whole BO optimization process again and again when the system condition is changed, it can predict the optimal solution just requiring providing the new system conditions to the leaning model.

Chapter 7 - High-Dimensional Bayesian Optimization Algorithm with Recurrent Neural Network for Complex Disease Optimal Control Models

Abstract

Bayesian Optimization algorithm has become a well-received approach for nonlinear global optimization problems and many machine learning applications. Over the past few years, improvements and enhancements have been brought forward and they have shown some promising results in solving the complex dynamic problems, systems of ordinary differential equations where the objective functions are computationally expensive to evaluate. Besides, the straightforward implementation of Bayesian Optimization algorithm performs well merely for optimization problems with 10-20 dimensions. Study presented in this paper proposes a new high-dimensional Bayesian Optimization algorithm combining Recurrent neural network (RNN-BO algorithm), which is expected to predict the optimal solution for the global optimization problems with high-dimensional or time-series decision models. The proposed RNN-BO algorithm can solve the optimal control problems in the lower dimension space, and then learn from the historical data using the recurrent neural network to learn the historical optimal solution data and predict the optimal control strategy for any new initial system value setting (initial parameter values or initial system state values). In addition, accurately and quickly providing the optimal control strategy is essential to control the epidemic's spread while minimizing the associated financial costs. Therefore, to verify the effectiveness of the proposed algorithm, computational experiments are carried out on a deterministic SEIR epidemic model and a stochastic SIS optimal control model.

Finally, we also discuss the impacts of different number of the RNN layers and training epochs on the trade-off between solution quality and related computational efforts.

Keywords: Bayesian Optimization, Recurrent neural network, high-dimension, time series, optimal control, epidemic model.

7.1 Introduction

Providing the optimal control strategies for epidemic models has increasingly attracted attentions from both research and health organizations or agencies. During the epidemic, the health organizations or agencies may take a series of control strategies (epidemic prevention or intervention measures) for mitigating the local outbreak, e.g., vaccination, quarantine, disinfection, or regional closures. All these control measures could be associated with certain financial costs, directly or indirectly. If health organizations or agencies do not control the epidemic, it may also cause inevitable economic consequences, such as workforce losses due to outbreaks, increased community healthcare costs, local business downturns, and declined related travels. Thus, the optimal control strategy of epidemic should balance the corresponding financial cost of control and the epidemic progression. During recent years several studies on the optimal control to control the spread of epidemic and relieve healthcare financial burden have been carried out [197, 199, 235, 236]. Therefore, it is important for public health purposes to figure out the optimal control policy for the trade-off of strategies effectiveness and cost efficacy [235].

Although many works on studying the optimal control strategy for different epidemic diseases have been made, their results only provided the optimal control policy for the specific regions (city/state/country) or virus type of epidemic. Those optimal control strategies may no longer be effective or optimal if the epidemic outbreaks in different regions or the epidemic viruses mutate. For instance, when the influenza viruses mutate into three different types, the control

treatment for a specific type of virus cannot work for the infective individuals infected by another type of virus or virus variation [237]. This means that researchers need to build a new model to study the relationship of optimal control and epidemic progression caused by different virus. At the end of 2019, the COVID-19 emerged in Wuhan, China and rapidly spread to the rest of the world. Due to the different transmission dynamics and economic situation of different regions of the world, the optimal control policies and the related control intensity usually are different [238]. Recently, due to the variant of COVID-19 virus, the unprecedented increase happens in several countries. The existing vaccines may lack the efficacy on controlling the variant virus, which means the government officials need to re-plan the control policy regarding the new situation of the epidemic [239]. The above challenge offers guidance for authors to focus on the algorithm development of optimal control learning and prediction. Since the initial epidemic system value setting is associated with the epidemic regions or virus types. The target algorithm is expected to have ability to learn the historical epidemic data (including initial system state/parameter data and corresponding optimal control strategy data), and then quickly predict the new optimal control solution to respond to new epidemic region or virus variation.

Our main purpose is to develop such a general learning and prediction algorithm, which can predict the optimal control solution only based on the known historical epidemic data, even though this data is from different epidemic regions or different types of viruses of same epidemic. For example, for some poor regions or countries, they may have no enough financial supports to collect local epidemic data. However, the data of other regions or countries under the same epidemic is available to access, it will be helpful and meaningful if the poor regions or countries can leverage those available data to generate the effective control policy for themselves though the data is from different places. Besides this, it’s necessary to develop the framework according to

some characteristics of the epidemic control model, which can guarantee the effectiveness and efficiency of the framework. To our knowledge, the epidemic control model with hundreds of thousands of time epochs is considered as high-dimensional and time-series [240]. If we consider each time epoch as one dimension of the model, hence the epidemic model is high-dimensional. Also, time-series means the values of the state variables and control variables of the model at current time will affect subsequent state variable values and control variable values. Therefore, considering these characteristics, we intent to develop a new algorithm combining a high-dimensional global optimization algorithm and Recurrent Neural Network (RNN) algorithm.

Conventional global optimization techniques, such as particle swarm optimization algorithm, genetic algorithm, simulated annealing algorithm, stochastic gradient descent, etc., are suitable for solving the low-dimensional systems with the nature of time-independent or dimensions-independent. They may not be enough effective to solve high-dimensional optimization systems. Bayesian Optimization (BO) is popular and powerful global optimization approach, it is also computationally challenging to handle high-dimensional systems [47]. However, BO is a promising learning-based method to dig out more hidden or posterior information from historical data. Some improved BO algorithms are proposed for handling the high-dimensional global optimization problems. For example, Moriconi *et. al.* proposed a high-dimensional BO algorithm by learning a nonlinear feature mapping to reduce the inputs' dimension, this improvement allows the algorithm to easily optimize the acquisition function in low-dimensional space [47]. Zhang *et. al.* introduced a sliced inverse regression method to BO to learn the intrinsic low-dimensional structure of the objective function in high-dimensional space, which can automatically study the intrinsic structure of objective function during the optimization process [48]. Li *et. al.* developed a new method for high-dimensional BO by using dropout strategy to

reduce dimensions and optimize a subset of variables, and then provide three "fill-in" strategies to guide how to fill-in the left-out dimensions at each acquisition function optimization [49]. However, these high-dimensional BO algorithms need to reconstruct the variables from low-dimensional space back into its original dimension space at each iteration, and then calculate the corresponding objective function value in high-dimensional space. Although those new BO algorithms overcome the high-dimensional difficulty, they didn't realize computational efficiency. Also, those BO algorithms are not suitable to solve the time-series optimization system. Therefore, we attempt to develop the target algorithm combining an BO algorithm with RNN algorithm. The BO algorithm used in the target algorithm is like the improved BO algorithm proposed in our previous work [240].

The target algorithm is in short denoted as RNN-BO algorithm. By combining RNN algorithm, the proposed algorithm keeps the advantage of RNN to learn the optimal control data on past epidemics (epidemics from same/different regions), then predict the optimal control strategy toward future outbreaks happened in different regions or happened due to virus variation. Our extensive computational experiments have shown that the RNN-BO algorithm can effectively overcome some of the shortcomings in the existing high-dimensional BO algorithms and epidemic optimal control optimization algorithms. In this paper, we use the time-dependent deterministic SEIR and stochastic SIS epidemic control models to illustrate the benefits and advantages of the RNN-BO algorithm. The main contributions of this paper are summarized below:

- Propose a novel RNN-BO algorithm that is effective and computationally efficient for high-dimensional global optimization problems with time-series epidemic model.
- The RNN-BO algorithm is capable to learn the relationship between the optimal control solution and initial system value setting of complex epidemic model. Then construct a

predictive model based on historical data, which can quickly and accurately predict the corresponding optimal control strategy once given any new initial system value setting (initial system state values or system parameter values).

- The RNN-BO algorithm reduces the high-dimensional variables into low-dimensional space when solves optimal control solution using BO algorithm, it does not require to reconstruct the control variables back to high-dimensional space at each iteration.
- The RNN-BO algorithm takes advantage of historical epidemic data from different regions or virus variation, which can continually learn and modify the predictive model so that it can offer effective and accurate optimal control strategy even there is less knowledge about new outbreak of same epidemic.

The rest of the paper is structured as follows. Section 7.2 introduces the epidemic control optimization systems as the application under this study. Section 7.3 provides the background and presents the RNN-BO algorithm in detail. Section 7.4 demonstrates the effectiveness of the RNN-BO algorithm and makes comparison with the standard Bayesian Optimization algorithm and a high-dimensional Bayesian Optimization algorithm through numerical simulation experiments. Finally, conclusions and future works are drawn in Section 7.5.

7.2 Problem Formulation

The model we attempt to research is high-dimensional time-series epidemic control model. In this paper, we plan to research the RNN-BO algorithm on two different high-dimensional time-series epidemic control models: deterministic SEIR control model and stochastic SIS control model. These two control models are developed based on the standard deterministic SEIR [193] and stochastic SIS model [224], respectively. Two original standard epidemic models didn't consider the control variables, which only can be used to study the natural progression of the

epidemic without any control strategy (epidemic prevention or intervention). However, in real world, the health organizations or agencies usually take a series of control strategies for mitigating the local outbreak.

The control strategy can affect contact rate or infection rate between individuals and finally affect the progression of the epidemic. For example, during COVID-19 epidemic, CDC noticed that control measures like facemasks, cloth mask or respirator can prevent the spread of respiratory secretions. Those control measures provide different levels of protection for people against exposure to infectious droplets and particles produced by infected people [194]. Also, encouraging and guaranteeing the safe social distance is a control strategy to decrease the contact and infection rate [195]. The control variables can represent the level/degree/intensity of restrictions on activities, mask wearing, quarantines or medicine care, it also can represent the vaccination coverage rates [195, 196, 199]. These facts indicate that the contact rate or infected rate can be controlled through practical control approaches, the control variable of the epidemic models in this paper has practical meaning, and is truly controllable. Thus, we consider the control variables into the standard SEIR and SIS epidemic model, and solve the optimal control strategy that minimizes the overall financial cost associated with control strategies and controls the spread of the epidemic.

The optimization system with the deterministic SEIR control model developed based on standard SEIR model [193] is formulated as follows:

$$\text{Min } V = \int_{t_1}^{t_f} C_1 I(t) + C_2 f(u_1, u_2, t) \tag{7.1}$$

$$s.\ t. \quad \frac{dS(t)}{dt} = \tau - (1 - u_1(t))\beta S(t)I(t) - \tau S(t) \tag{7.2}$$

$$\frac{dE(t)}{dt} = (1 - u_1(t))\beta S(t)I(t) - (\tau + \alpha)E(\text{t}) \tag{7.3}$$

$$\frac{dI(t)}{dt} = \alpha E(t) - (\tau + \gamma)I(t) - u_2(t)I(t) \tag{7.4}$$

$$\frac{dR(t)}{dt} = \gamma I(t) - \tau R(t) + u_2(t)I(t) \tag{7.5}$$

$$S(t) + E(t) + I(t) + R(t) = 1 \tag{7.6}$$

where t_1 is the start time of control, t_f is the end time of control. V indicates the overall cost due to control measures and the cost due to infected population if the health organizations or agencies don't take any control measure during time period $[t_1, t_f]$. The parameters C_1 and C_2 in Eq. (7.1) represent the financial cost of system without control and with control, respectively.

$f(u_1, u_2, t)$ in Eq. (7.1) is the cost function due to the control strategy. Most existing studies consider the cost function associated with the control strategy as convex [32, 199]. However, in the real world, the cost function is possible non-convex [226]. To better verify the effectiveness and efficiency of the proposed RNN-BO algorithm, the cost function $f(u_1, u_2, t)$ will be considered as non-convex in this paper.

$S(t)$, $E(t)$, $I(t)$, $R(t)$ in Eqns. (7.1)-(7.6) are the system state variables, they represent the fraction of susceptible, exposed, infected, and recovery population at time t, respectively. S represents the individuals who might be infected the disease; E represents the individuals who have been infected but are not infectious, they are not capable to transmit the disease; I represents the individuals who have been infected and are able to transmit the disease; R represents the individuals who have become immune.

Parameter τ in Eqns. (7.2)-(7.5) represents the natural birth rate, we assume the natural death rate is equal to the natural birth rate in this paper. Parameter β in Eqns. (7.2)-(7.3) represents the natural contact rate between S and I when there is not any control strategy like quarantine or activity restriction. Parameter α in Eqns. (7.3)-(7.4) represents transfer rate from state E to I. Parameter γ in Eqns. (7.4)-(7.5) represents natural recovery rate from state I to R when there is not any control strategy like medicine treatment or hospitalization.

u_1 and u_2 are the system decision variables (control variables), their values represent the level/degree/intensity of the corresponding control measures. u_1 in Eqns. (7.2)-(7.3) represents prevention control strategy that can slow down the probability of S being infected by I, such as vaccination, quarantine, activity restriction, social distance restriction, etc. u_2 in Eqns. (7.4)-(7.5) represents intervention control strategy that can speed up the population's recovery from state I to state R, such as medicine treatment, hospitalization, advanced medical facilities and equipment, etc.

Assume each control strategy contains ($\mathcal{D} = t_f - t_1$) time epochs. If each time epoch is considered as one time dimension of the system, it means the control variable is $\mathcal{D}$ dimensions. Define the control variables as $u_1 = \{u_1(t_1), \dots, u_1(t_f)\}$ and $u_2 = \{u_2(t_1), \dots, u_2(t_f)\}$, where $u_1(t), u_2(t) \in [u_l, u_u]$ $(t_1 \le t \le t_f)$, u_l and u_u represent the lower and upper bound of control variable, respectively. $u_1(t)$ and $u_2(t)$ mean the level/degree of the prevention and intervention control strategy at time t, respectively. Therefore, the lower and upper bound of control variables are assumed as $u_l = 0, \text{and } u_u = 1$.

Next, the stochastic SIS control model studied in this paper only contains two states: susceptible S and infected I. In addition, in real world the natural contact rate is possible uncertain, which may be affected by some stochastic environment factors like seasonal variations, climate change, air humidity. Hence, the stochastic SIS control model with a stochastic contact rate is formulated based on standard SIS model [224]:

$$s.t. \quad \frac{dS(t)}{dt} = \tau - \big(1 - u_1(t)\big)\beta S(t)I(t) + \gamma I(t) - \tau S(t) + u_2(t)I(t) - \sigma S(t)I(t)dB(t)/dt \tag{7.7}$$

$$\frac{dI(t)}{dt} = (1 - u_1(t))\beta S(t)I(t) - (\tau + \gamma)I(t) - u_2(t)I(t) + \sigma S(t)I(t)dB(t)/dt \tag{7.8}$$

$$S(t) + I(t) = 1 \tag{7.9}$$

where $B(t)$ is a standard Brownian motion, we use it to describe the uncertainty of the contact rate in the stochastic SIS control model. Eq. (7.7) means that the stochastic contact rate is normally distributed with mean βdt and variance $\sigma^2 dt$, we refer readers to paper [224] to get more exact details and definitions of $B(t)$ and σ.

In this paper, we use a standard Brownian motion to describe the uncertainty of the contact rate in the stochastic SIS control model. Therefore, the time-series optimal control problem with complex and high-dimensional stochastic SIS epidemic model researched in this paper can be formulated as follows:

$$\text{Min } V = \int_{t_1}^{t_f} C_1 I(t) + C_2 f(u_1, u_2, t) \tag{7.10}$$

$$\textit{s. t.} \quad dS(t) = \Big(\tau - \big(1 - u_1(t)\big)\beta S(t)I(t) + \gamma I(t) - \tau S(t) + u_2(t)I(t)\Big)\,dt$$

$$-\sigma S(t)I(t)dB(t) \tag{7.11}$$

$$dI(t) = \big((1 - u_1(t))\beta S(t)I(t) - (\tau + \gamma)I(t) - u_2(t)I(t)\big)dt + \sigma S(t)I(t)dB(t) \tag{7.12}$$

$$S(t) + I(t) = 1 \tag{7.13}$$

where $B(t)$ denotes the standard Brownian motion with the intensity of noise σ. The term $(1 - u_1(t))\beta$ and $u_2(t)I(t)$ have the similar meaning as shown in SEIR model.

7.3 High-dimensional Bayesian Optimization Algorithm with RNN

In this section, we develop a new high-dimensional Bayesian Optimization algorithm (RNN-BO algorithm) by combining an improved BO algorithm and RNN for time-series epidemic control models. The BO algorithm used in RNN-BO algorithm is like the improved BO algorithm proposed in our previous work [240]. Herein, we just briefly introduce it, we refer readers to paper [240] to get more details of the BO algorithm. The RNN-BO algorithm can predict a time-series

optimal control strategy quickly that can minimize the cost function V and effectively control the disease spread once given any new initial epidemic system value setting. The RNN-BO algorithm includes two parts: BO part and RNN part. BO part is mainly to generate enough historical data for further RNN part use. In BO part, we vary the initial system value setting (change the system parameter values or initial system state values), then solve the corresponding final optimal control strategy using the BO algorithm. Store each initial system value setting and corresponding optimal control strategy as one historical data pair. We can obtain many data pairs in the BO part by changing different initial system state values or parameter values. RNN part is to learn all historical data pair (initial system value setting as input and corresponding optimal control strategy as output), then generate a predictive model. This predictive model can be used to predict the optimal control solution once given any new input. In this section, the BO part is briefly introduced from section 7.3.1 to 7.3.5. The RNN part is introduced in section 7.3.6.

7.3.1 Time-Dimensions Reduction

Unlike the standard Bayesian optimization, the RNN-BO algorithm attempts to solve the optimal control strategy in a low-dimensional space. There are two purposes for making time-dimensions reduction of the control strategy variable. One is to find the optimal solution quickly and accurately, two is to generate data sequences with the nature of time-series for further RNN use. For the control strategy variable with full $\mathcal{D}$ dimensions, we select d dimensions ($d < \mathcal{D}$) of the control variable at each iteration.

7.3.2 Gaussian Process

The surrogate model used in the RNN-BO algorithm is the Gaussian process model. The Gaussian process is used to find the prior belief based on historical data and dig the posterior information, which it's better to evaluate the complex nonconvex objective function and find the

optimal solution. For a Gaussian process, we assume that for any control strategy samples $\{\dots, u^i, \dots\} \in [0,1]^{t_f - t_1}$, we do the time-dimensions reduction and generate d-dimensional $u^i = \{u(t_1), \dots, u(t_d)\} \in [0,1]^d$ for each control sample, the corresponding objective function value set $[\dots, V(u^i), \dots]^T$ for all samples set $\{\dots, u^i, \dots\} \in [0,1]^d$ follows the multivariate Gaussian distribution:

$$[\dots, V(u^i), \dots]^T \sim \mathcal{GP}(M, K) \tag{7.14}$$

where M is a mean vector $[\dots, m(u^i), \dots]^T$ and K is a covariance matrix as below:

$$K = \begin{bmatrix} k(u^1, u^1) & \cdots & k(u^1, u^i) \\ \vdots & \ddots & \vdots \\ k(u^i, u^1) & \cdots & k(u^i, u^i) \\ k(u^{i+1}, u^1) & \cdots & k(u^{i+1}, u^{i+1}) \\ \vdots & \ddots & \vdots \end{bmatrix} \tag{7.15}$$

$m(u^i)$ is mean function that is usually defined as a linear function or zero [204]. $k(u^i, u^j)$ is called covariance function or kernel function of two control strategies u^i and u^j. There are many different kernel function choices, such as radial basis function (RBF), Matern 52, Linear, Exponential, etc. In the RNN-BO algorithm, we use a common choice Matern 52 as the kernel function [241], it is formulated as:

$$k(u^i, u^j) = (1 + \sqrt{5} * \frac{|u^i - u^j|}{l} + \frac{5}{3} * \frac{|u^i - u^j|^2}{l^2}) \exp\left(-\sqrt{5} * \frac{|u^i - u^j|}{l}\right) \tag{7.16}$$

where l is the length-scale hyperparameter. Different kernel functions and the value of l may lead to different global optimization performances, which can be tested to pick the better choice through implementing numerical experiments [226]. Since it's not the main contribution of this paper, we will not provide more detail here.

The mean vector M and covariance matrix K can be viewed as the prior belief. From the Gaussian process model, for any new control strategy $u^{new} \in [0,1]^d$, the objective function value $V(u^{new})$ at the new point u^{new} will follows the distribution:

$$V(u^{new})|D \sim \mathcal{GP}(M^{new}, K^{new}) \tag{7.17}$$

where D is the dataset storing the historical data. M^{new} and K^{new} represent the posterior mean and posterior covariance, respectively. They can be expressed as:

$$D = \{\dots \left(u^i, V\left(u^i\right)\right), \dots\} \tag{7.18}$$

$$M^{new} = \mu(V(u^{new})|D) = m(u^{new}) + K'K^{-1}(V - M) \tag{7.19}$$

$$K^{new} = \sigma(V(u^{new})|D) = K'' - K'K^{-1}K'^{T} \tag{7.20}$$

where:

$$K' = [k(u^{new}, u^1), \dots, k\left(u^{new}, u^i\right), \dots] \tag{7.21}$$

$$K'' = k(u^{new}, u^{new}) \tag{7.22}$$

$$V = [\dots, V\left(u^i\right), \dots]^T \tag{7.23}$$

7.3.3 Acquisition Function

The acquisition function that we used to estimate the original objective function during the optimization process of the RNN-BO algorithm is the lower confidence bound (LCB) function [240]. The goal of using acquisition function is to utilize the posterior information to find a better new sampling point at each iteration, and this new sampling point can balance the purpose of exploration and exploitation. The exploration means that the algorithm tends to sample the next points with highly uncertainty. The exploitation means the algorithm will sample the next points with the lower objective function value in the minimization problems. We know that for any new control strategy, we have the posterior information $\mu(V(u^{new})|D)$ and $\sigma(V(u^{new})|D)$ from

Gaussian process. The posterior mean $\mu(V(u^{new})|D)$ can represent the exploitation, the posterior covariance $\sigma(V(u^{new})|D)$ can represent the explotation. The LCB acquisition function can be calculated as:

$$\mathrm{LCB}(u) = \mu(V(u^{new})|D) - k\sigma(V(u^{new})|D) \tag{7.24}$$

where k is the weight to balance the posterior mean and the covariance. A large value of k indicates that the algorithm places more weight on sampling a new point with high uncertainty, A small value of k indicates that the algorithm places more weight on sampling a new point with a small objective function value. At each iteration, we sample the next control strategy point that minimizes the LCB acquisition function:

$$u^{new} = \arg\min_{u} \mathrm{LCB}(u) \tag{7.25}$$

7.3.4 Sampling Strategy

When the model is high-dimensional, it is usually impossible to search the entire feasible solution space to solve the optimal control strategy for Eq. (7.25) at each iteration. Therefore, an effective and efficient sampling strategy is necessary to improve the computational efficiency of the RNN-BO algorithm. In the BO part of the RNN-BO algorithm, we combine the multi-armed bandit and random search to sample new candidates for optimizing the acquisition function.

Multi-armed bandit (MAB) is a class reinforcement learning case of the trade-off between exploration and exploitation [242]. MAB means that we decide to choose one or some bandits from all bandits to play at each iteration. Each bandit is configured with a reward of how the decision-maker will likely earn a reward regarding the decision. In the RNN-BO algorithm , the steps using MAB to sample the new candidates are: (1) Divide the range of control strategy into some small ranges and consider them as bandits; (2) Define the reward of each small range is equal to n_{MAB}, and at each small range, sample n_{MAB} candidate points; (3) Calculate the corresponding

acquisition function values for those sampling candidates; (4) Find the largest and smallest acquisition function values, and update the reward n_{MAB} of each range; (5) Repeat (2)-(4) for some iterations, and then find the best candidate point u_{MAB}^{new} with the best acquisition function. Here, in step (4), we assume the range that the candidate point with the largest acquisition function value belongs to will earn one reward, the reward at this range will be updated as $n_{MAB} \leftarrow n_{MAB} + 1$, which means that the RNN-BO algorithm will sample $n_{MAB} + 1$ candidate points from this range at the next iteration. The range that the point with the smallest value belongs to will lose one reward, the reward at this range will be updated as $n_{MAB} \leftarrow n_{MAB} - 1$, which means that the algorithm will sample $n_{MAB} - 1$ candidate points from this range at the next iteration. Figure 7.1 is a sampling point example of MAB.

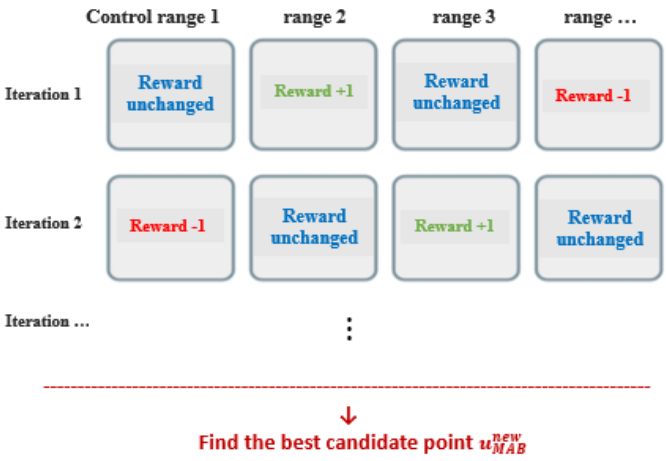

Figure 7.1 A sampling point example of MAB

Random research is another sampling method in the BO part. We randomly sample n_{RS} candidate points with lower bound u_l and upper bound u_u. Then calculate the corresponding acquisition function values for all candidates and pick the best one with the lowest acquisition function value as the optimal candidate u_{RS}^{new} generated by random search. At each iteration, we

compare the corresponding acquisition function values of candidate u_{MAB}^{new} and u_{RS}^{new}, choose the better one as the optimal new sampling point:

$$u^{new} = \begin{cases} u_{MAB}^{new}, & if\ \mathrm{LCB}(u_{MAB}^{new}) < \mathrm{LCB}(u_{RS}^{new}) \\ u_{RS}^{new}, & if\ \mathrm{LCB}(u_{MAB}^{new}) > \mathrm{LCB}(u_{RS}^{new}) \end{cases} \tag{7.26}$$

After some iterations, we can get the optimal solution u^* by comparing all u^{new}.

7.3.5 Local Search

To increase the final solution's accuracy, we add a local search after the acquisition function optimization. Since Adam method can faster converge to a local minimum with better quality [167]. Therefore, in the BO part of the RNN-BO algorithm, a local search based on Adam gradient descent is implemented starting from the optimal solution u^*. The final d-dimensional time-series optimal control solution is obtained after the local search.

7.3.6 Bayesian Optimization with Recurrent Neural Network

The proposed RNN-BO algorithm is expected to quickly and accurately predict the optimal control strategy when given any new initial system value setting. Therefore, this paper applies RNN to learn the historical data pairs obtained from the BO part, and find the relationship between the optimal control strategy and system initial system value setting. This section will describe how to utilize RNN to learn the historical data pairs and generate a predictive model.

RNN is a type of artificial neural network widely used to process sequential data or time series data, which is demonstrated to produce state-of-the-art results in various sequence learning problems [243]. Different from traditional neural networks, the inputs and outputs of RNN are dependent on each other. RNN depends on the prior data within the sequence, which utilizes the training data to learn the feature and position information. An application example of RNN is described in detail in [244]. An excellent advantage of RNN is it can take one data or a series of

data in time order as input and produce one value or a series of values as output. Therefore, there are many different types of RNN due to various inputs and outputs in length [245]. In the RNN-BO algorithm, we decide to use the one-to-one RNN, which means that the algorithm maps one input vector to one output.

Next, we introduce how to design the input and output data obtained from the BO part for further RNN training use. We use the SEIR model as an example. As shown in Figure 7.2, at iteration 1, initialize the system state values $(S_1(t_1), E_1(t_1), I_1(t_1), R_1(t_1))$, determine the values of system parameters, and randomly generate a d-dimensional control strategy. Then we can calculate all system state values in d time dimensions through Eqns. (7.2)-(7.6). We solve d-dimensional optimal control strategy using the BO algorithm described from section 7.3.1 to 7.3.5. Then update all state values from time t_1 to t_d. After iteration 1, we can obtain the data from time t_1 to t_d as:

$$\begin{bmatrix} S_1(t_1) & S_1(t_2) & S_1(t_3) & \dots & S_1(t_{d-1}) & S_1(t_d) \\ E_1(t_1) & E_1(t_2) & E_1(t_3) & \dots & E_1(t_{d-1}) & E_1(t_d) \\ I_1(t_1) & I_1(t_2) & I_1(t_3) & \dots & I_1(t_{d-1}) & I_1(t_d) \\ R_1(t_1) & R_1(t_2) & R_1(t_3) & \dots & R_1(t_{d-1}) & R_1(t_d) \end{bmatrix} \tag{7.27}$$

$$\{u_1(t_1) \quad u_1(t_2) \quad u_1(t_3) \quad \dots \quad u_1(t_{d-1}) \quad u_1(t_d)\} \tag{7.28}$$

Then, we choose the state value $(S_1(t_2), E_1(t_2), I_1(t_2), R_1(t_2))$ at time t_2 in Eq. (7.27) as the initial state values for iteration 2. Under the same parameter values, randomly generate a d-dimensional control strategy and calculate the state values, then optimize the control strategy and update the state values (do the same thing as iteration 1). After iteration 2, we can obtain the data from time t_2 to t_{d+1} as:

$$\begin{bmatrix} S_1(t_2) & S_2(t_3) & S_2(t_4) & \dots & S_2(t_d) & S_2(t_{d+1}) \\ E_1(t_2) & E_2(t_3) & E_2(t_4) & \dots & E_2(t_d) & E_2(t_{d+1}) \\ I_1(t_2) & I_2(t_3) & I_2(t_4) & \dots & I_2(t_d) & I_2(t_{d+1}) \\ R_1(t_2) & R_2(t_3) & R_2(t_4) & \dots & R_2(t_d) & R_2(t_{d+1}) \end{bmatrix} \tag{7.29}$$

$$\{u_2(t_2) \quad u_2(t_3) \quad u_2(t_4) \quad \dots \quad u_2(t_d) \quad u_2(t_{d+1})\} \tag{7.30}$$

Then choose the state value $(S_2(t_3), E_2(t_3), I_2(t_3), R_2(t_3))$ at time t_3 in Eq. (7.29) as the initial state values for iteration 3. Do the same things and obtain the data from t_3 to t_{d+2}, and so on. Stop the algorithm until it obtains the data from time t_{f-d+1} to t_f as:

$$\begin{bmatrix} S_{f-d}(t_{f-d+1}) & S_{f-d+1}(t_{f-d+2}) & S_{f-d+1}(t_{f-d+3}) & \dots & S_{f-d+1}(t_{f-1}) & S_{f-d+1}(t_f) \\ E_{f-d}(t_{f-d+1}) & E_{f-d+1}(t_{f-d+2}) & E_{f-d+1}(t_{f-d+3}) & \dots & E_{f-d+1}(t_{f-1}) & E_{f-d+1}(t_f) \\ I_{f-d}(t_{f-d+1}) & I_{f-d+1}(t_{f-d+2}) & I_{f-d+1}(t_{f-d+3}) & \dots & I_{f-d+1}(t_{f-1}) & I_{f-d+1}(t_f) \\ R_{f-d}(t_{f-d+1}) & R_{f-d+1}(t_{f-d+2}) & R_{f-d+1}(t_{f-d+3}) & \dots & R_{f-d+1}(t_{f-1}) & R_{f-d+1}(t_f) \end{bmatrix} \tag{7.31}$$

$$\{u_{f-d+1}(t_{f-d+1}) \quad u_{f-d+1}(t_{f-d+2}) \quad u_{f-d+1}(t_{f-d+3}) \quad \dots \quad u_{f-d+1}(t_{f-1}) \quad u_{f-d+1}(t_f)\} \tag{7.32}$$

After iterations, we obtain the data for the specific initial system state value setting $(S_1(t_1), E_1(t_1), I_1(t_1), R_1(t_1))$ and system parameter value setting. By changing the initial system state value or system parameter values and do the same process, then we can obtain many data and consider all those data as historical data.

Now we design the training inputs and outputs using those historical data. Consider the one-to-one RNN in the RNN-BO algorithm , we denote system value setting $S_{iteration}(t_i), E_{iteration}(t_i), I_{iteration}(t_i), R_{iteration}(t_i), \beta)$ as one input vector, where β is the specific infection rate (system parameter). The correspond output is the control value $u_{iteration}(t_i)$ at time t_i. Thus, for a specific initial system value setting $(S_1(t_1), E_1(t_1), I_1(t_1), R_1(t_1), \beta)$, there are $d * (f - d + 1)$ input-output data pairs as shown in Table 7.1. The RNN-BO algorithm doesn't require that the input must be all system state variables or all system parameters, such as the input as $(S_{iteration}(t_i), I_{iteration}(t_i), \beta)$. The objective function values or other system parameter values also can be used as inputs. We can adjust different elements as input according to the accuracy of final predictive solution.

If enough data is ready to use by changing different initial system value setting, we apply RNN to learn the data and generate a predictive model named RNN-BO predictive model. For any new initial system state values of the same epidemic, we don't have to implement the BO algorithm to solve the optimal control strategy through several optimization iterations. We only need to use the RNN-BO predictive model to predict the optimal control value at the beginning time, then calculate the state values for the next time using Eqns. (7.2)-(7.6). After that, the predictive model will predict the optimal control value at the next time. Repeat the process until we obtain t_f-dimensional time-series optimal control strategy. Once the RNN-BO predictive model is ready, the algorithm can easily and accurately predict the time-series optimal control strategy. The computational time of predictive process only takes a few seconds. The excellent computational efficiency and global optimization performance of the RNN-BO algorithm will be demonstrated in later simulation section. The implementation flowchart of the RNN-BO algorithm is shown in Figure 7.3.

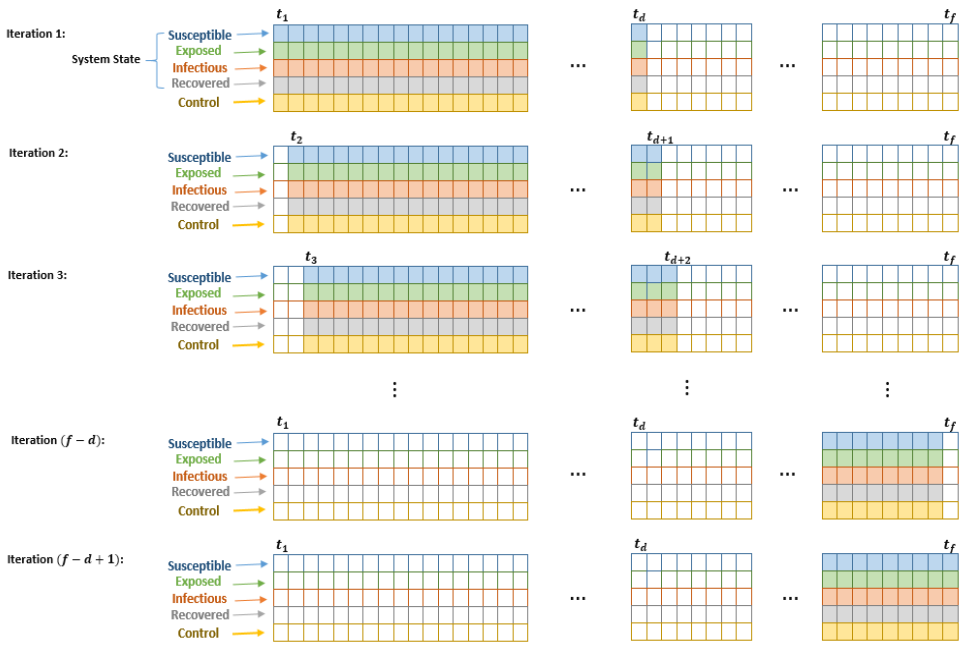

Figure 7.2 Data collection process of the RNN-BO algorithm

Table 7.1 Data pairs obtained from initial system setting $S_1(t_1), E_1(t_1), I_1(t_1), R_1(t_1), \beta$

inputs	outputs
$(S_1(t_1), E_1(t_1), I_1(t_1), R_1(t_1), \beta)$	$u_1(t_1)$
$(S_1(t_2), E_1(t_2), I_1(t_2), R_1(t_2), \beta)$	$u_1(t_2)$
⋮	⋮
$(S_1(t_d), E_1(t_d), I_1(t_d), R_1(t_d), \beta)$	$u_1(t_d)$
$(S_1(t_2), E_1(t_2), I_1(t_2), R_1(t_2), \beta)$	$u_2(t_2)$
$(S_2(t_3), E_2(t_3), I_2(t_3), R_2(t_3), \beta)$	$u_2(t_3)$
⋮	⋮
$(S_2(t_{d+1}), E_2(t_{d+1}), I_2(t_{d+1}), R_2(t_{d+1}), \beta)$	$u_2(t_{d+1})$
⋮	⋮
$(S_{f-d}(t_{f-d+1}), E_{f-d}(t_{f-d+1}), I_{f-d}(t_{f-d+1}), R_{f-d}(t_{f-d+1}), \beta)$	$u_{f-d+1}(t_{f-d+1})$
⋮	⋮
$(S_{f-d+1}(t_f), E_{f-d+1}(t_f), I_{f-d+1}(t_f), R_{f-d+1}(t_f), \beta)$	$u_{f-d+1}(t_f)$

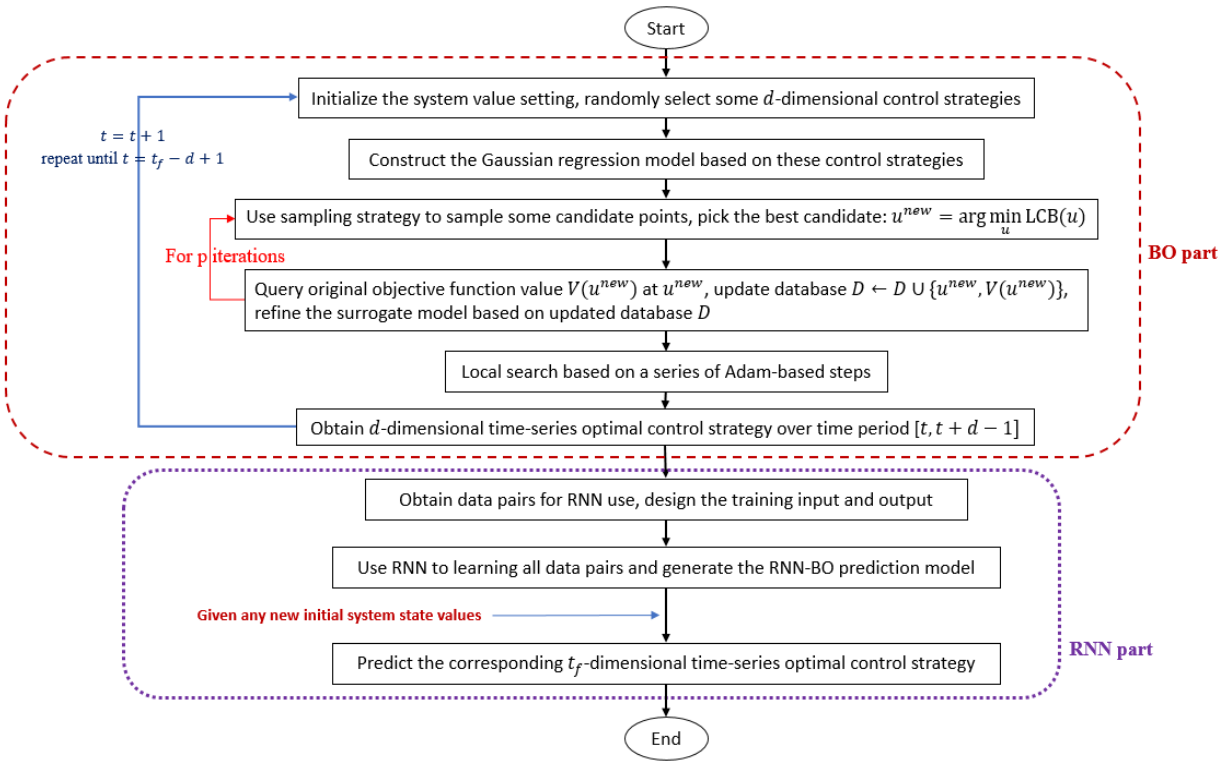

Figure 7.3 Flowchart of the RNN-BO algorithm

7.4 Numerical Simulation

In this section, some simulation experiments are carried out to illustrate the efficiency and effectiveness of the RNN-BO algorithm. All experiments are implemented on Python version 3.7 with Intel Core i5 CPUs and 32G memory. The simulation experiments are carried out on the deterministic SEIR control model and the stochastic SIS control model. (Some extra simulation tests on some synthetic functions are also implemented, we will show the related results for reader's interests in **Appendix 2**. The comparison of different types of RNN (RNN, LSTM, and GRU) are conducted, the results are shown in **Appendix 2**)

7.4.1 Effectiveness of the RNN-BO Algorithm

This section tests the efficiency and effectiveness of the RNN-BO algorithm on the deterministic SEIR control model formulated in Eqns. (7.1)-(7.6). We also demonstrate that the optimal control generated by the BO algorithm for other initial system value settings may not be the optimal and effective for the model with new different initial system value setting. That's also the reason why we propose the RNN-BO algorithm, a model is capable to learn from historical data and predict for new situations.

Figure 7.4 shows the trends of accumulated objective function values under different optimal control strategies. In the tests of this section, we set the system parameter infection rate as $\beta = 0.25$, $\beta = 0.3$, and $\beta = 0.4$. For each infection rate, vary the initial system state values. For example, in Figure 7.4(a), OptimalControl1 represents the optimal control strategy solved by the BO algorithm when the initial system state values are $S_1(t_1) = 0.4$, $E_1(t_1) = 0.13$, $I_1(t_1) = 0.47$, $R_1(t_1) = 0.0$, and system parameter $\beta = 0.25$. The line under OptimalControl1 means that the accumulated objective function values when we applied this OptimalControl1 to the model with new system state values $S(t_1) = 0.5$, $E(t_1) = 0.3$, $I(t_1) = 0.2$, $R(t_1) = 0.0$ and same system

parameter $\beta = 0.25$. OptimalControl2 represents the optimal control strategy solved by the BO algorithm when the initial system state values $S_1(t_1) = 0.8$, $E_1(t_1) = 0.0$, $I_1(t_1) = 0.2$, $R_1(t_1) = 0.0$ and system parameter $\beta = 0.25$. The line under OptimalControl2 means that the accumulated objective function values when we applied this OptimalControl2 to the model with new system state values $S(t_1) = 0.5$, $E(t_1) = 0.3$, $I(t_1) = 0.2$, $R(t_1) = 0.0$ and same system parameter $\beta = 0.25$. OptimalControl3 is associated with the initial system state values $S_1(t_1) = 0.6$, $E_1(t_1) = 0.03$, $I_1(t_1) = 0.37$, $R_1(t_1) = 0.0$, OptimalControl4 is associated with initial system state values $S_1(t_1) = 0.3$, $E_1(t_1) = 0.3$, $I_1(t_1) = 0.4$, $R_1(t_1) = 0.0$, OptimalControl5 is associated with initial system state values $S_1(t_1) = 0.5$, $E_1(t_1) = 0.2$, $I_1(t_1) = 0.3$, $R_1(t_1) = 0.0$.

RNN-BO OptimalControl represents the optimal control strategy predicted by the RNN-BO predictive model, the line under RNN-BO OptimalControl means that the accumulated objective function values when we applied this RNN-BO OptimalControl to the model with new system state values $S(t_1) = 0.5$, $E(t_1) = 0.3$, $I(t_1) = 0.2$, $R(t_1) = 0.0$ and same system parameter $\beta = 0.25$. RealOptimalControl represents the actual optimal control strategy generated by the BO algorithm for the model with the new initial system state values $S(t_1) = 0.5$, $E(t_1) = 0.3$, $I(t_1) = 0.2$, $R(t_1) = 0.0$.

The small figures in Figure 7.4(a)-(c) are the zoom figures to show the trends clearly. From three figures 7.4(a) to 7.4(c), we can see that for the model with a new different initial system value setting, the optimal control strategies (OptimalControl1 – OptimalControl5) generated for other different initial system value settings don't perform good for the model with new initial system state value. This means that those optimal controls are the optimal control solutions for specific situation, they are not the optimal control solution for different situation. However, whatever the infection rate is, RNN-BO OptimalControl behaves similar effect as

RealOptimalControl. That means although sometimes RNN-BO OptimalControl doesn't perform better than RealOptimalControl, the RNN-BO algorithm is flexible and accurate enough to predict the optimal solution or predict the solution closer to the actual optimal solution. Besides, different from other control strategies, the RNN-BO OptimalControl is predicted without going through the optimization iterations anymore, which is computationally efficiency.

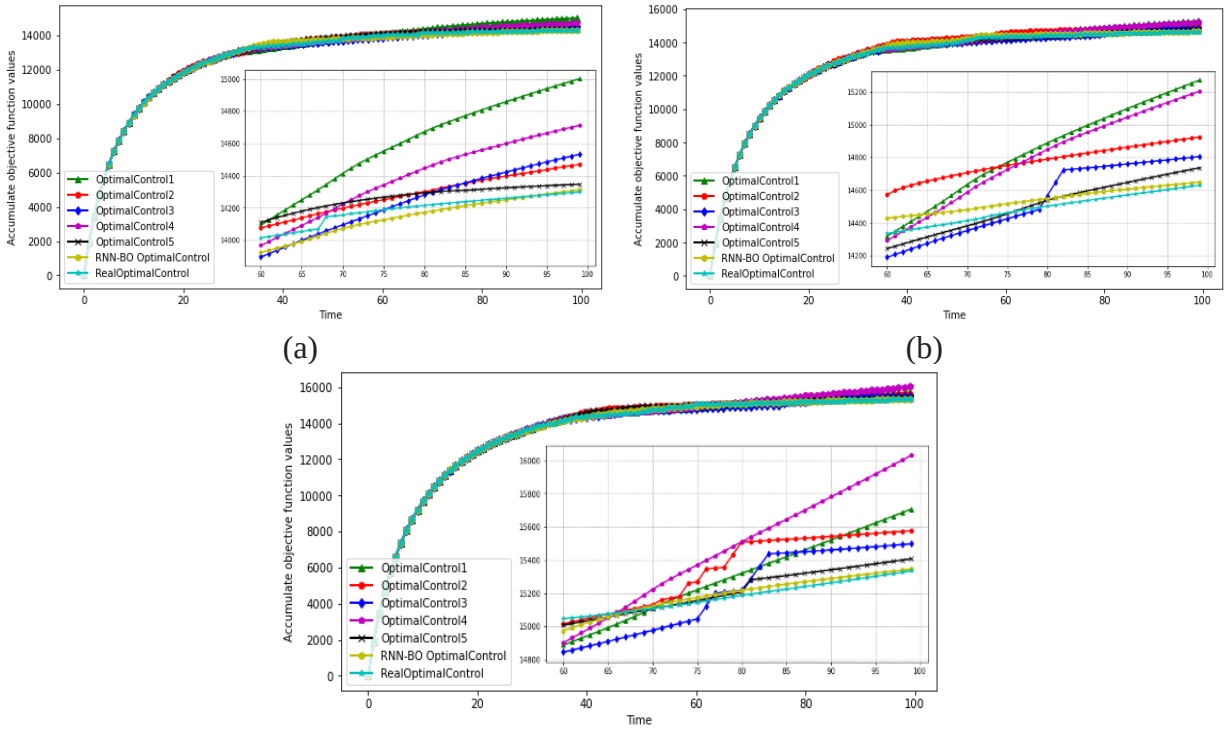

Figure 7.4 Simulation results on deterministic SEIR control model. (a) Accumulate objective function values generated by different optimal control when $\beta = 0.25$. (b) Accumulate objective function values generated by different optimal control when $\beta = 0.3$. (c) Accumulate objective function values generated by different optimal control when $\beta = 0.4$.

7.4.2 Analysis of Different RNN Layers and Different Training Epochs

This section studies the impact of different RNN layers and training epochs on the algorithm's performances in deterministic SEIR control model. For all simulation tests in this

section, the parameters of the RNN-BO predictive model are set as Dropout = 0.2, the activation = 'relu', the compile model optimizer = 'adam', loss = 'mse' during the implementation in Python. Set the new initial system value setting need to be predicted is $S(t_1) = 0.5$, $E(t_1) = 0.3$, $I(t_1) = 0.2$, $R(t_1) = 0.0$, $\beta = 0.4$. Then use the predictive model with different RNN layers and different training epochs to predict the corresponding optimal control strategies, observe the training loss of the predictive model and the final best objective function values under these optimal control strategies.

First, we study the impact of different RNN layers on the training loss. In this simulation experiment, the training epochs is fixed as 9, the number of RNN layers that we test are 2, 3, 4, 5, 6, and 7. The simulation result is shown in Figure 7.5(a). The trends of the training loss of different RNN layers are almost similar. All of them decrease a lot during the first three training epochs then gradually subside after that. When the number of RNN layers is 7, the training loss is relatively worse than those in other situations.

Next, we study the impact of different training epochs on the final best objective function value. In this simulation experiment, the number of RNN layers of the predictive model that we test are 2, 3, 4, 5, 6, and 7. The training epoch that we test is from 1 to 16. The simulation result is shown in Figure 7.5(b). While the training epoch is 1, the best objective function values of different number of layers are all higher than 15500. However, when the number of layers is 3, 4, 5, and 6, if the training epoch is between 2 to 16, the RNN-BO algorithm archives robust performances, it always solves low final best objective function values. When the number of layers is 2 or 7, the results show that the RNN-BO algorithm doesn't perform well on the global optimization for the studied SEIR control model. The best objective function value is sensitive to the training epoch when the number of layers is 2 or 7.

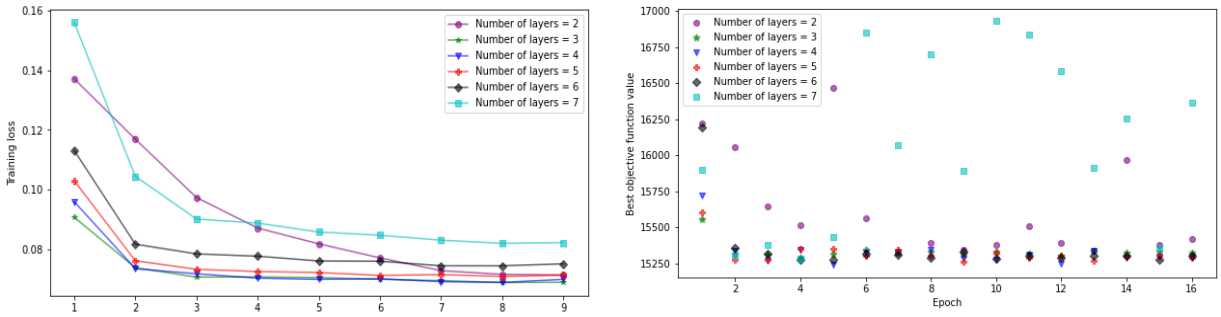

(a) (b)

Figure 7.5 Simulation results of different RNN layers and training epochs. (a) Training loss of different RNN layers when the training epochs = 9. (b) Best objective function value of different RNN layers under different number of training epochs.

7.4.3 Comparison with Other Algorithms

In this section, we compare the RNN-BO algorithm to the standard Bayesian Optimization algorithm (standard BO algorithm) and a high-dimensional Bayesian Optimization algorithm proposed in [49]. For simplify, we name this high-dimensional Bayesian Optimization algorithm as '**Reference BO algorithm**' in this section. Since we test the RNN-BO algorithm on the deterministic SEIR control model in section 7.4.1 and 7.4.2. To further prove the effectiveness of the RNN-BO algorithm on other model, we conduct the simulation of this section on the stochastic SIS control model formulated in Eqns. (7.10)-(7.13). All system parameter values remain unchanged for all tests in this section, the initial system values what we test is $S[0] = 0.6, I[0] = 0.4$. Referenced BO algorithm in its original paper is tested with different chosen dimensions d [49]. Therefore, in here we also select different dimensions for the reference BO algorithm to do the comparison.

The simulation results are shown in Figure 7.6. We can see that when the SIS model is without any control, the fraction of the infectious population over time behaves the oscillation property shown in Figure 7.6(a). It means that the epidemic would repeat outbreak. Also, the

accumulated objective function value under null control condition keeps going up shown in Figure 7.6(c). When we use different Bayesian Optimization algorithms to solve the optimal control strategy, the corresponding fraction of the infectious population over time and the accumulated objective function value are obtained. For the Reference BO algorithm in this paper, we only show the results when the number of chosen dimensions d is equal to$5, 30, 60, 90$ out of 100 dimensions. We tested $d = 5, 10, 20, 30, 40, 50, 60, 70, 80, 90$ for the Reference BO algorithm, it achieved the best objective function value when d is equal to 30. From Figure 7.6, we can see that all tested Bayesian Optimization algorithms significantly control the spread of epidemic. The corresponding accumulated objective function values over time also are about 6 times less than that when the model is without any control. For different Bayesian Optimization algorithms, the simulation results indicate that the Reference BO algorithm performs better than the standard BO algorithm, no matter what the number of chosen dimensions is. By comparing to the standard BO algorithm and the Reference BO algorithm, the RNN-BO algorithm achieves the best performance on controlling the spread of epidemic, decreasing infectious population, and minimizing the objective function value.

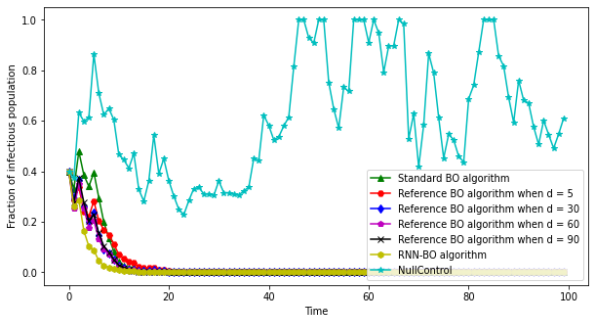

(a)

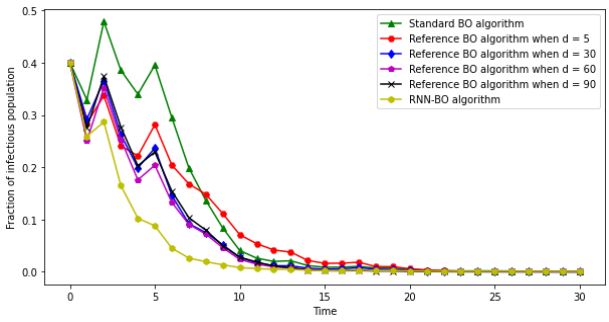

(b)

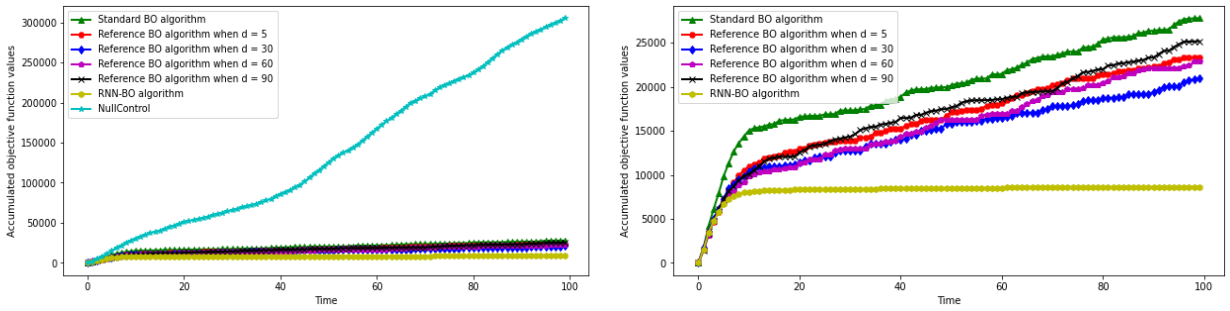

(c) (d)

Figure 7.6 Simulation results on stochastic SIS control model. (a) The trends of infectious population over under different BO algorithms and null control condition. (b) Zoom figure of the trends of infectious population under different BO algorithms. (c) Accumulated objective function value under different BO algorithms and null control condition. (d) Zoom figure of accumulated objective function value under different BO algorithms.

7.5 Conclusions

In this paper, a new RNN-BO high-dimensional optimization algorithm is proposed by combining the high-dimensional Bayesian Optimization and recurrent neural network to improve computational efficiency and effectiveness. This proposed RNN-BO algorithm is flexible, it can be applied to predict the optimal control solution for different cities, counties, or countries. For example, the same epidemic outbreaks in different countries, the related disease data in the developed countries like the United States might be quickly available to be used, more adequate and comprehensive than some developing countries. Although the optimal control strategy plan of a specific place may not be the optimal or effective for other places, the RNN-BO algorithm can utilize the historical data from different places to develop a general and flexible RNN-BO predictive model. It means that for some developing countries, if they are not willing to spend a lot of time and money to collect the useful disease data, they can learn the available historical data of the same disease from other countries, and then generate the predictive model to predict the

corresponding optimal control plan that is effective and applicable to their own countries. Some simulation experiments are implemented to prove that the RNN-BO algorithm is a promising approach. Different simulations also demonstrate the RNN-BO algorithm is robust and effective on the deterministic SEIR control model and stochastic SIS control model. We study the impact of different RNN layers and different training epochs on the RNN-BO algorithm's performances. In the future research, the RNN-BO algorithm should be studied and applied into more complicated and famous models. It would also be meaningful to design more effective sampling strategy, and tuning the parameters of the RNN-BO algorithm to speed up the calculations and predict the optimal result more accurate.

Chapter 8 - An Improved Mathematical Model of Sepsis: Modeling, Bifurcation Analysis, and Optimal Control Study for Complex Nonlinear Infectious Disease System

Abstract

Sepsis is a life-threatening medical emergency caused by extreme host immune response to infection, which is a major cause of death worldwide and the second highest cause of mortality in the United States. The immune response is a complicated system. Thus, a more accurate mathematical model is an important tool to study the progression of sepsis. On top of that, researching the optimal control treatment or intervention strategy on the comprehensive sepsis system is key in reducing mortality. For this purpose, first, this paper improves a complex nonlinear sepsis model proposed in our previous work. Then, bifurcation analyses are conducted for each sepsis subsystem to study the model behaviors under some system parameters. The bifurcation analysis results also further indicate the necessity of control treatment and intervention therapy. If the sepsis system is without adding any control under some parameter and initial system value settings, the system will perform persistent inflammation outcomes as time goes by. Therefore, we develop our complex improved nonlinear sepsis model into a sepsis optimal control model, and then use some effective biomarkers recommended in existing clinic practices as optimization objective function to measure the development of sepsis. Besides that, a Bayesian optimization algorithm by combining Recurrent neural network (RNN-BO algorithm) is introduced to predict the optimal control strategy for the studied sepsis optimal control system. The difference between the RNN-BO algorithm from other optimization algorithms is that once given any new initial system value setting (initial value is associated with the initial conditions of

patients), the RNN-BO algorithm is capable of quickly predicting a corresponding time-series optimal control based on the historical optimal control data for any new sepsis patient. To demonstrate the effectiveness and efficiency of the RNN-BO algorithm on solving the optimal control solution on the complex nonlinear sepsis system, some numerical simulations are implemented by comparing with other optimization algorithms in this paper.

Keywords: Nonlinear sepsis model, bifurcation analysis, optimal control, Bayesian optimization, Recurrent neural network.

8.1 Introduction

Sepsis is defined as life-threatening medical emergency caused by the body's extreme systemic immunological response to infection [246]. If there is not any therapeutic treatment, sepsis will further develop into septic shock, organ dysfunction and ultimately result in death. Sepsis is the major causes of death worldwide, with approximately 48.9 million incident sepsis cases in 2017 and estimated 20% of all global deaths [247]. In the early stage of sepsis, source control and antibiotics is normal therapeutic treatment to treat sepsis patients [248]. Some patients are benefit from the early administration of antibiotics [249]. If the patients present persistent inflammation in the later stage of sepsis when bacterial clearance is finished, some studies reported that the anti-TNF-α treatment is an effective therapy [250, 251]. Successful sepsis treatments involve the timing of control therapy and optimal dosing, delayed administration or improper dosage might lead to detrimental outcomes [252]. Thus, providing optimal treatment (involves timing and dosing of administration of control therapy) is the key in reducing the mortality of sepsis and improving patients' quality of care. In the past, attempts to discover the optimal treatments for sepsis have been focused on clinic trails. However, these attempts took much time to manipulate. Also, patients may present different clinical phenotypes if they perform different

pathophysiological mechanisms [249], it raises the difficulty to timely provide the effective and appropriate optimal control or intervention treatment through manipulating clinic trails for patients. Therefore, we attempt to address this challenge by the combining use of Bayesian optimization (BO) algorithm and Recurrent neutral network (RNN) applied to a sufficiently complex, nonlinear, mathematical sepsis model.

There are some previous studies on mathematical sepsis model. In 2004, Kumar *et al.* proposed a simplified sepsis mathematical model, this model contains three equations to roughly describe the dynamics between pathogen, early pro-inflammatory and late pro-inflammatory mediators [131]. In 2006, Reynolds *et al.* proposed a sepsis mathematical model to capture scenarios of inflammatory response to infection, this model presents more details of pro-inflammatory and anti-inflammatory mediators [253]. In 2015, We proposed an 18-equation complex sepsis model [254]. This model considers the basic and key components of sepsis progression incorporating innate with adaptive immunities, which studies details immune response among cell, pro-inflammatory cytokines, and anti-inflammatory cytokines. These mathematical models offer insights into complex dynamic immune response. However, these models do not consider the control or intervention treatment as variables into the system, to study the impact of control treatment on sepsis progression and look for the optimal treatment. To achieve our original goal, addressing the challenge and studying the method that can timely generate the optimal treatment, in this paper we are therefore developing our previous model into an optimal control model of sepsis.

To construct the sepsis optimal control model, the primary thing is to determine the practical and controllable parameters of the system. Past clinical studies show that appropriate antibiotics therapy in the early hours of sepsis onset can effectively control the pathogen infection,

control the pathogen replication/growth rate, and decrease absolute mortality [255 - 257]. In addition, during the immune response process, the release of the key pro-inflammatory cytokine such as tumor necrosis factor-α (TNF- α) is a double-edged sword in sepsis [258], which release rate can positively or negatively influence the outcomes of sepsis progression [254]. Some experimental studies show that anti-TNF-α therapy contributes to control the release rate of TNF-α, effective anti-TNF-α therapy can improve the outcome [259, 260]. Therefore, some key parameters such as the growth rate of pathogen and the release rate of TNF- α are controllable in real world, considering their related controls in the researched optimal control model will be more meaningful. Moreover, the model behaviors under some important system parameters is studied via stability and bifurcation analysis.

Besides the controllable parameters, the objective function for the sepsis optimal control model is also needed to be determined. What is a good biomarker that is well suited for the measure of immune response or development of sepsis? Some important immune system components can be used as biomarkers to detect changes and development of sepsis [261]. Those components can be pro-inflammatory cytokines such as TNF- α, interleukin-1 beta (IL-1β), interleukin-6 (IL-6), interleukin-8, and high mobility group box 1 (HMGB-1) [262 - 264]. Those pro-inflammatory components are associated to the clearance of pathogen. Some anti-inflammatory cytokines related to the downregulation of the immune system also can be used as biomarkers, such as interleukin-10 (IL-10), transforming growth factor-β (TGF- β), IL-1 receptor antagonists (IL-1ra) [262, 265]. In addition, TNF- α is a major pro-inflammatory cytokine and IL-10 is a crucial anti-inflammatory cytokine [266]. Thus, in many clinical practices, the ratio between TNF- α and IL-10 served as measure and biomarker to monitor sepsis progression [266 - 268]. Besides the inflammatory cytokines, several activation markers of immune cells have been recommended as biomarkers of

sepsis, such as neutrophil and monocyte/macrophage immune cells [262, 269]. According to the activation state and functions, monocyte immune cells can develop into monocyte-derived type-1 macrophage (M1 macrophage) and monocyte-derived type 2 macrophage (M2 macrophage) [270, 271]. M1 macrophage can promote the inflammation, M2 macrophage contributes to inhibit inflammation [271]. M1 macrophage is defined as the up-regulation biomarker and M2 macrophage is the down-regulation biomarker of inflammatory [272]. Thus, it is reasonable and convincing to establish the objective function based on some of these biomarkers.

For quickly providing the optimal control treatment strategy of the sepsis optimal control model that optimizes the objective function, the next step we aimed to develop an optimization algorithm by the combining use of BO algorithm and RNN. Solving the optimal control strategy of disease model can be viewed as a nonlinear optimization of control problem with time-series system [34, 226]. BO algorithm has been demonstrated to be an effective algorithm to optimize the optimal control strategy of the complex time-series disease system in our previous works [226, 240]. By combining RNN is because, RNN is great at learning the past data in sequence [273]. Since the initial value of sepsis system parameters and system state variables are associated with the initial conditions of patients, different initial values may lead to different outcomes, and may have different optimal control strategies. If we always use the BO algorithm to solve the optimal control solution when the sepsis patient is associated with new different initial value, the optimization process may take a lot of time, which may miss the best time for treatment. Our main idea is to use BO algorithm to generate the corresponding time-series optimal control strategies for system with different initial values. Consider those different system initial values and corresponding optimal control strategies as known historical data. Then leverage RNN to learn those historical data to catch the relationship between initial value and the optimal control strategy

obtained by BO algorithm. Once given a new initial value associated with patient's initial condition, the RNN-BO algorithm can timely and effectively predict the corresponding time-series optimal control strategy for this patient. The most contribution of RNN-BO algorithm is that it learns the historical data and generate a predictive model. Once the RNN-BO predictive model is ready, the RNN-BO algorithm only takes about 2 seconds to predict the optimal control strategy for any new given initial system values. It doesn't take time to do the optimization iterations anymore.

The remainder of this paper is organized as follows. Section 8.2 formulates the comprehensive optimal control model from some subsystems. Section 8.3 studies the model behaviors under various parameter settings via stability and bifurcation analysis. Section 8.4 presents the optimization scheme that will be used for solving the optimal control strategy of sepsis system. Then Section 8.5 implements the numerical simulation experiments to evaluate the effectiveness of proposed optimization scheme on researched sepsis model. Finally, Section 8.6 provides the conclusions and discusses our future work.

8.2 Model Formulation

Our sepsis optimal control model is developed based on our previous sepsis mathematical model [254]. This model describes the dynamic immune response of liver injury or infection among pathogen, pro-inflammatory cytokines, anti-inflammatory cytokines, and immune cells. We develop this optimal control model by incorporating three subsystems.

8.2.1 Neutrophil Immune Response Subsystem

Macrophage is one of the innate host's first lines of defense against bacterial pathogens [274]. In the initial stage of infection, once the intruding pathogens are detected, the resident immune cells such as tissue macrophages and hepatic macrophage (also known as Kupffer cells or resident liver macrophages) will migrate to the site of pathogens to remove pathogen and resolve

infections [253, 254]. Meanwhile, those macrophages release signal to resting phagocytes such as neutrophil immune cells. Resting phagocytes are activated and reach to the infection site to engulf the pathogens. In the meantime, these activated phagocytes release pro-inflammatory cytokines such as TNF- α, IL-6, IL-8. The pro-inflammatory cytokines will active and recruit more resting phagocytes to the infection site to clear the pathogen. The activation and recruitment of neutrophil promote the clearance of pathogen. However, the chemical substances such as reactive oxygen species (ROS) released by neutrophil cells is harmful, which will damage host tissue and accelerate the death of apoptotic hepatocytes [275 - 277]. We have developed this innate immune response process occurring in the early stage of infection into a mathematical model in the previous works [254]. In this paper, we call it neutrophil immune response subsystem, which consists of the following:

$$\frac{dP}{dt} = k_{pg}P\left(1 - \frac{P}{P_\infty}\right) - r_{pmk}\frac{[P^n]}{[P^n + k_{c1}^n]}M_{kf}P^* - r_{pn}\frac{[P^n]}{[P^n + k_{c2}^n]}(N_f + N_b)P^* \tag{8.1}$$

$$\frac{dM_{kf}}{dt} = k_{mk}M_{kf}\left(1 - \frac{M_{kf}}{K_\infty}\right) + k_{mkub}M_{kb} - \frac{[P^n]}{[P^n + k_{c1}^n]}M_{kf}P^* - u_{mk}M_{kf} \tag{8.2}$$

$$\frac{dM_{kb}}{dt} = \frac{[P^n]}{[P^n + k_{c1}^n]}M_{kf}P^* - k_{mkub}M_{kb} \tag{8.3}$$

$$\frac{dT}{dt} = \left(\frac{r_{t1max}M_{kb}}{m_{t1} + M_{kb}}\right)M_{kb} + \left(\frac{r_{t2max}N_b}{m_{t2} + N_b}\right)N_b - u_tT \tag{8.4}$$

$$\frac{dN_R}{dt} = k_{rd}N_R\left(1 - \frac{N_R}{N_S}\right) - r_1N_R(T + P)^* - u_{nr}N_R \tag{8.5}$$

$$\frac{dN_f}{dt} = r_1N_R(T + P)^* + k_{nub}N_b - \frac{[P^n]}{[P^n + k_{c2}^n]}N_fP^* - u_nN_f \tag{8.6}$$

$$\frac{dN_b}{dt} = \frac{[P^n]}{[P^n + k_{c2}^n]}N_fP^* - k_{nub}N_b \tag{8.7}$$

$$\frac{dr_1}{dt} = k_{r1}\left(1 + \tanh\left(N_f^*\right)\right) - u_{r1}r_1 \tag{8.8}$$

$$\frac{dD}{dt} = r_{hn}\frac{[D^n]}{[D^n + k_{c3}^n]}N_fD^*\left(1 - \frac{D}{A_\infty}\right) - r_{ah}D \tag{8.9}$$

where P, M_{kf}, M_{kb}, T, N_R, N_f, N_b, r_1, D are t_f-dimensional system state variables, $t \in [t_1, t_f]$, t_1 is the start time and t_f is the end time. They represent the levels of pathogen, free Kupffer cell that is waiting for binding with pathogen, binded Kupffer cell that is binding with pathogen, TNF- α, resting neutrophil that is waiting for activation, free activated neutrophil that is activated and is waiting for binding with pathogen, binded activated neutrophil that is binding with pathogen, the rate of resting neutrophil activated under infection, and damaged tissue or dead hepatocytes, respectively. In Eq. (8.1), P^* represents the pathogen concentration defined as $P^* = \frac{P}{P_\infty}$. In Eq. (8.8), N_f^* represents the free activated neutrophil concentration as $N_f^* = \frac{N_f}{N_S}$. In Eq. (8.9), D^* represents the damage tissue concentration as $D^* = \frac{D}{A_\infty}$. The rest of symbols are system parameters, their definition and corresponding values for later simulation experiments are summarized in Table shown in **Appendix 3**. We refer readers to our previous work [254] to get more details about the construction of this neutrophil immune response subsystem.

8.2.2 Monocyte Immune Response Subsystem

In our previous work [254], we have also constructed the monocyte immune response subsystem. However, the previous work did not consider the further development of monocytes. To better describe the dynamics of immune response, we attempt to improve the monocyte immune response model in this paper.

During the innate immune response process, besides the presence of Kupffer cell and neutrophil phagocyte contributing to the clearance of pathogen, recent works from the literature have already shown that monocyte immune cell is also a key phagocyte [278]. Monocyte is activated and recruited by HMGB-1 and TNF- α, which can clear the pathogen and phagocytizing the aging binded activated neutrophils, it has significant impact on liver inflammation [254, 279 -

281]. On the other hand, according to existing literature, HMGB-1 can be released by activated monocytes and necrotic cells (means dead cells in this paper) [281 - 283]. Besides the release of HMGB-1, monocytes also release the anti-inflammatory cytokines such as IL-10 [284]. IL-10 contributes to prevent the subsequent tissue damage by inhibiting the activation of phagocytes such as neutrophils and monocytes [285].

About the monocyte development, much experimental evidence indicates that monocytes will develop into monocyte-derived type 1 macrophage (M1 macrophage) when they encounter pathogen, TNF-α, or GM-CSF, then M1 macrophage contributes to kill the pathogens through phagocytosis [286, 287]. During this process, M1 macrophages will release pro-inflammatory cytokines such as TNF- α, IL-6, and IL-12 [288, 289]. Thus, M1 macrophages are inflammatory microphages that can promote inflammation and cause damage to host tissues [288]. In addition, monocytes also will develop into monocyte-type 2 macrophage (M2 macrophage) when they encounter apoptotic T cells, IL-10, or TGF-β [286 - 288]. M2 macrophages will release anti-inflammatory cytokines IL-10 and TGF- β when they phagocytize apoptotic T cells [290]. Thus, M2 macrophages are healing macrophages that plays an important impact on the healing and tissue repair [288]. A simplified mechanism of monocyte development is drawn as Figure 8.1.

Due to the immune response of M2 macrophages is associated with T cell, it belongs to adaptive immunity. Therefore, in this monocyte immune response subsystem, we will only consider M1 macrophages. The mathematical expression of M2 macrophage will be constructed in immune system with adaptive immunity shown in Section 8.2.3. Base on the original model proposed in previous work [254] and the development of monocytes, the monocyte immune response subsystem is revised by remodeling the expression of monocytes as following:

$$\frac{dP}{dt} = k_{pg}P(1-P^*) - r_{pmk}\frac{[P^n]}{[P^n+k_{c1}^n]}M_{kf}P^* - r_{pn}\frac{[P^n]}{[P^n+k_{c2}^n]}\left(N_f+N_b\right)P^* - E_1 \quad (8.10)$$

$$\frac{dN_f}{dt} = \frac{r_1 N_R (T+P)^*}{(1+\frac{C_A}{C_\infty})} + k_{nub} N_b - \frac{[P^n]}{[P^n + k_{c2}^n]} N_f P^* - u_n N_f \tag{8.11}$$

$$\frac{dN_b}{dt} = \frac{[P^n]}{[P^n + k_{c2}^n]} N_f P^* - u_{mn} N_b M_f^* - k_{nub} N_b \tag{8.12}$$

$$\frac{dM_R}{dt} = k_{mr} M_R \left(1 - \frac{M_R}{M_S}\right) - r_2 M_R (H+T)^* - u_{mr} M_R \tag{8.13}$$

$$\frac{dM_f}{dt} = \frac{r_2 M_R (H+T)^*}{(1+\frac{C_A}{C_\infty})} + k_{umb} M_b - E_1 - u_m M_f \tag{8.14}$$

$$\frac{dM_b}{dt} = E_1 - k_{umb} M_b \tag{8.15}$$

$$E_1 = \frac{dM_1}{dt} = r_{pm} \frac{[P^n]}{[P^n + k_{c4}^n]} M_f P^* \tag{8.16}$$

$$\frac{dH}{dt} = \left(\frac{r_{h1max}(M_b+D)}{mh_1 + M_b + D}\right)(M_b + D) - u_h H \tag{8.17}$$

$$\frac{dC_A}{dt} = \left(\frac{r_{camax} M_b}{C_{Ah} + M_b}\right) M_b - u_{ca} C_A \tag{8.18}$$

where M_R, M_f, M_b, M_1, H, C_A are t_f-dimensional system state variables, $t \in [t_1, t_f]$, t_1 is the start time and t_f is the end time. They represent the levels of resting monocyte that is waiting for activation, free activated monocyte that is activated and is waiting for phagocytizing, binded activated monocyte that is involving in the immune response with pathogen and T cells, monocyte-derived type 1 macrophage, HMGB-1, and IL-10, respectively.

Eq. (8.10) is developed from Eq. (8.1) by incorporating the clearance effect of monocytes. Eq. (8.11) is developed from Eq. (8.6) due to the inhibition of IL-10. Eq. (8.12) is developed from Eq. (8.7) by incorporating the phagocytosis effect of monocytes. In Eq. (8.12), M_f^* represents the free activated monocyte concentration as $M_f^* = \frac{M_f}{M_S}$. Eq. (8.16) represents the changing number of M1 macrophages due to M1 macrophages phagocytize pathogen, this term is associated with the solid line numbered with ① in Figure 8.1. The rest of symbols without mentioned before are

system parameters, their definition and corresponding values for later simulation experiments are summarized in Table shown in **Appendix 3**.

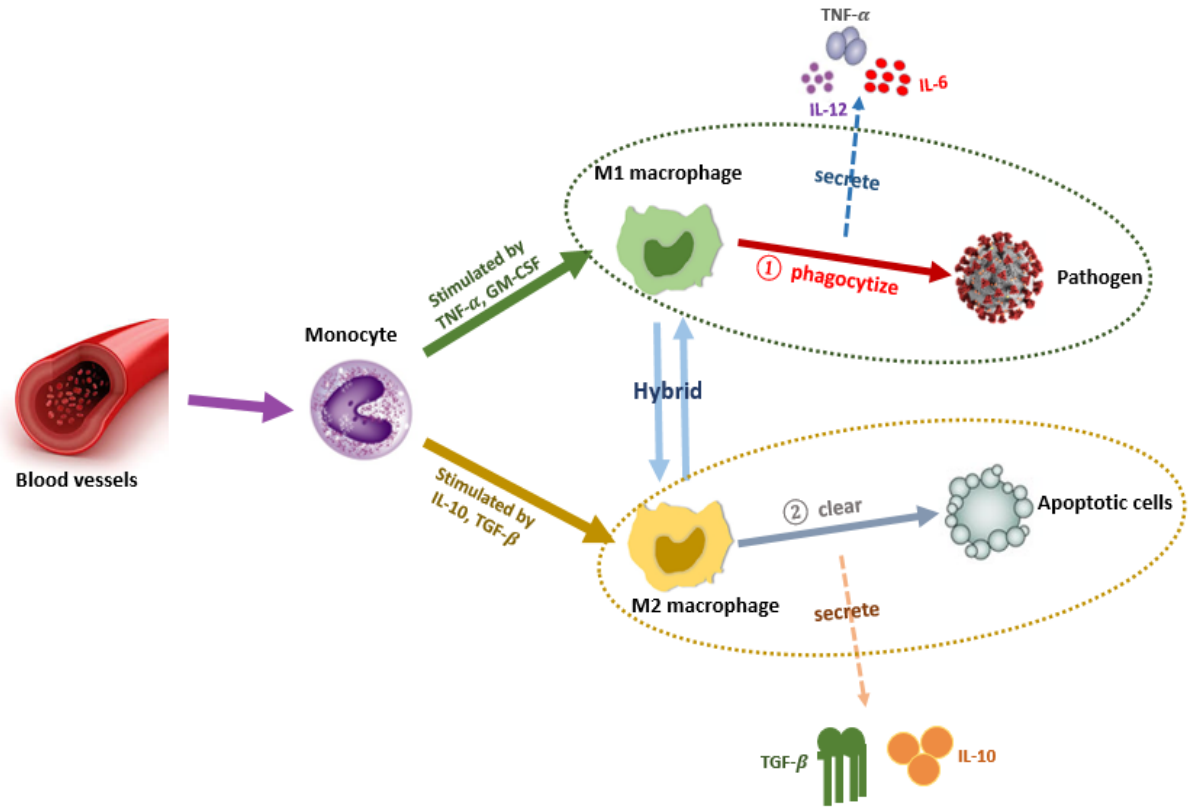

Figure 8.1 Simplified mechanism of monocyte development

8.2.3 Immune Response System Incorporated with Adaptive Immunity

Innate immunity plays an important role in the clearance of pathogen in the early stage of inflammation. Compared to innate immunity, adaptive immunity is activated in the late stage of inflammation [291]. The dynamics of adaptive immunity is more complicated than innate immunity. To simplify adaptive immunity, in this paper we will remain the model including B cells, and antibodies proposed in [254]. On this basis, this paper will provide the expression of M2 macrophages, and remodel the expression of monocytes. At the same time, this paper will improve the expression of T cells due to some T cell's functions.

The T cells we will study and model in this paper are CD4+ T cell and CD8+ T cell. CD4+ T cells play an important role on clearing the pathogen and achieving a regulated effective immune response to infection [292]. Activated monocytes that phagocytize pathogen is one type of antigen-presenting cells (APCs) [293]. CD4+ T cells are activated and recruited by APCs, APCs also can enhance and recruit more CD4+ T cells [290, 291]. CD4+ T cells that undergo apoptotic are phagocytized by M2 macrophages [294]. The activation of CD8+ T cells go through a major histocompatibility complex class I peptide (MHCI)-TCR mechanism, which is like the activation process of CD4+ T cells [254]. CD8+ T cells that undergo apoptotic are phagocytized by M2 macrophages as well [294]. Unlike CD4+ T cells, CD8+ T cells are cytotoxic cells, their primary function is to kill the infected target cells [290, 295]. In previous work, we have modeled the clearance function of CD4+ T cells on pathogen expression and cytotoxic function of CD8+ T cells through the decrease on expressions of binded Kupffer cells, binded activated neutrophils, and binded activated monocytes. However, the previous work doesn't model the clearance function on expression of CD4+ T cells and cytoxic function on expression of CD8+ T cells. Thus, we not only remain the modeling of those functions on pathogen, binded Kupffer cells, binded activated neutrophils, and binded activated monocytes, but also revise the expression of CD4+ T cells and CD8 T cells in this paper. A simplified mechanism of T cells in this paper is drawn as Figure 8.2.

Some experimental studies shown have shown that CD4+ T cells are activated by APCs to proliferate and differentiate into T_H1 and T_H2 effector cells [290, 296]. T_H1 and T_H2 effector cells can activate B cells to secrete antibodies [291]. The antibodies released by B cells play an important role on the clearance of pathogen at the later stage of inflammation [291, 293].

Base on the original model proposed in previous work [254] and our improvement on monocytes and T cells, the improved immune response system incorporated with adaptive immunity is revised as following:

$$\frac{dP}{dt} = k_{pg}P(1-P^*) - r_{pmk}\frac{[P^n]}{[P^n+k_{c1}^n]}M_{kf}P^* - r_{pn}\frac{[P^n]}{[P^n+k_{c2}^n]}\left(N_f+N_b\right)P^* -$$

$$M_1 - r_{pcd4}\frac{[P^n]}{[P^n+k_{c6}^n]}T_{CD4}P^* - r_{pAb}\frac{[P^n]}{[P^n+k_{c5}^n]}AP^* \tag{8.19}$$

$$\frac{dM_{kf}}{dt} = k_{mk}M_{kf}\left(1-\frac{M_{kf}}{K_\infty}\right) + k_{mkub}M_{kb} - \frac{[P^n]}{[P^n+k_{c1}^n]}M_{kf}P^* - u_{mk}M_{kf} \tag{8.20}$$

$$\frac{dM_{kb}}{dt} = \frac{[P^n]}{[P^n+k_{c1}^n]}M_{kf}P^* - r_{Mkbcd8}\frac{[M_{kb}^n]}{[M_{kb}^n+k_{c6}^n]}T_{CD8}M_{kb}^* - k_{mkub}M_{kb} \tag{8.21}$$

$$\frac{dT}{dt} = \left(\frac{r_{t1max}M_{kb}}{m_{t1}+M_{kb}}\right)M_{kb} + \left(\frac{r_{t2max}N_b}{m_{t2}+N_b}\right)N_b - u_tT \tag{8.22}$$

$$\frac{dN_R}{dt} = k_{rd}N_R\left(1-\frac{N_R}{N_S}\right) - r_1N_R(T+P)^*/(1+\frac{C_A}{C_\infty}) - u_{nr}N_R \tag{8.23}$$

$$\frac{dN_f}{dt} = r_1N_R(T+P)^*/(1+\frac{C_A}{C_\infty}) + k_{nub}N_b - \frac{[P^n]}{[P^n+k_{c2}^n]}N_fP^* - u_nN_f \tag{8.24}$$

$$\frac{dN_b}{dt} = \frac{[P^n]}{[P^n+k_{c2}^n]}N_fP^* - u_{mn}N_bM_f^* - r_{Nbcd8}\frac{[N_b^n]}{[N_b^n+k_{c7}^n]}T_{CD8}N_b^* - k_{nub}N_b \tag{8.25}$$

$$\frac{dr_1}{dt} = k_{r1}\left(1+\tanh\left(N_f^*\right)\right) - u_{r1}r_1 \tag{8.26}$$

$$\frac{dD}{dt} = r_{hn}\frac{[D^n]}{[D^n+k_{c3}^n]}N_fD^*(1-\frac{D}{A_\infty}) - r_{ah}D \tag{8.27}$$

$$\frac{dM_R}{dt} = k_{rm}M_R\left(1-\frac{M_R}{M_S}\right) - r_2M_R(H+T+T_{CD4}+T_{CD8})^*/(1+\frac{C_A}{C_\infty}) - u_{mr}M_R \tag{8.28}$$

$$\frac{dM_f}{dt} = \frac{r_2M_R(H+T+T_{CD4}+T_{CD8})^*}{1+\frac{C_A}{C_\infty}} + k_{umb}M_b - E_1 - E_2$$

$$-r_{cd4Mb}\frac{\left[M_f^n\right]}{\left[M_f^n+k_{c8}^n\right]}T_{CD4}M_f^* - r_{cd8Mb}\frac{\left[M_f^n\right]}{\left[M_f^n+k_{c8}^n\right]}T_{CD8}M_f^* - u_mM_f \tag{8.29}$$

$$\frac{dM_b}{dt} = E_1 + E_2 + r_{cd4Mb}\frac{\left[M_f^n\right]}{\left[M_f^n+k_{c8}^n\right]}T_{CD4}M_f^* + r_{cd8Mb}\frac{\left[M_f^n\right]}{\left[M_f^n+k_{c8}^n\right]}T_{CD8}M_f^*$$

$$-r_{Mbcd8}\frac{[M_b^n]}{[M_b^n+k_{c7}^n]}T_{CD8}M_b^* - k_{umb}M_b \tag{8.30}$$

$$E_1 = \frac{dM_1}{dt} = r_{pm}\frac{[P^n]}{[P^n+k_{c4}^n]}M_f P^* \tag{8.31}$$

$$E_2 = \frac{dM_2}{dt} = k_{cd4M}\frac{[T_{CD4}^n]}{[T_{CD4}^n+k_{c10}^n]}M_f T_{CD4}^* + k_{cd8M}\frac{[T_{CD8}^n]}{[T_{CD8}^n+k_{c10}^n]}M_f T_{CD8}^* \tag{8.32}$$

$$\frac{dH}{dt} = \left(\frac{r_{h1max}(M_b+D)}{mh_1+M_b+D}\right)(M_b+D) - u_h H \tag{8.33}$$

$$\frac{dC_A}{dt} = \left(\frac{r_{camax}M_b}{C_{Ah}+M_b}\right)M_b - u_{ca}C_A \tag{8.34}$$

$$\frac{dT_{CD4}}{dt} = k_{cd4}T_{CD4}\left(1-\frac{T_{CD4}}{T_{CD4\infty}}\right) + r_{cd4Mb}\frac{\left[M_f^n\right]}{\left[M_f^n+k_{c8}^n\right]}T_{CD4}M_f^*$$

$$-k_{cd4M}\frac{[T_{CD4}^n]}{[T_{CD4}^n+k_{c10}^n]}M_f T_{CD4}^* - r_{pcd4}\frac{[P^n]}{[P^n+k_{c6}^n]}T_{CD4}P^* - u_{cd4}T_{CD4} \tag{8.35}$$

$$\frac{dT_{CD8}}{dt} = k_{cd8}T_{CD8}\left(1-\frac{T_{CD8}}{T_{CD8\infty}}\right) + r_{cd8Mb}\frac{\left[M_f^n\right]}{\left[M_f^n+k_{c8}^n\right]}T_{CD8}M_f^* - k_{cd8M}\frac{[T_{CD8}^n]}{[T_{CD8}^n+k_{c10}^n]}M_f T_{CD8}^*$$

$$-r_{Mkbcd8}\frac{[M_{kb}^n]}{[M_{kb}^n+k_{c6}^n]}T_{CD8}M_{kb}^* - r_{Nbcd8}\frac{[N_b^n]}{[N_b^n+k_{c7}^n]}T_{CD8}N_b^*$$

$$-r_{Mbcd8}\frac{[M_b^n]}{[M_b^n+k_{c7}^n]}T_{CD8}M_b^* - u_{cd8}T_{CD8} \tag{8.36}$$

$$\frac{dB}{dt} = k_B B\left(1-\frac{B}{B_\infty}\right) + r_{Bt}\frac{[B^n]}{[B^n+k_{c9}^n]}T_{CD4}B^* - u_B B \tag{8.37}$$

$$\frac{dA}{dt} = \left(\frac{r_{Abmax}B}{m_{Ab}+B}\right)B - u_{Ab}A \tag{8.38}$$

where M_2, T_{CD4}, T_{CD8}, B, A are t_f-dimensional system state variables, $t \in [t_1, t_f]$, t_1 is the start time and t_f is the end time. They represent the levels of monocyte-derived type 2 macrophage, CD4+ T cell, CD8+ T cell, B cell, and Antibodies, respectively. In Eq. (8.21), M_{kb}^* represents the binded Kupffer cell concentration defined as $M_{kb}^* = \frac{M_{kb}}{K_\infty}$. In Eq. (8.8), N_b^* represents the binded activated neutrophil concentration as $N_b^* = \frac{N_b}{N_S}$. In Eq. (8.25), M_b^* represents the binded activated

monocytes concentration as $M_b^* = \frac{M_b}{M_S}$. In Eq. (8.32), T_{CD4}^* represents the CD4+ T cell concentration as $T_{CD4}^* = \frac{T_{CD4}}{T_{CD4\infty}}$, T_{CD8}^* represents the CD8+ T cell concentration as $T_{CD8}^* = \frac{T_{CD8}}{T_{CD8\infty}}$. In Eq. (8.38), B^* represents B cell concentration as $B^* = \frac{B}{B_\infty}$. Eq. (8.32) represents the changing number of M2 macrophages due to M2 macrophages phagocytize apoptotic T cells, this term is associated with the solid line numbered with ② in Figure 8.1.

In Eq. (8.35), the first term represents the recruiting process of CD4+ T cells during adaptive immunity, which is associated with the solid line numbered with ① in Figure 8.2. The second term represents the increasing number of CD4+ T cells that are enhanced by APCs, which is associated with the solid line numbered with ③ in Figure 8.2. The third term represents the decreasing number of CD4+ T cells since the apoptotic CD4+ T cells are phagocytized by monocytes, which is associated with the solid line numbered with ⑦ in Figure 8.2. The fourth term represents the decreasing number of CD4+ T cells since they are binding with pathogen and kill pathogen, which is associated with the solid line numbered with ⑤ in Figure 8.2. The fifth term represents the decreasing number of CD4+ T cells due to normal degradation, which is associated with the solid line numbered with ⑥ in Figure 8.2.

In Eq. (8.36), the first term represents the recruiting process of CD8+ T cells during adaptive immunity, which is associated with the solid line numbered with ② in Figure 8.2. The second term represents the increasing number of CD8+ T cells that are enhanced by APCs, which is associated with the solid line numbered with ④ in Figure 8.2. The third term represents the decreasing number of CD8+ T cells since the apoptotic CD8+ T cells are phagocytized by monocytes, which is associated with the solid line numbered with ⑧ in Figure 8.2. The fourth, fifth, sixth terms represent the decreasing number of CD8+ T cells since CD8+ T cells are binding

with Kupffer cells, neutrophils, monocytes and kill them, which are associated with the solid lines numbered with ⑨, ⑩, ⑪ in Figure 8.2, respectively. The seventh term represents the decreasing number of CD8+ T cells due to normal degradation, which is associated with the solid line numbered with ⑫ in Figure 8.2.

The rest of symbols without mentioned before are system parameters, their definition and corresponding values for later simulation experiments are summarized in Table shown in **Appendix 3**.

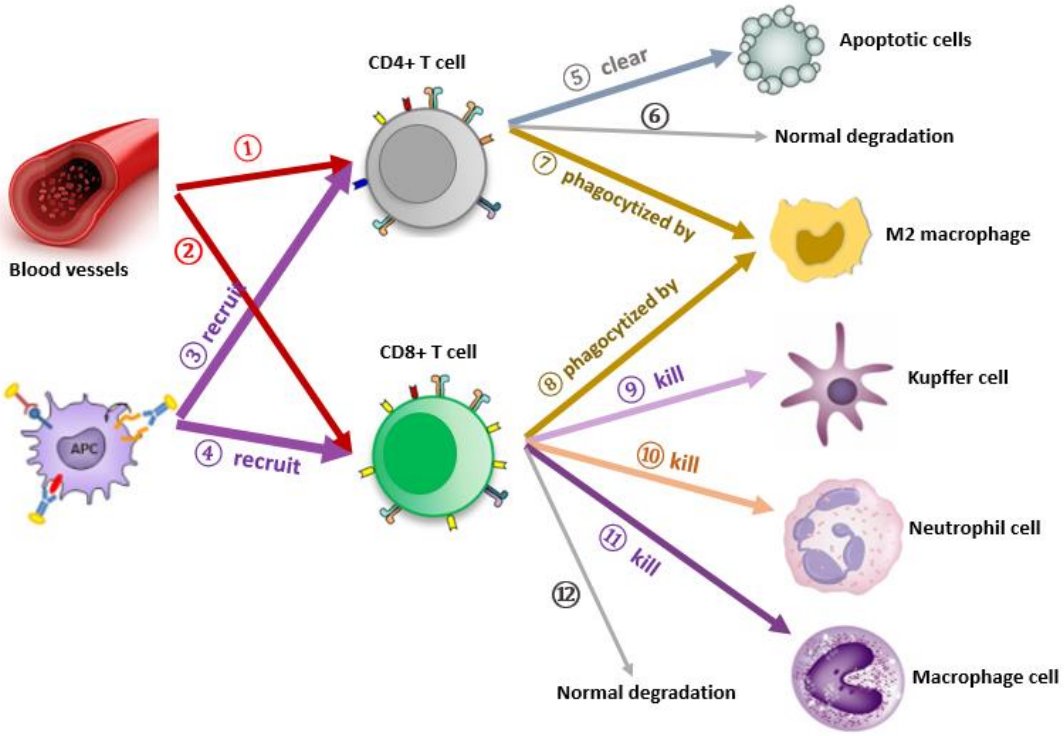

Figure 8.2 Simplified mechanism of T cells

8.3 Bifurcation Analysis

To study the model dynamics behaviors under various parameter settings, we will conduct the bifurcation analysis for each subsystem in this section. Bifurcation is the qualitative behavior change (change in number or numerical value of equilibrium points) of the system by varying

parameters [297]. The objective of bifurcation analysis is to study and identify the key parameters in sepsis development. In this paper we will use numerical analysis to realize bifurcation analysis due to the complexity of sepsis system. Since our current nonlinear sepsis model is too complicated, there is no existing programming tools or packages that can directly solve the bifurcation diagrams of system. Bifurcation value is a value of the equilibrium point moving from stable equilibrium to unstable equilibrium [298]. Therefore, we will start the bifurcation analysis by varying the values of key parameters, then plot all equilibrium points over the key parameters. The bifurcation will be intuitively and clearly caught. In this paper, all bifurcation diagrams are numerically generated by Python.

8.3.1 Bifurcation Analysis in Neutrophil Subsystem

The parameters we analyze in neutrophil subsystem are k_{pg}, r_{pn}, and u_n. For each parameter, only the system state variables with obvious equilibrium behavior are presented. The bifurcation diagrams of neutrophil subsystem are shown in Figure 8.3.

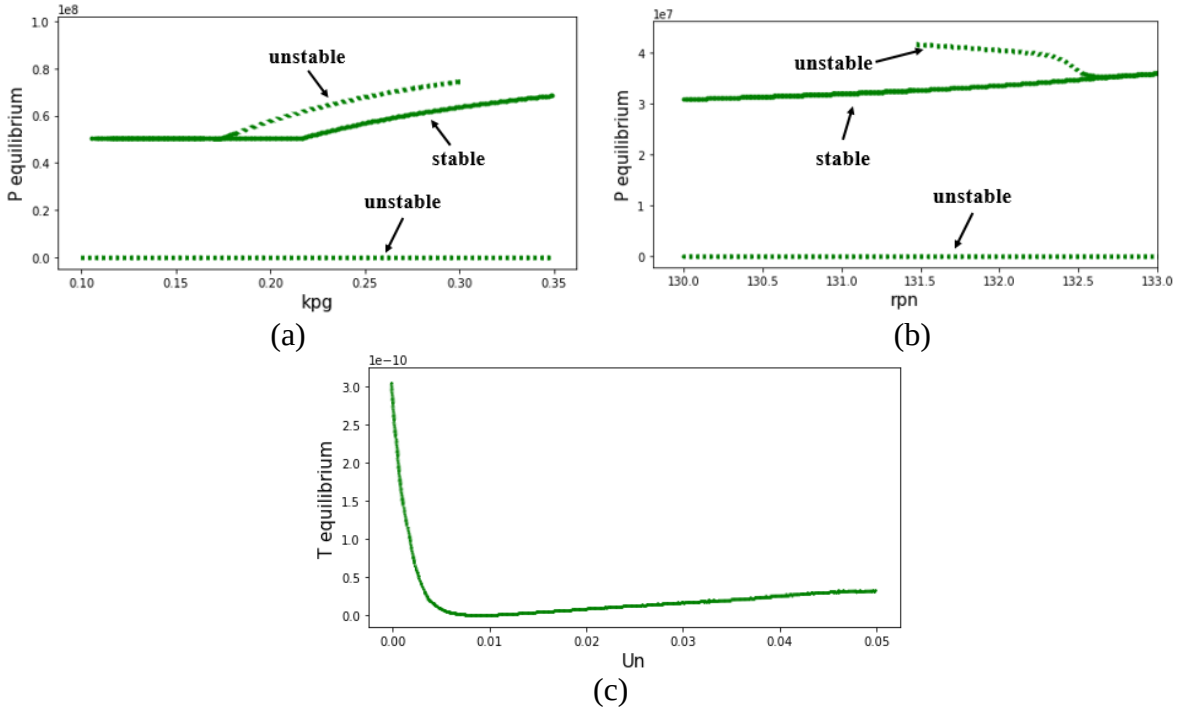

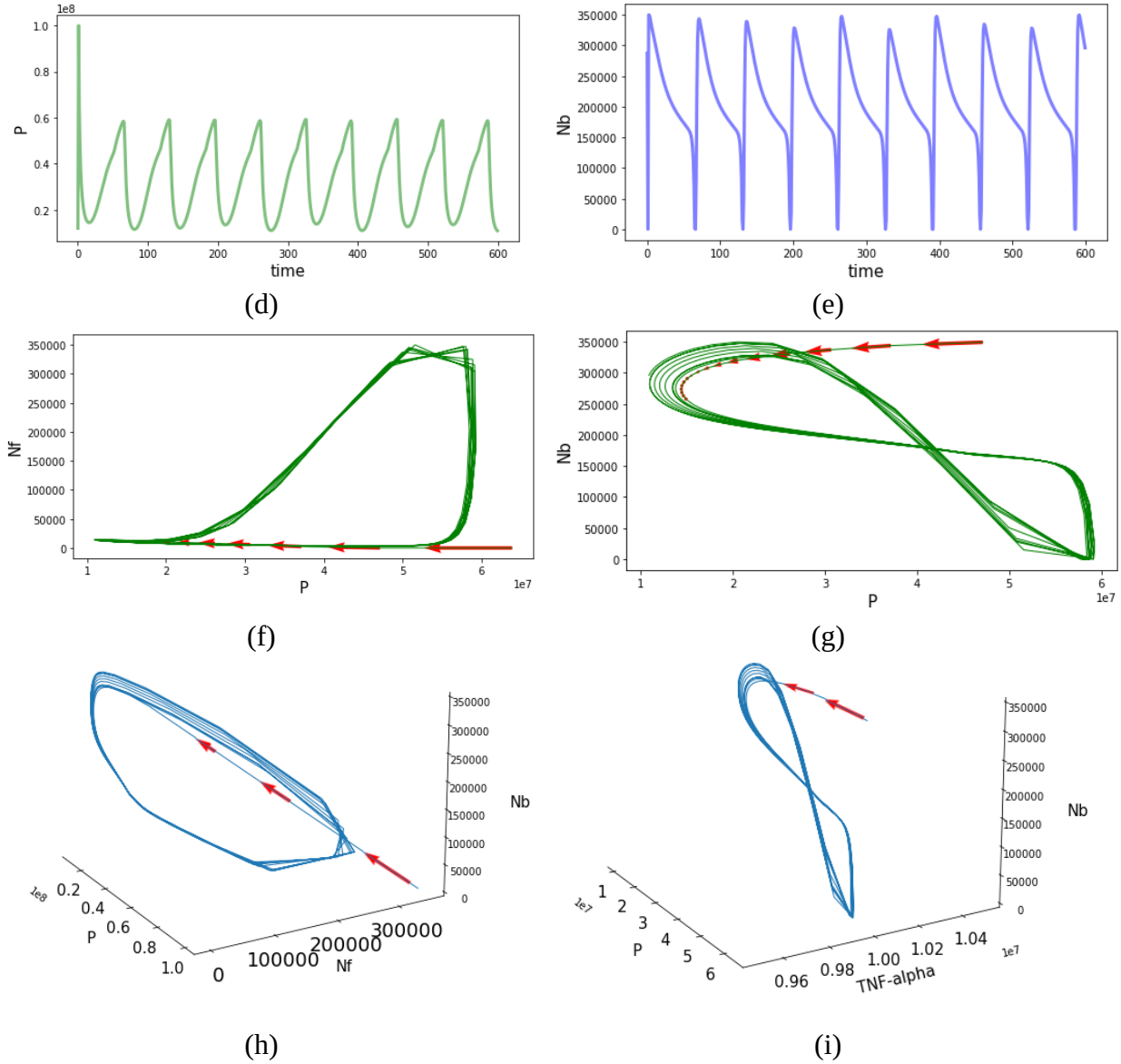

(d) (e)

(f) (g)

(h) (i)

Figure 8.3 Bifurcation analysis results in neutrophil subsystem. (a) Numerical equilibrium curve of pathogen related to parameter k_{pg}. (b) Numerical equilibrium curve of pathogen related to parameter r_{pn}. (c) Numerical equilibrium curve of TNF-α related to parameter u_n. (d) Oscillation behavior of pathogen when k_{pg} is equal to 0.1. (e) Oscillation behavior of Nb when k_{pg} is equal to 0.1. (f) Phase trajectory in P-Nf plane. (g) Phase trajectory in P-Nb plane. (h) Phase trajectory in (P, Nf, Nb) space. (i) Phase trajectory in (P, TNF-α, Nb) space.

In Figure 8.3, X axis represents the parameter values, Y axis represents the equilibrium values of the system state variable. According to the definition of bifurcation, Figure 8.3(a) and Figure 8.3(b) both show the changes in the number of equilibrium and the change in the numerical values of equilibrium when the parameter value is change. In (a) and (b), the solid line represents the stable equilibrium, dash line represents the unstable equilibrium. Stable equilibrium means that the points nearing this equilibrium (on both sides of this equilibrium) converge to this equilibrium, unstable equilibrium means that there exist points nearing this equilibrium (on both sides of this equilibrium) diverge from this equilibrium [299]. In Figure 8.3(a), stable equilibrium points of pathogen are observed when system parameter k_{pg} increases from 0.11 to 0.35. At the same range of parameter k_{pg}, unstable equilibrium points of pathogen are observed as well. When $k_{pg} = 0.175$, a bifurcation point is identified, and new unstable equilibrium point of pathogen are generated as k_{pg} increases from 0.175 to 0.3. In Figure 8.3(b), stable equilibrium points of pathogen are observed when system parameter r_{pn} increases from 130 to 133. At the same range of parameter r_{pn}, unstable equilibrium points of pathogen are observed as well. When $r_{pn} = 132.6$, a bifurcation point is identified, and new unstable equilibrium point of pathogen are generated as r_{pn} decreases from 132.6 to 131.5. In Figure 8.3(c), the changes on numerical value of equilibrium points of TNF-α is observed by varying the system parameters u_n.

Figure 8.3(d) and Figure 8.3(e) show the oscillation behaviors of pathogen and N_b when k_{pg} is equal to 0.1 in neutrophil subsystem. As k_{pg} is equal to 0.1, pathogen and binded activated neutrophil diverge at unstable equilibria in neutrophil subsystem. These trends indicate that inflammation oscillation requires the additional intervention or control treatment. Otherwise, the inflammation will constantly occur as time goes by. Figure 8.3(f) and Figure 8.3(g) display the phase trajectories in pathogen-free activated neutrophil plane and pathogen-binded activated

neutrophil plane, respectively. The arrow in the figure represents the direction of phase trajectory. The stable limit cycles are reach in these phase spaces. Stable limit cycle means that all neighboring trajectories approach the limit cycle as the time approaches infinity [300]. Therefore, Figure 8.3(f) and Figure 8.3(g) also reflect that pathogen, free activated neutrophil, binded activated neutrophil will converge to a dynamic equilibrium, not converges a single point. Their values even repeatedly remain in a high level, which will lead to persistent inflammatory. Figure 8.3(h) and Figure 8.3(i) display the phase trajectories in (pathogen, free activated neutrophil plane, binded activated neutrophil) space and (pathogen, TNF-α, binded activated neutrophil) space, respectively. The stable limit cycles are observed in these two phase space as well.

8.3.2 Bifurcation Analysis in Monocyte Subsystem

Continued bifurcation analysis on the monocyte subsystem are researched. The parameter we analyze in monocyte subsystem is k_{pg}. For each parameter, only the system state variables with obvious equilibrium behavior are presented. The bifurcation diagrams of neutrophil subsystem are shown in Figure 8.4.

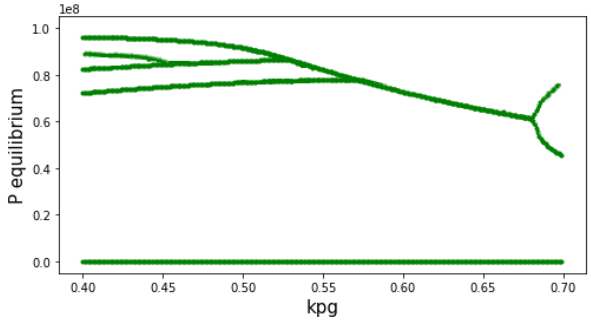

(a)

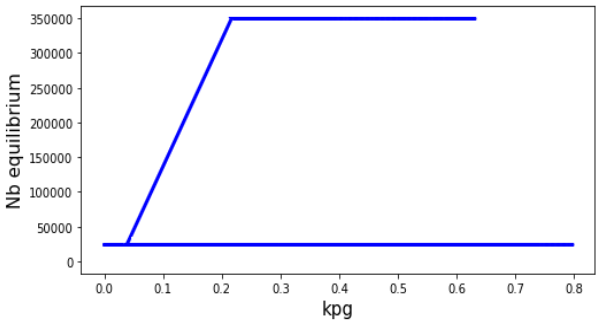

(b)

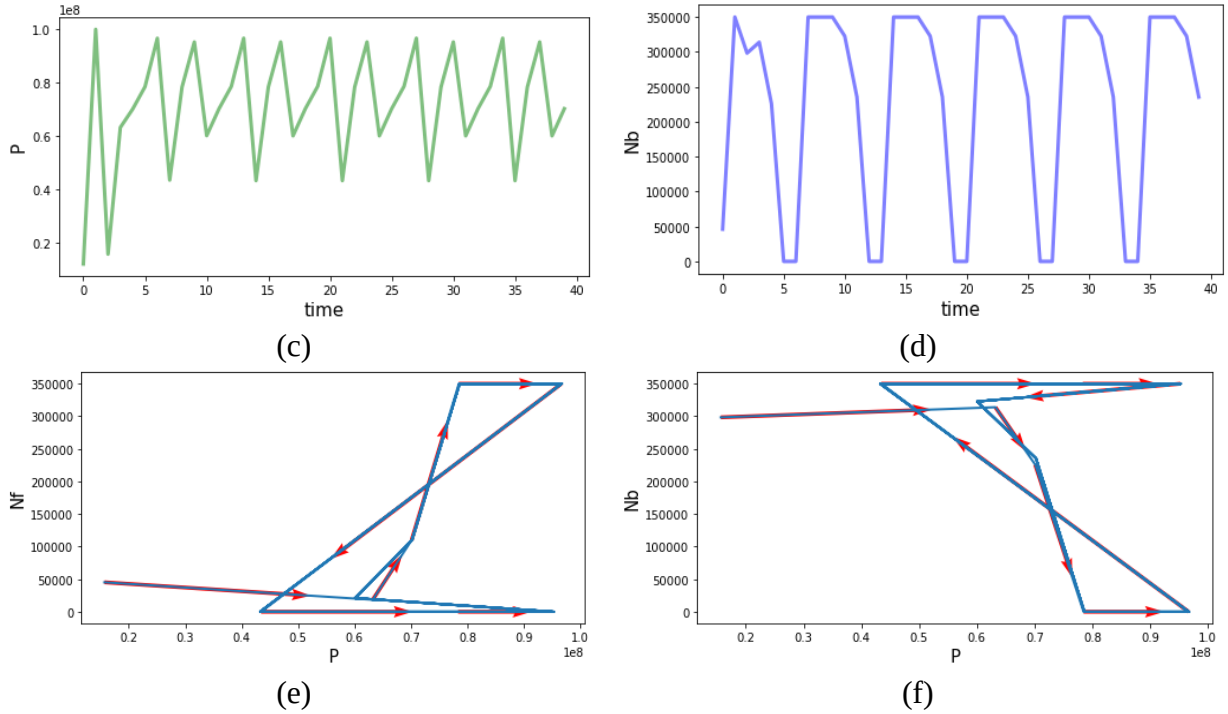

Figure 8.4 Bifurcation analysis results in monocyte subsystem. (a) Numerical equilibrium curve of pathogen related to parameter k_{pg}. (b) Numerical equilibrium curve of Nb related to parameter k_{pg}. (c) Oscillation behavior of pathogen when k_{pg} is equal to 0.65. (d) Oscillation behavior of Nb when k_{pg} is equal to 0.65. (e) Phase trajectory in P-Nf plane. (f) Phase trajectory in P-Nb plane.

According to the definition of bifurcation, Figure 8.4(a) and Figure 8.4(b) both show the changes in the number of equilibrium and the change in the numerical values of equilibrium when the parameter value is change. In Figure 8.4(a), we observe that more complicate bifurcation behavior of pathogen related to parameter k_{pg} is catch in the monocyte subsystem. There are several bifurcation points representing the change on the number of equilibria. In Figure 8.4(b), when $0 < k_{pg} < 0.1$, there is a bifurcation point leading to the change on the number of N_b equilibrium. Figure 8.4(c) and Figure 8.4(d) show the oscillation behaviors of pathogen and N_b when k_{pg} is equal to 0.65. Both pathogen and binded activated neutrophil diverge at unstable

equilibria in monocyte subsystem. These trends indicate that in this case the inflammation oscillation will keep happening if there is not any intervention or control measure to change the value of k_{pg}. Figure 8.4(e) and Figure 8.4(f) display the phase trajectories in pathogen-free activated neutrophil plane and pathogen-binded activated neutrophil plane, respectively. The arrow represents the direction of phase trajectory. The stable limit cycles are observed in these phase spaces. This also can reflect that pathogen, free activated neutrophil and binded activated neutrophil will not converge to a stable equilibrium as time approaches infinite when k_{pg} is equal to 0.65. Their values even repeatedly increase to high level, which will induce the persistent inflammatory.

8.4 Optimal Control and RNN-BO Optimization Algorithm

This section will develop the sepsis model into optimal control model and solve the optimal control strategy using a time-series optimization algorithm named RNN-BO algorithm we detailed proposed in [301]. In this paper, we will consider control strategy variables into sepsis model to represent the level/intensify of sepsis control or intervention treatment strategy. This paper only considers two types of control strategies under two different undesirable consequences in sepsis: one is the control strategy when the load of pathogen remains at high level, but the pro-inflammatory cytokines go down to low level in the early stage of inflammation, and the immune response can't work to the clearance of pathogen; another is the control strategy when the load of pathogen is low, but the inflammatory response is still active.

8.4.1 Control Strategy on Pathogen and Corresponding Optimal Control Model's Objective Function

Clinical studies show that appropriate antibiotics treatment is effective therapy when the load of pathogen remains at high level, which can effectively control the pathogen

replication/growth rate and decrease absolute mortality [255 - 257]. Thus, the pathogen growth rate is a controllable parameter. Our sepsis model parameter k_{pg} in Eq. (8.19) represents the pathogen growth rate (definition provided in **Appendix 3**). We will consider a t_f-dimensional control strategy variable $u_p = \{u_p(t_1), \dots, u_p(t_f)\}$ to represent the level/intensify of antibiotics treatment control. $u_p(t) \in [u_{pL}, u_{pU}]$ represents the control value at time t, u_{pL} and u_{pU} represent the lower bound and upper bound of antibiotics treatment control, respectively. The Eq. (8.19) will be developed as follows by incorporating the control strategy variable u_p:

$$\frac{dP}{dt} = \big(1 - u_p\big)k_{pg}P(1 - P^*) - r_{pmk}\frac{[P^n]}{[P^n + k_{c1}^n]}M_{kf}P^* - r_{pn}\frac{[P^n]}{[P^n + k_{c2}^n]}\big(N_f + N_b\big)P^*$$

$$-r_{pm}M_1 - r_{pcd4}\frac{[P^n]}{[P^n + k_{c6}^n]}T_{CD4}P^* - r_{pAb}\frac{[P^n]}{[P^n + k_{c5}^n]}AP^* \quad (8.39)$$

where $(1 - u_p)$ represents the decrease in pathogen growth rate due to the antibiotics treatment control strategy.

For the optimal control model, the next thing is to determine the objective function for the model. Some good biomarkers/components usually are used as the measure/objective function of immune response or development of sepsis [261]. During the immune response process, the level of pathogen can affect the outcomes of sepsis [302]. M1 macrophage contributes to pathogen clearance but will promote the inflammation as well, M2 macrophage contributes to the removal of apoptotic cells and inhibit inflammation as the same time [271]. M1 macrophage is defined as the up-regulation biomarker and M2 macrophage is the down-regulation biomarker of inflammatory [272]. The ratio of M1/M2 is used as a biomarker correlated with the tissue health status, inflammation associates with higher ratio of M1/M2 [303].

In addition, healthy adaptive immune system plays important role on the recovery of inflammation, CD4+ T cells and CD8+ T cells are two important T cells during adaptive immunity

process. CD4+ T cells accelerate the clearance of pathogen [292]. But CD8+ T cells are cytotoxic cells, their primary function is to kill the binded Kupffer cells, binded activated neutrophils, and binded activated monocytes, which will reduce the pathogen clearance ability of immune system [290, 293]. Therefore, the ratio of CD8+ T cell/CD4+ T cell is recognized a biomarker of the ability of adaptive immune system and disease severity, a high CD8+ T cell/CD4+ T cell is associated with increased morbidity and mortality [304, 305].

Therefore, we decide to use the ratio of M1/M2 and the ratio of CD8+ T cell/CD4+ T cell as the objective function when the load of pathogen is high in the early stage of inflammation, to measure the effectiveness of antibiotics treatment control strategy to the development of sepsis. The corresponding objective function is defined as:

$$\min_{u_p \in [u_{pL}, u_{pU}]^{t_f}} w_1 \frac{M1}{M2} + w_2 \frac{T_{CD8}}{T_{CD4}} \tag{8.40}$$

where w_1 and w_2 are constant parameters of weight.

8.4.2 Control Strategy on TNF-α and Corresponding Optimal Control Model's Objective Function

When the load of pathogen is low in the later stage of inflammation, the inflammation may still present due to the uncontrolled immune response, which will lead to persistent inflammation. If the immune system of host body is weak or uncontrolled, the activated neutrophil cells will still release the toxic chemical substance ROS after finishing pathogen clearance, which is harmful to host tissue and accelerate the death of apoptotic hepatocytes [254]. At the same time neutrophil cells will release TNF-α. When TNF-α detects the apoptotic hepatocytes, it will activate and recruit more neutrophil cells to migrate to the site of apoptotic cells. Since phagocytes will constantly attack the host's healthy cells even though there is no pathogen existing in the body, this is a vicious circle to induce persistent infection and eventually develop into server sepsis or

organ dysfunction. Some experimental studies show that anti-TNF-α therapy contributes to control the release rate of TNF- α for the above situation, effective anti-TNF-α therapy can improve the outcome of inflammation and save life [259, 260]. No doubt, the release rate of TNF-α is a controllable parameter. Our sepsis model parameter r_{t2max} in Eq. (8.22) represents the release rate of TNF-α by activated neutrophil (definition provided in **Appendix 3**). We will consider a t_f-dimensional control strategy variable $u_T = \{u_T(t_1), \dots, u_T(t_f)\}$ to represent the level/intensify of anti-TNF-α treatment control. $u_T(t) \in [u_{TL}, u_{TU}]$ represents the control value at time t, u_{TL} and u_{TU} represent the lower bound and upper bound of anti-TNF-α treatment control, respectively. The Eq. (8.22) will be developed as follows by incorporating the control strategy variable u_T:

$$\frac{dT}{dt} = \left(\frac{r_{t1max}M_{kb}}{m_{t1}+M_{kb}}\right)M_{kb} + \left(\frac{(1-u_T)r_{t2max}N_b}{m_{t2}+N_b}\right)N_b - u_t T \tag{8.41}$$

where $(1 - u_T)$ represents the decrease in release rate of TNF-α by activated neutrophil due to the anti-TNF-α treatment control strategy.

During the immune response process, the level of inflammatory cytokines both can affect the outcomes of sepsis [302]. TNF- α is a major pro-inflammatory cytokine and IL-10 is a crucial anti-inflammatory cytokine [293]. In many clinical practices, the ratio of TNF- α/IL-10 is used as a biomarker to monitor sepsis progression [266 - 268]. Therefore, we decide to use the ratio of TNF- α/IL-10 as the objective function when the immune response is still active in the later stage of inflammation, to measure the effectiveness of anti-TNF-α treatment control strategy to the development of sepsis. The corresponding objective function is defined as:

$$\min_{u_T \in [u_{TL}, u_{TU}]} {}^{t_f}\frac{T}{C_A} \tag{8.42}$$

8.4.3 RNN-BO Optimization Algorithm

One of our purposes is not only to solve the optimal control that minimizes the objective function value, but also to quickly provide the optimal control strategy when the parameter values or system state variable values are changed. Since the initial system value setting (initial value of sepsis system parameters and system state variables) are associated with the initial conditions of patients, different initial system value settings may lead to different outcomes, and may have different corresponding optimal control strategies. That will waste a lot of time to generate an optimal control strategy if use the optimization algorithm to solve the optimal control model each time for every new given initial values. We know that successful sepsis treatments involve not only optimal dosing of control treatment strategy, but the timing of control therapy is also important [252]. Therefore, an efficient optimization algorithm is key to quickly generate an optimal control strategy, which can reduce the mortality of sepsis and improve patients' quality of care.

The optimization algorithm we use in this paper is named RNN-BO optimization algorithm. The RNN-BO algorithm is a time-series optimization algorithm detailed proposed in our previous paper [301], which combines RNN and an improved BO algorithm. Herein, we briefly introduce the RNN-BO algorithm. The main idea of the RNN-BO algorithm is to use an improved BO algorithm to solve different corresponding low-dimensional optimal control strategies by varying the initial parameter values or system state variable values. Low-dimensional control strategy in here means that the dimension of control strategy what we aim to solve is d ($d < t_f$) rather than full dimension t_f during this process. The improved BO algorithm is different from the standard BO algorithm. The standard BO algorithm is detailed introduced in [190]. This improved BO algorithm samples the optimal control candidates by combining multi-armed bandit [242] and

random search algorithm [306]. Then pick the best solution that minimizes the acquisition function. Acquisition function we used in our RNN-BO algorithm is an approximation function of objective function using lower confidence bound function (LCB) [190]. After the optimization of acquisition function, to increase the solution's accuracy, RNN-BO algorithm does a local search to further optimize this optimal control strategy, which is different from the standard BO algorithm.

For each initial system value setting, we can generate $(t_f - d + 1)$ d-dimensional control strategies by using the improved BO algorithm. Since we solve the first d-dimensional optimal control strategy starts from time 1 to time d, the system state variables values over this time period ($t \in [1, d]$) can be calculated based on this first d-dimensional optimal control strategy. Then use these system state variables values at time 2 as the initial values, we solve the second d-dimensional optimal control strategy starts from time 2 to time $d + 1$, the system state variables values over this time period ($t \in [2, d + 1]$) can be calculated based on this second d-dimensional optimal control strategy, and so on. If we change the initial parameter value or initial system state variables value, we can generate another $(t_f - d + 1)$ d-dimensional control strategies. All these optimal control strategies are time-series. Store all data pairs (consisting of initial system value settings and corresponding optimal strategies) for further use. For example, if we vary the initial system value setting for n times, then the total number of data pairs we can obtain is $n * (t_f - d + 1)$.

Next, design system value setting as input data and the corresponding optimal control strategy as output. Then use the RNN algorithm to learn those data pairs and generate a model named RNN-BO predictive model. Once provide any initial system value setting, the RNN-BO predictive model can quickly and effectively predict a corresponding t_f-dimensional time-series

optimal control strategy. The implementation flowchart of the RNN-BO optimization algorithm is shown in Figure 8.5.

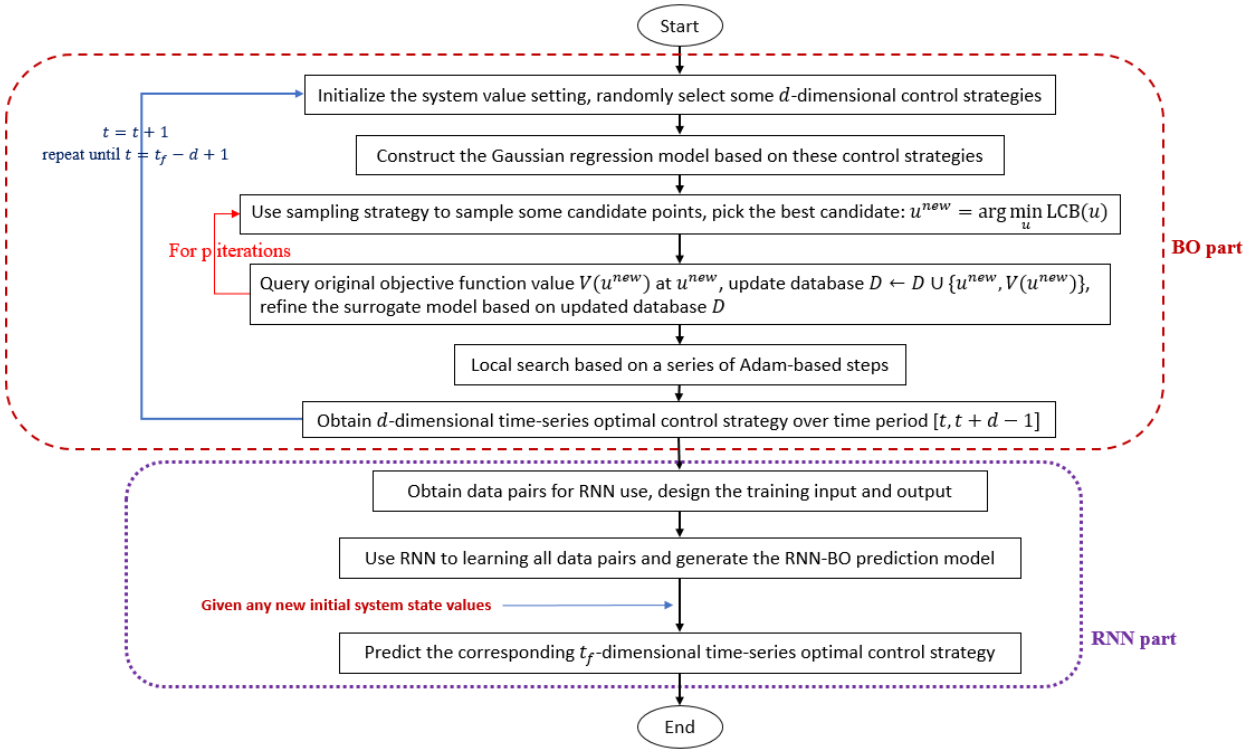

Figure 8.5 Implementation flowchart of the RNN-BO optimization algorithm

8.5 Numerical simulation

In this section, we implement numerical simulation tests to solve the optimal control strategy for the sepsis optimal control system in Eqns. (8.19)-(8.38) using the RNN-BO algorithm. There are two inflammatory situations that can be controlled as we discussed in Section 8.4.1 and 8.4.2: one is when the load of pathogen remains at high level, but the pro-inflammatory cytokines go down to low level in the early stage of inflammation, and the immune response can't work to the clearance of pathogen; two is when the load of pathogen is low, but the immune response is still active. To better demonstrate the effectiveness and efficiency of the RNN-BO algorithm to solve the optimal control strategy on this complex sepsis system, we compare it with the situation

without any control, and other two BO algorithms (the standard BO algorithm and a high-dimensional DR-DF BO algorithm proposed in [240])

8.5.1 Numerical Results When the Optimal Control Strategy is on Pathogen

For the first inflammatory situation, the load of pathogen remains in high level over time, the host's immune system isn't capable to the clearance of pathogen and the pro-inflammatory cytokines go down sooner. In this situation, antibiotics treatment is the effective therapy to control the pathogen replication/growth rate [255 - 257]. The first situation can be shown as Figure 8.6(a). TNF- α is an important pro-inflammatory cytokine during immune response process. We can see that when the pathogen goes up in the early stage of inflammation, but TNF- α sharply goes down, it means that the macrophages that are responsible to the clearance of pathogen couldn't be recruited and activated. In this case, the load of pathogen will remain in high level, this may lead to the death due to pathogen infection.

When the control strategy is antibiotics treatment control strategy, the objective function is to minimize the sum of ratio of M1/M2 and the ratio of CD8+ T cell/CD4+ T cell. Higher ratio is associated with severe inflammation. The simulation results are shown in Figure 8.6. The running time of the standard BO algorithm to generate the optimal control strategy is about 45 seconds. The running time of the DR-DF BO algorithm is about 25 seconds. But the RNN-BO algorithm is different from other two algorithms, it learns the historical data. Once the RNN-BO predictive model is ready, the RNN-BO algorithm only takes about 2 seconds to predict the optimal control strategy by giving the same initial system values as the other two BO algorithms.

Figure 8.6(b) shows the control strategies from three algorithms. The optimal control strategy of standard BO algorithm performs obvious fluctuation over time. The optimal control strategy of DR-DF BO algorithm is more stable. The optimal control predicted from RNN-BO

algorithm is lower at the early stage of inflammation, then become high level at the later stage of inflammation when it recognizes the load of pathogen is still in high level. According to the trends of the optimal control strategies, the optimal control strategy predicted by RNN-BO algorithm may be more reasonable.

Figure 8.6(c) shows the comparison on ratio of CD8+ T cell/CD4+ T cell over time. We can see that the ratio when the system is without control is significantly higher than the ration when the system is with control. From the smaller figure in Figure 8.6(c), after applying the optimal control strategies generated by the standard BO algorithm, DR-DF BO algorithm, and RNN-BO algorithm, the ratios of CD8+ T cell/CD4+ T cell perform the same trends. That means those three algorithms reach similar optimization performances on this ratio for our sepsis optimal control system, they all have effective impact on controlling the inflammation. Figure 8.6(c) shows the comparison on ratio of M1/M2 over time. We can see that the ratio when the system is without control is also significantly higher than the ration when the system is with control. The ratio without control will gradually increase up to 40,000. From the smaller figure in Figure 8.6(d), the ratios with control are effectively controlled at low level. The DR-DF BO algorithm and RNN-BO algorithm have similar great performance, both slightly outperform the standard BO algorithm on the ratio of M1/M2. Figure 8.6(e) shows the accumulated objective function values over time of different methods. Since the objective function is the sum of ratio of CD8+ T cell/CD4+ T cell and ratio of M1/M2, the trends of accumulated objective function value are like the trends of the ratios.

According to Figure 8.6, taking antibiotics treatment control is necessary to control the progression of inflammation when the load of pathogen is high in the early stage of inflammation. Overall, the optimal control predicted by the RNN-BO algorithm is slightly better than the standard BO algorithm and DR-DF BO algorithm with only 2 seconds running time.

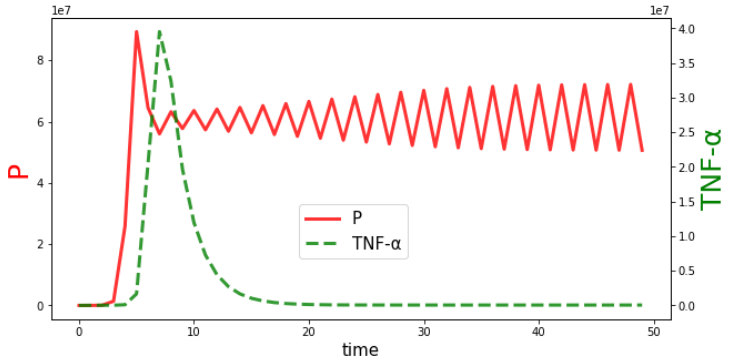

(a)

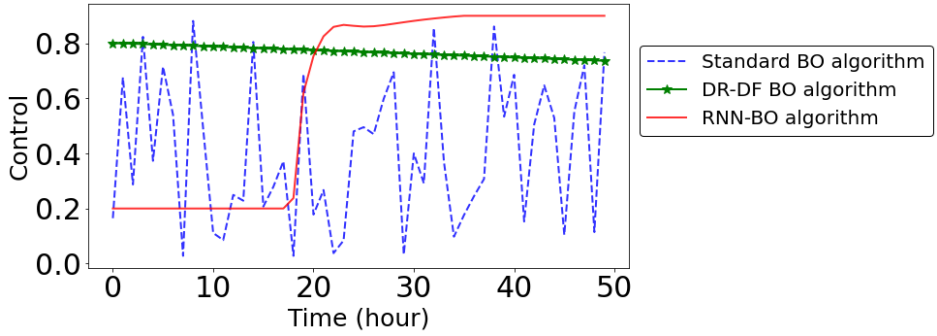

(b)

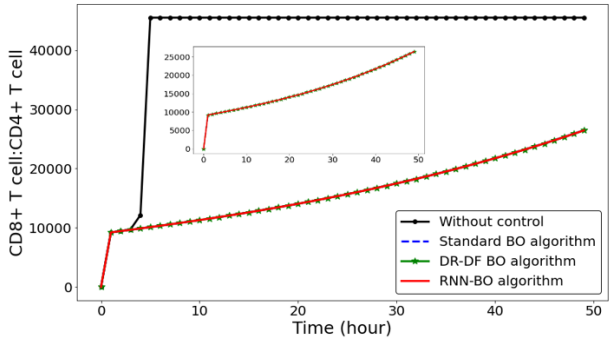

(c)

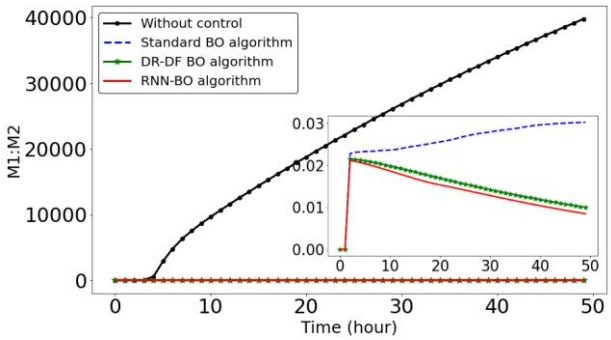

(d)

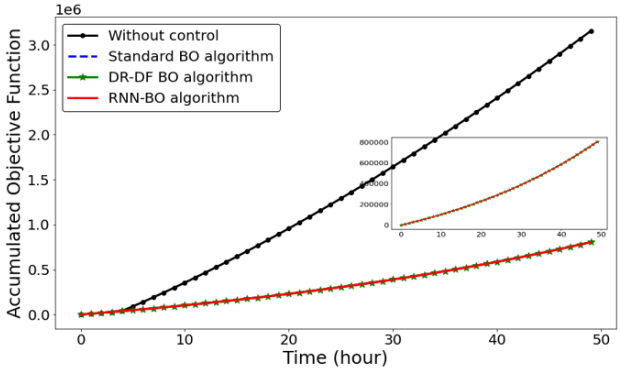

(e)

Figure 8.6 Simulation results for the first inflammatory situation. (a) Trends of Pathogen and TNF-α. (b) Optimal control strategies of different optimization algorithms. (c) Ratio of

$\frac{T_{CD8}}{T_{CD4}}$ comparison by different algorithms. (d) Ratio of $\frac{M1}{M2}$ comparison by different algorithms. (e) Accumulated objective function values over time of different algorithms.

8.5.2 Numerical Results When the Optimal Control Strategy is on TNF-α

For the second inflammatory situation, the immune response is still active when the load of pathogen is low. This means that macrophages constantly attack the host's healthy cells after they finish the clearance of pathogen. In this situation, the host will perform persistent inflammation and tend to develop into organ dysfunction. From previous clinic practices, anti-TNF-α therapy is an effective control treatment to the second situation [259, 260]. The second situation can be shown as Figure 8.7(a). We can see that the load of pathogen grows up quickly in the early stage of inflammation, the immune response is activated. After the load of pro-inflammatory cytokine TNF- α increases, the pathogen starts to go down until all pathogens are cleared. However, after all pathogens are cleared, the load of TNF- α remains in a high level. The immune response keeps active even there is no pathogen in the host's body. This case may lead to the death due to persistent inflammation.

When the control strategy is anti-TNF-α treatment control strategy, the objective function is to minimize the ratio of TNF- α/IL-10. The simulation result is shown in Figure 8.7. Higher ratio is associated with severe inflammation. The running times of different algorithms in this section are similar as they performed in Section 8.5.1.

Figure 8.7(b) shows the control strategies from three algorithms. The optimal control strategy of standard BO algorithm performs obvious fluctuation over time. The optimal control strategy of DR-DF BO algorithm is more stable. The optimal control predicted from RNN-BO algorithm is lower at the early stage of inflammation, then sharply increase to a high level when it

recognizes the load of TNF- α keeps increasing even the pathogen has already started to decrease. According to the trends of the optimal control strategies, the optimal control strategy predicted by RNN-BO algorithm may be more reasonable.

Figure 8.7(c) shows the comparison on ratio of TNF- α/IL-10 over time. We can see that the ratio when the system is without control is significantly higher than the ration when the system is with control. The ratio without control will gradually increase up to 2.5×10^9. From the smaller figure in Figure 8.7(c), the ratios with control are effectively controlled, the highest ratios with control are about 10^3 times lower than the highest ratio of without control. The RNN-BO algorithm outperforms the standard BO algorithm and the DR-DF BO algorithm. Figure 8.7(d) shows the accumulated objective function values over time of different methods. Since the objective function in the second inflammatory situation is the ratio of M1/M2, the trend of accumulated objective function value performs like the trends of the ratio.

According to Figure 8.7, taking anti-TNF-α treatment control is necessary to control the progression of inflammation when the load of pathogen is low, but the immune response is still active in the later stage of inflammation. Overall, the optimal control generated by the RNN-BO algorithm is better than the standard BO algorithm and DR-DF BO algorithm.

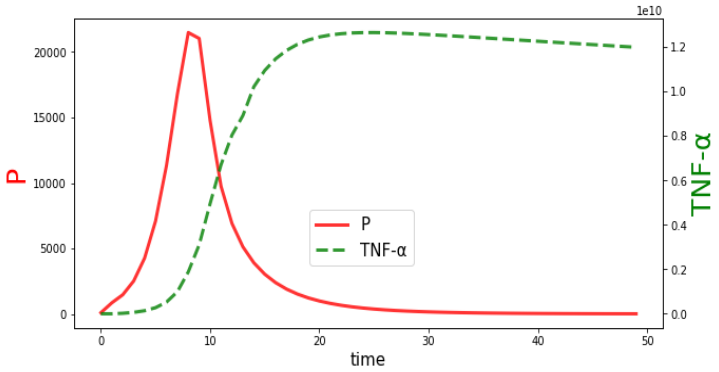

(a)

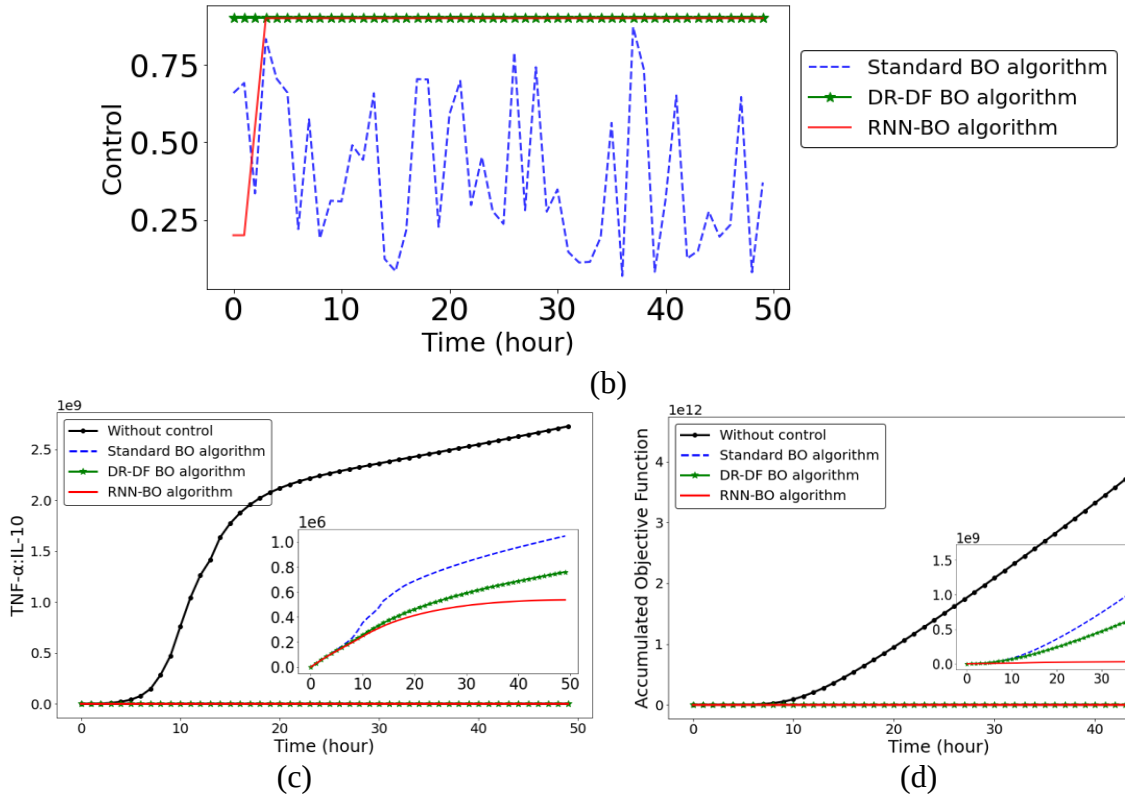

Figure 8.7 Simulation results for the second inflammatory situation. (a) Trends of Pathogen and TNF- α. (b) Optimal control strategies of different optimization algorithms. (c) Ratio of $\frac{T}{C_A}$ comparison by different algorithms. (d) Accumulated objective function values over time of different algorithms.

8.6 Conclusion and Future Work

This paper improves a complex nonlinear sepsis model on the monocyte part and adaptive immunity part, which more accurately study the progression of the delicate immune response system. The bifurcation analysis of our sepsis subsystem presents the model behaviors under some system parameters, but also shows the necessary of control treatment and intervention therapy for the sepsis development. If the sepsis system is without considering any control treatment under some parameter and initial system value settings, the system will perform persistent inflammation outcomes (harmful infection oscillation outcomes) as time goes by. Thus, this paper develops the

improved nonlinear sepsis model into an optimal control system. According to some existing clinic practices, this paper determines to apply some authorized and recommended sepsis biomarkers as our objective functions of studied sepsis optimal control system to measure the sepsis progression. Next, an RNN-BO optimization algorithm is introduced to predict the optimal control strategy. The most advantage of RNN-BO algorithm is that it learns the historical optimal control strategies and generates a predictive model. Once there is a new sepsis patient with different initial condition (is associated with initial system value setting), the RNN-BO algorithm is capable to predict the corresponding optimal control strategy for this patient in short time. Some comparison simulation experiments with other optimization algorithms are carried out. Simulation results demonstrate the effectiveness and efficiency of the RNN-BO algorithm on driving the optimal control solution for a complex nonlinear sepsis optimal control system. As the healthcare field develops, the mathematical study and optimal control research of sepsis will continue to grow. To better express sepsis via mathematical model, and propose more effective optimization algorithm for providing the optimal control strategy to improve quality of clinic therapy or reduce the mortality of sepsis, are both our further research directions.

Chapter 9 - Conclusion, Contribution and Future Works

9.1 Conclusions

As one meaningful and necessary topic in healthcare, the optimal control strategy of disease plays a crucial role in controlling the transmission or progression of the disease, reducing human mortality, and saving lives. This dissertation introduces the mathematical modeling of disease based on the optimal control strategy theory. The diseases studied in this dissertation are mainly divided into two types: epidemic disease and sepsis (a severe infectious disease). In this dissertation, nonlinear complex deterministic, stochastic, convex, possible non-convex, time-series, and high-dimensional disease optimal control systems, are studied to address the importance and impact of the optimal control strategy on controlling the development of diseases. Several practical and effective optimization algorithms are proposed to solve the optimal control strategy for disease optimal control systems. Analytical and numerical simulations are carried out to help us better understand the model behavior, the effectiveness and necessity of the optimal control strategy, and demonstrate the effectiveness and efficiency of the proposed optimization algorithms.

The main conclusions drawn from this dissertation are:

1. This dissertation synthesizes local and global contact networks and perceptual and rational information to mathematically explain how the information related to epidemic cause human fear and lead to human behaviors of choosing control strategy. This dissertation finds four necessary conditions of the epidemic disease model through the stability analysis.
2. The traditional optimal control strategy is researched in the disease system without considering uncertain error. However, medical measurement errors or system

uncertainty potentially exist in the real world. The traditional optimal control may be no longer optimal and effective in this situation. To improve the quality of care and increase the survival possibility of patients, it is necessary to study these errors so that we can make the optimal control strategy more accurate and effective for the disease model.

3. For the severe infectious disease named 'sepsis', the activated monocytes will develop into monocyte-derived type 1 macrophage (M1 macrophage) when they encounter pathogens, TNF-α, or GM-CSF, or develop into monocyte-type 2 macrophage (M2 macrophage) when they meet apoptotic T cells, IL-10, or TGF-β. CD4+ T cells play an important role in clearing pathogens. CD8+ T cells can kill the binded Kupffer cells, binded activated neutrophils, and binded activated monocytes due to the cytotoxic property.
4. For the severe infectious disease 'sepsis', the pathogen growth rate k_{pg} and the release rate of TNF-α by neutrophils r_{t2max} are two important controllable parameters. When the load of pathogen remains at a high level, but the pro-inflammatory cytokines go down to a low level in the early stage of inflammation, antibiotics treatment is an effective control strategy to control the pathogen growth rate k_{pg}. When the load of the pathogen is low, but the immune response is still active, anti-TNF-α therapy is an effective control strategy to control the release rate of TNF-α by neutrophils r_{t2max}.
5. For epidemic diseases, the cost of control strategy could be affected by various factors like inpatient days, cost of treatment equipment, wages, logistics, and infrastructure. Therefore, the cost function associated with the control strategy may be possible non-

convex. The possible non-convex objective function can make the optimal control strategy more meaningful and practical.

6. When considering the non-convex objective function in the epidemic disease optimal control model, this dissertation finds that the conventional optimization algorithms and the standard Bayesian Optimization algorithm are not effective and computationally efficient enough to solve the optimal control strategy.
7. Besides the possible non-convex, the studied disease systems in this dissertation are time-series and high-dimensional. Through some simulation comparison experiments, this dissertation finds that the existing conventional optimization algorithms, standard Bayesian Optimization algorithm, and some existing high-dimensional Bayesian Optimization algorithms are not effort-effective and computationally efficient to solve the optimal control strategy for the complex time-series and high-dimensional systems.
8. The initial system value setting of the disease system, such as system state value and system parameter values, is associated with disease regions, virus type, infection rate, etc. Through numerical simulation experiments, this dissertation finds that the optimal control strategies generated for some specific initial system settings are no longer optimal for the system with new different initial system settings. Also, to develop the corresponding optimal control strategy for the new system setting, the existing optimization algorithms need to be implemented again, which isn't effort-effective and time-efficient enough. Therefore, developing an optimization algorithm capable of accurately and efficiently predicting the optimal control strategy for the new system setting is meaningful to realize control effectiveness and computational efficacy.

9.2 Contributions

Major contributions of this dissertation to the area of mathematical modeling of disease systems, optimal disease control, and the optimization algorithms of solving the optimal control strategy for complex systems are listed as follows:

1. This dissertation first mathematically models how human fear influences their control behavior during the epidemic (IFF model). It also solves the optimal control strategy that controls the spread of the epidemic and minimizes the financial cost associated with the control strategy for this nonlinear epidemic disease optimal control model.
2. This dissertation improves an existing sepsis model by reconstructing the monocyte subsystem and adaptive immune subsystem and developing it into a complex nonlinear sepsis optimal control model. Compared to the original mathematical model, the improved sepsis optimal control model provides a more accurate expression of some critical system state variables. Also uses three important biomarkers recognized by existing sepsis literatures as objective functions and makes significant performances on these three biomarkers after control.
3. Compared to the existing disease control models, this dissertation develops a stochastic disease optimal control model to study the dynamics of disease systems with medical measurement error or system error. It also proposes an optimization algorithm combining the traditional optimal control and machine learning algorithm (EBOC algorithm). This proposed algorithm can learn the error from the historical system data and accurately and effectively solve the optimal control strategy for further disease systems with errors.

4. Compared to the existing epidemic disease control models, this dissertation considers possible non-convex objective function, which is more accurate and meaningful to express the practical cost function associated with the control strategy. Moreover, this dissertation proposes an improved Bayesian Optimization algorithm (IBO algorithm) to effectively and efficiently solve the corresponding optimal control solution.
5. Compared to the existing optimization algorithms, this dissertation proposes a more effective and computational efficient high-dimensional Bayesian Optimization algorithm by combining dimension reduction and different dimension fill-in strategies (DR-DF BO algorithm). This new novel algorithm can effectively and efficiently solving the optimal control strategy for complex nonlinear time-series and high-dimensional disease control systems.
6. Compared to the existing optimization algorithms, this dissertation proposes a novel Bayesian Optimization algorithm by combining Recurrent Neural Network (RNN-BO algorithm). This RNN-BO algorithm can learn the historical optimal control data and system data to quickly and accurately predict the optimal control strategy for further epidemic or sepsis diseases. For the system with a new initial value setting, the RNN-BO algorithm doesn't need to implement the optimization process again to provide the optimal control solution as other optimization algorithms do, which is highly accurate, effort-effective, and computationally efficient.

9.3 Future Works

Major future works to the area of disease mathematical modeling, disease optimal control, and optimization algorithms are listed as follows:

1. In this dissertation, the optimal control discussed in the disease models is theoretical. The future work will combine the actual disease data to mathematically construct the disease control models to better reflect the reality.
2. In this dissertation, the optimal control discussed in the diseases models is a single variable. Future work will attempt to simultaneously design multi-control variables to describe different control strategies, which may be more accurate in expressing the decision-making situation in the real world.
3. This dissertation proposed a new Bayesian Optimization algorithm by combining RNN, which is demonstrated the effectiveness and efficiency. Thus, the optimization algorithm may have better prediction and optimization performance by combining machine learning algorithms. Future work attempts to develop more effective and efficient Bayesian Optimization algorithms by combining different machine learning algorithms, such as Convolutional Neural Network (CNN), or mix CNN and RNN, etc. In this case, the proposed algorithms can solve more complex systems.
4. The models studied in this dissertation focus on disease models (healthcare field). Future work can apply the proposed optimization algorithms to other different areas and see if the proposed methodologies are still effective for other models with different structure.

Reference

1. Omachonu, V.K. and Einspruch, N.G., 2007. Systems engineering in the healthcare service industry. *International journal of healthcare technology and management*, *8*(1-2), pp.161-172.
2. Gregor, M., Grznár, P., Pedan, M. and Cudráková, M., 2016. Knowledge in healthcare. In *Annals of DAAAM. Proceedings of the 26-th DAAAM International symposium on intelligent manufacturing and automation. ISSN* (pp. 1726-9679).
3. Breslow, L., 1999. From disease prevention to health promotion. *Jama*, *281*(11), pp.1030-1033.
4. Ioannidis, J.P. and Lau, J., 2001. Evidence on interventions to reduce medical errors. *Journal of general internal medicine*, *16*(5), pp.325-334.
5. Sommerfeld, J., Ramsay, A., Pagnoni, F., Terry, R.F., Guth, J.A. and Reeder, J.C., 2015. Applied research for better disease prevention and control. *PLoS neglected tropical diseases*, *9*(1), p.e3378.
6. Anderson, R.M. and Garnett, G.P., 2000. Mathematical models of the transmission and control of sexually transmitted diseases. *Sexually transmitted diseases*, *27*(10), pp.636-643.
7. Angstmann, C.N., Henry, B.I. and McGann, A.V., 2016. A fractional order recovery SIR model from a stochastic process. *Bulletin of mathematical biology*, *78*(3), pp.468-499.
8. El-Saka, H.A.A., 2014. The fractional-order SIS epidemic model with variable population size. *Journal of the Egyptian Mathematical Society*, *22*(1), pp.50-54.
9. Özalp, N. and Demirci, E., 2011. A fractional order SEIR model with vertical transmission. *Mathematical and Computer Modelling*, *54*(1-2), pp.1-6.
10. Almeida, R., 2018. Analysis of a fractional SEIR model with treatment. *Applied Mathematics Letters*, *84*, pp.56-62.
11. Hossain, M.T., Miah, M.M. and Hossain, M.B., 2017. Numerical study of kermack-mckendrik SIR model to predict the outbreak of ebola virus diseases using euler and fourth order runge-kutta methods. *American Academic Scientific Research Journal for Engineering, Technology, and Sciences*, *37*(1), pp.1-21.
12. Eikenberry, S.E. and Gumel, A.B., 2018. Mathematical modeling of climate change and malaria transmission dynamics: a historical review. *Journal of mathematical biology*, *77*(4), pp.857-933.
13. Allen, L.J.S., Brown, V.L., Jonsson, C.B., Klein, S.L., Laverty, S.M., Magwedere, K., Owen, J.C. and Van Den Driessche, P., 2012. Mathematical modeling of viral zoonoses in wildlife. *Natural resource modeling*, *25*(1), pp.5-51.
14. Leonenko, V.N. and Ivanov, S.V., 2018. Prediction of influenza peaks in Russian cities: Comparing the accuracy of two SEIR models. *Mathematical Biosciences & Engineering*, *15*(1), p.209.
15. Oliveira, J.F., Jorge, D.C., Veiga, R.V., Rodrigues, M.S., Torquato, M.F., da Silva, N.B., Fiaccone, R.L., Cardim, L.L., Pereira, F.A., de Castro, C.P. and Paiva, A.S., 2021. Mathematical modeling of COVID-19 in 14.8 million individuals in Bahia, Brazil. *Nature communications*, *12*(1), pp.1-13.

16. Ivorra, B., Ferrández, M.R., Vela-Pérez, M. and Ramos, A.M., 2020. Mathematical modeling of the spread of the coronavirus disease 2019 (COVID-19) taking into account the undetected infections. The case of China. *Communications in nonlinear science and numerical simulation*, *88*, p.105303.
17. Anirudh, A.J.I.D.M., 2020. Mathematical modeling and the transmission dynamics in predicting the Covid-19-What next in combating the pandemic. *Infectious Disease Modelling*, *5*, pp.366-374.
18. Ganiny, S. and Nisar, O., 2021. Mathematical modeling and a month ahead forecast of the coronavirus disease 2019 (COVID-19) pandemic: an Indian scenario. *Modeling earth systems and environment*, *7*(1), pp.29-40.
19. Simsir, A., Kismali, E., Mammadov, R., Gunaydin, G. and Cal, C., 2010. Is it possible to predict sepsis, the most serious complication in prostate biopsy?. *Urologia internationalis*, *84*(4), pp.395-399.
20. Parrillo, J.E., Parker, M.M., Natanson, C., Suffredini, A.F., Danner, R.L., Cunnion, R.E. and Ognibene, F.P., 1990. Septic shock in humans: advances in the understanding of pathogenesis, cardiovascular dysfunction, and therapy. *Annals of internal medicine*, *113*(3), pp.227-242.
21. Yamanaka, Y., Uchida, K., Akashi, M., Watanabe, Y., Yaguchi, A., Shimamoto, S., Shimoda, S., Yamada, H., Yamashita, M. and Kimura, H., 2019. Mathematical modeling of septic shock based on clinical data. *Theoretical Biology and Medical Modelling*, *16*(1), pp.1-22.
22. McDaniel, M., Keller, J.M., White, S. and Baird, A., 2019. A whole-body mathematical model of Sepsis progression and treatment designed in the BioGears physiology engine. *Frontiers in physiology*, *10*, p.1321.
23. Zuev, S.M., Kingsmore, S.F. and Gessler, D.D., 2006. Sepsis progression and outcome: a dynamical model. *Theoretical Biology and Medical Modelling*, *3*(1), pp.1-15.
24. Wu, C.H.J., Shi, Z., Ben-Arieh, D. and Simpson, S.Q., 2016. Mathematical modeling of innate immunity responses of sepsis: modeling and computational studies. *Healthcare Analytics: From Data to Knowledge to Healthcare Improvement. Hoboken, NJ: John Wiley & Sons, Inc*, pp.221-59.
25. Joshi, H.R., Lenhart, S., Li, M.Y. and Wang, L., 2006. Optimal control methods applied to disease models. *Contemporary Mathematics*, *410*, pp.187-208.
26. Bussell, E.H., Dangerfield, C.E., Gilligan, C.A. and Cunniffe, N.J., 2019. Applying optimal control theory to complex epidemiological models to inform real-world disease management. *Philosophical Transactions of the Royal Society B*, *374*(1776), p.20180284.
27. Fish, D.N., 2002. Optimal antimicrobial therapy for sepsis. *American journal of health-system pharmacy*, *59*(suppl_1), pp.S13-S19.
28. Khouzani, M.H.R., Sarkar, S. and Altman, E., 2011, April. Optimal control of epidemic evolution. In 2011 Proceedings IEEE INFOCOM (pp. 1683-1691). IEEE.
29. Di Giamberardino, P. and Iacoviello, D., 2017. Optimal control of SIR epidemic model with state dependent switching cost index. Biomedical signal processing and control, 31, pp.377-380.
30. Berhe, H.W., Makinde, O.D. and Theuri, D.M., 2018. Optimal control and cost-effectiveness analysis for dysentery epidemic model. Applied Mathematics & Information Sciences, 12(6), pp.1183-1195.

31. Gubar, E. and Zhu, Q., 2013, July. Optimal control of influenza epidemic model with virus mutations. In 2013 European Control Conference (ECC) (pp. 3125-3130). IEEE.
32. Reluga, T.C., 2010. Game theory of social distancing in response to an epidemic. *PLoS computational biology*, *6*(5), p.e1000793.
33. Modares, H. and Sistani, M.B.N., 2011. Solving nonlinear optimal control problems using a hybrid IPSO–SQP algorithm. *Engineering Applications of Artificial Intelligence*, *24*(3), pp.476-484.
34. Friesz, T.L., 2010. Nonlinear programming and discrete-time optimal control. In *Dynamic optimization and differential games* (pp. 33-78). Springer, Boston, MA.
35. Linder, A., Åkesson, P., Inghammar, M., Treutiger, C.J., Linnér, A. and Sundén-Cullberg, J., 2012. Elevated plasma levels of heparin-binding protein in intensive care unit patients with severe sepsis and septic shock. *Critical care*, *16*(3), pp.1-11.
36. Masino, A.J., Harris, M.C., Forsyth, D., Ostapenko, S., Srinivasan, L., Bonafide, C.P., Balamuth, F., Schmatz, M. and Grundmeier, R.W., 2019. Machine learning models for early sepsis recognition in the neonatal intensive care unit using readily available electronic health record data. *PloS one*, *14*(2), p.e0212665.
37. Schuetz, P., Maurer, P., Punjabi, V., Desai, A., Amin, D.N. and Gluck, E., 2013. Procalcitonin decrease over 72 hours in US critical care units predicts fatal outcome in sepsis patients. *Critical Care*, *17*(3), pp.1-8.
38. Joshi, H.R., Lenhart, S., Li, M.Y. and Wang, L., 2006. Optimal control methods applied to disease models. *Contemporary Mathematics*, *410*, pp.187-208.
39. Tauchnitz, N., 2015. The Pontryagin maximum principle for nonlinear optimal control problems with infinite horizon. *Journal of Optimization Theory and Applications*, *167*(1), pp.27-48.
40. Misra, A.K., Sharma, A. and Shukla, J.B., 2015. Stability analysis and optimal control of an epidemic model with awareness programs by media. *Biosystems*, *138*, pp.53-62.
41. Aldila, D., Padma, H., Khotimah, K., Desjwiandra, B. and Tasman, H., 2018. Analyzing the MERS disease control strategy through an optimal control problem. *International Journal of Applied Mathematics and Computer Science*, *28*(1).
42. Laubenbacher, R., Hinkelmann, F. and Oremland, M., 2013. Agent-based models and optimal control in biology: a discrete approach. *Mathematical concepts and methods in modern biology*, pp.143-178.
43. Ali, M.M. and Kaelo, P., 2008. Improved particle swarm algorithms for global optimization. Applied mathematics and computation, 196(2), pp.578-593.
44. Mahmoodabadi, M.J. and Nemati, A.R., 2016. A novel adaptive genetic algorithm for global optimization of mathematical test functions and real-world problems. Engineering Science and Technology, an International Journal, 19(4), pp.2002-2021.
45. Kirkpatrick, S., Gelatt, C.D. and Vecchi, M.P., 1983. Optimization by simulated annealing. science, 220(4598), pp.671-680.
46. Mutný, M. and Krause, A., 2019. Efficient high dimensional bayesian optimization with additivity and quadrature fourier features. Advances in Neural Information Processing Systems 31, pp.9005-9016.

47. Moriconi, R., Deisenroth, M.P. and Kumar, K.S., 2020. High-dimensional Bayesian optimization using low-dimensional feature spaces. Machine Learning, 109(9), pp.1925-1943.
48. Zhang, M., Li, H. and Su, S., 2019. High dimensional bayesian optimization via supervised dimension reduction. arXiv preprint arXiv:1907.08953.
49. Li, C., Gupta, S., Rana, S., Nguyen, V., Venkatesh, S. and Shilton, A., 2018. High dimensional bayesian optimization using dropout. arXiv preprint arXiv:1802.05400.
50. Rana, S., Li, C., Gupta, S., Nguyen, V. and Venkatesh, S., 2017, July. High dimensional Bayesian optimization with elastic Gaussian process. In International conference on machine learning (pp. 2883-2891). PMLR.
51. Albuquerque, M.F.P.M. and Morais, H.M., 1997. Decentralization of endemic disease control: an intervention model for combating bancroftian filariasis. *Revista Panamericana de Salud Pública*, *1*, pp.155-163.
52. Mandal, S., Bhatnagar, T., Arinaminpathy, N., Agarwal, A., Chowdhury, A., Murhekar, M., Gangakhedkar, R.R. and Sarkar, S., 2020. Prudent public health intervention strategies to control the coronavirus disease 2019 transmission in India: A mathematical model-based approach. *The Indian journal of medical research*, *151*(2-3), p.190.
53. Neilan, R.M. and Lenhart, S., 2010. An Introduction to Optimal Control with an Application in Disease Modeling. In *Modeling Paradigms and Analysis of Disease Trasmission Models* (pp. 67-81).
54. Modares, H. and Sistani, M.B.N., 2011. Solving nonlinear optimal control problems using a hybrid IPSO–SQP algorithm. *Engineering Applications of Artificial Intelligence*, *24*(3), pp.476-484.
55. Friesz, T.L., 2010. Nonlinear programming and discrete-time optimal control. In *Dynamic optimization and differential games* (pp. 33-78). Springer, Boston, MA.
56. Hontelez, J.A., De Vlas, S.J., Tanser, F., Bakker, R., Bärnighausen, T., Newell, M.L., Baltussen, R. and Lurie, M.N., 2011. The impact of the new WHO antiretroviral treatment guidelines on HIV epidemic dynamics and cost in South Africa. *PloS one*, *6*(7), p.e21919.
57. Chen, Y., Bi, K., Zhao, S., Ben-Arieh, D. and Wu, C.H.J., 2017. Modeling individual fear factor with optimal control in a disease-dynamic system. *Chaos, Solitons & Fractals*, *104*, pp.531-545.
58. Chen, Y., Bi, K., Wu, C.H.J. and Ben-Arieh, D., 2019. A new evidence-based optimal control in healthcare delivery: a better clinical treatment management for septic patients. *Computers & Industrial Engineering*, *137*, p.106010.
59. Funk, Sebastian, Marcel Salathé, and Vincent AA Jansen. "Modelling the influence of human behaviour on the spread of infectious diseases: a review." *Journal of the Royal Society Interface* (2010): rsif20100142.
60. Polgar, S., 1962. Health and human behavior: areas of interest common to the social and medical sciences. *Current Anthropology*, 3(2), pp.159-205.
61. Morse, Stephen S. "Factors in the emergence of infectious diseases." *Plagues and Politics*. Palgrave Macmillan UK, 2001. 8-26.
62. Cohen, Mitchell L. "Changing patterns of infectious disease." *Nature* 406.6797 (2000): 762-767.

63. Lemerise, E.A. and Arsenio, W.F., 2000. An integrated model of emotion processes and cognition in social information processing. *Child Development*, 71(1), pp.107-118.
64. Dunn, J.R. and Schweitzer, M.E., 2005. Feeling and believing: the influence of emotion on trust. *Journal of Personality and Social Psychology*, 88(5), p.736.
65. Griskevicius, V., Shiota, M.N. and Neufeld, S.L., 2010. Influence of different positive emotions on persuasion processing: a functional evolutionary approach. *Emotion*, 10(2), p.190.
66. Zhao, S., Kuang, Y. and Ben-Arieh, D., 2015, January. Information dissemination and human behaviors in epidemics. In IIE Annual Conference. Proceedings (p. 1907). *Institute of Industrial Engineers-Publisher*.
67. Johnston, A.C. and Warkentin, M., 2010. Fear appeals and information security behaviors: an empirical study. *MIS quarterly*, pp.549-566.
68. Geer, J.H., 1965. The development of a scale to measure fear. *Behaviour Research and Therapy*, 3(1), pp.45-53.
69. Funk, S., Gilad, E., Watkins, C. and Jansen, V.A., 2009. The spread of awareness and its impact on epidemic outbreaks. *Proceedings of the National Academy of Sciences*, *106*(16), pp.6872-6877.
70. Newman, M.E., 2002. Spread of epidemic disease on networks. *Physical review E*, 66(1), p.016128.
71. Tien, J.H. and Earn, D.J., 2010. Multiple transmission pathways and disease dynamics in a waterborne pathogen model. *Bulletin of Mathematical Biology*, 72(6), pp.1506-1533.
72. Korobeinikov, A., 2006. Lyapunov functions and global stability for SIR and SIRS epidemiological models with non-linear transmission. *Bulletin of Mathematical Biology*, 68(3), pp.615-626.
73. Parkinson, B., 2011. Interpersonal emotion transfer: Contagion and social appraisal. *Social and Personality Psychology Compass*, 5(7), pp.428-439.
74. Epstein, J.M., Parker, J., Cummings, D. and Hammond, R.A., 2008. Coupled contagion dynamics of fear and disease: mathematical and computational explorations. *PLoS One*, 3(12), p.e3955.
75. Chen, F.H., 2009. Modeling the effect of information quality on risk behavior change and the transmission of infectious diseases. *Mathematical Biosciences*, 217(2), pp.125-133.
76. Hogg, M.A. and Reid, S.A., 2006. Social identity, self-categorization, and the communication of group norms. *Communication Theory*, 16(1), pp.7-30.
77. Wöllmer, M., Eyben, F., Reiter, S., Schuller, B., Cox, C., Douglas-Cowie, E. and Cowie, R., 2008, September. Abandoning emotion classes-towards continuous emotion recognition with modelling of long-range dependencies. *In INTERSPEECH* (Vol. 2008, pp. 597-600).
78. Gunes, H., 2010. Automatic, dimensional and continuous emotion recognition.
79. Suls, J., Green, P. and Hillis, S., 1998. Emotional reactivity to everyday problems, affective inertia, and neuroticism. *Personality and Social Psychology Bulletin*, 24(2), pp.127-136.
80. Ebner-Priemer, U.W., Eid, M., Kleindienst, N., Stabenow, S. and Trull, T.J., 2009. Analytic strategies for understanding affective (in) stability and other dynamic processes in psychopathology. *Journal of Abnormal Psychology*, 118(1), p.195.
81. Jahng, S., Wood, P.K. and Trull, T.J., 2008. Analysis of affective instability in ecological momentary assessment: Indices using successive difference and group comparison via multilevel modeling. *Psychological Methods*, 13(4), p.354.

82. Trull, T.J., Solhan, M.B., Tragesser, S.L., Jahng, S., Wood, P.K., Piasecki, T.M. and Watson, D., 2008. Affective instability: measuring a core feature of borderline personality disorder with ecological momentary assessment. *Journal of Abnormal Psychology*, 117(3), pp.647.
83. Zhao, S., Wu, J. and Ben-Arieh, D., 2015. Modeling infection spread and behavioral change using spatial games. *Health Systems*, 4(1), pp.41-53.
84. Steimer, T., 2002. The biology of fear-and anxiety-related behaviors. *Dialogues in Clinical Neuroscience*, 4, pp.231-250.
85. McEwen, B.S., 2007. Physiology and neurobiology of stress and adaptation: central role of the brain. *Physiological Reviews*, 87(3), pp.873-904.
86. Baker, G.A., 2003. Food safety and fear: Factors affecting consumer response to food safety risk. *International food and agribusiness management review*, 6(1), pp.1-11.
87. Scoglio, C.M., Bosca, C., Riad, M.H., Sahneh, F.D., Britch, S.C., Cohnstaedt, L.W. and Linthicum, K.J., 2016. Biologically informed individual-based network model for Rift Valley fever in the US and evaluation of mitigation strategies. *PloS one*, 11(9), p.e0162759.
88. Meyers, L., 2007. Contact network epidemiology: Bond percolation applied to infectious disease prediction and control. *Bulletin of the American Mathematical Society*, 44(1), pp.63-86.
89. Sahneh, F.D. and Scoglio, C., 2013. May the best meme win!: new exploration of competitive epidemic spreading over arbitrary multi-layer networks. arXiv preprint arXiv:1308.4880.
90. Poli, R., Kennedy, J. and Blackwell, T., 2007. Particle swarm optimization. *Swarm intelligence*, 1(1), pp.33-57.
91. Bandura, A., 2001. Social cognitive theory of mass communication. *Media Psychology*, 3(3), pp.265-299.
92. Lo, A.W., Repin, D.V. and Steenbarger, B.N., 2005. Fear and greed in financial markets: A clinical study of day-traders (No. w11243). *National Bureau of Economic Research*.
93. Das, E. and Fennis, B.M., 2008. In the mood to face the facts: When a positive mood promotes systematic processing of self-threatening information. *Motivation and Emotion*, 32(3), pp.221-230.
94. Shakeri, H., Sahneh, F.D., Scoglio, C., Poggi-Corradini, P. and Preciado, V.M., 2015. Optimal information dissemination strategy to promote preventive behaviours in multilayer epidemic networks. Math. *Biosc. Eng*, 12(3), pp.609-623.
95. Eberhart, R. and Shi, Y., 2001. Particle swarm optimization: developments, applications and resources. In evolutionary computation, 2001. Proceedings of the 2001 Congress on (Vol. 1, pp. 81-86). *IEEE*.
96. Emvudu, Y., Demasse, R. and Djeudeu, D., 2011. Optimal control of the lost to follow up in a tuberculosis model. *Computational and Mathematical Methods in Medicine*, 2011.
97. Neyman, J. and Pearson, E.S., 1933, October. The testing of statistical hypotheses in relation to probabilities a priori. In Mathematical Proceedings of the Cambridge Philosophical Society (Vol. 29, No. 04, pp. 492-510). *Cambridge University Press*.
98. Lyapunov, A.M., 1992. The general problem of the stability of motion. *International Journal of Control*, *55*(3), pp.531-534.
99. Van Den Bergh, F., 2006. An analysis of particle swarm optimizers (Doctoral dissertation, University of Pretoria).
100. Ruf, B.M., Muralidhar, K., Brown, R.M., Janney, J.J. and Paul, K., 2001. An empirical investigation of the relationship between change in corporate social performance and financial performance: A stakeholder theory perspective. *Journal of Business Ethics*, 32(2), pp.143-156.

101. Brammer, S. and Millington, A., 2008. Does it pay to be different? An analysis of the relationship between corporate social and financial performance. *Strategic Management Journal*, 29(12), pp.1325-1343.
102. Pontryagin, L.S., *Mathematical theory of optimal processes*. 2018: Routledge.
103. Greco, D.B. and Simao, M., 2007. Brazilian policy of universal access to AIDS treatment: sustainability challenges and perspectives. *Aids*, 21, pp.S37-S45.
104. Renneboog, L., Ter Horst, J. and Zhang, C., 2008. Socially responsible investments: Institutional aspects, performance, and investor behavior. *Journal of Banking & Finance*, 32(9), pp.1723-1742.
105. Guo, M., Li, B., Zhang, Z., Wu, S., and Song, J., 2013. Efficiency evaluation for allocating community-based health services. *Computers & Industrial Engineering*, *65*(3), pp.395-401.
106. Rais, A., and Viana, A., 2011. Operations research in healthcare: a survey. *International transactions in operational research*, *18*(1), pp.1-31.

107. Bi, K., Chen, Y., Zhao, S., Ben-Arieh, D., and Wu, C.H.J., 2018. Modeling learning and forgetting processes with the corresponding impacts on human behaviors in infectious disease epidemics. *Computers & Industrial Engineering*.
108. Coşgun, Ö. and Büyüktahtakın, İ.E., 2018. Stochastic dynamic resource allocation for HIV prevention and treatment: An approximate dynamic programming approach. *Computers & Industrial Engineering*, *118*, pp.423-439.
109. Kar, T.K., and Batabyal, A., 2011. Stability analysis and optimal control of a SIR epidemic model with vaccination. *Biosystems*, *104*(2-3), pp.127-135.
110. Ren, Y., Ordóñez, F. and Wu, S., 2013. Optimal resource allocation response to a smallpox outbreak. *Computers & Industrial Engineering*, *66*(2), pp.325-337.

111. Ng, C.T., Cheng, T.C.E., Tsadikovich, D., Levner, E., Elalouf, A., and Hovav, S., 2018. A multi-criterion approach to optimal vaccination planning: Method and solution. *Computers & Industrial Engineering*, *126*, pp.637-649.
112. Blayneh, K., Cao, Y. and Kwon, H.D., 2009. Optimal control of vector-borne diseases: treatment and prevention. *Discrete and Continuous Dynamical Systems B*, *11*(3), pp.587-611.
113. Bircher, J., Scientific Contribution Towards a dynamic definition of health and disease. Medicine, Health Care, and Philosophy, 2005. 81335: p. 341.
114. Hernandez-Mejia, G., Alanis, A.Y. and Hernandez-Vargas, E.A., 2018. Neural inverse optimal control for discrete-time impulsive systems. *Neurocomputing*, *314*, pp.101-108.
115. Makary, M.A., and Daniel, M., 2016. Medical error—the third leading cause of death in the US. *BMJ*, *353*, p.i2139.
116. Liu, D. and Q. Wei, Finite-approximation-error-based optimal control approach for discrete-time nonlinear systems. IEEE Transactions on Cybernetics, 2013. 43(2): p. 779-789.
117. Kong, E.B. and T.G. Dietterich, Error-correcting output coding corrects bias and variance, in *Machine Learning Proceedings 1995*. 1995, Elsevier. p. 313-321.
118. Togai, M., and O. Yamano. Analysis and design of an optimal learning control scheme for industrial robots: A discrete system approach. in Decision and Control, *1985 24th IEEE Conference on*. 1985. IEEE.
119. Gaudiano, P. and S. Grossberg, Vector associative maps: Unsupervised real-time error-based learning and control of movement trajectories. Neural networks, 1991. 4(2): p. 147-183.

120. Lee, D.S. and J.M. Park, Neural network modeling for on-line estimation of nutrient dynamics in a sequentially-operated batch reactor. Journal of Biotechnology, 1999. 75(2-3): p. 229-239.
121. Lin, C.-T., and C.S.G. Lee, Neural-network-based fuzzy logic control and decision system. IEEE Transactions on computers, 1991. 40(12): p. 1320-1336.
122. Hoyert, D.L., et al., *Deaths: final data for 1999*. National vital statistics reports: from the Centers for Disease Control and Prevention, National Center for Health Statistics, National Vital Statistics System, 2001. 49(8): p. 1-113.
123. Dellinger, R.P., et al., Surviving Sepsis Campaign: international guidelines for management of severe sepsis and septic shock: 2008. Intensive care medicine, 2008. 34(1): p. 17-60.
124. Angus, D.C., et al., Epidemiology of severe sepsis in the United States: analysis of incidence, outcome, and associated costs of care. Critical care medicine, 2001. 29(7): p. 1303-1310.
125. Cohen, J., et al., Sepsis: a roadmap for future research. The Lancet infectious diseases, 2015. 15(5): p. 581-614.
126. Brent, A.J., Sepsis. Medicine, 2017. 45(10): p. 649-653.
127. Rangel-Frausto, M.S., et al., The natural history of the system inflammatory response syndrome (SIRS): a prospective study. Jama, 1995. 273(2): p. 117-123.
128. Bhattacharjee, P., D.P. Edelson, and M.M. Churpek, Identifying patients with sepsis on the hospital wards. Chest, 2017. 151(4): p. 898-907.
129. Cook, S.A. The complexity of theorem-proving procedures. in *Proceedings of the third annual ACM symposium on Theory of computing*. 1971. ACM.
130. Ladner, R.E., N.A. Lynch, and A.L. Selman, *A comparison of polynomial time reducibilities.* Theoretical Computer Science, 1975. 1(2): p. 103-123.
131. Kumar, R., et al., The dynamics of acute inflammation. Journal of theoretical biology, 2004. 230(2): p. 145-155.
132. Malliaris, A.G., Stochastic optimal control, in *Finance*. 1989, Springer. p. 246-251.
133. Padkin, A., et al., Epidemiology of severe sepsis occurring in the first 24 hrs in intensive care units in England, Wales, and Northern Ireland. Critical care medicine, 2003. 31(9): p. 2332-2338.
134. Neuhaus, K., J. Dulout, and C. Alonso. LVDC Grid Based on PV Energy Sources and Multiple Electrochemical Storage Technologies. in Ubiquitous Intelligence & Computing, Advanced and Trusted Computing, Scalable Computing and Communications, Cloud and Big Data Computing, Internet of People, and Smart World Congress (UIC/ATC/ScalCom/CBDCom/IoP/SmartWorld), *2016 Intl IEEE Conferences*. 2016. IEEE.
135. Quinlan, J.R., Induction of decision trees. Machine learning, 1986. 1(1): p. 81-106.
136. Alpaydin, E., Introduction to machine learning. *sl*. 2010, The MIT Press.
137. Mohri, M., A. Rostamizadeh, and A. Talwalkar, Foundations of machine learning. 2012: MIT press.
138. Odom, M.D., and R. Sharda. A neural network model for bankruptcy prediction. in Neural Networks, *1990., 1990 IJCNN International Joint Conference on*. 1990. IEEE.

139. Day, J., J. Rubin, and G. Clermont, Using Nonlinear Model Predictive Control to Find Optimal Therapeutic Strategies to Modulate Inflammation. Mathematical Biosciences and Engineering, 2010. 7(4): p. 739-763.
140. Bartolini, G., Ferrara, A. and Usai, E., 1997. Applications of a sub-optimal discontinuous control algorithm for uncertain second order systems. International Journal of Robust and Nonlinear Control: IFAC-Affiliated Journal, 7(4), pp.299-319.
141. Sahni, S., Computationally related problems. SIAM Journal on Computing, 1974. 3(4): p. 262-279.
142. De Jong, K.A. and W.M. Spears. Using genetic algorithms to solve NP-complete problems. in *ICGA*. 1989.
143. Song, J., He, S., Liu, F., Niu, Y. and Ding, Z., 2016. Data-driven policy iteration algorithm for optimal control of continuous-time Itô stochastic systems with Markovian jumps. *IET Control Theory & Applications*, *10*(12), pp.1431-1439.
144. Xu, H. and Jagannathan, S., 2013. Stochastic optimal controller design for uncertain nonlinear networked control system via neuro dynamic programming. *IEEE Transactions on Neural Networks and Learning Systems*, *24*(3), pp.471-484.
145. Liu, D., Wang, D., Zhao, D., Wei, Q. and Jin, N., 2012. Neural-network-based optimal control for a class of unknown discrete-time nonlinear systems using globalized dual heuristic programming. *IEEE Transactions on Automation Science and Engineering*, *9*(3), pp.628-634.
146. Shousong, H. and Qixin, Z., 2003. Stochastic optimal control and analysis of stability of networked control systems with long delay. *Automatica*, *39*(11), pp.1877-1884.
147. Araya-Sassi, C., Paredes-Belmar, G. and Gutiérrez-Jarpa, G., 2020. Multi-commodity inventory-location problem with two different review inventory control policies and modular stochastic capacity constraints. *Computers & Industrial Engineering*, p.106410.
148. Chen, Y., Bi, K., Wu, C.H.J. and Ben-Arieh, D., 2019. A new evidence-based optimal control in healthcare delivery: A better clinical treatment management for septic patients. *Computers & Industrial Engineering*, *137*, p.106010.
149. Kushner, H.J., 1965. On the stochastic maximum principle: Fixed time of control. *Journal of Mathematical Analysis and Applications*, *11*, pp.78-92.
150. Haussmann, U.G., 1978. On the stochastic maximum principle. *SIAM Journal on Control and Optimization*, *16*(2), pp.236-251.
151. Bensoussan, A., 1983. Stochastic maximum principle for distributed parameter systems. *Journal of the Franklin Institute*, *315*(5-6), pp.387-406.
152. Framstad, N.C., Øksendal, B. and Sulem, A., 2004. Sufficient stochastic maximum principle for the optimal control of jump diffusions and applications to finance. *Journal of optimization theory and applications*, *121*(1), pp.77-98.
153. Li, J., 2012. Stochastic maximum principle in the mean-field controls. *Automatica*, *48*(2), pp.366-373.
154. Buckdahn, R., Djehiche, B. and Li, J., 2011. A general stochastic maximum principle for SDEs of mean-field type. *Applied Mathematics & Optimization*, *64*(2), pp.197-216.
155. Rajagopal, K., Balakrishnan, S.N. and Busemeyer, J.R., 2016. Neural network-based solutions for stochastic optimal control using path integrals. *IEEE transactions on neural networks and learning systems*, *28*(3), pp.534-545.
156. Kang, K. and Subramaniam, V., 2018. Joint control of dynamic maintenance and production in a failure-prone manufacturing system subjected to deterioration. *Computers & Industrial Engineering*, *119*, pp.309-320.

157. Liu, Z., 2018. Design of nonlinear optimal control for chaotic synchronization of coupled stochastic neural networks via Hamilton–Jacobi–Bellman equation. *Neural Networks*, *99*, pp.166-177.
158. Chavanasporn, W. and Ewald, C.O., 2012. A numerical method for solving stochastic optimal control problems with linear control. *Computational Economics*, *39*(4), pp.429-446.
159. Simpkins, A. and Todorov, E., 2009, March. Practical numerical methods for stochastic optimal control of biological systems in continuous time and space. In *Adaptive Dynamic Programming and Reinforcement Learning, 2009. ADPRL'09. IEEE Symposium on* (pp. 212-218). IEEE.
160. Huschto, T. and Sager, S., 2014. Solving stochastic optimal control problems by a wiener chaos approach. *Vietnam Journal of Mathematics*, *42*(1), pp.83-113.
161. Tönissen, D.D., van den Akker, J.M. and Hoogeveen, J.A., 2017. Column generation strategies and decomposition approaches for the two-stage stochastic multiple knapsack problem. *Computers & Operations Research*, *83*, pp.125-139.
162. Todorov, E. and Li, W., 2005, June. A generalized iterative LQG method for locally-optimal feedback control of constrained nonlinear stochastic systems. In *American Control Conference, 2005. Proceedings of the 2005* (pp. 300-306). IEEE.
163. Hatami-Marbini, A., Sajadi, S.M. and Malekpour, H., 2020. Optimal control and simulation for production planning of network failure-prone manufacturing systems with perishable goods. *Computers & Industrial Engineering*, p.106614.
164. Wang, Z., Wang, X. and Liu, L., 2016. Stochastic optimal linear control of wireless networked control systems with delays and packet losses. *IET Control Theory & Applications*, *10*(7), pp.742-751.
165. Devolder, P., Princep, M.B. and Fabian, I.D., 2003. Stochastic optimal control of annuity contracts. *Insurance: Mathematics and Economics*, *33*(2), pp.227-238.
166. Blanc, X., Costaouec, R., Le Bris, C. and Legoll, F., 2012. Variance reduction in stochastic homogenization using antithetic variables. *Markov Processes and Related Fields*, *18*(1), pp.31-66.
167. Kingma, D.P. and Ba, J., 2014. Adam: A method for stochastic optimization. *arXiv preprint arXiv:1412.6980*.
168. Zhao, Y., Jiang, D. and O'Regan, D., 2013. The extinction and persistence of the stochastic SIS epidemic model with vaccination. *Physica A: Statistical Mechanics and Its Applications*, *392*(20), pp.4916-4927.
169. Grange, J.M. and Zumla, A., 2002. The global emergency of tuberculosis: what is the cause?. *The journal of the Royal Society for the Promotion of Health*, *122*(2), pp.78-81.
170. Burgos, M., Gonzalez, L.C., Paz, E.A., Gournis, E., Kawamura, L.M., Schecter, G., Hopewell, P.C. and Daley, C.L., 2005. Treatment of multidrug-resistant tuberculosis in San Francisco: an outpatient-based approach. *Clinical Infectious Diseases*, *40*(7), pp.968-975.
171. Snyder, D.C., Paz, E.A., Mohle-Boetani, J.C., Fallstad, R., Black, R.L. and Chin, D.P., 1999. Tuberculosis prevention in methadone maintenance clinics: effectiveness and cost-effectiveness. *American Journal of Respiratory and Critical Care Medicine*, *160*(1), pp.178-185.
172. Side, S., Mulbar, U., Sidjara, S. and Sanusi, W., 2017, April. A SEIR model for transmission of tuberculosis. In *AIP Conference Proceedings* (Vol. 1830, No. 1, p. 020004). AIP Publishing.
173. Shier, R., 2004. Statistics: 1.1 Paired t-tests. *Mathematics Learning Support Centre*, *12*.

174. Lemos-Paião, A.P., Silva, C.J. and Torres, D.F., 2017. An epidemic model for cholera with optimal control treatment. *Journal of Computational and Applied Mathematics*, *318*, pp.168-180.
175. Ullah, S. and Khan, M.A., 2020. Modeling the impact of non-pharmaceutical interventions on the dynamics of novel coronavirus with optimal control analysis with a case study. *Chaos, Solitons & Fractals*, *139*, p.110075.
176. Silva, C.J. and Maurer, H., 2020. Optimal control of HIV treatment and immunotherapy combination with state and control delays. *Optimal Control Applications and Methods*, *41*(2), pp.537-554.
177. Morris, D.H., Rossine, F.W., Plotkin, J.B. and Levin, S.A., 2021. Optimal, near-optimal, and robust epidemic control. *Communications Physics*, *4*(1), pp.1-8.
178. Cheong, K.H., Wen, T. and Lai, J.W., 2020. Relieving cost of epidemic by parrondo's paradox: a COVID-19 case study. *Advanced Science*, *7*(24), p.2002324.
179. Pronk, N., 2012. An optimal lifestyle metric: four simple behaviors that affect health, cost, and productivity. *ACSM's Health & Fitness Journal*, *16*(3), pp.39-43.
180. Andersen, B., Gundgaard, J., Kretzschmar, M., Olsen, J., Welte, R. and Øster-gaard, L., 2006. Prediction of costs, effectiveness, and disease control of a population-based program using home sampling for diagnosis of urogenital Chlamydia trachomatis infections. *Sexually transmitted diseases*, *33*(7), pp.407-415.
181. Gomory, R., 1960. An algorithm for the mixed integer problem. RAND CORP SANTA MONICA CA.
182. Land, A.H. and Doig, A.G., 2010. An automatic method for solving discrete programming problems. In *50 Years of Integer Programming 1958-2008* (pp. 105-132). Springer, Berlin, Heidelberg.
183. Metropolis, N., 1987. The beginning of the Monte Carlo method. *Los Alamos Science*, *15*, pp.125-130.
184. Goldberg, D.E. and Holland, J.H., 1988. Genetic algorithms and machine learning.
185. Kirkpatrick, S., Gelatt, C.D. and Vecchi, M.P., 1983. Optimization by simulated annealing. *science*, *220*(4598), pp.671-680.
186. Kennedy, J. and Eberhart, R., 1995, November. Particle swarm optimization. In *Proceedings of ICNN'95-International Conference on Neural Networks* (Vol. 4, pp. 1942-1948). IEEE.
187. Westerlund, T. and Pettersson, F., 1995. An extended cutting plane method for solving convex MINLP problems. *Computers & Chemical Engineering*, *19*, pp.131-136.
188. Stidsen, T., Andersen, K.A. and Dammann, B., 2014. A branch and bound algorithm for a class of biobjective mixed integer programs. *Management Science*, *60*(4), pp.1009-1032.
189. Gong, Y.J., Li, J.J., Zhou, Y., Li, Y., Chung, H.S.H., Shi, Y.H. and Zhang, J., 2015. Genetic learning particle swarm optimization. *IEEE transactions on cybernetics*, *46*(10), pp.2277-2290.
190. Torun, H.M., Swaminathan, M., Davis, A.K. and Bellaredj, M.L.F., 2018. A global Bayesian optimization algorithm and its application to integrated system design. *IEEE Transactions on Very Large Scale Integration (VLSI) Systems*, *26*(4), pp.792-802.
191. Sameen, M.I., Pradhan, B. and Lee, S., 2020. Application of convolutional neural networks featuring Bayesian optimization for landslide susceptibility assessment. *Catena*, *186*, p.104249.
192. Abbasimehr, H. and Paki, R., 2021. Prediction of COVID-19 confirmed cases combining deep learning methods and Bayesian optimization. *Chaos, Solitons & Fractals*, *142*, p.110511.

193. Pandey, G., Chaudhary, P., Gupta, R. and Pal, S., 2020. SEIR and Regression Model based COVID-19 outbreak predictions in India. *arXiv preprint arXiv:2004.00958*.
194. Prem, K., Liu, Y., Russell, T.W., Kucharski, A.J., Eggo, R.M., Davies, N., Flasche, S., Clifford, S., Pearson, C.A., Munday, J.D. and Abbott, S., 2020. The effect of control strategies to reduce social mixing on outcomes of the COVID-19 epidemic in Wuhan, China: a modelling study. *The Lancet Public Health*, *5*(5), pp.e261-e270.
195. Shah, N.H., Suthar, A.H. and Jayswal, E.N., 2020. Control strategies to curtail transmission of covid-19. *International Journal of Mathematics and Mathematical Sciences*, *2020*.
196. Lemecha Obsu, L. and Feyissa Balcha, S., 2020. Optimal control strategies for the transmission risk of COVID-19. *Journal of biological dynamics*, *14*(1), pp.590-607.
197. Wang, X., Peng, H., Shi, B., Jiang, D., Zhang, S. and Chen, B., 2019. Optimal vaccination strategy of a constrained time-varying SEIR epidemic model. *Communications in Nonlinear Science and Numerical Simulation*, *67*, pp.37-48.
198. Bakare, E.A., Nwagwo, A. and Danso-Addo, E., 2014. Optimal control analysis of an SIR epidemic model with constant recruitment. *International Journal of Applied Mathematics Research*, *3*(3), p.273.
199. Lü, X., Hui, H.W., Liu, F.F. and Bai, Y.L., 2021. Stability and optimal control strategies for a novel epidemic model of COVID-19. *Nonlinear Dynamics*, pp.1-17.
200. Kabir, K.A. and Tanimoto, J., 2019. Modelling and analysing the coexistence of dual dilemmas in the proactive vaccination game and retroactive treatment game in epidemic viral dynamics. *Proceedings of the Royal Society A*, *475*(2232), p.20190484.
201. Castilho, C., Gondim, J.A., Marchesin, M. and Sabeti, M., 2020. Assessing the efficiency of different control strategies for the coronavirus (COVID-19) epidemic. *arXiv preprint arXiv:2004.03539*.
202. Shahriari, B., Swersky, K., Wang, Z., Adams, R.P. and De Freitas, N., 2015. Taking the human out of the loop: A review of Bayesian optimization. *Proceedings of the IEEE*, *104*(1), pp.148-175.
203. Gramacy, R.B. and Apley, D.W., 2015. Local Gaussian process approximation for large computer experiments. *Journal of Computational and Graphical Statistics*, *24*(2), pp.561-578.
204. Lee, D., Park, H. and Yoo, C.D., 2015. Face alignment using cascade gaussian process regression trees. In *Proceedings of the IEEE Conference on Computer Vision and Pattern Recognition* (pp. 4204-4212).
205. Wang, J.M., Fleet, D.J. and Hertzmann, A., 2008. Gaussian process dynamical models for human motion. *IEEE transactions on pattern analysis and machine intelligence*, *30*(2), pp.283-298.
206. Chowdhary, G., Kingravi, H.A., How, J.P. and Vela, P.A., 2015. Bayesian nonparametric adaptive control using gaussian processes. *IEEE transactions on neural networks and learning systems*, *26*(3), pp.537-550.
207. Brochu, E., Cora, V.M. and De Freitas, N., 2010. A tutorial on Bayesian optimization of expensive cost functions, with application to active user modeling and hierarchical reinforcement learning. *arXiv preprint arXiv:1012.2599*.
208. Roman, I., Santana, R., Mendiburu, A. and Lozano, J.A., 2014. Dynamic kernel selection criteria for Bayesian optimization. In *BayesOpt 2014: NIPS Workshop on Bayesian Optimization*.

209. De Palma, A., Mendler-Dünner, C., Parnell, T., Anghel, A. and Pozidis, H., 2019. Sampling acquisition functions for batch Bayesian optimization. *arXiv preprint arXiv:1903.09434*.
210. Wang, H., van Stein, B., Emmerich, M. and Back, T., 2017, October. A new acquisition function for Bayesian optimization based on the moment-generating function. In *2017 IEEE International Conference on Systems, Man, and Cybernetics (SMC)* (pp. 507-512). IEEE.
211. Montgomery, D.C., Peck, E.A. and Vining, G.G., 2021. Introduction to linear regression analysis. John Wiley & Sons.
212. Schulz, E., Speekenbrink, M. and Krause, A., 2018. A tutorial on Gaussian process regression: Modelling, exploring, and exploiting functions. *Journal of Mathematical Psychology*, *85*, pp.1-16.
213. Endres, S.C., Sandrock, C. and Focke, W.W., 2018. A simplicial homology algorithm for Lipschitz optimisation. *Journal of Global Optimization*, *72*(2), pp.181-217.
214. Xiang, Y., Sun, D.Y., Fan, W. and Gong, X.G., 1997. Generalized simulated annealing algorithm and its application to the Thomson model. *Physics Letters A*, *233*(3), pp.216-220.
215. Storn, R. and Price, K., 1997. Differential evolution–a simple and efficient heuristic for global optimization over continuous spaces. *Journal of global optimization*, *11*(4), pp.341-359.
216. Wales, D.J. and Scheraga, H.A., 1999. Global optimization of clusters, crystals, and biomolecules. *Science*, *285*(5432), pp.1368-1372.
217. Bai, B., Zhou, C. and Ye, N., 2021. Application of multi-failure mode reliability-based particle swarm optimization algorithm. *Computers & Industrial Engineering*, *161*, p.107627.
218. Park, H.J., Cho, S.W. and Lee, C., 2021. Particle swarm optimization algorithm with time buffer insertion for robust berth scheduling. *Computers & Industrial Engineering*, *160*, p.107585.
219. Nguyen, H., Moayedi, H., Foong, L.K., Al Najjar, H.A.H., Jusoh, W.A.W., Rashid, A.S.A. and Jamali, J., 2020. Optimizing ANN models with PSO for predicting short building seismic response. *Engineering with Computers*, *36*(3), pp.823-837.
220. Sierra, M.R. and Coello, C.A.C., 2005, March. Improving PSO-based multi-objective optimization using crowding, mutation and∈-dominance. In *International conference on evolutionary multi-criterion optimization* (pp. 505-519). Springer, Berlin, Heidelberg.
221. Madubueze, C.E., Dachollom, S. and Onwubuya, I.O., 2020. Controlling the spread of COVID-19: optimal control analysis. *Computational and Mathematical methods in Medicine*, *2020*.
222. Sergeyev, Y.D., Kvasov, D.E. and Mukhametzhanov, M.S., 2018. On strong homogeneity of a class of global optimization algorithms working with infinite and infinitesimal scales. *Communications in Nonlinear Science and Numerical Simulation*, *59*, pp.319-330.
223. Sergeyev, Y.D. and Kvasov, D.E., 2015. A deterministic global optimization using smooth diagonal auxiliary functions. *Communications in Nonlinear Science and Numerical Simulation*, *21*(1-3), pp.99-111.
224. Gray, A., Greenhalgh, D., Hu, L., Mao, X. and Pan, J., 2011. A stochastic differential equation SIS epidemic model. *SIAM Journal on Applied Mathematics*, *71(3)*, pp.876-902.
225. Liu, B., Grout, V. and Nikolaeva, A., 2017. Efficient global optimization of actuator based on a surrogate model assisted hybrid algorithm. *IEEE Transactions on Industrial Electronics*, *65*(7), pp.5712-5721.

226. Chen, Y., Bi, K., Wu, C.H.J., Ben-Arieh, D. and, Ashesh, S., 2017. A New Bayesian Optimization Algorithm for Complex High-Dimensional Disease Epidemic Systems and Related Computational Studies. *arXiv preprint arXiv: 2108.00062*.
227. Duvenaud, D., 2014. The Kernel cookbook: Advice on covariance functions. *URL https://www. cs. toronto. edu/~ duvenaud/cookbook*.
228. Močkus, J., 1975. On Bayesian methods for seeking the extremum. In *Optimization techniques IFIP technical conference* (pp. 400-404). Springer, Berlin, Heidelberg.
229. Kushner, H.J., 1964. A new method of locating the maximum point of an arbitrary multipeak curve in the presence of noise.
230. Thompson, W.R., 1933. On the likelihood that one unknown probability exceeds another in view of the evidence of two samples. *Biometrika, 25(3/4)*, pp.285-294.
231. Srinivas, N., Krause, A., Kakade, S.M. and Seeger, M., 2009. Gaussian process optimization in the bandit setting: No regret and experimental design. *arXiv preprint arXiv:0912.3995*.
232. Koulouriotis, D.E. and Xanthopoulos, A., 2008. Reinforcement learning and evolutionary algorithms for non-stationary multi-armed bandit problems. *Applied Mathematics and Computation, 196(2)*, pp.913-922.
233. Emaasit, D., 2018. Pymc-learn: practical probabilistic machine learning in Python. *arXiv preprint arXiv:1811.00542*.
234. Pelikan, M., Goldberg, D.E. and Cantú-Paz, E., 1999, July. BOA: The Bayesian optimization algorithm. In *Proceedings of the genetic and evolutionary computation conference GECCO-99* (Vol. 1, pp. 525-532).
235. Zhang, H., Yang, Z., Pawelek, K.A. and Liu, S., 2020. Optimal control strategies for a two-group epidemic model with vaccination-resource constraints. *Applied Mathematics and Computation*, *371*, p.124956.
236. Izzati, N., Andriani, A. and Robi'Aqolbi, R., 2020, October. Optimal control of diphtheria epidemic model with prevention and treatment. In *Journal of Physics: Conference Series* (Vol. 1663, No. 1, p. 012042). IOP Publishing.
237. Xu, D., Xu, X., Xie, Y. and Yang, C., 2017. Optimal control of an SIVRS epidemic spreading model with virus variation based on complex networks. *Communications in Nonlinear Science and Numerical Simulation*, *48*, pp.200-210.
238. Zugarini, A., Meloni, E., Betti, A., Panizza, A., Corneli, M. and Gori, M., 2020. An Optimal Control Approach to Learning in SIDARTHE Epidemic model. *arXiv preprint arXiv:2010.14878*.
239. Nabi, K.N., Kumar, P. and Erturk, V.S., 2021. Projections and fractional dynamics of COVID-19 with optimal control strategies. *Chaos, Solitons & Fractals*, *145*, p.110689.
240. Chen, Y., Bi, K., Wu, C.H.J., Ben-Arieh, D. and Sinha, A., 2021. High dimensional Bayesian Optimization Algorithm for Complex System in Time Series. *arXiv preprint arXiv:2108.02289*.
241. Moriconi, R., Kumar, K.S. and Deisenroth, M.P., 2020. High-dimensional Bayesian Optimization with projections using quantile Gaussian processes. *Optimization Letters*, *14*(1), pp.51-64.

242. Vakili, S., Liu, K. and Zhao, Q., 2013. Deterministic sequencing of exploration and exploitation for multi-armed bandit problems. *IEEE Journal of Selected Topics in Signal Processing*, *7*(5), pp.759-767.
243. Mikolov, T. and Zweig, G., 2012, December. Context dependent recurrent neural network language model. In *2012 IEEE Spoken Language Technology Workshop (SLT)* (pp. 234-239). IEEE.
244. Kamijo, K.I. and Tanigawa, T., 1990, June. Stock price pattern recognition-a recurrent neural network approach. In *1990 IJCNN international joint conference on neural networks* (pp. 215-221). IEEE.
245. Lipton, Z.C., Berkowitz, J. and Elkan, C., 2015. A critical review of recurrent neural networks for sequence learning. *arXiv preprint arXiv:1506.00019*.
246. Gyawali, B., Ramakrishna, K. and Dhamoon, A.S., 2019. Sepsis: The evolution in definition, pathophysiology, and management. *SAGE open medicine*, *7*, p.2050312119835043.
247. Rudd, K.E., Johnson, S.C., Agesa, K.M., Shackelford, K.A., Tsoi, D., Kievlan, D.R., Colombara, D.V., Ikuta, K.S., Kissoon, N., Finfer, S. and Fleischmann-Struzek, C., 2020. Global, regional, and national sepsis incidence and mortality, 1990–2017: analysis for the Global Burden of Disease Study. *The Lancet*, *395*(10219), pp.200-211.
248. Dellinger, R.P., Levy, M.M., Rhodes, A., Annane, D., Gerlach, H., Opal, S.M., Sevransky, J.E., Sprung, C.L., Douglas, I.S., Jaeschke, R. and Osborn, T.M., 2013. Surviving Sepsis Campaign: international guidelines for management of severe sepsis and septic shock, 2012. *Intensive care medicine*, *39*(2), pp.165-228.
249. Schinkel, M., Paranjape, K., Panday, R.N., Skyttberg, N. and Nanayakkara, P.W., 2019. Clinical applications of artificial intelligence in sepsis: a narrative review. *Computers in biology and medicine*, *115*, p.103488.
250. Aikawa, N., Maruyama, T., Takahashi, T., Fujimi, S., Yokoyama, T., Yoshihara, K., Ikeda, T., Sadamitsu, D. and Momozawa, M., 2013. A Phase II study of polyclonal anti-TNF-α (AZD9773) in Japanese patients with severe sepsis and/or septic shock. *Journal of Infection and Chemotherapy*, *19*(5), pp.931-940.
251. Lv, S., Han, M., Yi, R., Kwon, S., Dai, C. and Wang, R., 2014. Anti-TNF-α therapy for patients with sepsis: a systematic meta-analysis. *International journal of clinical practice*, *68*(4), pp.520-528.
252. Martínez, M.L., Plata-Menchaca, E.P., Ruiz-Rodríguez, J.C. and Ferrer, R., 2020. An approach to antibiotic treatment in patients with sepsis. *Journal of thoracic disease*, *12*(3), p.1007.
253. Reynolds, A., Rubin, J., Clermont, G., Day, J., Vodovotz, Y. and Ermentrout, G.B., 2006. A reduced mathematical model of the acute inflammatory response: I. Derivation of model and analysis of anti-inflammation. *Journal of theoretical biology*, *242*(1), pp.220-236.
254. Shi, Z., Wu, C.H.J., Ben-Arieh, D. and Simpson, S.Q., 2015. Mathematical model of innate and adaptive immunity of sepsis: a modeling and simulation study of infectious disease. *BioMed research international*, *2015*.
255. Chun, K., Syndergaard, C., Damas, C., Trubey, R., Mukindaraj, A., Qian, S., Jin, X., Breslow, S. and Niemz, A., 2015. Sepsis pathogen identification. *Journal of laboratory automation*, *20*(5), pp.539-561.

256. Vazquez-Grande, G. and Kumar, A., 2015, February. Optimizing antimicrobial therapy of sepsis and septic shock: focus on antibiotic combination therapy. In *Seminars in respiratory and critical care medicine* (Vol. 36, No. 01, pp. 154-166). Thieme Medical Publishers.
257. Gillis, A., Beil, M., Halevi-Tobias, K., van Heerden, P.V., Sviri, S. and Agur, Z., 2019. Alleviation of exhaustion-induced immunosuppression and sepsis by immune checkpoint blockers sequentially administered with antibiotics—analysis of a new mathematical model. *Intensive care medicine experimental*, *7*(1), pp.1-16.
258. Chaudhry, H., Zhou, J., Zhong, Y.I.N., Ali, M.M., McGuire, F., Nagarkatti, P.S. and Nagarkatti, M., 2013. Role of cytokines as a double-edged sword in sepsis. *In vivo*, *27*(6), pp.669-684.
259. Vincent, J.L., Sun, Q. and Dubois, M.J., 2002. Clinical trials of immunomodulatory therapies in severe sepsis and septic shock. *Clinical infectious diseases*, *34*(8), pp.1084-1093.
260. Rigato, O., Ujvari, S., Castelo, A. and Salomão, R., 1996. Tumor necrosis factor alpha (TNF-α) and sepsis: evidence for a role in host defense. *Infection*, *24*(4), pp.314-318.
261. Biron, B.M., Ayala, A. and Lomas-Neira, J.L., 2015. Biomarkers for sepsis: what is and what might be?. *Biomarker insights*, *10*, pp.BMI-S29519.
262. Faix, J.D., 2013. Biomarkers of sepsis. *Critical reviews in clinical laboratory sciences*, *50*(1), pp.23-36.
263. Aderem, A. and Ulevitch, R.J., 2000. Toll-like receptors in the induction of the innate immune response. *Nature*, *406*(6797), pp.782-787.
264. Cao, X.H., Stojkovic, I. and Obradovic, Z., 2014, October. Predicting sepsis severity from limited temporal observations. In *International Conference on Discovery Science* (pp. 37-48). Springer, Cham.
265. Gogos, C.A., Drosou, E., Bassaris, H.P. and Skoutelis, A., 2000. Pro-versus anti-inflammatory cytokine profile in patients with severe sepsis: a marker for prognosis and future therapeutic options. *The Journal of infectious diseases*, *181*(1), pp.176-180.
266. Tsurumi, A., Que, Y.A., Ryan, C.M., Tompkins, R.G. and Rahme, L.G., 2016. TNF-α/IL-10 ratio correlates with burn severity and may serve as a risk predictor of increased susceptibility to infections. *Frontiers in public health*, *4*, p.216.
267. Goswami, B., Rajappa, M., Mallika, V., Shukla, D.K. and Kumar, S., 2009. TNF-α/IL-10 ratio and C-reactive protein as markers of the inflammatory response in CAD-prone North Indian patients with acute myocardial infarction. *Clinica Chimica Acta*, *408*(1-2), pp.14-18.
268. Dimopoulou, I., Armaganidis, A., Douka, E., Mavrou, I., Augustatou, C., Kopterides, P., Lyberopoulos, P., Tzanela, M., Orfanos, S.E., Pelekanou, E. and Kostopanagiotou, G., 2007. Tumour necrosis factor-alpha (TNFα) and interleukin-10 are crucial mediators in post-operative systemic inflammatory response and determine the occurrence of complications after major abdominal surgery. *Cytokine*, *37*(1), pp.55-61.
269. Yang, J., Zhang, L., Yu, C., Yang, X.F. and Wang, H., 2014. Monocyte and macrophage differentiation: circulation inflammatory monocyte as biomarker for inflammatory diseases. *Biomarker research*, *2*(1), pp.1-9.
270. Mosser, D.M. and Edwards, J.P., 2008. Exploring the full spectrum of macrophage activation. *Nature reviews immunology*, *8*(12), pp.958-969.

271. Italiani, P. and Boraschi, D., 2014. From monocytes to M1/M2 macrophages: phenotypical vs. functional differentiation. *Frontiers in immunology*, *5*, p.514.
272. Cunha, C., Gomes, C., Vaz, A.R. and Brites, D., 2016. Exploring new inflammatory biomarkers and pathways during LPS-induced M1 polarization. *Mediators of Inflammation*, *2016*.
273. Kim, Y.J., Choi, S., Briceno, S. and Mavris, D., 2016, September. A deep learning approach to flight delay prediction. In *2016 IEEE/AIAA 35th Digital Avionics Systems Conference (DASC)* (pp. 1-6). IEEE.
274. Rosenberger, C.M. and Finlay, B.B., 2003. Phagocyte sabotage: disruption of macrophage signalling by bacterial pathogens. *Nature reviews Molecular cell biology*, *4*(5), pp.385-396.
275. Wright, H.L., Moots, R.J., Bucknall, R.C. and Edwards, S.W., 2010. Neutrophil function in inflammation and inflammatory diseases. *Rheumatology*, *49*(9), pp.1618-1631.
276. Lacy, P. and Stow, J.L., 2011. Cytokine release from innate immune cells: association with diverse membrane trafficking pathways. *Blood, The Journal of the American Society of Hematology*, *118*(1), pp.9-18.
277. Jaeschke, H., 2006. Mechanisms of neutrophil-induced liver cell injury during hepatic ischemia-reperfusion and other acute inflammatory conditions. *Am. J. Physiol. Gas-trointest. Liver Physiol*, *290*, pp.1083-1088.
278. Karlmark, K.R., Weiskirchen, R., Zimmermann, H.W., Gassler, N., Ginhoux, F., Weber, C., Merad, M., Luedde, T., Trautwein, C. and Tacke, F., 2009. Hepatic recruitment of the inflammatory Gr1+ monocyte subset upon liver injury promotes hepatic fibrosis. *Hepatology*, *50*(1), pp.261-274.
279. Schiraldi, M., Raucci, A., Muñoz, L.M., Livoti, E., Celona, B., Venereau, E., Apuzzo, T., De Marchis, F., Pedotti, M., Bachi, A. and Thelen, M., 2012. HMGB1 promotes recruitment of inflammatory cells to damaged tissues by forming a complex with CXCL12 and signaling via CXCR4. *Journal of experimental medicine*, *209*(3), pp.551-563.
280. Tacke, F., 2012, December. Functional role of intrahepatic monocyte subsets for the progression of liver inflammation and liver fibrosis in vivo. In *Fibrogenesis & tissue repair* (Vol. 5, No. 1, pp. 1-8). BioMed Central.
281. Chen, G., Li, J., Ochani, M., Rendon-Mitchell, B., Qiang, X., Susarla, S., Ulloa, L., Yang, H., Fan, S., Goyert, S.M. and Wang, P., 2004. Bacterial endotoxin stimulates macrophages to release HMGB1 partly through CD14-and TNF-dependent mechanisms. *Journal of leukocyte biology*, *76*(5), pp.994-1001.
282. Gregory, S.H., Sagnimeni, A.J. and Wing, E.J., 1996. Bacteria in the bloodstream are trapped in the liver and killed by immigrating neutrophils. *The Journal of Immunology*, *157*(6), pp.2514-2520.
283. Willenbrock, S., Braun, O., Baumgart, J., Lange, S., Junghanss, C., Heisterkamp, A., Nolte, I., Bullerdiek, J. and Escobar, H.M., 2012. TNF-α induced secretion of HMGB1 from non-immune canine mammary epithelial cells (MTH53A). *Cytokine*, *57*(2), pp.210-220.
284. Couper, K.N., Blount, D.G. and Riley, E.M., 2008. IL-10: the master regulator of immunity to infection. *The Journal of Immunology*, *180*(9), pp.5771-5777.

285. Bhatia, M., Brady, M., Shokuhi, S., Christmas, S., Neoptolemos, J.P. and Slavin, J., 2000. Inflammatory mediators in acute pancreatitis. *The Journal of Pathology: A Journal of the Pathological Society of Great Britain and Ireland*, *190*(2), pp.117-125.
286. Sindrilaru, A., Peters, T., Wieschalka, S., Baican, C., Baican, A., Peter, H., Hainzl, A., Schatz, S., Qi, Y., Schlecht, A. and Weiss, J.M., 2011. An unrestrained proinflammatory M1 macrophage population induced by iron impairs wound healing in humans and mice. *The Journal of clinical investigation*, *121*(3), pp.985-997.
287. Liaskou, E., Wilson, D.V. and Oo, Y.H., 2012. Innate immune cells in liver inflammation. *Mediators of inflammation*, *2012*.
288. Black, S., Kushner, I. and Samols, D., 2004. C-reactive protein. *Journal of Biological Chemistry*, *279*(47), pp.48487-48490.
289. Ballou, S.P. and Lozanski, G., 1992. Induction of inflammatory cytokine release from cultured human monocytes by C-reactive protein. *Cytokine*, *4*(5), pp.361-368.
290. Kasten, K.R., Tschöp, J., Adediran, S.G., Hildeman, D.A. and Caldwell, C.C., 2010. T cells are potent early mediators of the host response to sepsis. *Shock*, *34*(4), pp.327-336H.
291. Kindt, T.J., Goldsby, R.A., Osborne, B.A. and Kuby, J., 2007. Kuby immunology. Macmillan.
292. Luckheeram, R.V., Zhou, R., Verma, A.D. and Xia, B., 2012. CD4+ T cells: differentiation and functions. *Clinical and developmental immunology*, *2012*.
293. Batrla, R., Linnebacher, M., Rudy, W., Stumm, S., Wallwiener, D. and Gückel, B., 2002. CD40-expressing carcinoma cells induce down-regulation of CD40 ligand (CD154) and impair T-cell functions. *Cancer research*, *62*(7), pp.2052-2057.
294. Bellingan, G.J., Caldwell, H., Howie, S.E., Dransfield, I. and Haslett, C., 1996. In vivo fate of the inflammatory macrophage during the resolution of inflammation: inflammatory macrophages do not die locally, but emigrate to the draining lymph nodes. *The Journal of Immunology*, *157*(6), pp.2577-2585.
295. Lodish, H., Berk, A., Kaiser, C.A., Kaiser, C., Krieger, M., Scott, M.P., Bretscher, A., Ploegh, H. and Matsudaira, P., 2008. Molecular cell biology. Macmillan.
296. Alberts, B., Johnson, A., Lewis, J., Morgan, D., Raff, M., Roberts, K., Walter, P., Wilson, J. and Hunt, T., 2017. Molecular biology of the cell. WW Norton & Company.
297. McCann, C., 2013. Bifurcation Analysis of Non-linear Differential Equations. *University of LiverPool*.
298. Ahmed, N., Raza, A., Rafiq, M., Ahmadian, A., Batool, N. and Salahshour, S., 2021. Numerical and bifurcation analysis of SIQR model. *Chaos, Solitons & Fractals*, *150*, p.111133.
299. Absil, P.A. and Kurdyka, K., 2006. On the stable equilibrium points of gradient systems. *Systems & control letters*, *55*(7), pp.573-577.
300. Keith, W.L. and Rand, R.H., 1985. Dynamics of a system exhibiting the global bifurcation of a limit cycle at infinity. *International journal of non-linear mechanics*, *20*(4), pp.325-338.
301. Chen, Y., Bi, K., Wu, C.H.J., Ben-Arieh, D. and Sinha, A., 2022. High-dimensional Bayesian Optimization Algorithm with Recurrent Neural Network for Disease Control Models in Time Series. *arXiv preprint arXiv:2201.00147*.

302. Netea, M.G., Van Der Meer, J.W., Van Deuren, M. and Kullberg, B.J., 2003. Proinflammatory cytokines and sepsis syndrome: not enough, or too much of a good thing?. *Trends in immunology*, *24*(5), pp.254-258.
303. Yang, J., Zhu, Y., Duan, D., Wang, P., Xin, Y., Bai, L., Liu, Y. and Xu, Y., 2018. Enhanced activity of macrophage M1/M2 phenotypes in periodontitis. *Archives of oral biology*, *96*, pp.234-242.
304. Jiang, M., Guo, Y., Luo, Q., Huang, Z., Zhao, R., Liu, S., Le, A., Li, J. and Wan, L., 2020. T-cell subset counts in peripheral blood can be used as discriminatory biomarkers for diagnosis and severity prediction of coronavirus disease 2019. *The Journal of infectious diseases*, *222*(2), pp.198-202.
305. Serrano-Villar, S., Sainz, T., Lee, S.A., Hunt, P.W., Sinclair, E., Shacklett, B.L., Ferre, A.L., Hayes, T.L., Somsouk, M., Hsue, P.Y. and Van Natta, M.L., 2014. HIV-infected individuals with low CD4/CD8 ratio despite effective antiretroviral therapy exhibit altered T cell subsets, heightened CD8+ T cell activation, and increased risk of non-AIDS morbidity and mortality. *PLoS pathogens*, *10*(5), p.e1004078.
306. Solis, F.J. and Wets, R.J.B., 1981. Minimization by random search techniques. *Mathematics of operations research*, *6*(1), pp.19-30.
307. Beuzón, C.R., Salcedo, S.P. and Holden, D.W., 2002. Growth and killing of a Salmonella enterica serovar Typhimurium sifA mutant strain in the cytosol of different host cell lines. *Microbiology*, *148*(9), pp.2705-2715.
308. Hess, J., Ladel, C., Miko, D. and Kaufmann, S.H., 1996. Salmonella typhimurium aroA-infection in gene-targeted immunodeficient mice: major role of CD4+ TCR-alpha beta cells and IFN-gamma in bacterial clearance independent of intracellular location. *The Journal of Immunology*, *156*(9), pp.3321-3326.
309. Friedman, R.L. and Moon, R.J., 1977. Hepatic clearance of Salmonella typhimurium in silica-treated mice. *Infection and immunity*, *16*(3), pp.1005-1012.
310. Stossel, T.P., Mason, R.J., Hartwig, J. and Vaughan, M., 1972. Quantitative studies of phagocytosis by polymorphonuclear leukocytes: use of emulsions to measure the initial rate of phagocytosis. *The Journal of clinical investigation*, *51*(3), pp.615-624.
311. Hampton, M.B., Vissers, M.C. and Winterbourn, C.C., 1994. A single assay for measuring the rates of phagocytosis and bacterial killing by neutrophils. *Journal of leukocyte biology*, *55*(2), pp.147-152.
312. Bouwens, L., Baekeland, M., De Zanger, R. and Wisse, E., 1986. Quantitation, tissue distribution and proliferation kinetics of Kupffer cells in normal rat liver. *Hepatology*, *6*(4), pp.718-722.
313. Gog, J.R., Murcia, A., Osterman, N., Restif, O., McKinley, T.J., Sheppard, M., Achouri, S., Wei, B., Mastroeni, P., Wood, J.L. and Maskell, D.J., 2012. Dynamics of Salmonella infection of macrophages at the single cell level. *Journal of The Royal Society Interface*, *9*(75), pp.2696-2707.
314. Bemelmans, M.H., Gouma, D.J. and Buurman, W.A., 1993. Influence of nephrectomy on tumor necrosis factor clearance in a murine model. *The Journal of Immunology*, *150*(5), pp.2007-2017.

315. Boxio, R., Bossenmeyer-Pourié, C., Steinckwich, N., Dournon, C. and Nüße, O., 2004. Mouse bone marrow contains large numbers of functionally competent neutrophils. *Journal of leukocyte biology*, *75*(4), pp.604-611.
316. Coxon, A., Tang, T. and Mayadas, T.N., 1999. Cytokine-activated endothelial cells delay neutrophil apoptosis in vitro and in vivo: a role for granulocyte/macrophage colony-stimulating factor. *The Journal of experimental medicine*, *190*(7), pp.923-934.
317. Santos, S.A.D., Andrade Júnior, D.R.D. and Andrade, D.R.D., 2011. Tnf-a production and apoptosis in hepatocytes after listeria monocytogenes and salmonella typhimurium invasion. *Revista do Instituto de Medicina Tropical de São Paulo*, *53*(2), pp.107-112.
318. Bauer, A.L., Beauchemin, C.A. and Perelson, A.S., 2009. Agent-based modeling of host–pathogen systems: The successes and challenges. *Information sciences*, *179*(10), pp.1379-1389.
319. Gallin, J.I., Goldstein, I.M. and Snyderman, R. eds., 1992. Inflammation: basic principles and clinical correlates (pp. 511-533). New York: Raven press.
320. Shi, C., Velázquez, P., Hohl, T.M., Leiner, I., Dustin, M.L. and Pamer, E.G., 2010. Monocyte trafficking to hepatic sites of bacterial infection is chemokine independent and directed by focal intercellular adhesion molecule-1 expression. *The Journal of immunology*, *184*(11), pp.6266-6274.
321. Lund, P.K., Namork, E., Brorson, S.H., Westvik, Å.B., Joø, G.B., Øvstebø, R. and Kierulf, P., 2002. The fate of monocytes during 24 h of culture as revealed by flow cytometry and electron microscopy. *Journal of immunological methods*, *270*(1), pp.63-76.
322. Yang, H., Ochani, M., Li, J., Qiang, X., Tanovic, M., Harris, H.E., Susarla, S.M., Ulloa, L., Wang, H., DiRaimo, R. and Czura, C.J., 2004. Reversing established sepsis with antagonists of endogenous high-mobility group box 1. *Proceedings of the National Academy of Sciences*, *101*(1), pp.296-301.
323. Nagl, M., Kacani, L., Müllauer, B., Lemberger, E.M., Stoiber, H., Sprinzl, G.M., Schennach, H. and Dierich, M.P., 2002. Phagocytosis and killing of bacteria by professional phagocytes and dendritic cells. *Clinical and vaccine immunology*, *9*(6), pp.1165-1168.
324. Underhill, D.M., Bassetti, M., Rudensky, A. and Aderem, A., 1999. Dynamic interactions of macrophages with T cells during antigen presentation. *The Journal of experimental medicine*, *190*(12), pp.1909-1914.
325. Macdonald, S.H.F., Woodward, E., Coleman, M.M., Dorris, E.R., Nadarajan, P., Chew, W.M., McLaughlin, A.M. and Keane, J., 2012. Networked T cell death following macrophage infection by Mycobacterium tuberculosis. *PloS one*, *7*(6), p.e38488.
326. van Schaik, S.M. and Abbas, A.K., 2007. Role of T cells in a murine model of Escherichia coli sepsis. *European journal of immunology*, *37*(11), pp.3101-3110.
327. Ahuja, A., Anderson, S.M., Khalil, A. and Shlomchik, M.J., 2008. Maintenance of the plasma cell pool is independent of memory B cells. *Proceedings of the National Academy of Sciences*, *105*(12), pp.4802-4807.
328. Langley, W.A., Mueller, S.N. and Ahmed, R., 2009. Memory B cells are required to maintain long-lived plasma cells in mice following viral infections (132.16).
329. Vieira, P. and Rajewsky, K., 1988. The half-lives of serum immunoglobulins in adult mice. *European journal of immunology*, *18*(2), pp.313-316.

Appendix 1

Simulation of the IBO Algorithm on Synthetic Functions

We benchmarked three widely used, non-strictly convex, single-objected, and lower-dimensional functions that are particularly hard to optimize due to the presence of multiple local or global minima or deep valley-like regions (Eggholder function, Rosenbrock function, McCormick function). Thus, they are well-known test problems for global optimization and have been widely used as the benchmarks for various optimization characteristics [214]. Figure 10.1 presents the benchmark results by comparing the IBO algorithm to simplicial homology global optimization [213], dual annealing optimization [214], differential evolution [215], and basin-hopping [216], on three qualitatively different test functions mentioned above. The simulation experiments are conducted 10 times for each algorithm to calculate the average result. The running time of the IBO and other four algorithms are very close when they solve the same test function, which are about 5 seconds.

The red dot in the three figures represents the global minimum for given test functions. In Figure 10.1(a), the global minimum for the Eggholder function locates in position (512, 404.2319, −959.6407). The IBO algorithm catches the solution (511.95715, 404.26605, −959.48926) shown as a black star sign in the figure, which performs exceptionally well comparing to other algorithms. The solutions generated by simplicial homology global optimization and dual annealing optimization are closer to the global minimum. Differential evolution and basin-hopping algorithms do not perform well on the Eggholder function. Their final solutions are far off from the global minimum.

Figure 10.1(b) presents the computational results using the Rosenbrock function. The global minimum of 2D Rosenbrock is in (1, 1, 0). All five optimization algorithms perform well

for reaching the global minimum within a reasonable amount of run time. Figure 10.1(c) illustrates the computational results using the McCormick function. The global minimum for the McCormick function is located at (−0.54719, −1.54719, −1.9133). Our computational experiments show, IBO algorithm, dual annealing, and differential evolution outperform simplicial homology global optimization and basin-hopping. The IBO algorithm, dual annealing optimization, and differential evolution found the global minimum for the McCormick function, while both simplicial homology (blue dot) and the Basin-hopping algorithm ended (green cross) far from the global minimum.

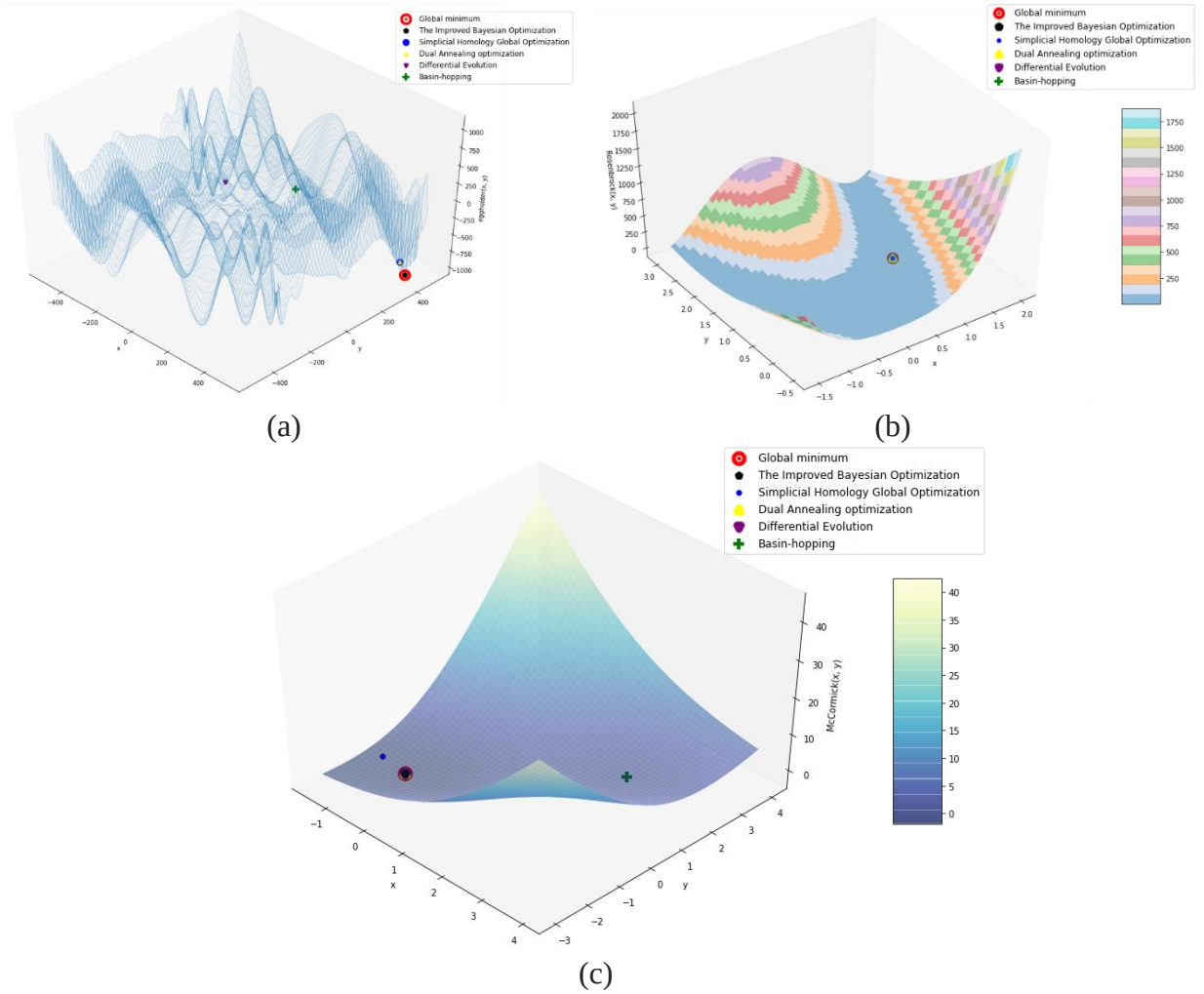

(a) (b)

(c)

Figure 10.1 Simulation results of the IBO algorithm on synthetic function. (a) Algorithms' comparison for optimization of Eggholder function. (b) Algorithms' comparison for

optimization of Rosenbrock function. (c) Algorithms' comparison for optimization of McCormick function.

Based on our simulation experiments, the IBO algorithm for these objective functions shows the best performance. Compared to the other four optimization algorithms, the IBO algorithm performs well on the low-dimensional global optimization problems. It can reach a very accurate optimal solution for the three standard test functions.

Appendix 2

Simulation of the RNN-BO Algorithm on Synthetic Functions

We test the solution accuracy generated by the RNN-BO algorithm on three high-dimensional synthetic functions (Rastrigin function, Rosenbrock function, Styblinski-Tang function). Due to the synthetic test functions don't contain constraints, there is no system state value designed in the input. We implement the tests by changing the initial start point of variable for each test function. Unless noted otherwise, we assume the variables of three test functions are 100 dimensions during simulation experiments. We conduct the simulation for each function across 5 runs to collect the data and 10 runs to evaluate the global optimal solution by changing the initial start points.

For Rastrigin function, the theoretical global optimal solution is $f(0,\dots,0)=0$. For Rosenbrock function, the theoretical global optimal solution is $f(1,\dots,1)=0$. For 100-dimensional Styblinski-Tang function, the theoretical global optimal solution is $f(-2.903534,\dots,-2.903534)=-3916.617$. During the historical data collecting process in BO part of the RNN-BO algorithm, we firstly randomly sample some points to construct the Gaussian process model, and then pick the best candidate at each iteration to optimize the acquisition function, finally do the local search to gradually converge to the global optimal point. To provide an intuitive display of the sampling point trajectory across one run in optimization part of the RNN-BO algorithm, we show a 3-dimensional plotting of each test function in Figure 11.1. We can see that the RNN-BO algorithm always can figure out the global optimal point in finite iterations for each test function. For 10 evaluation runs to predict the global optimal solution by changing the initial start points, the results are summarized in Table 11.1.

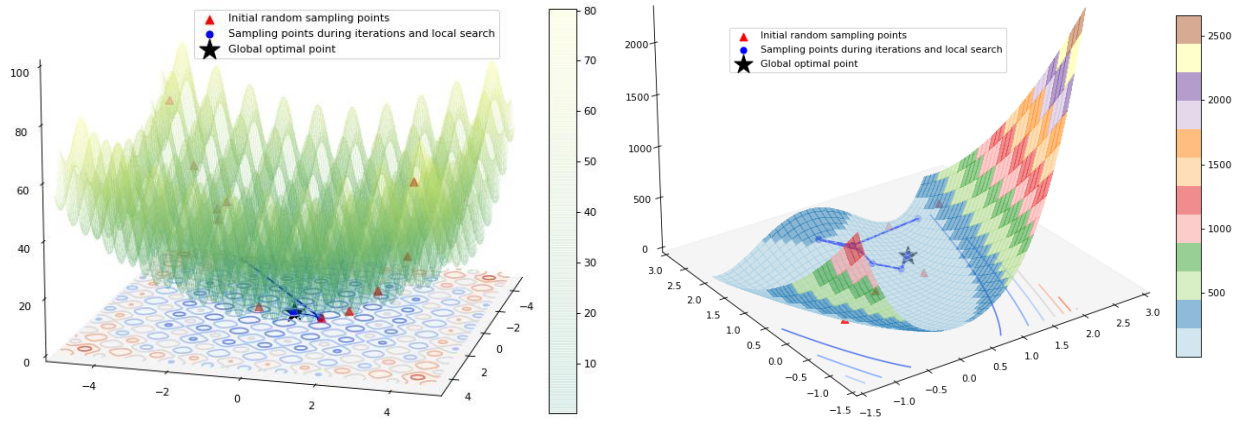

(a)

(b)

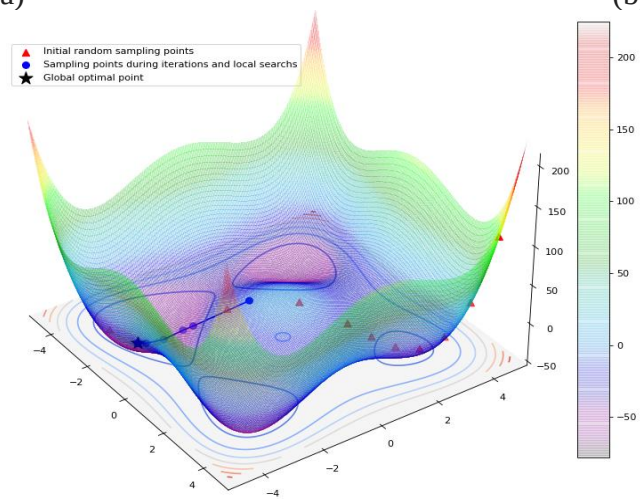

(c)

Figure 11.1 Simulation results of the RNN-BO algorithm on synthetic function. (a) 3-dimensional plotting of Rastrigin function. (b) 3-dimensional plotting of Rosenbrock function. (c) 3-dimensional plotting of Styblinski-Tang function.

Table 11.1 The optimal solutions of three synthetic functions crossing 10 runs

Function	Evaluation Dimension	Evaluation Domain	Evaluation Run	Evaluation Global Minimum	Plot Variable Dimension	Plot Domain
Rastrigin	100	[-5.12, 5.12]	10	0.0±0.00003051	2	[-5.12, 5.12]
Rosenbrock	100	[-∞, ∞]	10	0.000431±0.0013	2	[-1.5, 3]
Styblinski-Tang	100	[-5, 5]	10	-3916.608±0.0007	2	[-5, 5]

Comparison of RNN, LSTM, and GRU on 100-dimensional SEIR control model

We test different types of RNN during algorithm implementation process in Python. The different types are RNN, Long-short term memory (LSTM), and Gated recurrent unit (GRU). We conduct the comparison on a 100-dimensional SEIR control model. For the predictive model generated by each algorithm, we implement 10 runs of simulation to calculate the mean and standard deviation. The comparison results are shown in below.

Table 11.2 The comparison results of RNN, LSTM and GRU crossing 10 runs

	RNN	**LSTM**	**GRU**
Training time	7 seconds	11 seconds	11 seconds
Predictive time	3 seconds	3 seconds	3 seconds
Objective value (mean of 10 runs)	14,682	12,857	13,511
Std of 10 runs of objective value	245.187	210.363	232.56

Appendix 3

Table 12.1 Definition and experimental simulation values of parameters in improved sepsis system

Parameter	Definition	Value	Reference
k_{pg}	Pathogen growth rate	0-3.6/h	[307]
P_{∞}	Pathogen carrying capacity	10^8 cells	[308]
r_{pmk}	Rate at which pathogens are killed by Kupffer cells	0.03/per kupffer cell/h	[309]
n	The extent of pathogen binding to Kupffer cells	2	[254]
k_{c1}	Number of Kupffer cells which phagocytose half of pathogen	0.03 cells/h	[309]
r_{pn}	Rate at which pathogens are killed by neutrophils	20-100/per neutrophil/h	[310]
k_{c2}	Concentration of neutrophils which phagocytose half of pathogen	1.5×10^{-4}/h	[311]
k_{mk}	Proliferation rate of Kupffer cells under inflammation	0.015 – 2/h	[254]
K_{∞}	Kupffer cells carrying capacity	(16-20)$\times 10^6$ cells/g liver	[312]
k_{mkub}	Unbinding rate of binding Kupffer cells	0.1-0.77/h	[313]
u_{mk}	Killing rate of free Kupffer cells induced by binding to pathogen	0.23-0.9/h	[313]
r_{t1max}	The maximum number of TNF- α being released by Kupffer cells per enzyme molecule per hour	10/h	[254]
m_{t1}	Number of Kupffer cells at which the reaction rate is half of maximal production rate	10000 cells	[254]
r_{t2max}	The maximum number of TNF- α being released by neutrophils per enzyme molecule per hour	1000/h	[254]
m_{t2}	Number of activated neutrophils at which the reaction rate is half of maximal production rate	10000 cells	[254]
u_t	Degradation rate of TNF- α	0.025-0.5/h	[314]
k_{rd}	Influx rate of neutrophils into blood vessel	0.1-0.72/h	[315]
N_S	Maximum amount of neutrophils in liver	3.5×10^5/h	[282]
u_{nr}	Apoptotic rate of resting neutrophils	0.069-0.12/h	[316]
k_{nub}	Unbinding rate of activated neutrophils	0.01-0.5/h	[254]
u_n	Apoptotic rate of activated neutrophils	0.05/h	[316]
k_{r1}	Auxiliary parameter associated with the activation rate of resting neutrophils	3/h	[254]
u_{r1}	Degradation rate of parameter r_1 to maintain a slow-saturation curve	0.003/h	[254]
r_{hn}	Rate at which activated neutrophils kill apoptotic hepatocytes	9000/per neutrophil/h	[254]
k_{c3}	Concentration of activated neutrophils which phagocytose half of apoptotic hepatocytes	0.04 cells/h	[254]
A_{∞}	Number of hepatocytes in liver	3.2×10^8 cells/h	[254]

r_{ah}	Recovery rate of apoptotic hepatocytes	0.5-2/h	[317]
C_{∞}	Dissociation rate of IL-10	0.02	[254]
u_{mn}	Rate at which activated neutrophils are killed by inflammatory monocytes	200/monocyte/h	[254]
k_{mr}	Influx rate of monocytes into blood vessel	0.5/h	[318]
M_S	Resting monocyte carrying capacity in blood vessel	50000 cells	[319]
r_2	Influx rate of monocytes in liver	80/h	[320]
u_{mr}	Apoptotic rate of resting monocytes	0.2	[254]
u_m	Apoptotic rate of activated monocytes	0.08	[321]
k_{umb}	Unbinding rate of binding activated monocytes	0.4	[322]
r_{pm}	Rate at which pathogens are killed by inflammatory monocytes	7/monocyte/h	[323]
k_{c4}	Number of monocytes that phagocytose half of pathogen	0.002 cells/h	[323]
r_{h1max}	The maximum number of HMGB-1 being released by monocytes per enzyme molecule per hour	0.001	[254]
mh_1	Number of monocytes generate half of maximal HMGB-1 production rate	10,000	[254]
u_h	Degradation rate of HMGB-1	0.5–3	[254]
r_{camax}	The maximum number of IL-10 being released by monocytes per enzyme molecule per hour	10,000	[254]
C_{Ah}	Number of monocytes generate half of maximal HMGB-1 production rate	10,000	[254]
u_{ca}	Degradation rate of IL-10	0.02	[254]
r_{pcd4}	Rate at which pathogens are killed by CD4+ T cells	8	[323]
k_{c5}	Concentration of antibody which kills half of pathogen	0.035	[254]
k_{c6}	Concentration of CD4+ T cells which kill half of pathogen	0.0015	[254]
r_{pAb}	Rate at which pathogens are killed by antibody	1	[254]
r_{Mkbcd8}	Rate at which binding Kupffer Cells are killed by CD8+ T cells	0.25	[324]
r_{Nbcd8}	Rate at which binding activated neutrophils are killed by CD8+ T cells	0.25	[324]
k_{c7}	Concentration of CD8+ T cells which kill half of binding antigen presenting cell	0.0015	[254]
r_{cd4Mb}	Rate at which CD4+ T cells bind to activated monocytes	4	[324]
r_{cd8Mb}	Rate at which CD8+ T cells bind to activated monocytes	4	[324]
k_{c8}	Activated monocyte concentration produces half occupation on T cells	0.0075	[254]
r_{Mbcd8}	Rate at which binding activated monocytes are killed by CD8+ T cells	0.25	[324]
k_{cd4M}	Rate at which binding CD4+ T cells are killed by activated monocytes	0.73–2	[325]

k_{cd8M}	Rate at which binding CD8+ T cells are killed by activated monocytes	0.73–2	[325]
k_{c9}	B cell concentration produces half occupation on T cells	0.045	[254]
k_{c10}	Concentration of activated monocytes which kill half of binding T cells	0.018	[254]
k_{cd4}	The influx rate of CD4+ T cells to blood vessel	0.014	[326]
$T_{CD4\infty}$	CD4+ T cell carrying capacity in the blood vessel	27.4×10^6	[326]
u_{cd4}	Degradation rate of CD4+ T cells	0.00083–0.001	[326]
k_{cd8}	The influx rate of CD8+ T cells to blood vessel	0.0625	[326]
$T_{CD8\infty}$	CD8+ T cell carrying capacity in the blood vessel	5×10^6	[326]
u_{cd8}	Degradation rate of CD8+ T cells	0.00079–0.001	[326]
k_B	The influx rate of B cells to blood vessel	0.0122	[326]
B_∞	B cell carrying capacity in the blood vessel	28.6×10^6	[326]
r_{Bt}	Rate at which B cells bind to T cells	1–10	[254]
u_B	Degradation rate of B cells	0.00012–0.00016	[327, 328]
r_{Abmax}	The maximum production amount of antibody by B cells	0.00053	
m_{Ab}	Number of B cells at which the reaction rate is half of maximum production rate	10,000	[254]
u_{Ab}	Degradation rate of antibody	0.0035–0.01	[329]